UNIVERSITAT DE BARCELONA

Bioactive glass coatings obtained by thermal spray techniques

Beatriz Garrido Domínguez

Bioactive glass coatings obtained by thermal spray techniques

Beatriz Garrido Domínguez

UNIVERSITAT DE BARCELONA

Programa de doctorat: Enginyeria i ciències aplicades

Bioactive glass coatings obtained by thermal spray techniques

Memòria presentada per optar al grau de doctor per la Universitat de Barcelona

Beatriz Garrido Domínguez

Directora de la tesi: Irene Garcia Cano

Professora catedràtica Universitat de Barcelona

Director de la tesi: Sergi Dosta Parras

Professor agregat Universitat de Barcelona

Tutora de la tesi: Irene Garcia Cano

Professora catedràtica Universitat de Barcelona

UNIVERSITAT DE BARCELONA

Agradecimientos / Acknowledgments

Escribir estas líneas, de alguna forma, es admitir que termina este periodo de formación tan especial e inolvidable. La realización de esta tesis no hubiera sido posible sin la ayuda y colaboración de muchas personas, y me gustaría dedicarles unas palabras de agradecimiento.

En primer lugar, a mis directores de tesis, Irene y Sergi, agradecerles haberme guiado y apoyado en este camino, para llegar finalmente, a este momento tan esperado. Debo agradecerles la confianza, haberme permitido aprender, conocer, decidir, errar y seguir.

Además, quiero hacer una mención especial al profesor Josep Mª Guilemany que de alguna forma siempre ha estado presente en este camino.

Gracias también al resto de compañeros del CPT, estudiantes de doctorado, posdoctorados, profesores y técnico. Juntos hemos compartido unos años intensos, y como decía uno de ellos “convivimos más tiempo con los compañeros de trabajo que con nuestra familia”, y solo por ello vale la pena cuidarnos y apoyarnos en el día a día. La calidad humana de los compañeros del grupo ha hecho que me haya sentido como una más, y es por ello que guardaré un gran recuerdo de esta etapa, que me ha generado nostalgia viendo llegar su final.

La tesis doctoral no se ha realizado únicamente en los espacios del Centro de Proyección Térmica de la Universitat de Barcelona, por ello también quiero extenderles mi agradecimiento. Al Instituto de Cerámica y Vidrio de Madrid, en especial a Miguel Ángel, que desde el primer día me hizo sentir como si estuviera en casa, y eso no tiene precio cuando acabas de llegar a otra ciudad. Al Instituto Hospital del Mar de Investigaciones Médicas, en especial a Natalia, por ser tan acogedora y permitirme unirme al laboratorio sin dudarlo.

Afrontar una etapa de altibajos como ésta hubiera sido más complicado sin la estabilidad, cariño y tranquilidad que me aporta siempre mi familia, por ello no puedo terminar estas líneas sin un agradecimiento para ellos.

Funding received

Thanks to the financial support received, this work has been possible: Grant MAT2016-76928-C2-1-R funded by MCIN/AEI/ 10.13039/501100011033.

MINISTERIO DE CIENCIA E INNOVACIÓN

UNIÓN EUROPEA
Fondo Social Europeo
El FSE invierte en tu futuro

AGENCIA ESTATAL DE INVESTIGACIÓN

Thesis by compendium of the following publications

This thesis is presented as a compendium of publications. The publications that have been made in indexed journals guarantee the scientific interest and quality of the work developed. They are listed in order of appearance in the thesis, and for each publication, the SCImago Journal Rank indicator (SJR) is detailed. This indicator measures the current average prestige per paper of journals and is developed from the information contained in the Scopus® database.

- **Authors**: Beatriz Garrido, Sergi Dosta, Irene García-Cano
  Title: Bioactive glass coatings obtained by thermal spray: Current status and future challenges
  Journal: Boletín de la Sociedad Española de Cerámica y Vidrio, In press
  SJR (2020): 0.462
  Rank by Journal Impact Factor (2020): 43/110 - Q2 in category: Materials Science - Ceramics and Composites
  Date: April 2021
  DOI: 10.1016/j.bsecv.2021.04.001

- **Authors**: Beatriz Garrido, Irene García-Cano, Sergi Dosta
  Title: Adhesion improvement and in vitro characterisation of 45S5 bioactive glass coatings obtained by atmospheric plasma spraying
  Journal: Surface and Coatings Technology, Volume 405, 126560
  SJR (2020): 0.904
  Rank by Journal Impact Factor (2020): 20/123 - Q1 in category: Materials Science - Surfaces, Coatings and Films
  Date: January 2021
  DOI: 10.1016/j.surfcoat.2020.126560

- **Authors**: Beatriz Garrido, Vicente Albaladejo, Irene García-Cano, Sergi Dosta
  Title: Development of Bioglass/PEEK Composite Coating by Cold Gas Spray for Orthopedic Implants
  Journal: Journal of Thermal Spray Technology, Volume 31-1, pp. 186-196
  SJR (2020): 0.686
  Rank by Journal Impact Factor (2020): 27/123 - Q1 in category: Materials Science - Surfaces, Coatings and Films
  Date: January 2022
  DOI: 10.1007/s11666-021-01312-w

Participation in conferences and other scientific events

In addition to the detailed publications, the results obtained throughout the development of the thesis have been widely extended. The contributions presented in national and international scientific events are listed below.

- **Authors**: Beatriz Garrido, Irene García-Cano, Sergi Dosta
  Title: Improvement of the adhesion strength of bioactive glass coatings obtained by Atmospheric Plasma Spraying
  Type of contribution: Poster
  Conference: International Thermal Spray Conference (ITSC)
  Dates and place: May 4-6, 2022 - Vienna, Austria

- **Authors**: Beatriz Garrido, Vicente Albaladejo, Sergi Dosta, Irene García-Cano
  Title: Characterization of bioactive glass-PEEK coatings obtained by CGS
  Type of contribution: Oral presentation
  Conference: International Thermal Spray Conference (ITSC)
  Dates and place: May 24-28, 2021 - Virtual event

- **Authors**: Beatriz Garrido, Vicente Albaladejo, Sergi Dosta, Irene García-Cano
  Title: Caracterización de recubrimientos de PEEK y vidrio bioactivo obtenidos por proyección fría
  Type of contribution: Oral presentation
  Conference: Congreso de la Sociedad Española de Cerámica y Vidrio (SECV)
  Dates and place: October 26-29, 2020 - Castellón, Spain

- **Authors**: Beatriz Garrido, Raisha Garcia, Javier Fernández, Sergi Dosta, Irene García-Cano
  Title: In-vitro test evaluation of bioactive glass coatings obtained by APS and CGS
  Type of contribution: Oral presentation
  Conference: Les Rencontres Internationales de la Projection Thermique (RIPT)
  Dates and place: December 11-13, 2019 - Jülich, Germany

- **Authors**: Beatriz Garrido, Sergi Dosta, Irene García-Cano
  Title: Properties of plasma sprayed bioactive glass coatings: role and control of the microstructure
  Type of contribution: Oral presentation
  Conference: Workshop for Young Researchers in Ceramics and Glasses for Medical Applications
  Dates and place: October 10-11, 2019 - Madrid, Spain

- **Authors**: Beatriz Garrido, Sergi Dosta, Irene García-Cano
  Title: Biological evaluation of bioactive glass coatings obtained by different thermal spray technologies
  Type of contribution: Poster
  Conference: International Thermal Spray Conference (ITSC)
  Dates and place: May 26-29, 2019 - Yokohama, Japan

- **Authors**: Beatriz Garrido, Sergi Dosta, Irene García-Cano
  Title: Bioactive glass coatings for biomedical applications deposited by different thermal spray techniques
  Type of contribution: Oral presentation
  Conference: Congreso de la Sociedad Española de Cerámica y Vidrio (SECV) / Congreso Hispano-Luso de Cerámica y Vidrio
  Dates and place: October 8-11, 2018 - Barcelona, Spain

- **Authors**: Beatriz Garrido, Sergi Dosta, Irene García-Cano
  Title: Bioactive glass coatings obtained by different thermal spray technologies
  Type of contribution: Oral presentation
  Conference: Congreso Nacional de Materiales (CNMAT) / Iberian Meeting on Materials Science
  Dates and place: July 4-6, 2018 - Salamanca, Spain

- **Authors**: Sergi Dosta, Irene García-Cano, Beatriz Garrido, Javier Sánchez, Núria Cinca
  Title: Functional bioactive glass coatings: Analysis of microstructure and in vitro bioactivity
  Type of contribution: Poster
  Conference: International Thermal Spray Conference (ITSC)
  Dates and place: May 7-10, 2018 - Orlando, Florida, USA

Table of contents

Table of contents

Abstract

Abstract

Bone tissue has an excellent healing response, recovering functional and structural properties when damaged. Notwithstanding, severe damage to the bone implies the need for surgery to recover. Different orthopaedic devices are used to replace long-term hard bone tissue and are designed to last as long as possible. However, despite the significant advances in the design of implants, there is still a failure rate that cannot be underestimated. The implant failure, mainly due to aseptic loosening or infection, leads to revision surgery, which is expensive and implies more pain and time for the patient's recovery. This thesis studies surface modifications strategies by incorporating bioactive glass coatings to produce implants with materials capable of replacing bone and stimulating its regeneration to promote more efficient osseointegration.

Atmospheric plasma spray is a coating process in which materials are deposited as fine particles by applying thermal and kinetic energy to form a coating on a prepared substrate. The poor bond strength of bioactive glass coatings to the metallic substrates, partly because of the thermal expansion coefficients mismatch, is one of the main challenges faced through different strategies. To evaluate the bond strength of the developed coatings, ASTM C633 has been followed. By modifying the morphology of the bioactive glass powders and creating agglomerated particles, the cohesion between coating and substrate can be increased. Also, using hydroxyapatite in combination with bioactive glass, as a mixture of both powders or as an anchor layer, can improve the affinity of the coating with the substrate. Furthermore, applying a pre-heating to the substrate immediately prior to the deposition enhances the coating adhesion of bioactive glasses. An improvement in adhesion can be achieved if a thermal post-treatment is performed on the coatings. The different strategies evaluated have increased the bond strength of bioactive glass coatings with respect to the standard powder deposition. Some of the strategies evaluated have provided coatings with high bonding values that comply with the regulations for implantation.

In order to understand the role of the elements forming the structure of the glass and their proportion, bioactive glass coatings with different compositions have been deposited by atmospheric plasma spray onto titanium alloy substrates. The different elements forming the glass affects the mechanical and biological properties of the coatings. These elements produce a change in the coating's microstructure, affecting the coating's porosity and thus its cohesion. Also, some of the elements contained in the glass structure are able to stimulate bone cell response. Moreover, the coating's reaction in physiological solution is also affected by the content of network-forming oxides and the crystalline phases present on the coating. The analysis of the ability of the coatings to form a hydroxyl carbonate apatite and the evaluation of their dissolution behaviour has clarified how the composition of the glass can

influence the osseointegration process. In vitro tests with osteoblasts have shown that the non-commercial 62W composition has a better cellular response and stronger bond to the substrate than the commercial glass formulations. Thus, this formulation can be optimal for replacing the current hydroxyapatite-coated implants.

Cold gas spray can generate coatings with relatively low heat, making it possible to maintain the feedstock powder's material chemistry and phase composition in the resulting coatings. However, the brittleness of the glasses and the low temperatures involved during the process make it a challenge to produce glass coatings by this technique. Mixing the bioactive glasses with PEEK powder have allowed the deposition of a composite coating by low-pressure cold gas spraying, where brittle particles are embedded in a polymeric matrix. The amount of glass in the mixture affects the coating's properties and influences the deposition efficiency of the coatings. Another approach considered is to design formulations with adequate viscosity for the operating temperatures of the cold gas technique, which makes it possible to deposit the coating. However, the high degree of dissolution compromises the bioactive behaviour of these glass coatings.

0. Chapter: Thesis structure

0. Thesis structure

This thesis has been structured in several chapters as follows.

Chapter 1 presents a current and complete state of the art and is divided into three parts: the first one consist of an overview of biomaterials, with a particular emphasis on the bioactive materials used for hard tissue replacement; the second one introduces the surface modification techniques where the thermal spray techniques used in this thesis, Atmospheric Plasma Spray and Cold Gas Spray, are detailed; the las part consist of a review paper that covers bibliographic reports that have investigated bioactive glass deposition using different thermal spray techniques and the future challenges in this area.

Chapter 2 describes the motivation and goal of the thesis, including the description of specific objectives. It also tries to explain the relationship between objectives and articles contained in this thesis.

Chapter 3 introduces the methodology used to perform the experimental activity of the research, starting with the feedstock materials and following with the techniques and equipment used to characterise and evaluate the materials and coatings created. Finally, the procedures followed to produce the appropriate coatings are detailed.

The results are divided into several parts included in **Chapter 4**, with some results reported in article form. The first section details the different approaches studied to improve the adhesion of bioactive glass coatings; these results are presented in two papers. The following section shows a study with glasses of different compositions, the effect on the biological response is evaluated according to the elements present in the glass. The third section covers the development of composite bioglass/PEEK coatings by the Cold Gas Spray technique; these results are displayed in two papers, one focused on the coating production and mechanical properties and the other discussing the biological response. Finally, the last section corresponds to the development of new bioactive glass formulations with adjusted properties to be used by cold gas spray.

All the results are outlined and thoroughly discussed in **Chapter 5**.

Finally, the conclusions drawn from this thesis are summarized in **Chapter 6**.

1. Chapter: Introduction

1. Chapter: Introduction

1.1. Overview on biomaterials

Biomaterials have been gaining an increasingly important role in medicine, particularly in the regenerative field. Furthermore, it will become more and more frequent that we need the help of a biomaterial throughout our lives since life expectancy is increasing, and the deterioration of our bodies is inevitable. For this reason, the field of biomedicine has been continuously growing for decades, and today it is an area of great interest for researchers. However, materials to replace or treat damaged parts of the body date back to ancient times, even though the materials we use today are different from the first ones used.

The first evidence of using materials to repair damaged parts of the body is found in dentures. Approximately in 2500 B.C., the ancient Egyptians stabilized the periodontally affected teeth using a **gold wire**. It is known that years later, around the year 500 a. C., **teeth from animals** were used to replace the missing human teeth, and those were held with gold bands. Around the year 300 A.D., the carved **ivory** was used to replace the teeth, and again the gold wire was the element that facilitated the fastening of the pieces. Years later (600 A.D.), **seashells** were used as dental implants. From the 16th century to about the 19th century, teeth from humans who passed away were collected for use in teeth replacement. In 1829, Henry Levert carried out the first studies in vivo to determine the biological compatibility of some materials for use in dental implants; these were silver, gold, lead, and platinum (Ref 1).

Although the first advances were made in dental applications, the time for orthopaedic applications arrived in the eighteenth century. During the Middle Ages and the Modern Age, the development of implants was scarce.

The first wire fixation for orthopaedics could have been done around 1770, but there is some controversy. In 1827, Dr. Kearny Rodgers (New York) performed a bone suture using a **silver wire** to retain bone fragments of a humerus suffering pseudarthrosis. Sixteen days after the surgery, the cannula fell out of the wound with the entire wire. Despite this, bones remained in the correct position, and the fragments joined 69 days after the operation (Ref 2).

The following case, detailed in the first book published on internal fixation by Bérenger Féraud, describes a case of 1851 in which a worker suffered a closed and comminuted fracture of the lower leg after falling down a staircase. After several unsuccessful attempts to recover his fracture, it was decided to amputate his leg, but at the patient's request, this amputation was avoided. Instead, Bérenger exposed the bone ends and hold them together with three **lead wire** ligatures. After three weeks, the fracture was united, and the lead wires were removed. The patient left the hospital after 105 days.

The fixation of bones by screws could start around 1850. The French surgeons, Cucel and Rigaud, used **wood screws** and a leather strap to fixate satisfactorily a sternum and an olecranon fracture, respectively (Ref 3).

After knowing the work of the chemist Louis Pasteur on fermentation caused by germs, the surgeon Joseph Lister, suspected that microbes, invisible to the human eye, might be responsible for the infections in wounds. This theory motivated the surgeon to find a chemical that would allow him to kill germs. Thus, in 1865 Lister was able to heal a fracture without infection. This achievement led him to develop aseptic surgery protocols (Ref 4).

Another progress for orthopaedics happened in 1886, with the beginning of osteosynthesis, the subcutaneous fixation of bone fragments with plates and screws. The German surgeon Carl Hansmann performed the first internal plate fixation using a removable **steel nickel-coated plate and screws** in 1886 (Ref 5). However, after four to eight weeks, the plates and screws were removed, and frequently it was necessary to reinsert the plates to achieve healing of the fracture (Ref 6).

In 1895 when Lane introduced a **steel plate** for use in internal fixation. However, it caused problems with corrosion and needed a modification in composition and design to reduce the stress concentrations (Ref 7).

In the 20th century, one factor that promoted the development of implants and new biomaterials was the sharp increase in demand due to the need to rehabilitate the millions of wounded from the First and Second World Wars. This need arose when some of the critical advances in medicine and surgery happened, such as the development of anaesthesia and the sterile surgical techniques mentioned previously. The discovery of X-rays was another significant progress and rapidly was used in medicine. View into the human skeletal system was possible with these novel rays that facilitated diagnoses and the evaluation of the treatments used. It also allowed locating the remains of shrapnel in the wounded people. In this way, a particular scenario with favourable conditions to achieve a notable advance in the development of bone repair techniques and systems with new materials was created.

At that time, the prevailing opinion was that the materials suitable for implantation in the body were considered inert since they had minimal interaction with the biological system. However, over time, all the implants deteriorated rapidly in the human body; metals suffered corrosion, and the human body rejected other materials. In addition, the materials used did not meet the mechanical properties necessary to perform the function for which they were designed correctly. Because of these drawbacks, it was necessary to search for new metal alloys. In the 20th century, **stainless steel** was introduced to replace metallic components, the surgeon William O'Neill Sherman developed the first, a vanadium steel alloy in 1912, which was discarded in the following years due to corrosion (Ref 7). **Cobalt-based alloys** for

orthopaedic surgery appeared in 1936, thanks to Chadles S. Venable and co-workers, which analysed many metals' corrosion resistance (aluminium, copper, iron, lead, nickel, gold...) (Ref 8). Other attractive metals for orthopaedics appeared in the following years. The first trials with **tantalum** date back to 1936, and the first attempts with **titanium** were in 1947, with a variety of orthopaedic devices such as plates and screws (Ref 9).

The development of hip prostheses took many years, given the complexity of the joint. The first sketches of a hip replacement were shown in the German Congress of Surgery in the 1890s. Nevertheless, it was not until 1938 that the first total hip arthroplasty appeared, preceded by a partial hip arthroplasty in 1931. However, these first trials did not obtain favourable results. Then, in 1959, surgeon John Charnley began a study of total hip replacements with a low coefficient of friction, being the first to introduce **Teflon** polymer as a component of hip replacement and **polymethylmethacrylate (PMMA)** as bone cement (Ref 10). These innovations represent a significant improvement in the duration of hip implants.

The good results of these materials and new alloys developed led to **the first generation of biomaterials**. This generation began in the 1950s and was characterised by inert materials that did not cause harm to the patient, did not corrode in an aqueous environment, and at the same time could perform the function of the replaced tissue. Among the biomaterials considered from the first generation, it is possible to find metals (stainless steel, cobalt-chrome-based alloys, titanium, and its alloys), ceramics (alumina and zirconia), and polymers (silicone rubber, acrylic resins).

A new generation of materials was explored in the 1970s; **the second generation of biomaterials** intended to cause a controlled reaction with the tissues to induce a desired therapeutic effect. The biomaterials belonging to this era were designed to be resorbable or bioactive. This generation included the development of degradable biomaterials, active proteins, and other macromolecules in a localized site. For example, biodegradable polymeric sutures can be designed with suitable mechanical strength and specific degradation time. These kinds of polymers are polyglycolic acid (PGA), polylactic acid (PLA), or copolymer poly(lactic-co-glycolic acid) PLGA. Another example of the second generation of biomaterials are heparin coatings for blood-contacting devices (syringe needles and polymer tubing for artificial hearts) addressed to improve blood compatibility. Drug-eluting endovascular stents were used to prevent vascular restenosis after the balloon angioplasty. Since the slow release of drugs causes a delay in the growth of the coronary endothelium. This new generation also represented substantial progress for orthopaedic and dental applications by incorporating various bioactive glasses and ceramics compositions in this area.

In the 1990s, **the third generation of biomaterials** emerged to support and stimulate the regeneration of functional tissue. These biomaterials combine the properties of the previous generation (bioactive and resorbable), developing materials that help the body heal itself. The third generation of biomaterials covers two approaches, tissue engineering and in situ tissue regeneration. Porous foams designed to activate genes that stimulate the regeneration of living tissues were developed in this era. These temporary 3D porous structures combine materials with bioactive and bioresorbable capabilities that provide repair or replacement that will last as long as the patient. Biomaterials in the form of powders, solutions, or doped particles can stimulate local tissue repair. In addition, the ionic dissolution products of some bioactive materials can promote cell proliferation, differentiation, and extracellular matrix (ECM) production and organization. Mg alloys are also classified as third-generation biomaterials. These materials provide temporary mechanical support while degraded progressively as host tissues replace them. These alloys have been used more widely in cardiovascular stents than in orthopaedic implants (Ref 11).

In the 2010s, advances in nanotechnology and cell biology have allowed the development of tissue engineering and regenerative medicine toward **the fourth generation of biomaterials**. Scientific progress is giving rise to these new biomaterials, which try to mimic the extracellular matrix of tissues, their molecular architecture, and the biochemical environment to give proper cells stimulus.

Classification of biomaterials

The first definition of biomaterials dates from 1986, a conference supported by the European Society of Biomaterials was held to reach a consensus and establish definitions in the area of biomaterials. Biomaterials were defined as: “a nonviable material used in a medical device, intended to interact with biological systems.” (Ref 12)

The progress of science and technology meant that the concept of biomaterial became obsolete. It has evolved several times with scientific advances; D. F. Williams proposed in 2009 the following definition: “A biomaterial is a substance that has been engineered to take a form which, alone or as part of a complex system, is used to direct, by control of interactions with components of living systems, the course of any therapeutic or diagnostic procedure, in human or veterinary medicine.” (Ref 13)

Finally, in 2018 a conference was held in Chengdu to eliminate unnecessary terms, update others, and include new definitions regarding biomaterials. D. F. Williams presented a simplified version of its last biomaterials definition, which the assistants approved: “A material designed to take a form which can direct, through interactions with living systems, the course of any therapeutic or diagnostic procedure.” (Ref 14) Biomaterials can be classified according to tissue response or their origin, as shown in Figure 1.1.

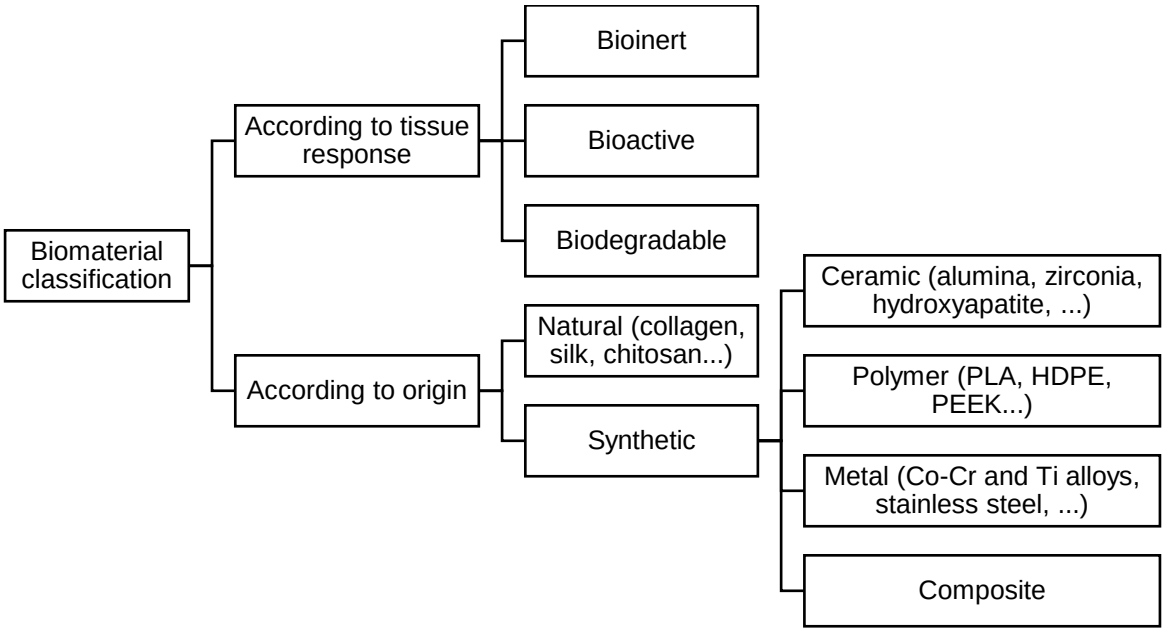

Figure 1.1 Classification of biomaterials according to their tissue response and origin

Bioinert materials are encapsulated by fibrous tissues when inserted into the body. The implanted biomaterials are isolated from the surrounding bone because the body considers it a foreign object. On the contrary, the **bioactive** materials promote bonding with the tissue. Moreover, **biodegradable** materials can decompose gradually over time, releasing their mass into the surrounding tissue. Generally, metallic biomaterials are inert; when polymers are implanted in the body, they can show a bioinert or biodegradable behaviour. We find all kinds of responses among ceramics since they can be bioinert, biodegradable, or bioactive.

1.2. Biomaterials for hard tissue replacement

The body's ability to maintain and regulate its internal conditions is known as homeostasis, and this aspect precisely limits which materials can be implanted in the human body. Biocompatibility is defined as the ability of a material to perform with an appropriate host response in a specific application. It means that the host's response to its implantation and presence cannot have adverse effects on either the implant or the host organism. In addition, the degradation products of the material must be taken into account, and these cannot cause harmful effects either in the area of implantation or for other organs or tissues. However, the interaction between the material and the biological environment is not the only factor to consider. The demands of mechanical resistance (young modulus, tensile strength, compression, bending, behaviour to fatigue and friction) and adequate corrosion determine which materials can be implantable and their ability to be processed, machined, and even to be sterilisable.

Consequently, the amount of materials to choose from to produce an implant is reduced. However, on the other hand, to choose the ideal candidate, there are more requirements: the

exact position of the implantation, the function that it will carry out, the time that it must remain implanted (temporary or permanent) or even the patient's medical history.

Bone tissue performs vital functions for the human body. It is responsible for providing the mechanical support to the body that allows locomotion, and in addition, the bone is the main protective barrier of the vital organs. Nevertheless, this tissue is susceptible to injury and deterioration, compromising its function. The leading biomaterials used to restore damaged bone are detailed in Table 1.1.

Table 1.1 Main biomaterials and its applications in bone defect repair and replacement

Materials		**Applications**	**References**
Metals	Cobalt-based alloys	Dental implants: - Partial denture frameworks and orthodontic wires Orthopaedic implants: - Joint replacement (components on knee, ankle, shoulder, wrist and hip arthroplasty) - Fracture fixation devices (screws and plates) Spine surgery: - Spinal rods	(Ref 15–17)
	Stainless steel	Orthopaedic implants: - Joint replacement (components on hip arthroplasty) - Fracture fixation devices (Kirschner wires and Schanz screws)	(Ref 18,19)
	Titanium and its alloys	Dental implants: - Implants, crowns, bridges and other components Orthopaedic implants: - Joint replacement (components on knee, elbow, shoulder, ankle and hip arthroplasty) - Fracture fixation devices (screws and plates)	(Ref 17,20,21)
Ceramics	Aluminium oxide and alloys	Dental implants: - Implants, crowns, bridges and abutments Orthopaedic implants: - Joint replacement (components on hip arthroplasty)	(Ref 22)
	Zirconium oxide and alloys	Dental implants: - Implants, crowns and bridges Orthopaedic implants: - Joint replacement (components on knee and hip arthroplasty)	(Ref 23)

Polymers	Polyethylene (UHMWPE)	Orthopaedic implants: - Joint replacement (components on knee, wrist, elbow, shoulder, ankle and hip arthroplasty)	(Ref 16,24)
	PEEK and its composites	Dental implants: - Implants and abutments Orthopaedic implants: - Joint replacement (components on knee arthroplasty) - Fracture fixation devices (screws and plates) Spine surgery: - Spinal rods and interbody fusion cages Other applications: - Rib cage replacement, cranial reconstructions	(Ref 25)

1.2.1. Osseointegration

For permanent orthopaedic or dental implants, osseointegration is key to achieving implant success. Osseointegration is defined as the direct structural and functional connection between the living bone and the surface of a load-bearing implant. When the osteoblasts adhere to the implant substrate, they can produce a strong bond with the surrounding host bone. Osseointegration is a complex process that depends on osteoinduction and osteoconduction of the implant material. If the osseointegration is insufficient, the formation of fibrous tissues around the implant can occur, causing loosening and failure of the prostheses.

The bone healing process is initiated then the bone matrix is exposed to extracellular fluid, proteins, and growth factors. This activation, followed by the osseointegration process, occurs in any lesion of the pre-existing bone matrix, including minor bone defects, fractures, and even when an artificial implant is needed to replace or repair a bone-damaged area. Once activated the bone healing, the osseointegration process starts, which can be subdivided into three stages (Ref 26–28):

- Woven bone formation: when osteoblasts reach the implant surface, a rapid bone matrix formation takes place to restore continuity and **first stability** of the implant. This woven bone consists of irregular-shaped and non-oriented packed collagen fibers, and the mechanical properties of this matrix are lower than the desired.
- Lamellar bone deposition: most of the woven bone is replaced by the lamellar bone, with an orientation that allows obtaining better mechanical properties.

- Bone remodelling: the bone structure is adapted to load and offers **biological stability** through bone regeneration and remodelling.

Implant design plays an essential role in achieving good osseointegration. The osseointegration process needs several months, usually from three to six months after the implant placement (Ref 29). The duration of the process depends on systemic and local factors, such as the implant material, the surface topography of the implant, the loading conditions of the implant, or the remodelling bone capacity of the patient. During the osseointegration process, the stability of the implant-bone fixation depends on initial mechanical stability that decreases over time and biological stability that increases over time. The variation in the implant stability can be observed in Figure 1.2.

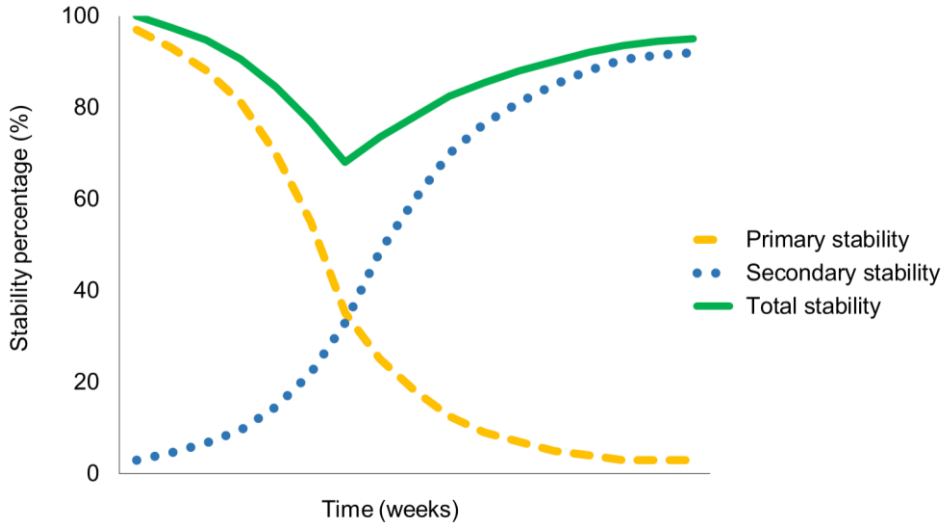

Figure 1.2 Stability of the implant over time. Figure adapted from (Ref 30)

1.2.2. Causes of implant failure

Most implants used to replace long-term hard bone tissue are designed to last as long as possible while being functional for the patient. However, there is a failure rate that cannot be underestimated. The two leading causes of implant failure are aseptic loosening and infection.

Aseptic loosening can be the result of unsuitable initial fixation. For this reason, it is crucial that the surgery team achieves good stability of the implant, not only to obtain this initial stability but also to prevent aseptic loosening of the implant in the long term, which can occur due to several factors that are detailed below:

- Gaps at the implant-tissue interface which difficult the stabilization of the prosthesis and cause **micromotion**; this instability tends to evolve to the necessity of revision surgery (Ref 31).
- The generation of **wear particles** from the implant induces a severe inflammatory response and can lead to bone resorption (Ref 32).

- Some materials do not favour **bony in-growth** on implants, making it difficult to achieve a proper fixation due to the poor osseointegration of the prosthesis (Ref 33).
- Lack of osteoinduction causes **poor bone deposition** on implant surfaces, and the stabilization of the prosthesis can be challenging in patients with poor bone quality or slow healing rates (Ref 33).

Infection of orthopaedic implants is the other leading cause of implant failure and the necessity of revision surgery. If bacteria attachment to the implant surface occurs, these begin to proliferate and can form a biofilm, which protects the bacterial colony from antibiotics and infection defense mechanisms. Therefore, it is crucial to prevent biofilm formation to avoid microbial infections. Therefore, different strategies are studied, some focused on the rapid inhibition of the infection and others that act in the long term (Ref 34). In 1989, the surgeon Gristina described the concept “race for the surface” as a competition between microbial adhesion and tissue integration to colonize the implant surface. If cells cover the surface first, it is easier to avoid bacterial colonization of the implant. On the other hand, if bacteria occupy first the implant surface, it will be covered by a biofilm (Ref 35,36).

Some of the causes that lead to infection are:

- **Initial microbial adhesion** and subsequent infection may occur at the implantation site, leading to implant failure.
- Some organisms can cause chronic **infections in late stages**.
- Infection leading to **osteolysis** occurs in the long term. The wear particles from the implant stimulate the inflammatory cells to promote bone resorption.

Implant design must consider both the need for strong osseointegration and infection prevention to achieve a successful implant.

1.3. Bioactive materials

The bioactive materials (bioactive glasses, glass-ceramics, and calcium orthophosphates) consist of a group of inorganic non-metallic solids capable of causing a specific biological response on its surface that promotes a direct, adherent, and strong bond between the surrounding tissue and the material itself. These biomaterials exhibit a bioactive behaviour and can bond to the bone tissue and support the adhesion and proliferation of the osteoblasts.

There is increasing clinical use of these biomaterials because they offer the possibility of enhancing the lifetime of prostheses. However, their clinical applications are limited to fillers, scaffolds, and coatings due to their poor mechanical properties.

1.3.1. Bioactive glasses

Glasses are mainly formed by **network-forming oxides** (SiO_2, B_2O_3, P_2O_5 y GeO_2), which allow the formation of the characteristic disordered structure of amorphous solids. To achieve a vitreous structure, it is also necessary to avoid crystallization during the cooling of the molten oxides. The glassy silica network is the most common and is composed of tetrahedrons that share the oxygens located at their vertices. The oxygen shared by two tetrahedrons forms a bridge between them called **bridging oxygen** (BO). In a glassy silica network, almost all oxygens are BO and the structure presents high connectivity.

Network-modifying oxides are introduced into the glassy structure of glass during melting. These oxides break down the structure and convert some of the BO to **not bridging oxygens** (NBO). The disorder produced in the network by these oxides gives rise to different properties. Modifying oxides can be alkaline (Na_2O, K_2O) or alkaline earth (CaO, MgO). While bonds between cations of the network-formers and oxygens are covalent, the modifying oxides are linked by ionic bonds.

When an **alkaline oxide** such as Na_2O ($2Na^+ + O^{2-}$) is added to the silica network, the reaction described in Figure 1.3 occurs. The addition of Na_2O breaks the chain of linked tetrahedrons so that each alkali ion creates a new NBO. Sodium ions (Na^+) bond ionically with NBO oxygens, filling the gaps between the tetrahedrons of the glassy matrix and neutralizing the network. As a result, alkaline oxides cause a decrease in the glass transition temperature and the viscosity of the glass, an increase in density and CTE, and a reduction in resistance to chemical attack.

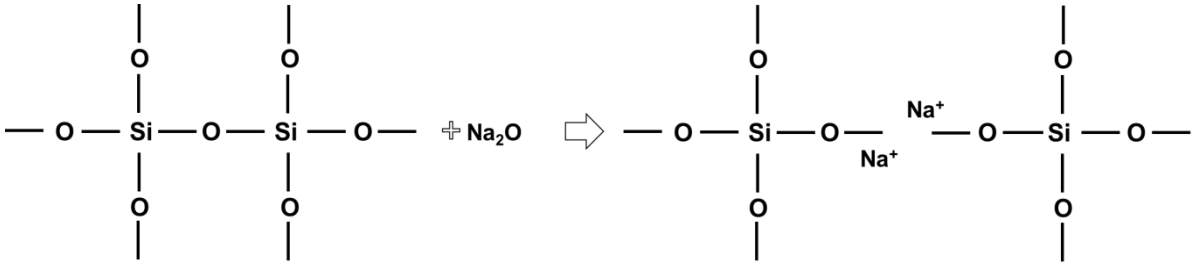

Figure 1.3 Incorporation of sodium oxide (alkaline) into the silica network

By incorporating **alkaline earth oxides** such as CaO ($Ca^{2+} + O^{2-}$), the network is disrupted by the lengthening of the chains. The addition of CaO causes each Ca^{2+} ion to create two new NBOs, and it ionically bonds to them, as can be seen in Figure 1.4. The calcium ions function as a bridge between the tetrahedrons and neutralize the network. Alkaline earth oxides stabilize the vitreous network, provide durability, prevent crystallization and improve the resistance to chemical attacks.

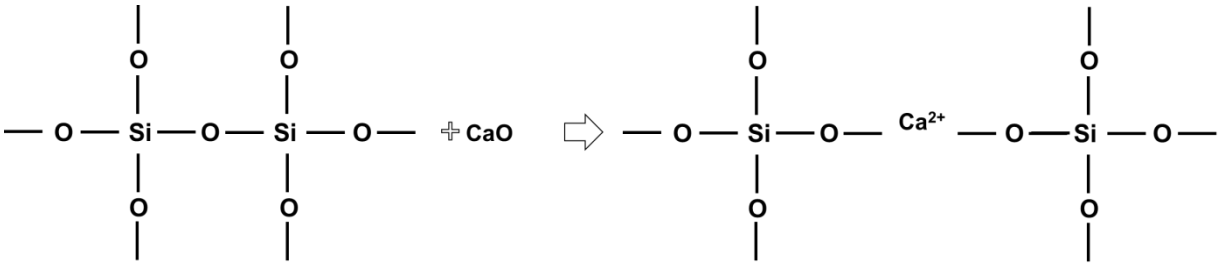

Figure 1.4 Incorporation of calcium oxide (alkaline earth) into the silica network

When alkali and alkaline earth oxides are incorporated, the properties of the resulting glassy matrix depend on the concentration of each oxide.

The ceramic engineer Larry Hench was concerned about the large number of soldiers who were handicapped after they participated in the Vietnam War. So Hench started to think about how to “make materials to repair people” (Ref 37), This way, he focused on his research on a material that the body could tolerate and discovered a family of glasses that replaced bone and helped its regeneration. In 1969, professor Hench patented Bioglass®, the first bioactive glass, with the composition of 45SiO_2, 6P_2O_5, 24.5Na_2O, 24.5CaO (in wt.%) and commonly known as 45S5 (Ref 29).

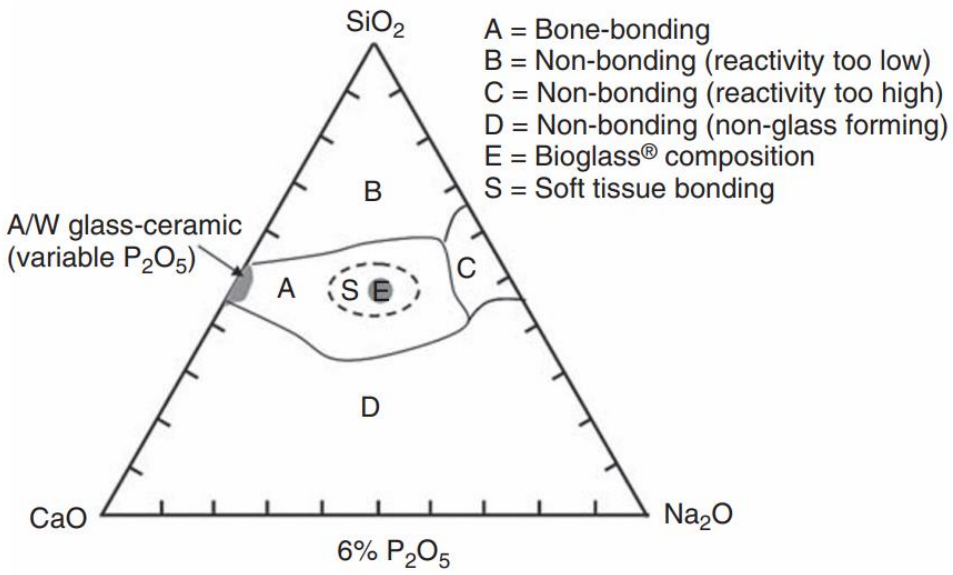

Figure 1.5 Bioactivity for Na_2O-CaO-SiO_2 diagram with constant 6% in weight of P_2O_5. Figure from (Ref 38)

Hench studied the quaternary system SiO_2-CaO-Na_2O-P_2O_5, fixing the concentration of the phosphorous oxide (Figure 1.5). Depending on the content of each oxide, he found glasses with different biological stability, from soluble to non-degradable compositions. The maximum SiO_2 content that provides bioactivity is 60% in weight; above this content, glasses are bioinert. When SiO_2 content varies from 55 to 60% in weight, moderated reactivity is achieved, and these compositions can bond to hard tissue. Ranging from 45% to 52% in weight, the bioactivity of the compositions is faster, and these glasses can bond to soft and hard tissues.

Regarding the content of network modifiers, below 15% in weight of CaO content, the reactivity of the compositions is too high and is non-stable. When Na_2O content is below 5% in weight, the structure obtained is glass-ceramic.

The structure that each glass acquires according to its composition determines its bioactivity. Bioactive glasses are amorphous solids, exhibiting an open structure and lacking great structural order. High silica and phosphate content produces a highly interconnected structure, very stable upon exposure to body fluids. The addition of network modifiers disrupts the structure causing bridging oxygen turns into non-bridging oxygen atoms, thus generating a more open structure where fluids are allowed to pass.

In the developed glasses by Hench, silica is the main network former, and it is shown as SiO_4 tetrahedron, connected to the same units through Si-O-Si bonds. The phosphate is displayed as orthophosphate (PO_4^{3-}) and is surrounded by the modifier cations to balance its charge (Ref 39).

The theoretical value of network connectivity (N_c) of the glass can be calculated to predict bioactivity and other properties of bioactive glasses. Furthermore, different authors have developed models to calculate N_c of the glasses considering the number of bridging oxygen atoms per network former based on their molar composition (Ref 40).

The equation (1) is commonly used to calculate the N_c with reliable results for the quaternary system studied by Hench. However, when more components are involved, other models should be used (Ref 41).

$$N_c = \frac{4[SiO_2] - 2\left[M_2^I O + M^{II} O\right] + 6[P_2O_5]}{[SiO_2]} \quad (1)$$

Where $M_2^{I}O$ and $M_2^{II}O$ are the mono- and divalent modifier oxides, the equation clearly shows that the addition of network modifiers is an effective strategy to alter the structure of the glass and increase its bioactivity. Low N_c is related to low glass transition and melting temperature, great reactivity, and solubility (Ref 42). Glasses with N_c between 2.0 and 2.6 are expected to be bioactive, with a higher rate between 2.11 and 2.56 (Ref 43). Particularly, Bioglass® composition has a N_c value of 2.11. Even if the proportion of modifiers oxides (sodium and calcium) does not alter the N_c, other properties of the glass can be affected. For example, if sodium oxide is replaced by calcium oxide, the resulting compositions have higher glass transition and melting temperature, which also causes an increase in density and hardness (Ref 44). The reason is the difference in ionic radii of the two ions. Regarding cellular behaviour, bioactive glasses have been demonstrated to promote attachment, proliferation, differentiation, and mineralization of bone cells compared to non-reactive surfaces (Ref 45,46).

Hench proposed how bioactive glass degraded in body fluid solutions and bonded with bone. This process results from a rapid sequence of chemical and tissue reactions on the glass surface when being in contact with the biological medium, represented in Figure 1.6. The proposed mechanism is related to bioactive glasses of the SiO_2-CaO-Na_2O-P_2O_5 family. There may be slight variations for other compositions depending on the elements forming the network.

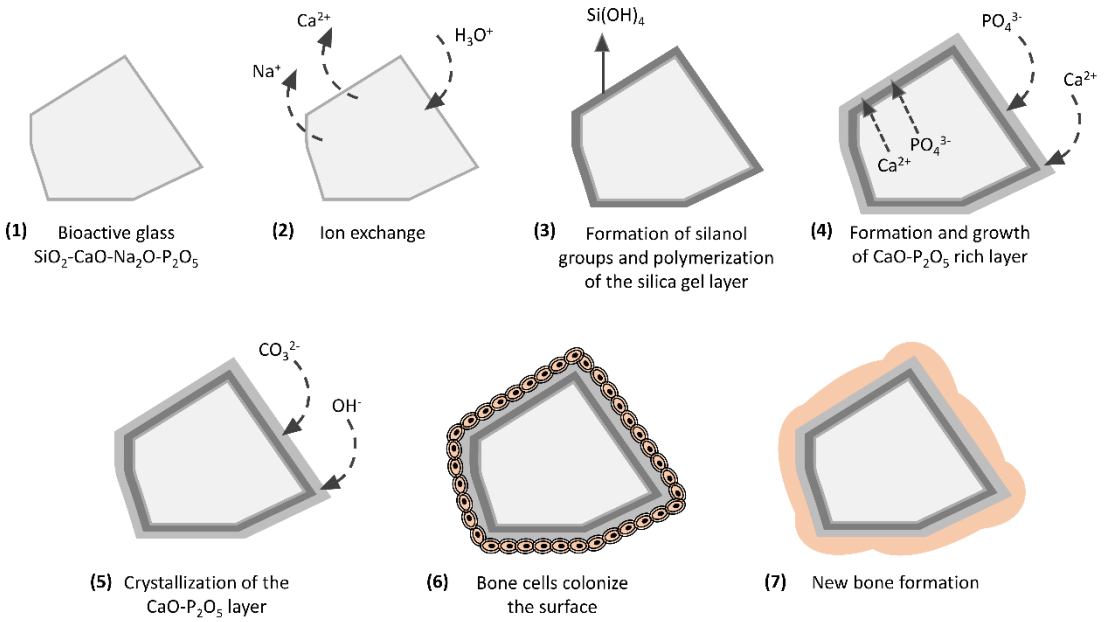

Figure 1.6 Reactions on the surface of a bioactive glass when is in contact with the biological medium

The first step involves the ion exchange of sodium and calcium ions of the glass for hydrogen ions (H_3O^+) present in the fluids, increasing the pH solution. The increase in pH generates the breaking of the Si-O-Si bonds, generating silanol groups (SiOH) at the glass surface. The continued formation of silanols causes condensation and re-polymerization of the silanols, leading to a silica-rich layer on the glass surface. After that, Ca^{2+} and PO_4^{3-} groups from the glass migrate through the silica layer forming an amorphous CaO-P_2O_5-rich layer on its top. This layer grows with the Ca^{2+} and PO_4^{3-} ions from the surrounding solution. Incorporating OH^- and CO_3^{2-} ions from the solution contributes to the crystallization of the CaO-P_2O_5-rich layer, forming the hydroxyl carbonate apatite layer (HCA). Bone cells that generate the bone matrix colonize the HCA layer and start the deposition of hydroxyapatite crystals that become the mineralized bone (Ref 42).

1.3.2. Calcium orthophosphates

Calcium orthophosphates are salts of the orthophosphoric acid (H_3PO_4) that can form compounds containing $H_2PO_4^-$, HPO_3^{2-}, or PO_4^{3-} (Ref 47). It was 1769 when the chemist and metallurgist Johan Gottlieb Gahn discovered the existence of calcium phosphate in bones.

The first clinical use of a calcium phosphate compound was in successfully repairing a bone defect in 1920 (Ref 48). To the date, up to eleven non-ion-substituted calcium orthophosphates in the ternary system $Ca(OH)_2$-H_3PO_4-H_2O were found, with a calcium to phosphate molar ratio Ca/P between 0.5 and 2.0. However, not all of them have a biological interest.

Table 1.2 Calcium orthophosphates compounds

Name	Formula	Ca/P molar ratio
Monocalcium phosphate monohydrate (MCPM)	$Ca(H_2PO_4)_2 \cdot H_2O$	0.5
Monocalcium phosphate anhydrous (MCPA)	$Ca(H_2PO_4)_2$	0.5
Dicalcium phosphate dehydrate (DCPD)	$CaHPO_4 \cdot 2H_2O$	1.0
Dicalcium phosphate anhydrous (DCPA)	$CaHPO_4$	1.0
Octacalcium phosphate (OCP)	$Ca_8(HPO_4)_2(PO_4)_4 \cdot 5H_2O$	1.33
α-Tricalcium phosphate (α-TCP)	α-$Ca_3(PO_4)_2$	1.5
β-Tricalcium phosphate (β-TCP)	β-$Ca_3(PO_4)_2$	1.5
Amorphous calcium phosphate (ACP)	$Ca_xH_y(PO_4)_z \cdot nH_2O$ (n=3-4.5; 15-20% H_2O)	1.2-2.2
Calcium-deficient hydroxyapatite (CDHA)	$Ca_{10-x}(HPO_4)_x(PO_4)_{6-x}(OH)_{2-x}$ (0 < x < 1)	1.5–1.67
Hydroxyapatite (HA)	$Ca_{10}(PO_4)_6(OH)_2$	1.67
Tetracalcium phosphate (TTCP or TetCP)	$Ca_4(PO_4)_2O$	2.0

Calcium orthophosphate biomaterials are not recognized as foreign in the body due to their chemical similarity to the mineral component of human bones and teeth. Depending on their composition, different ranges of solubility or crystallinity are found. Most calcium orthophosphates are scarcely soluble in water. The lower the Ca/P ratio, the more soluble the calcium phosphate phase; the compounds with a Ca/P ratio of less than 1 imply a high solubility when implanted into the body and are not suitable for biomedical application (Ref 49–51).

Hydroxyapatite (HA) is the calcium orthophosphate more studied and more present in the medical field. Its chemical formula is $Ca_{10}(PO_4)_6(OH)_2$ and has a stoichiometric molar ratio Ca/P of 1.67. Two structures can occur when synthetizing stoichiometric HA, monoclinic and hexagonal phases. In the biological environment, HA has the hexagonal phase that is more stable. It is the most stable calcium orthophosphate with low solubility in physiological fluids. Its surface can act as a nucleating site for the deposition of bone minerals from the solutions.

This biomaterial allows the bone to grow and remodel over its surface. Furthermore, it does not cause an inflammatory reaction when applied to the body; however, this biomaterial is not osteoinductive (Ref 52,53).

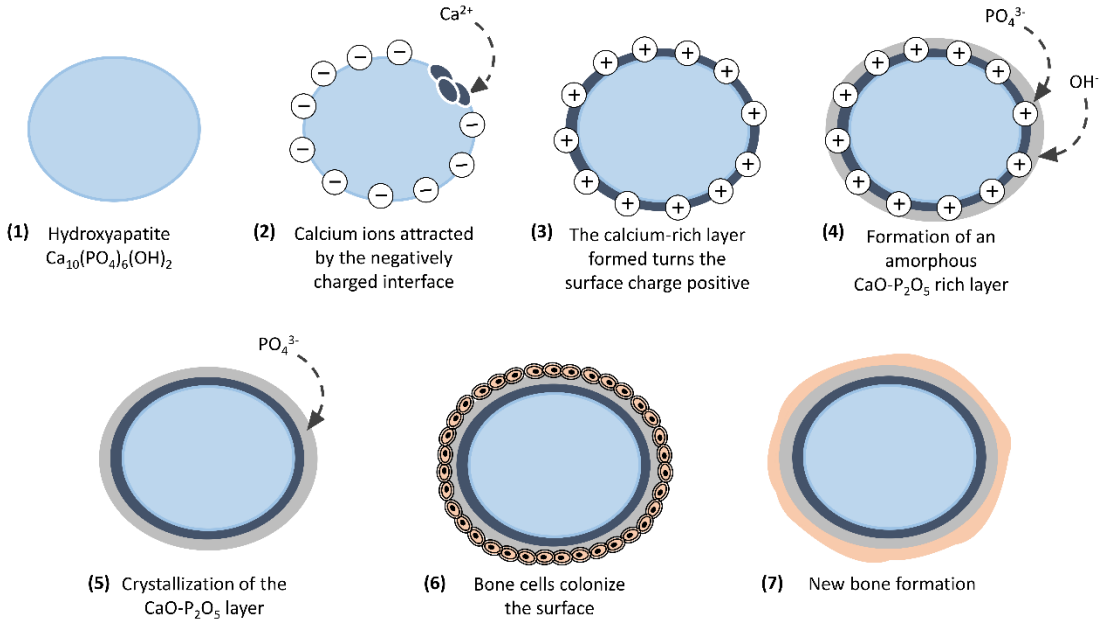

Figure 1.7 Reactions on the surface of HA when is in contact with the biological medium

The development of a bioactive bond between the implant and the surrounding bone is different for bioactive calcium orthophosphates than the proposed by Hench for bioactive glasses. Kokubo suggested (Ref 54) that for HA, the mechanism is initiated by the negative charge of the surface and not by the dissolution of ions from the material (Figure 1.7). The HA surface has an initial negative potential because of the OH^- and PO_4^{3-} ions (Ref 55). When it comes in contact with the solution, the Ca^{2+} from the solution accumulates at the interface, making the surface charge positive. By the inversion of the charge, the surface interacts with PO_4^{3-} ions from the solution, and an amorphous calcium phosphate layer is formed. Subsequently, this layer turns into a crystalline hydroxyl carbonate apatite layer by the ionic exchange.

The apatite formation process in HA can be corroborated by the electrostatic interaction of its functional groups with the ions in the fluid. However, in other ceramics, such as β-TCP or in some glass ceramics, such as A-W, the mechanism of apatite formation can be more complex since specific solubility alters the surface charge of the biomaterial. In these cases, an intermediate situation could occur to the mechanism described by Hench for bioactive glasses or by Kokubo for HA.

1.3.3. Glass-ceramics

Glass-ceramics appeared in the search for an improvement in the mechanical properties of bioactive glasses (Ref 56). These biomaterials are obtained by applying an appropriate thermal treatment to glass materials and result in the nucleation and growth of specific crystalline phases within the glassy matrix (Ref 47,57). Hence, this family of bioactive materials is partly crystalline and partly glassy. This new arrangement in the structure provides materials with high resistance to scratching and abrasion, low coefficient of thermal expansion, and tensile strength increased compared to either a glass or a ceramic of similar composition, as shown in Table 1.3 (Ref 58,59). The main drawback of glass-ceramics is its brittleness a feature that shares with glass and ceramic materials.

Table 1.3 Crystalline phases and fracture toughness of different bioactive materials

Material	Phases	Fracture Toughness ($MPa \cdot m^{1/2}$)	Young's Modulus (GPa)	References
45S5 bioactive glass	100% glass	0.7-1.1	35	(Ref 60)
A/W glass-ceramic	38% apatite + 34% wollastonite + 28% glass	2.0	117	(Ref 61)
Synthetic HA	100% hydroxyapatite	0.7-1.2	~100	(Ref 62)
Cortical bone	Mainly apatite and collagen	2-12	7–30	(Ref 60)

The developed glass-ceramics have a similar composition to Hench's glasses but with less content of alkali oxides (Ref 61). In 1973, Brömer and Pfeil discovered the first glass-ceramic material, named Ceravital®, which has an apatite ($CaO\text{-}P_2O_5$) phase in a $Na_2O\text{-}K_2O\text{-}MgO\text{-}CaO\text{-}SiO_2\text{-}P_2O_5$ glass matrix. Later, Kokubo and co-workers developed in the late 1980s the A/W glass-ceramic, commercially denominated Cerabone® A/W. This composition with remarkable clinical results contained two crystalline phases: oxyfluorapatite ($Ca_{10}(PO_4)_6(O,F_2)$) and wollastonite ($\beta\text{-}CaSiO_3$) in a residual glass matrix. In the following years, other four glass-ceramics developed reached clinical use.

1.4. Surface modification

The durability and the success of an implant are marked by its design, which includes a proper geometry and a good choice of the biomaterials that form it, and the surface characteristics significantly affect the biological response. It must be noted that cellular response and bone formation are affected by a series of surface properties and not only by one in particular. For

this reason, when a surface is altered, its characteristics should be evaluated in the whole context.

It is possible to find different approaches depending on which aspects are intended to be modified in an implant. Some of these are increasing bioactivity, promoting cell growth after implantation, supporting antibacterial effect, reducing the wear rate (particularly in join applications) by increasing hardness, and preventing ion release into the body.

Therefore, surface modification plays an essential role in developing implants with a better response in the biological system. Different strategies allow the superficial modification of the implants:

- Alter the surface layer in the existing biomaterial by chemical or physical methods. For example, biomolecules with specific functional groups can be incorporated into the surface material to trigger specific behaviours. Also, the roughness of the implant can be modified by acid or alkaline etching.
- Incorporate a thin layer of material, which usually has a different composition, on the existing surface. This overcoating can be produced by different methods such as solvent coating, electrophoretic deposition, or thermal spray.
- Topographical modification of surfaces creates three-dimensional features in the existing biomaterial to favour initial stabilization or increase the contact area. Different patterns and textures can be designed, from the creation of pores to gratings, microgrooves, or columns. Moreover, this feature can be designed on a micro or nanoscale.

Regarding functionality, surfaces can be mono-functional or multi-functional. In recent years, research has focused on the attempt to develop surfaces that can hold multiple tasks.

1.5. Thermal spray technology

1.5.1. Overview on thermal spraying

Thermal spraying includes a group of coating processes in which materials are deposited as fine particles in a molten or semi-molten state or even in an entirely solid-state to form a coating on a prepared substrate.

The process of achieving the deposition of the coating on the substrate combines kinetic energy (acceleration of the particles) with thermal energy (heating of the particles). Each spraying technique works with a specific temperature and particle velocity range, as shown in Figure 1.8. The characteristics of the process determine this range. Depending on the feedstock material and the desired properties of the final coating, it is convenient to choose among the different spraying techniques the most suitable.

The heat source used for heating the feedstock material can be a combustion flame, an electric arc, or an ionized gas, depending on the spraying technique used. The feedstock material is introduced as powder, wire, rod, cord, or suspension and accelerated by an auxiliary gas fed into the spray gun, generating a continuous stream of hot and accelerated particles sprayed towards the substrate. The coating formation consists of two phases: when the particles impact the substrate, a union is created with it, and the following particles allow the growth of the coating due to the accumulation of particles.

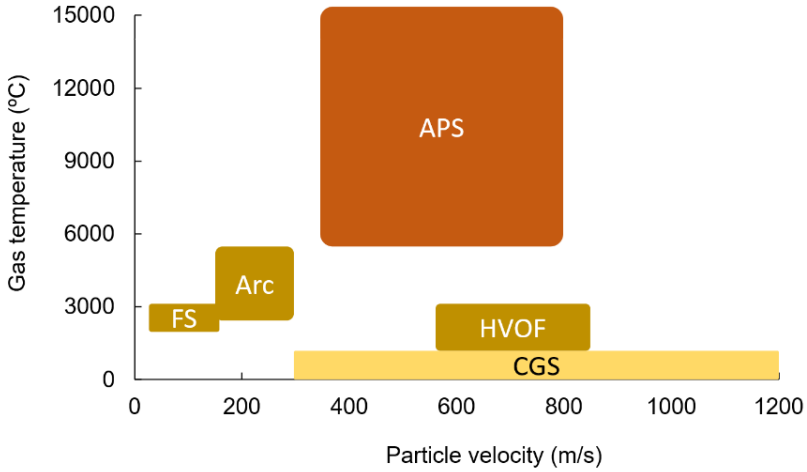

Figure 1.8 Gas temperature and particle velocity in different thermal spray techniques

1.5.2. Build-up and coating properties

The microstructure of thermal spray coatings is characterised by defects occurring due to the build-up coating process. Cracking can appear perpendicular to the substrate, within the splats microstructure (generally perpendicular to the substrate), or by generating a separation at the interface with the substrate or within the coating (parallel to the substrate). Cracks usually occur during residual stress relaxation. Due to the surface activation process, impurities are another defect for thermal spray coatings, particularly with contamination in the interface. It is also common to find non-flattened or partially flattened particles due to un-melted particles. The incomplete splat stacking can originate pores along inter-splat boundaries, often globular pores (Ref 63).

Almost all materials can be sprayed using thermal spray techniques. However, it is more appropriate to use one technique or another depending on the chosen material due to the process conditions. The microstructure and the properties of the coatings are the consequence of several factors involved in the coating formation. The factors that influence the properties of the sprayed coatings are listed above:

- Feedstock properties:
  - The **material composition** is essential for the quality of the obtained coatings. The feedstock material must be in optimal conditions (no humidity and no

oxidation) to obtain an accurate result. It is also important to remember that some materials can decompose, crystallize or oxidize during the spraying process.

- The **characteristics of the feedstock material** have a clear impact on the quality of the coating. For example, the material's thermal conductivity affects the effectiveness of heat transfer between the energy beam and the material. In the case of powder material, it should also be considered that the morphology of the particles, density, and the size of the particles affect the particle trajectory and particle heating and velocity.

- Pre-treatment of substrate: **pre-heating** the substrate prior to spraying can reduce residual thermal stress and support adhesion of the layer. Also, adequate **surface roughness** can favour the adhesion of the particles to the substrate (Ref 64,65).

- Thermal spray process:

  - Some materials can be sprayed by different **thermal spraying techniques**. Inevitably, the characteristics of each technique result in coatings with different properties.

  - The **process parameters** are decisive in the quality of the coatings, but some have a more significant impact. Some of these parameters are external such as the spraying distance and angle, speed of the thermal spray device across the surface, and the environment (inert gas chambers or atmosphere). Other parameters are internal, from the equipment: nozzle geometry, feed rate of the feedstock material, and the energy source (gas composition, temperature, gas flow, and power).

- Post-treatments: **thermal or chemical treatments** are applied to eliminate pores to improve cohesion strength and enhance bonding strength, modify the microstructure, crystallize amorphous coatings or form final compounds, among other possibilities (Ref 66,67).

Depending on the final application, different properties are desired. Therefore, when designing an implant or medical device, it is important to evaluate the requirements for the specific application, and some of the properties can be specified by international regulations.

The properties of the materials can be divided into mechanical, physical, chemical, and biological, and most of these categories are interconnected with each other. It is usually challenging to find a perfect candidate that meets all the requirements. For this reason, the material with the most adjusted mechanical properties is usually chosen as the substrate to avoid stress shielding. Bone remodelling is related to the loads the bone is subjected to; therefore, a rigidity and strain similar to the bone must be achieved when placing an implant

(Ref 68,69). The surface of the candidate material can be modified to provide an enhancement to a specific application. For example, hip or knee implants are subject to many friction stresses, so it is necessary to seek a low coefficient of friction between the materials in contact. The coatings for this part of the prosthesis can be oriented towards obtaining this improvement. These devices have another area that must be bonded with the bone tissue to acquire proper stability. So for this part of the components, a coating with a bioactive material or inducing a high specific surface area to increase the contact with the bone tissue are alternatives to promote the osseointegration. Otherwise, when plates are temporarily implanted to repair fractures, the weak integration of the screws with the bone tissues could facilitate their removal after the healing of the bone fracture. In this case, it would be favourable to use materials with less bioactive capacity.

1.5.3. Basics on atmospheric plasma spray

Plasma spraying is a deposition technique in which powder is injected within a plasma jet at very high temperatures (between 6000 and 15000 ºC) (Ref 70), the first industrial plasma spray torches (dc arcs) date from the 1960s (Ref 71). Figure 1.9 represents a scheme of dc plasma spraying equipment. The accelerated particles are partially or totally melted and driven to impact onto the substrate, where the coating is formed by the accumulation of flattened and solidified particles. Plasma spraying is a process where thermal energy is strongly involved, allowing the deposition of a wide range of materials, even the ceramic ones, and the substrate remains cold during the deposition.

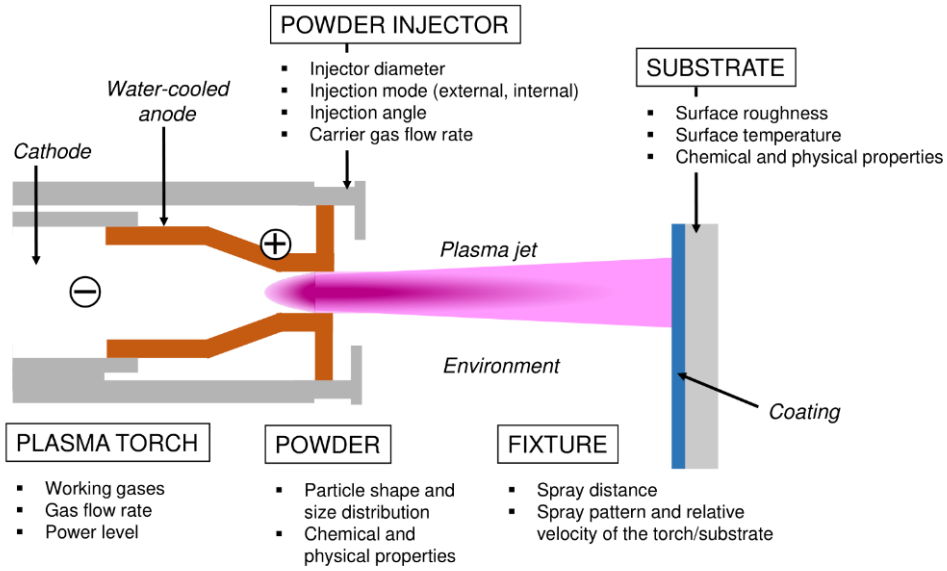

Figure 1.9 Schematic drawing of the plasma spraying process

Plasma spraying is a flexible and reliable technique, with the possibility of controlling many parameters that influence the coating properties.

The process can be divided into three different stages:

- Generation of thermal and kinetic energy includes parameters involved in the **plasma formation and its interaction with its environment**. For example, when spraying in an air environment, the atmosphere can react with the molten particles in certain situations, causing metal oxidation or carbide decomposition.
- Interaction of energy with sprayed material, related to the **powder and its injection properties**.
- Interaction of sprayed material with the substrate is associated with **splat formation and coating development**.

Achieving proper coatings requires special care and knowledge of the process.

Working gases heat up and expand to the atmosphere forming a plasma jet. Intense temperature and plasma velocity gradients exist in the plasma jet. The maximum temperature is achieved in the core zone, close to the nozzle exit and the centre line. This region is followed by a transitional region in which the temperature decreases rapidly. Finally, the powder suspended in a carrier gas is injected into the plasma jet.

Generation of thermal and kinetic energy

Different gases can be used to generate the plasma. The **plasma composition** also influences the jet velocity and enthalpy. Monoatomic gases such as argon and helium need only to be ionized to enter the plasma state, so they require less energy to initiate the plasma. The energy of these gases has a linear relationship with the gas temperature. In contrast, bimolecular gases (hydrogen and nitrogen) need to dissociate before entering the plasma state. The relationship between the energy of diatomic gases and the gas temperatures suffers deviations from linearity due to the dissociation previous to ionization (Ref 72).

Generally, the plasma gas is composed of argon or mixtures of argon + hydrogen, argon + helium and argon + nitrogen; less common is a mixture of nitrogen + hydrogen and argon + hydrogen + helium. The typical flow rate of the working gases is about 30-50 slm; in some equipment, it can be up to 80 slm (Ref 72). To improve the heat transfer to the particles, hydrogen, helium, or nitrogen are usually added as auxiliary gas to the primary gas, causing an increased plasma enthalpy (Ref 73).

The volume percentage of each gas in the mixture depends on the gas composition. For example, Janisson et al. (Ref 74) studied the effect of the ternary mixture argon-helium-hydrogen in the plasma jet properties, where argon and helium vary between 30 to 55 vol. %, while the contribution of hydrogen is minor, below 25%.

Powder injection characteristics

The success of a suitable coating is largely related to good control of the particle's trajectory and their heat transfer in the plasma. A slight deviation from the optimal conditions leads to poor results due to insufficient heating of the particles since large radial and axial temperature gradients exist on the plasma jet.

Injection of the particles into the plasma jet is an essential factor in controlling the trajectory of the particles and ensuring it is in the correct region of the plasma (the hot region, close to the centre line). **The powder injection** device can be located internal, inside the nozzle of the plasma torch, or external, at a short distance outside of the plasma torch exit. With the same spray conditions, internal injection allows the particles to pass through the plasma jet faster, introducing a perturbation in the plasma jet flow. In contrast, with external injection, the particles enter directly into the plasma jet during its expansion, when the impulse is lower (Ref 75). Moreover, the injection is usually performed perpendicular to the axis of the jet (90º), but sometimes the **injection angle** is done at a certain angle. When the injection of the powder is done with an unfavourable inclination to the flow direction, the particles reach higher temperatures due to their long residence time in the core zone of the jet. However, this inclination can cause sticking problems in the nozzle due to the lower injection velocity of the particles and the injection in a hotter zone of the jet compared with orthogonal injection.

Otherwise, when the powder injection is done with a favourable inclination to the flow, the particles enter the plasma jet in a less hot zone than orthogonal injection and the time of residence of the powder in the jet is reduced.

The most common gas used as the carrier gas for APS is argon due to its relatively high density, and the gas flow rate is usually in the range 2.5 to 8 slm (standard litre per minute). The **carrier gas flow rate** should be adjusted for each powder. It must be adequate for the particles to reach the hotter region of the plasma jet with a suitable velocity and travel close to its centre line, allowing the particles to acquire the necessary temperature conditions. If the carrier gas flow rate is insufficient, the particles do not reach the hotter zone of the plasma jet. While, if it is too high, the particles cross the plasma jet rapidly, remaining few time in the core zone and acquiring a trajectory far from the jet axis.

The trajectory of the particles through the plasma jet also depends on their **size and mass**. Small particles may not penetrate the plasma jet at the same carrier gas flow rate, and larger particles may cross the plasma jet. For this reason, a narrow particle size distribution can provide better results. When spraying powders with small particle sizes, a higher carrier gas flow rate should be used to acquire an axial trajectory. However, particles below 5-10 µm are not suitable for plasma spraying because the needed carrier gas flow rate disturbs the plasma jet (Ref 71). Then, the typical particle size used in plasma spraying goes from 10 to 70 µm.

Coating formation

The coating formation depends mainly on the **characteristics of the substrate surface**. For this reason, before spraying, surface preparation can be done by providing a surface free of contamination, modifying the roughness or morphology of the surface, or applying temperature to preheat the substrate.

Other aspects that can vary the properties of the coatings are related to **kinematic parameters**, such as the spray distance (usually between 60 and 150 mm for APS (Ref 73)), degree of overlapping (distance between passes), and traverse gun speed. Moreover, the impact angle of the particles has to be close to an orthogonal impact to the substrate.

The molten or semi-molten particles flatten, solidify and form splats. The solidification is commonly achieved before the following particle impacts the same area, and the coating results from their layering. The properties of the coatings are also linked to the quality of contact between de adhered splats. The **splat layering** depends on the temperature of the particles at the moment of impact and on their ability to accommodate onto the substrate or other solidified particles. For example, disc-shaped splats provide good contact and enhanced adhesion/cohesion (Figure 1.10(b)), while splats with extensively fingered have poor contact, with many bubbles, as represented in Figure 1.10(c); these types of splats correspond to fully molten particles. However, when the partially molten particles impact the substrate, they cannot spread properly (see Figure 1.10(a)); the unmelted core is still present in the centre of the splat, and the molten shell of the particles can spread out (Ref 76).

The powder feed rate, the use of cooling systems, the spray distance, and preheating of the substrate are the parameters that can help achieve splats with the proper flattening degree for good adhesion. Interesting coatings can be obtained by APS if a compromise between the different parameters is achieved to ensure that the particles melt at impact.

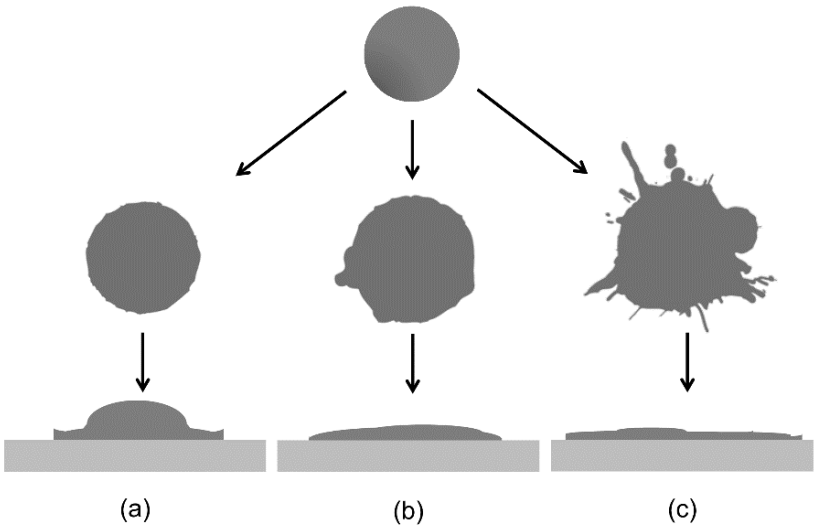

Figure 1.10 Scheme of different types of splat formation by APS

1.5.4. Basics on cold gas spray

Cold gas spray is a material deposition process included in thermal spray techniques. It was developed in the 1980s and involved the impact of particles on a substrate at very high speeds (300 to 1200 m/s) to form coatings or self-standing components (Ref 77). The suitable size of powder particles for this technique is relatively small, between 1 and 50 µm (Ref 78). Moreover, the spray distance is less than in other spraying techniques; it does not exceed 50 mm (Ref 79). Unlike other thermal spray processes, the particle deposition process in CGS is in solid-state, so the feedstock material does not reach melting to form the coating. The heat during the process is relatively low for both the spray material and the substrate, making it possible to maintain the feedstock material's material chemistry and phase composition in the obtained coatings, minimizing the oxidation and decomposition of the materials sprayed (Ref 80).

The kinetic energy governs the union between the particles and the formation of the coating; therefore, a high level of plastic deformation of the particles and adiabatic shear instability is required. A converging-diverging nozzle is usually used to produce supersonic gas flow in which particles achieve supersonic velocity. This supersonic velocity is created in the nozzle throat (in the diverging part of the nozzle). Convergent-barrel and convergent–divergent-barrel nozzles can also be used to accelerate particles. The different types of nozzles employed in CGS to get supersonic velocities are represented in Figure 1.11. The nozzle design is one of the key factors in achieving optimum spray conditions (Ref 81–83).

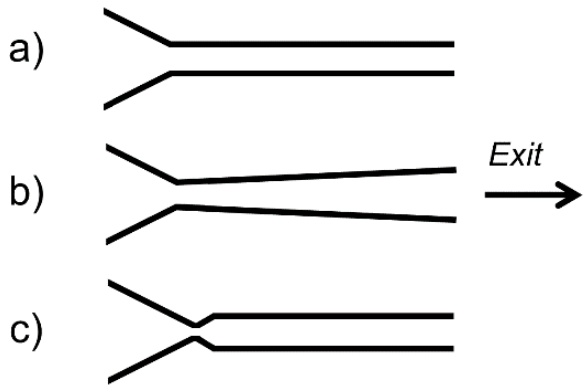

Figure 1.11 Scheme of types of nozzles for cold spray: convergent-barrel nozzle, convergent-divergent nozzle, convergent-divergent-barrel nozzle. Figure adapted from (Ref 81)

CGS allows the production of dense and pure coatings from metal and metal alloy powders. The formation mechanism of these coatings favours the low porosity level since the pressure during spraying causes packaging of the particles, forming a strong bond between them. Thus the coatings are less porous in the first layers and increase their porosity in the upper part (Ref 79). The quality of the coatings depends on the process parameters such as gas

temperature, nozzle design, and powder characteristics. The deposition of polymers and ceramics using this technique is not easy, but the research in this area has increased in recent years.

High-pressure cold spraying (HPCS) and low-pressure cold spraying (LPCS)

CGS is divided into two different processes depending on the pressure used: high-pressure cold spraying (HPCS) and low-pressure cold spraying (LPCS). A scheme of the different types of equipment can be seen in Figure 1.12.

In the HPCS process, pressurized gas (N_2, He, or a mixture of them) is heated and conducted to the nozzle; the **powder is fed** with a carrier gas and then mixed with the main gas before entering the nozzle **in the axial direction**. The acceleration of the particles is achieved through the converging-diverging nozzle. The accelerated particles reach high speed and impact the surface, forming the coating layer by layer. The HPCS process enables pressures between **10 bar and up to 70 bar**. The gas is preheated in a separate heating unit, and also, in the spraying gun, the gas preheating temperature can vary **from room temperature to 1100ºC**. Particle velocities as high as 1200 m/s can be achieved by this technique (Ref 84).

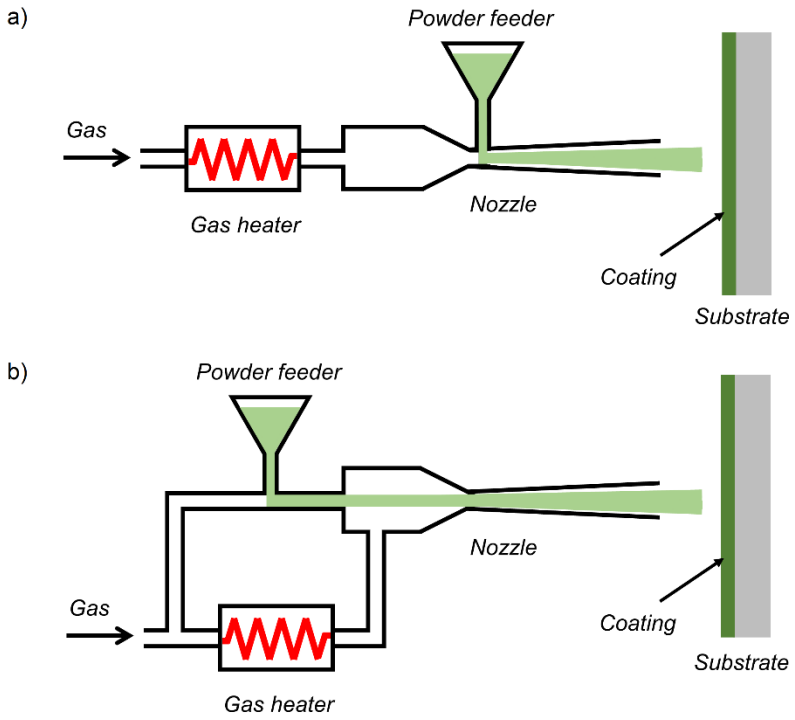

Figure 1.12 Schematic drawing of: a) LPCS and b) HPCS

In the LPCS process, compressed air is usually used as process gas to spray the powders; nitrogen or helium can also be used, and gas heating is done only in the spraying gun. The powder is fed to the heated gas perpendicularly to the diverging part of the nozzle (radial injection). The pressure in this process varies between 5 and 10 bar, depending on the equipment. Furthermore, the gas preheating temperature can be adjusted from room

temperature to 650ºC. Regarding the powder feed rate, in LPCS, lower ratios are used because of the higher particle concentration in the gas flow, usually between 5 to 50 g/min versus 75 to 220 g/min in HPCGS (Ref 85). The particle velocities reached in LPCGS are lower than in HPCGS, usually below 600 m/s. Even though the particle velocities are much lower, it is a technique belonging to CGS technology because the powders do not reach melting temperatures during the coating formation process (Ref 80).

Coating formation

The formation of a CGS coating is very different from conventional thermally sprayed coatings. It is produced in a solid-state without melting the material. The coating formation consists of two stages: in the initial one, the bonding of the first layer of particles occurs at the interface of the substrate; in the second stage, the following particles adhere to the previous particles, forming the structure of the coating by the layers generated. The voids are reduced as the particles are sprayed, and the coating structure is densified and work hardened.

Assadi et al. (Ref 86) studied **the bonding mechanism** in CGS with some metallic powders (crystalline materials). They attributed it to the adiabatic shear instability, which occurs when particles impact the substrate or deposited material interface at high velocity. The deposition of particles is accomplished when the impact velocity of the particles on the substrate exceeds the **critical velocity**, which is a value related to feedstock material characteristics (Ref 87). In Figure 1.13, a schematic correlation between particle velocity and deposition efficiency for a specific temperature is represented.

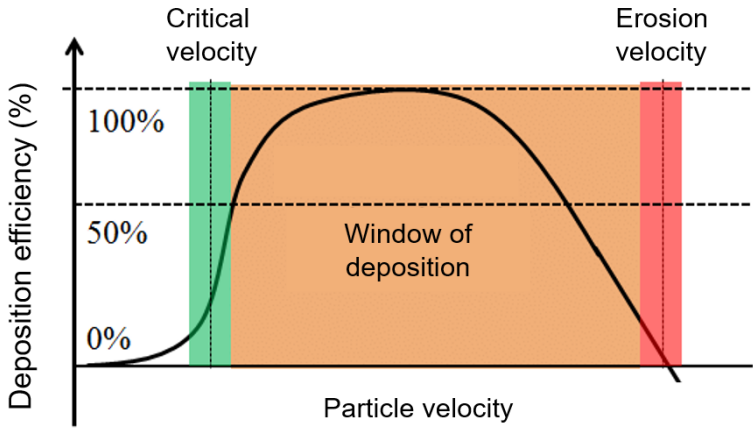

Figure 1.13 Correlation among particle velocity and deposition efficiency for a constant temperature. Figure adapted from (Ref 79)

Schmidt et al. (Ref 78) proposed the following equation for defining the critical velocity:

$$v_{critical} = \sqrt{A\sigma/\rho + BC_p(T_m - T)} \quad (2)$$

Where A and B are fitting constants, σ is the temperature-dependent flow stress, ρ is the density, C_p is the heat capacity of the sprayed powder, T_m is the melting temperature of the particles, and T is the mean temperature of particles upon impact.

If the particle velocity is lower than the critical velocity, the particles rebound and do not adhere. From the critical velocity to the erosion velocity exists a range of velocities (window of deposition) where the deposition of the particles can be accomplished and build up the coating. When the accelerated particles impact the substrate above the erosion velocity, particle rebound occurs, which can cause erosion.

The pressure and temperature of the gas are determining parameters to achieve the deposition of the particles. The velocity of the particles can be increased by using higher pressure values. It is possible to diminish the critical velocity that determines material deposition by increasing the gas temperature. The particles become more ductile and can be deformed more easily during impact by providing more temperature. The coating formation mechanism depends considerably on the pair of materials involved (powder/substrate). During spraying, the kinetic energy of the particles is transformed into strain energy and heat, causing the plastic deformation of particles and substrate or mostly one of them. When the substrate is much softer than the particles, the deformation can occur mainly on the substrate remaining the particles embedded; on the contrary, if the substrate is much harder than the particles, these tend to flatten (Ref 80).

Compared to conventional thermal spray techniques, cold spraying is a simpler process that makes it suitable for modelling. Furthermore, with a throughout understanding of the process, improvements can be made in obtaining quality coatings and in better design of commercial equipment (Ref 78).

The deformation mechanisms of particles impacting a metallic surface deposited by CGS are well-studied for crystalline materials. However, other kinds of materials need the consideration of other properties that can influence the deformation mechanism. Henao et al. (Ref 88) presented a model that described the **deformation mechanism of metallic glass** materials (MG) by CGs. In this, it was demonstrated that the window of deposition of MGs is dependent on their Reynolds number (Re), which is defined by the ratio between the inertial and viscous forces of MGs particles at impact. Deposition and bonding of MGs particles occur only at high Re values when the particles are in a viscous flow, achieved at the proper temperature and inertial forces. Higher Re values, achieved by increasing the kinetic and thermal energy of the particles, lead to greater deformation of the MG particles, enhanced deposition, and higher bonding strength. This deformation mechanism contrasts with that of crystalline materials, for which viscosity is not as affected by temperature.

1.5.5. Bioactive glass coatings obtained by thermal spray: Current status and future challenges (Review Paper)

The first publication of this thesis is a Review Paper, which describes the most relevant findings on the topic of bioactive glasses coatings obtained by thermal spray to clarify the current status of this strategy for improving biomedical implants.

This review comprehensively covers reports in the literature that have investigated the deposition of bioactive glasses using different thermal spray techniques.

The main problem of bioactive glass coatings obtained to date is detailed (insufficient coating adhesion), so they cannot commercially replace hydroxyapatite coatings. The different strategies studied to improve this aspect are presented and the main factors that affect the quality of these coatings. Finally, the different lines in which research can be continued to develop improved coatings are summarized.

BOLETÍN DE LA SOCIEDAD ESPAÑOLA DE CERÁMICA Y VIDRIO XXX (2021) XXX–XXX

BOLETIN DE LA SOCIEDAD ESPAÑOLA DE
Cerámica y Vidrio
www.elsevier.es/bsecv

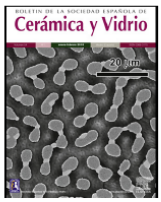

Original

Bioactive glass coatings obtained by thermal spray: Current status and future challenges

*Beatriz Garrido, Sergi Dosta, Irene Garcia Cano**

Thermal Spray Centre (CPT), Facultat de Química, Universitat de Barcelona (UB), Martí i Franqués 1, 7a Planta, 08028, Barcelona, Spain

Boletín de la Sociedad Española de Cerámica y Vidrio (April 2021), In Press

https://doi.org/10.1016/j.bsecv.2021.04.001

Abstract

Several inorganic materials such as bioactive glasses, glass–ceramics and calcium phosphates have been shown to be bioactive and resorbable which make them suitable for coating bone implants. This study focuses only on bioactive glasses. These biomaterials are highly biocompatible and can form a strong chemical bond with the tissues. This review comprehensively covers bibliographic reports that have investigated bioactive glass deposition using different thermal spray techniques.

The main drawback for the glass coating deposition is the low adherence with the substrate. Some strategies can favour a good bond such as using bond coats, blends, pre-heating the substrate or modifying the glass composition.

The characteristics of the feedstock powders are determinant for the properties of the coatings obtained. Porosity and thickness of the coatings can be modulated by using different thermal spray techniques and varying parameters of the process.

The degradation rate of some bioactive glasses can achieve kinetics similar to the new bone formation. Taking advantage of its dissolution capacity, glasses can be doped with functional elements.

While several biological studies have been performed with bioactive glass materials, there has been relatively little research on the biological response of coated glasses by thermal spray techniques. Research studies have demonstrated the opportunities of this promising material to enhance the bioactivity of the implants.

Keywords: Bioactive glass; Thermal spray; Coatings; Implants; Bioactive coating

1. Introduction

In recent decades there is an increase of life expectancy which is associated to age-related diseases. Traumatic injuries and pathological diseases such as osteoporosis or osteoarthritis affect bone function causing pain to the patient and also damage and fractures to the bones.

Bone represents the second most common tissue implanted in the body after blood (Ref 1). It has an excellent healing response when damaged, recovering both functional and structural properties. Notwithstanding severe damage to the bone implies the need of surgery to recover.

Most biomaterials and medical devices perform satisfactorily, improving the quality of life for the recipient. However, all manufactured devices have a failure rate affecting several patients annually (Ref 2,3). The demand for primary and revision surgery related to bone diseases are increasing last decades and represent a high cost to the health system (Ref 4–6).

So bone repair remains an important challenge in the field of orthopaedic and craniofacial surgery.

When designing an implant is important to consider special requirements: geometry, mechanical properties, the tissue-implant interaction, the anatomical site of the implant, etc. Besides human tissue is very sensitive to foreign substances, and the body can promote a rejection response.

Biomaterials that provide the structural support are required for replace skeletal hard connective tissues. In 1890 the surgeon Themistocles Gluck implanted the first total joint replacement, a hinged ivory prosthesis for knee (Ref 7). W. A. Lane introduced a metal plate for bone fracture fixation for the first time in 1895, however it was of current steel and corrosion occurred. It was not until 1926 that a stainless steel was discovered and used in the internal fixation of fractures which remain uncorroded for years (Ref 8,9). In recent times, titanium alloy, cobalt-chromium alloy, stainless steel, zirconia and aluminium oxides are the main biomaterials used for orthopaedic implants (Ref 3,10,11).

Implant failure analysis studies of the devices have been performed in order to modify the designs. These have evolved much over the last century, getting reasonable long-term viability for the current devices in the market. Surgeons and researchers still work hand by hand to improve them.

The most common failure mechanism is due to loosening. A poor osteointegration is responsible of the undesired mobility that causes loosening. To obtain a good fixation is required biological and mechanical stability by the formation of a structural and functional interface between the device and the surrounding bone. Also the presence of pathogens can cause biological reactions after the implantation of the device (Ref 12).

Aseptic loosening occurs at long term and is due to the mechanical failure of the device, this mechanism represents the 75% of the failures. While septic loosening is due to pathogens such viruses and bacteria, this mechanism represents the 7% of the failures and occurs at early stage (Ref 13). Other common causes of failure are the release of wear and corrosion particles into the body and fracturing of the device due to fatigue or creep (for polymeric components at early stage). The survivability of the implant also depends on the patient, for example wearing is more frequent in younger and more active patients.

To diminish these problems that can lead to failure surface devices can be modified.

The goal of the present article is to provide a literature review of the most relevant findings on the topic of bioactive glasses coatings obtained by thermal spray in order to clarify the current status of this strategy for improve biomedical implants. In this review, the effect of features related to the spray processes will be commented, such as the range of the particles sprayed and the raw material as powder or as suspension. Different approaches for achieve a good bond between substrate and coating will be introduced. The main features of the coatings will be discussed, with particular focus on coating thickness, porosity and bioactivity in simulated body fluid. Moreover, post treatments to modify the coating properties will be remarked. Finally, studies related to the biological behaviour of the coatings in vitro and in vivo will be presented.

2. Functionalization via surface modifications

Surface modifications are used for improving biological response of the implants. With this strategy, the structural support provided by the substrate is maintained. Among the different possibilities the methods can be broadly divided into three categories: (1) chemically or physically altering the atoms, compounds or molecules in the existing surface (chemical modification, etching, mechanical roughening), (2) overcoating the existing surface depositing materials with a different composition (coating, grafting, thin film deposition) and (3) creating surface textures or patterns. (Figure 1)

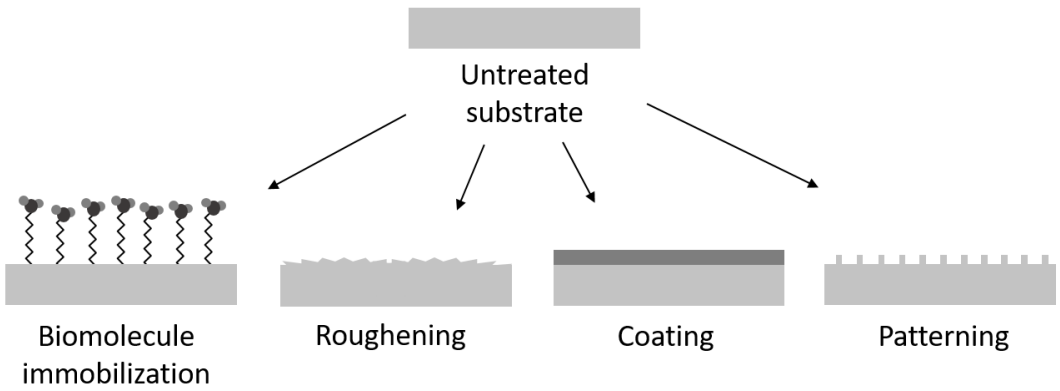

Figure 1. Some of the surface modification techniques commonly used

The similarity in composition, structure and morphology of the calcium orthophosphates to bone tissue make them good candidates for improve implants. Particularly, hydroxyapatite (HA) has been used for coating biomaterials due to the similarity with the inorganic mineral phase of the bone.

First studies of sprayed HA coatings started in the 1980s. In Netherlands, Geesink and co-workers reported some research studies with promising results (Ref 14–16), while Furlong and Osborn in the United States started also that research at the same period (Ref 17,18). The first clinical trials with HA coated implants started in Europe in 1987 and some months later, in 1988, in the United States with a coated femoral component (Omnifit-HA, Osteonics Corporation, Allendale) (Ref 19–25).

HA coatings enhance the bone formation on orthopaedic implants (Ref 26–28). First generation of HA coatings were thick and some adverse events were reported (Ref 29–31), current coatings are thinner and more uniform.

Hydroxyapatite coatings can be prepared by different techniques such as thermal spray, sol-gel, dip coating, electrophoretic deposition, dip coating, pulsed laser deposition, etc. (Ref 32) Nowadays only plasma spray is commercially accepted by the Food and Drug Administration (FDA) for producing HA coatings. The coatings should accomplish specific requirements, such as the tensile adhesion strength that shall have a value not less than 15 MPa, the Ca/P atomic ratio between 1.67 and 1.76, a crystallinity ratio major or equal to 45% or the content of harmful metals below 50 mg/kg, with a lower value for some specific elements (arsenic, cadmium, mercury, lead) (Ref 33).

HA offers a good bonding to the bone, however other bioactive materials can provide osteoinductive properties and a strongly osteointegration with the implant surface.

In the late 1960s bioactive glasses were developed by L. Hench, a particular range of glass compositions that react in physiological environment (Ref 34). These glasses bond to the bone by the formation of a hydroxyl carbonate apatite (HCA) layer and also promote bone cell growth along its surface. Moreover, the dissolution products of bioactive glasses can stimulate cellular differentiation (Ref 35).

In the last decades researchers have studied several compositions inspired in the first one developed, the 45S5, a highly reactive glass in the SiO_2-Na_2O-CaO-P_2O_5 system. Some of the most common constituents used for developing formulations are Al_2O_3, B_2O_3, MgO, K_2O or CaF_2, which have been added with particular purposes in any case (Ref 36–41). The bioactivity of a glass largely depends on its composition and surface reactivity, modifications should be analysed carefully since small variations can affect notably its properties.

The connectivity of the silicate network affects directly the dissolution rate of the glass. More disrupted networks make glasses more susceptible to degradation and then more bioactive. If the connectivity network is too high glasses are not bioactive, as the reactivity is promoted by the non-bridging oxygens of the open silicate network. Then connectivity can be diminished adding network modifiers such as sodium and calcium.

Bioactive glasses have gained a place in the market, mainly as bone grafts for orthopaedic and dental uses to regenerate and heal bone defects from trauma or tumour removal (Ref 42–45). But they also can be found as an attractive active component in toothpaste for reducing sensitivity in teeth (Ref 46–48).

Currently, there are many researchers investigating their use as scaffolds because of their osseous regenerative capacity, but further studies are still required before the translation to clinical trials (Ref 49).

Both bioactive glasses and HA are fragile materials, therefore their use as a bulk is not suitable. One more interesting application for bioactive glasses is the coating deposition in a similar approach to HA coatings, in this way can be used for load bearing applications.

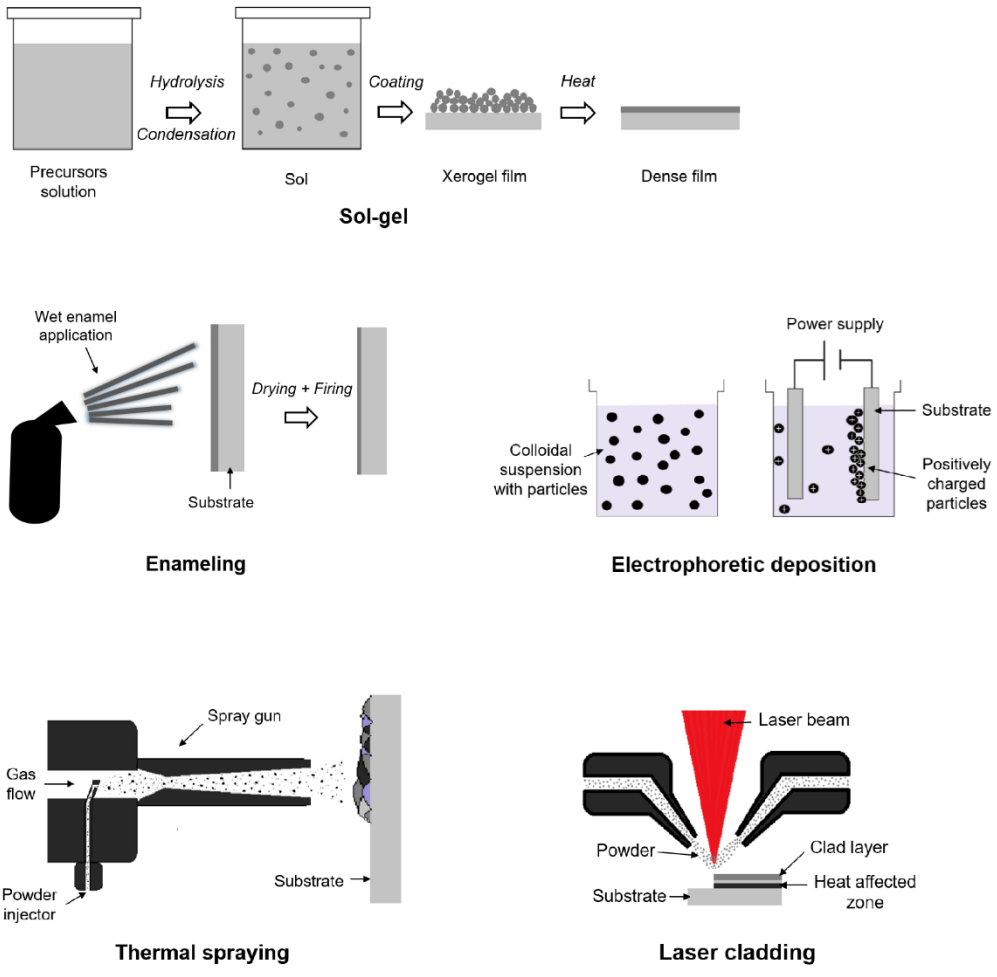

Figure 2. Principal techniques to develop bioactive glass coatings

Different strategies can be used for obtain the bioactive glass coatings, like sol-gel, laser cladding, enamelling, electrophoretic deposition and thermal spraying (Figure 2). The main disadvantage of all these methods is the poor adhesion strength of the coating to the metallic substrate, in part because of the mismatch of the thermal expansion coefficients. Being one of the main challenges, achieving coatings that comply with the regulations to be inserted into the body. In addition, each of these techniques is capable of producing coatings in a different thickness range (Figure 3). In particular, thermal spraying provides a wide and interesting range for this application.

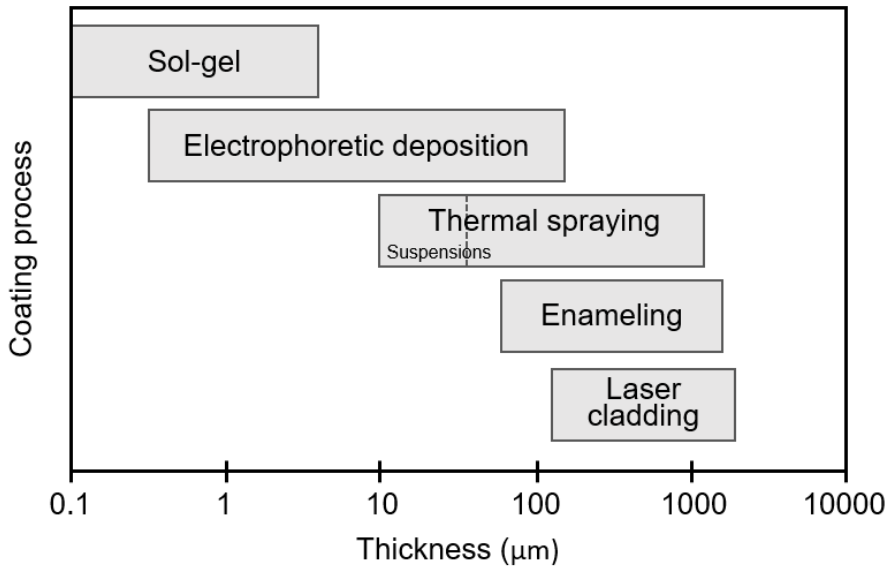

Figure 3. Typical thickness of coatings obtained by different methods.

3. Functionalization by thermal spray

Thermal spraying are coating processes where particles are melted (or partially melted) and deposited onto the substrate in the form of flattened drops that pile on each other to produce a layered coating (Ref 50–53).

The conventional techniques atmospheric plasma spraying (APS) and flame spraying (FS) have been used for produce coatings with bioactive glass materials (Ref 54–57). (Figure 4)

In the APS process a high temperature ionised plasma gas acts as heat source. The raw material, usually in powder form, is carried in an inert gas into the plasma jet where is heated and accelerated towards the substrate. The high temperature achieved during the process allow spraying materials with high melting points. Moreover, the high cooling rate of the particles can preserve the amorphous nature of the feedstock. The features of the APS process make it suitable for manufacture coatings with bioactive glasses.

FS is a process in which the heat from the combustion of a fuel gas (acetylene or propane) with oxygen is used to melt the feedstock material, the material is heated and propelled onto

a substrate. The flame temperature and velocity is lower than for APS. Few research of bioactive glass coatings involving this process can be found in the literature (Ref 56,57).

Suspension spraying is a particular group of thermal spray processes that differs from conventional ones by the use of liquid suspensions instead of dry powders as feedstock material while using the spray torches of the conventional techniques (Ref 58).

Suspension Plasma Spraying (SPS) was developed before the High Velocity Suspension Flame Spraying (HVSFS), for this reason there is more research done with SPS process (Ref 59). While HVSFS has been investigated by only a few research groups. By contrast more research with bioactive glass materials has been performed by HVSFS as can be appreciated in this review. In a comparative study of the development of bioactive glass coatings by both techniques, which will be discussed later, SPS was found to produce less suitable coatings for orthopaedic applications than with HVSFS (Ref 60). In addition, nanostructured coatings can be produced with Solution Precursor Plasma Spraying (SPPS), which could achieve better biological properties due to higher reactivity. In that case, precursor solutions are used instead of traditional feedstock (powders and suspensions) (Ref 61).

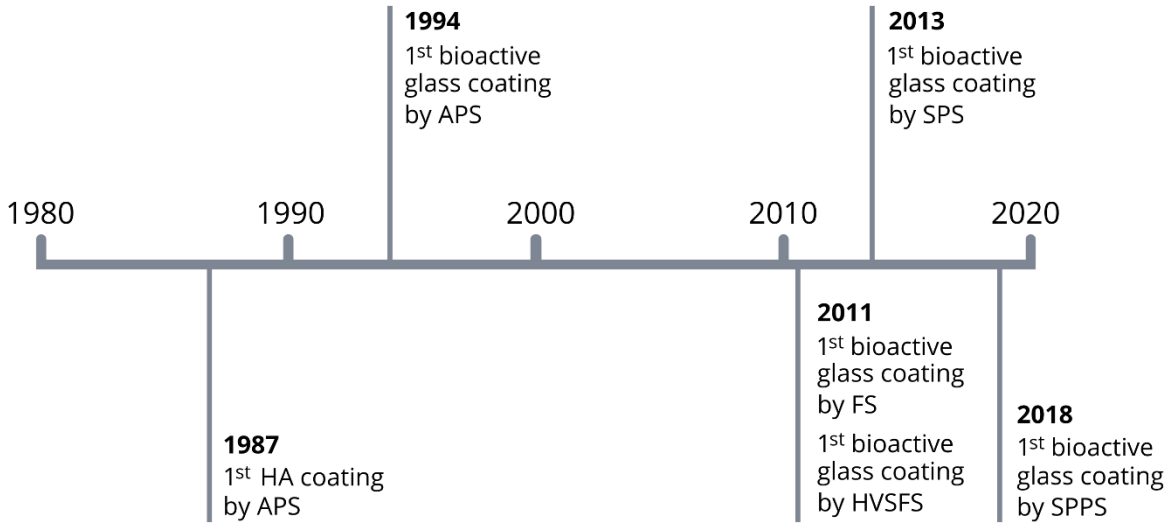

Figure 4. Timeline of the development of bioactive glass coatings by thermal spray

3.1. Influence of raw material

The main particularity of working with suspensions is that allow spraying very fine particles which tend to clog in the conventional powder feeders due to their low flowability.

In 2015 Bolelli et al. (Ref 60) published an interesting study comparing bioactive glass coatings sprayed by both suspension spraying above-mentioned techniques. The glass composition sprayed onto a TiO_2 bond coat applied by APS was in the system SiO_2-Na_2O-CaO-K_2O-P_2O_5. The SPS process produced highly porous and rough coatings where the

particles are incompletely flattened and partly attached among them. These coatings had a thickness ≤50 μm and were highly reactive in SBF due to its high specific surface area and porosity.

However, the HVSFS process produced denser bioactive glass coatings, containing few rounded pores and transverse microcracks. The thickness of the coatings achieved were between 20 and 50 μm. The HVSFS coatings reacted slower in SBF due to a much lower specific surface area than SPS ones. The microstructure and properties of the coatings developed by HVSFS in this study were more suitable for use in metallic implants.

Narrow particle size distribution favour the coating homogeneity. Furthermore, due to the low thermal conductivity of the glasses for the smaller particles is easier to reach the complete melting during the process. Then spraying fine particles results in more regular coatings.

In 2016 Cañas et al. (Ref 62) presented a work related to the effect of the particle size of the powder feedstock on the final coatings, for this purpose 45S5 glass was plasma sprayed onto stainless steel AISI 304L. For the fractions higher than 200 μm no coating was obtained because the melting of the particles was not achieved. For the intermediate fractions 200–63 μm coatings were obtained but not all the particles were fully melted. As a consequence of the insufficient melting, the coarser the particle size the more irregular the coating. Finally the finest fraction <63 μm needed a fluidiser (hydrophobic fumed silica) to be sprayed, more regular coatings were obtained with this fraction.

3.2. Adhesion strength

The main problem of thermal spraying bioactive glass materials is the poor adhesion to metal substrates. The effect of a large coefficient of thermal expansion (CTE) mismatch of the dissimilar materials create stress concentration in the glass near the metal. Furthermore, the rapid cooling of the particles characteristic of the thermal spray processes causes severe temperature gradients, which results into residual stresses across the coating-substrate interface.

A suitable coating must meet tensile strength values to be used in metallic implants. Depending on the coating material, this minimum required value may vary between 15-22 MPa according to the applicable regulations (ASTM F1147-05, ASTM F1185–03).

Many authors sandblast substrates before spraying for rise its roughness, which improves the mechanical adhesion; but this is not enough and other actions should be carried out. Several strategies have been studied in order to increase the abovementioned bonding strength of the coating with the substrate.

The first solution presented is the use of a bond coat, as was reported by Goller in 2004 (Ref 63). 45S5 bioactive glass was plasma sprayed onto titanium with and without Amdry 6250

(60% Al_2O_3 40% TiO_2) bond coat. The results show a uniform coating layer with 20 µm of bond coat and 80µm of top coat with a tensile strength of 27.18 MPa. While the coating without bond coat has a thickness of 110 µm and a tensile strength of 8.56 MPa. ASTM C633 was followed to obtain the strength values. In this study the application of the bond coat increase the bonding strength about three times, and the adhesive bonding observed at the bioactive glass metal interface turned into cohesive bonding.

A preceding study use a titanium bond coat to enhance adhesion reported by Lee et al. in 1996 (Ref 64). A bioactive glass in the system SiO_2-Na_2O-CaO-P_2O_5 was plasma sprayed onto Ti_6Al_4V substrates with a titanium bond coat. The thickness of the titanium bond coat and bioactive glass top coat are 130 µm and 50 µm respectively. The titanium bond coat was used to ensure adherence between the substrate and the bioactive glass coating.

Another study using a bond coat for improve adhesion strength was published by Bellucci et al. in 2012 (Ref 65). Bioactive glass composition based on the K_2O-CaO-P_2O_5-SiO_2 system, named “Bio-K”, was deposited by HVSFS onto titanium. The effect of deposit a TiO_2 bond coat by APS was investigated. In this study 5 different bioactive glass compositions in the system mentioned previously were used, the TiO_2 bond coat improve the adhesion for three of this compositions. Particularly in the Bio-K 5 reaches the higher tensile strength value of 17M Pa with bond coat, while presents 8 MPa without bond coat. The bond strength was measured following the ISO 4624 method. Besides the microstructure of the coatings and their bioactivity are not affected by the presence of the bond coat.

Blends are also used in order to improve the bonding strength as presented by Chern et al. in 1994 (Ref 54). A bioactive glass in the system SiO_2-Na_2O-CaO-P_2O_5 mixed with HA was deposited by APS onto Ti_6Al_4V. The aim of this study was enhance the bioactivity and the bonding strength of the common HA coating. The adhesion strength was measured following the ASTM C633 method, the values for HA, bioactive glass/HA (1:1 in powder weight) and bioactive glass coatings were 33.0 MPa, 39.1 MPa and 52.0 MPa respectively.

Ding et al. in 2000 published another study working with bioactive glass and HA blends (Ref 66). A series of HA mixed with a bioactive glass in the system SiO_2-Na_2O-CaO-P_2O_5 (10:3:5:2 in weight) was plasma sprayed on Ti_6Al_4V substrates. Blends with 2.5, 5, 10 and 25% wt. of bioactive glass were prepared by both sinter-granulation and direct mixing methods. The majority of coatings had a thickness in the range of 90-140 µm and the tensile strength values vary in the range 50-60 MPa. Getting the coating with higher amount of bioactive glass 55MPa of bond strength. The values were measured following the ASTM C633. High bond strengths were obtained from all coatings. The different methods used for mixing the powders does not show significant differences in bond strength of the coatings.

Another study working with bioactive glass blends was reported by Nelson et al. in 2014 (Ref 57). Blends of bioactive glass 45S5 with pure titanium or with Ti_6Al_4V were flame sprayed onto titanium. These blends are done with the 15% wt. of bioactive glass in both cases. Besides the blends are prepared with different particle size distribution for glass and metallic powders. ASTM C633 was followed for measure tensile strength. Blends with Ti_6Al_4V show an increase of strength as the size particles of bioactive glass is higher, while the blends with pure titanium present less variation of tensile strength with increasing the powder size of bioactive glass. The higher value of tension obtained for the blend with pure titanium is 13 MPa, and for Ti_6Al_4V 20 MPa. Concluding that the use of the mix of Ti_6Al_4V and 45S5 is a better choice.

In 2013 Cattini et al. designed various bioactive glass/hydroxyapatite (HA) functional coatings by SPS (Ref 67). The different designs included: composite coating with randomly distributed constituent phases, duplex coating with glass top layer onto HA layer and graded coating with a gradual changing, starting from pure HA at the interface with the substrate up to pure glass on the surface. The functionalized coatings were mechanical characterized using the scratch test. The critical load for the composite coating is 27.1 N, the lower 21.2 N for the duplex design, caused likely for the abrupt interface between the glass and the HA. While the graded design resist the maximum load of the test without reaching the substrate, concluding that the stresses could be progressively reduced with this design. With the graded coating, that provides better mechanical results, the authors continued the research to improve the functional coating (Ref 68).

An alternative presented by Altomare et al. in 2011 is pre heating the substrate to improve the adhesion (Ref 69). 45S5 bioactive glass was deposited by HVSFS on titanium substrates. This study was performed to understand the deposition mechanisms during the process. In fact, pre heating to 100ºC the substrate was crucial to deposit a homogeneous coating. If the substrate was not preheated or was allowed to cool before spraying the deposition was highly impaired. The most important role of pre heating is the mitigation of the rapid cooling of glass droplets in the first layer which hinders their adhesion.

Bolelli and co-workers reported in 2012 two studies (Ref 65,70) were bioactive glasses were deposited by HVSFS using a pre-heating step to enhance adhesion, in that occasion arriving to higher temperatures. The pre-heating of the substrate generally improves splat–substrate wetting and results in better adhesion. In these studies Bio-K was sprayed onto titanium substrates after pre-heating with two torch cycles with no suspension injection, coating deposition started when the substrate temperature was about 230-260ºC.

3.3. Influence of the thickness

According to the ASTM F1854-15 there is no specification for the thickness of thermal sprayed medical implant coatings. However is a critical feature for achieving long term stability and avoid the implant mobility. The coating thickness is a compromise between mechanical properties and its dissolution, thus is a parameter to analyse carefully when manufacturing a coating. Excessive thickness can favour delamination and fragmentation of the coating, by contrast very thin coatings can be degraded before achieving a good bonding with bone tissue. Most of the commercial HA coatings for orthopaedic implants have a thickness between 50–75 μm (Ref 71). So for bioactive glass coatings the value should be on near values.

The thickness can be modulated by controlling parameters of the process such as stand-off distance, number of passages or the melting of the particles. But also characteristics of the powder as powder size, glass composition or density. As can be seen in Table 1 the thickness for coatings produced with dry powder as feedstock material, by APS, vary from 40 to 150 μm while the coatings obtained by suspension spraying are in the range of 10 to 83 μm. This difference is due to the fine particle size used with the suspension spraying techniques.

3.4. Influence of porosity

Has long been known that material properties, such as chemical surface, porosity and surface finishing have a great influence in the biological response of the cells with the coating. High porosity is able to mimic biological structures, it plays an important role in tissue ingrowth through the pore size (Ref 72) and, more critical, the interconnected porosity (Ref 73). Some authors have reported that a minimum pore size about 100-150 μm was needed for the continued health of bony ingrowth (Ref 73,74), but smaller porosity can contribute also to cellular attachment (Ref 75). In vivo results on porous titanium implants showed that increase of porosity and pore size positively influence their osteoconductive properties (Ref 76). But porosity not only supports tissue adhesion, growth and vascularization, it also reduces the elastic modulus mismatch of the coating and substrate reducing the stress shielding associated. Therefore it is a very interesting parameter to take into account in the manufacture of these coatings.

In the aforementioned study by Chern et al. in 1994 a detailed description of the coating porosity is indicated (Ref 54). Blends of HA with bioactive glass in the system SiO_2-Na_2O-CaO-P_2O_5 were deposited by APS onto Ti_6Al_4V. The presence of bioactive glass increases the surface roughness of the coatings. When adding bioactive glass on HA coatings large open pores are formed because the glass particles went through a low viscosity stage, not being totally melted and flattened when impacting with the substrate and other particles. Chern et al. suggested that the porosity achieved could provide bone ingrowth.

Table 1. Summary of most relevant results of bioactive glass coatings without blends obtained by means of thermal spray

Raw material	Glass composition	Spraying process	Coatings phases	Thickness	Ref.
Powder	SiO_2-Na_2O-CaO-P_2O_5 system	APS	Amorphous	70µm	(Ref 54)
	Biovetro (SiO_2-Na_2O-K_2O-CaO-MgO-P_2O_5-Al_2O_3 system)	APS	Amorphous	80µm	(Ref 78)
	45S5	APS	Amorphous	130µm (titanium bond coat) 50µm (top coat)	(Ref 64)
	Biovetro	APS	Not reported	80µm	(Ref 35)
	SiO_2-Al_2O_3-CaO-Na_2O system	APS	Amorphous	80µm	(Ref 40)
	45S5	APS	Not reported	20µm (Al_2O_3-TiO_2 bond coat) 80µm (top coat) 110µm (without bond coat)	(Ref 63)
	45S5 and Bio-K (K_2O-CaO-P_2O_5-SiO_2 system)	APS	$Na_4Ca_4(Si_6O_{18})$ and $CaSi_2O_5$ phase (45S5) Amorphous (Bio-K)	150µm	(Ref 81)
	SrBioactiveGlass (K_2O-CaO-ZnO-MgO-Na_2O- P_2O_5-SiO_2 system)	APS	Amorphous	50-100µm	(Ref 37)
	45S5	APS	Some amorphous coatings and some with Ca_2-SiO_4 phase	40-100µm	(Ref 77)
	45S5	APS	Some amorphous coatings and some with $Na_6Ca_3Si_6O_{18}$	150µm	(Ref 55)
Suspension	45S5	HVSFS	Amorphous	41-83µm	(Ref 69)
	Bio-K	HVSFS	ZrO_2 (contamination) and other crystalline peaks with much lower intensity barely distinguishable	10-15µm	(Ref 65)
	45S5	HVSFS	Amorphous	10-25µm	(Ref 80)
	SiO_2-Na_2O-K_2O-CaO-P_2O_5 system	HVSFS and SPS	Mainly amorphous, some coatings present $Ca_3(Si_3O_9)$ phase	20-50µm	(Ref 60)
	SiO_2-Na_2O-CaO-P_2O_5 system	SPS	Ca_2SiO_4 phase	20µm (top coat)	(Ref 105)
	45S5	SPPS	Amorphous	35µm	(Ref 106)

A remarkable study about porosity was presented by Rojas et al. in 2020 where parameters of the APS process affecting the coating porosity are analysed (Ref 77). 45S5 bioactive glass is plasma sprayed onto stainless steel AISI 304L. The cross sectional structure of the coating reveals a significant amount of inter and intralamellar circular porosities produced by volatilization of chemical components, in this case P_2O_5 and Na_2O, from the feedstock powder. This phenomenon occurs at high temperatures as reported by Gabbi et al. (Ref 78) and Pawlowski (Ref 53). The wide particle size distribution of the feedstock causes a non-homogeneous heating of the in-flight particles during the manufacture of this coating. As a result a weak interlamellar interaction and a low spreading generate irregular porosity.

In the same study, the stand-off distance was analysed and could be observed that circular porosity increases with decreasing spray distance. Furthermore, it was observed that the porosity of coatings decreases when using air jets forward the samples to cool the coating during the process. This can be explained because the particles are cooled before their impact resulting in less volatilization. Finally, the amount of porosity can also be controlled by the plasma enthalpy being lower at high enthalpy. Control of the porosity can be achieved by adjusting the plasma enthalpy, the spraying distance and the air jet used to cool the substrate, in this study the variation of porosity was between 4 and 16%.

López et al. in 2014 reported a study of bioactive coatings obtained from feedstocks prepared by different routes (Ref 79). 45S5 was plasma sprayed onto stainless steel AISI 304L. The 45S5 frit was milled using two different routes: dry milling followed by sieving and wet milling followed by spray drying to obtain a powder comprising porous agglomerates. The coatings produced with spray dried powder reveal a quite heterogeneous microstructure with high porosity and a marked variation of pore sizes. The coated samples prepared with dry route feedstock present less porosity than the previous ones, however large and round pores are also observed in this coating. Furthermore, in both cases the particles with a size range higher than 63µm are few deformed due to the low thermal conductivity of the glass resulting in high roughness and heterogeneity. The characteristics of the feedstock strongly impact on the final coating microstructure. The spray-dried agglomerates present a high porosity. During the spraying process the low conductivity of the glass particles prevent the core from melting and maintain its high porosity. Thus particles arrive to the substrate with low melting degree and deformation, giving as a result a high porous coating.

Nelson et al. studied the deposition of a bioactive glass-titanium alloy composite in 2011 (Ref 56). Flame spray was used to manufacture porous composite coatings of 45S5 and Ti_6Al_4V with the aim of improve the bioactivity of the coatings. The amount of bioactive glass to the blend represent the 15% wt. and 38% wt., but in the latter the glass distribution through the coating was not homogeneous. So the blend with lower content of glass was selected. The

porosity of the coatings was increased with the presence of bioactive glass achieving 33% while the coatings without glass reach 26% of porosity.

In 2014 Nelson et al. published another work with titanium and bioactive glass composites (Ref 57). Blends of 15%wt. 45S5 glass with pure titanium or with Ti_6Al_4V were flame sprayed onto titanium. Porosity was characterized following the ASTM E2109. Blends with pure titanium get higher porosity (8-29%) than the ones with Ti_6Al_4V (5-18%). In pure titanium and bioactive glass composites, pores are localized around the glass particles suggesting that some interactions could occur between the materials. Some possible interactions could be poor stacking, viscous flow of molten glass, localized regions evolving gas or splashing of molten particles. In addition higher porosity was achieved when increasing the glass powder size. The larger particles result in lower particle temperatures and hence insufficient deformation of the particles when impact with the substrate or other particles.

Bolelli et al. in 2012 presented the comparison of a bioactive glass Bio-K and a tricalcium phosphate (TCP) bioactive ceramic deposited by HVSFS onto pre-heated titanium substrates (Ref 70). Cross-sections confirm more porous microstructure in Bio-K than TCP coatings. Bio-K particles are less flattened and often containing spherical central cavities which can be responsible for most of the fine porosity appreciated.

In 2019 Bano et al. presented a work where analyse the microstructure of glass coatings obtained by HVSFS (Ref 80). 45S5 glass was deposited onto stainless steel AISI 304L at three different flame powers (low, medium and high). Well adhered coatings with a thickness of 25µm were obtained at medium and high flame powers. Coating with higher porosity, 16%, correspond to the medium flame power. The coating produced with high flame power was 10% porous and present a higher roughness surface. With high flame there is more heat transfer to the particles and these are more melted resulting in a denser microstructure.

3.5. Influence of post-treatments

A post deposition heat treatment can be used to modify the microstructure of the coatings as reported by Cannillo et al. in 2010 (Ref 81). Two different bioactive glass powders Bio-K and 45S5 were plasma sprayed onto titanium substrates.

Bio-K was derived from the 45S5, just replacing all the sodium oxide with potassium oxide to reduce its tendency to crystallize at high temperature. In this study the sprayed coatings were treated at 700ºC for 1h, above the glass transition temperature of both glasses. This treatment maintain the Bio-K coating amorphous, while in the 45S5 coating two crystalline phases were detected, sodium-calcium silicates and calcium silicates. These phases were also identified in the 45S5 as-sprayed coatings, which were generated through the spraying process. After the heat treatment the peaks of the 45S5 coating were more intense meaning an increase in its crystallinity. As a result, the thermal treatment may be helpful to reduce the defectiveness

of the glass coatings. Exceeding the glass transition temperature it can soften and adapt between particles and to the substrate. Consequently, the mechanical properties are enhanced.

Another post treatment but in this case with a multifunctional approach was reported in 2009 by Verné et al. (Ref 82). Bioactive glass coatings were doped with silver to provide them antibacterial properties. A glass in the system SiO_2-Al_2O_3-CaO-Na_2O was plasma sprayed onto titanium alloy and stainless steel substrates. Amorphous coatings with a thickness of 80μm were obtained.

Coated samples were treated by a patented ion-exchange treatment to introduce silver ions in the surface in two different solution concentrations 0.5M and 0.05M. Leaching tests revealed that in both conditions, silver is rapidly released during the first day of immersion in SBF, this feature is interesting due to the incidence of infections just after surgical procedures. The in vitro test in SBF confirmed the low bioactivity of the coatings before and after the silver-doping, with no variation due to the silver. The low degree of bioactivity was expected due to the glass reactivity.

Antibacterial tests showed a marked bacteriostatic behaviour of Ag-coated samples, proportional to the silver content. The doped coatings inhibited the proliferation of most of the adherent bacteria on the coatings surfaces but not kill them. According to the good results of the antibacterial tests only the samples with less silver concentration were tested for biocompatibility. Cell culture tests for 6 and 24h confirmed the safety of the coatings for fibroblast cells.

3.6. In vitro evaluation for apatite-forming ability

When bioactive glasses are in contact with simulated body fluids a HCA layer, that allows the chemical bond to bone, is developed on its surface. The formation of the HCA starts at the surface of the glass and moves inward.

The development of the HCA layer starts with the formation of a silicon-rich layer almost instantaneously, this is covered in few minutes with a layer of amorphous calcium phosphate, which subsequently crystallizes with an apatite-like structure. L. Hench described in detail the interactions and reactions that take place in the formation of the HCA layer (Ref 83–86).

The bioactivity of a glass coating can be affected by many factors such as crystallinity, composition, porosity or specific surface area. So it is important to evaluate the apatite-forming ability of new formulations and processed coatings, due to alterations produced during the development.

Despite the fact that bioactive glasses exhibit an amorphous structure the deposition process or post-treatments can generate crystalline phases. These can affect mechanical properties

and also bioactivity, which tends to decrease with the level of crystallization, however some crystalline phases are not affecting its bioactivity, as can be checked in Table 1, most of the coatings obtained by thermal spray preserve its amorphous structure.

The variations on glass composition to adjust some properties can also affect the glass reactivity, which is specially linked to the network connectivity. Furthermore, high porosity and high specific surface area can accelerate the HCA layer formation process.

It is important to keep in mind that not always having a high degradation rate is beneficial, since if the coating degrades very quickly and a good bond with the bone has not been formed, it can negatively affect the mechanical stability of the implant. Therefore, the degree of reactivity must be adjusted to the specific application.

For bioactivity assessment many types of simulated body fluids can be used, which consist of similar ion concentrations to physiological plasma. SBF solution defined by Kokubo (Ref 87) has become the main used in current experiments as can be seen in Table 2. In many studies the solution is refreshed after certain time points (2-3 days), especially when longer time points are tested. Some studies have evaluated among other factors the role of the solution chosen, the frequency of the renewal of the solution, suggesting that the results can be affected depending on the testing solutions and conditions selected (Ref 41,88).

The aim of the test is to determine the mineralisation process by observing the apatite nucleation upon a surface over a period time. Moreover is important consider performing a mechanical evaluation of the samples after the SBF immersion to detect alterations in coating properties.

3.7. Biological behaviour of the bioactive glass coatings

Biomaterials designed to be implanted inside the body should integrate with host tissue and not become encapsulated by a dense layer of fibrous connective tissue (Ref 89). The success of the implant integration involves the formation of a bone-like interface that integrates the implant surface with the surrounding bone.

Implant materials are designed to promote osteoconduction and osteoinduction, essential features for osseointegration (Ref 90). The first is related to the capacity of the surface to allow bone growth, the latter refers to the process by which cells are guided to become differentiated osteogenic cells.

The basic reactions of osteoblasts on material surfaces involves the following phenomena: protein adsorption at the material surface, followed by the cellular attachment which occurs rapidly, then adhered cells migrate, proliferate and differentiate (Ref 91).

Some surface properties of the implanted materials can affect biological responses on the cell-material interface, such as composition, ion release, topography or chemistry (Ref 92).

Table 2. Summary of most relevant results of apatite-forming ability of the bioactive glass coatings obtained by means of thermal spray.

Sprayed material	Spraying process	Solution conditions	Apatite formation	Ref.
45S5	APS	SBF solution. Soaking times: 1, 2, 4, 8, 16, and 32 days.	After 1 day, the concentration of Ca^{2+} was enough to precipitate HCA on the surfaces of the coatings. The thickness of the Ca-P rich layer was about 10µm after 16 days.	(Ref 64)
Blend: HA + SiO_2-Na_2O-CaO-P_2O_5 system (10:3:5:2 in weight)	APS	SBF solution, agitated daily. Immersion time: 30 days.	Apatite thickness between 20±30µm after 30 days.	(Ref 66)
45S5	HVSFS	SBF solution. Soaking times: 1, 3, 7, 14 and 28 days.	Only 1 day soaking is needed to develop a continuous hydroxyapatite layer onto the surface of the samples.	(Ref 69)
Blend: Ti_6Al_4V + 45S5 (15%wt.)	FS	SBF solution, changed every 3 days. Soaking times: 1, 7 and 14 days.	No apatite layer was formed on the Ti_6Al_4V alloy control after 14 days. The bioactive glass-alloy shows evidence of crystalline HA formation after 14 days. The primary XRD peaks were observed at low intensities after 7 days of exposure to SBF.	(Ref 56)
45S5	APS	SBF solution. Soaking times: 1, 2, 3, 5 and 7 days.	An apatite layer was developed after 7 days of SBF exposure, but some areas are formed by silica gel which has not evolved yet to apatite.	(Ref 79)
45S5	SPPS	SBF solution. Soaking times: 1 and 7 days.	The coating exhibits the formation of a HCA layer after 1 week immersed.	(Ref 106)
45S5	HVSFS	SBF solution. Soaking times: 1, 2, 3 and 7 days.	After 7 days, no apatite precipitation on 25 kW coatings. Apatite layer of 24µm on 50 kW coatings and apatite layer of 17µm on 75 kW coatings. More degradation occurs on the coating produced at 50kW likely for the higher porosity.	(Ref 80)

For this reason cell culture tests and in vivo models are essential for validate the obtained coatings, ensuring the capability of the material to interact properly.

Gabbi et al. (Ref 78) published in 1995 an in vivo and in vitro study performed to evaluate the biological results of Biovetro (Na_2O-K_2O-CaO-MgO-Al_2O_3-SiO_2-P_2O_5 system) coatings obtained by APS on Ti_6Al_4V plates. For in vitro assays cells were seeded at a density of $1x10^5$ cells cm^{-2} and incubated for different intervals. A decrease in cell proliferation is observed for the samples coated with Biovetro but not for control samples, which is associated to the ionic release of the glass. For in vivo testing a group of rabbits was selected, for each animal a sample coated with Biovetro was introduced in one tibia and an uncoated sample in the other. The reabsorption of the Biovetro layer is confirmed at 180 days, which is replaced by newly formed bone thus preventing fibrous tissue from filling the gap between the implant and the bone tissue. This study confirms the biodegradability and osteoconductivity of the Biovetro glass.

To perform cell culture studies with bioactive glasses a preconditioning step for the materials is required to avoid cytotoxicity caused by the rapid pH increase. Different strategies have been proposed to avoid this problem, consisting of immersing samples in physiological solutions (Ref 93).

The second cellular study with thermal sprayed bioactive glasses is reported in 1998 by Oliva et al. (Ref 35). For this study two bioactive glasses from the Biovetro family, in the Na_2O-K_2O-CaO-MgO-Al_2O_3-SiO_2-P_2O_5 system, were used. As control were chosen a third composition without P_2O_5 resulting in a non-bioactive glass and the titanium alloy substrate. The glasses were sprayed by APS onto Ti_6Al_4V specimens.

Primary cultures of human osteoblasts were used in this research. The samples were preconditioned before the cellular assay, to stabilize the pH and avoid the cytotoxicity. This procedure consist of soaking the samples for 24h in phosphate-buffered saline (PBS) and process was repeated other three times refreshing the PBS to reach the stabilization of the pH. To evaluate the biological response on the different materials cells were seeded with a density of $2x10^4$ cells cm^{-2}. A similar adhesion for the different samples was assessed after 24h of incubation, except for one of the bioactive glass coatings that recorded lower adhesion. After 4 days the MTT test revealed higher amount of osteoblasts on the control surfaces rather than the bioactive ones. However for long periods of incubation, 8, 16 and 24 days, the results changed and the bioactive coated samples presented a higher proliferation than the control samples. Scanning electron microscopy was carried out for samples at 24 days of incubation, and the micrographs revealed that on bioactive glass coated samples the cells were fully spread forming a very close layer of osteoblasts. In contrast the micrographs related

to bio-inert glass surfaces revealed not completely spread of the cells and these were less close among them.

In 2011 Altomare et al. reported an in vitro study on 45S5 coatings sprayed by HVSFS onto titanium substrates (Ref 69). A human osteosarcoma cell line was used for the tests. Coated and acid-etched titanium samples (commonly used in bone-contact dental applications) were seeded with a cell density of $1x10^4$ cells cm^{-2}. After 7 days of incubation cells were able to proliferate in a similar way on both studied surfaces, confirming the ability of the coated samples to support adhesion and proliferation of the human osteoblast-like cells. Moreover, the morphological observation by scanning electron microscopy confirm no adverse changes in cell morphology. The in vitro tests corroborate that 45S5 coatings maintain the biocompatibility characteristic of bulk glass. Consequently, the results suggest that bioactive glass coatings are an alternative to thermally-sprayed hydroxyapatite.

Related to the in vivo studies, two works more have been published. In 1998 Lopez-Sastre et al. reported a comparative study between HA and Biovetro coatings onto titanium implants (Ref 94). APS technique was used to coat the implants with a thickness of 80µm.

The cylinders were implanted in the distal femoral epiphysis of six sheep, on the right side the bioactive glass implants, on the opposite the HA coated. The results were assessed at 6 different times. The implants coated with Biovetro present larger pore size and four times more porosity than HA ones. These bioactive glass coatings were less integrated into the bone, as was observed on histological examination of the interface. The authors attribute these results to the amount of aluminium oxide in the composition. It was demonstrated an accumulation of aluminium at the interface by aluminon staining. Above 3% its capacity to bond the bone is lost. These results are according to the literature, where is reported than the presence of alumina in the composition can inhibit the bone bonding. Up to 1.5%-2% of alumina can be included in a glass formulation without significantly diminish the glass bioactive capacity (Ref 86,95,96).

More than a decade later, in 2014 Newman et al. reported another in vivo study with bioactive glass coatings (Ref 37). The glass, in the system SiO_2-Na_2O-K_2O-CaO-MgO-ZnO-P_2O_5-SrO, was applied to Ti_6Al_4V implants by APS.

Glass and HA coated implants were inserted into the distal femur and proximal tibia of twenty-seven New Zealand White rabbits for the periods of 6, 12, or 24 weeks. The bioactive glass composition used in this research was designed to achieve a CTE similar to HA. Also with an amorphous structure and an appropriate network connectivity for bond to bone. Furthermore, the use of strontium has been used as treatment for osteoporosis (Ref 97,98). Degradation test reveals the rapid release of the Sr^{2+}. At 6 weeks an increase of the early bone formation

around bioactive glass coated implants was observed comparing with HA and the fixation of implants by 24 weeks is superior with bioactive glass coated specimens.

4. Summary and future outlook

There are key factors to be accomplished to obtain a successful coating.

Firstly, the good adhesion at the interface between the glass and substrate, which is likely the main drawback for the glass coatings deposited by thermal spray techniques. Different approaches can improved that bonding, as using a bond-coat between glass and substrate, the use of blends (mainly with HA), pre-heating the substrate or modifying the glass composition in order to achieve a closer CTE of the glass and the metallic substrate.

Secondly, to achieve a homogeneous coating a narrow particle size distribution is recommended. The low thermal conductivity of the glasses can result in irregular microstructures due to non-homogeneous heating of the particles. Moreover, the characteristics of the feedstock strongly impact on the final coating microstructure.

Thirdly, by using different thermal spray techniques and varying the parameters of the process we can control porosity and thickness of the coatings. The plasma enthalpy and the spraying distance seem to have an important paper in modulating the porosity, while thinner coatings can be achieved using suspension spraying processes because of the possibility of work with finer particles.

Keep the apatite forming ability of the coatings is a key point for the final coatings. Specific attention must be paid when varying glass compositions or when introduce crystalline phases during the deposition or the post-deposition processes. However not all the crystalline phases affect negatively the degree of bioactivity, and by other side can enhance the mechanical properties (Ref 55). In fact, the bioactive glass-ceramics are partially crystallized glasses with a similar degree of bioactivity than bioactive glasses and improved mechanical properties, some of them have a clear presence in clinical use (Ref 85,99).

Another key factor is the assessment of the coating stability and its biological response. Few studies involving cell culture or in vivo tests have been performed with bioactive glass coatings obtained by thermal spraying and some of them are not concluding. Further research is necessary to corroborate the response of the materials for long-term applications.

Besides the improvement of bonding to the bone, other functionalities can be achieved for the coatings. Taking advantage of its ability to dissolve, it could be possible to add functional elements and get a release of this elements over time to provide an improvement. For example, enhance angiogenesis capacity (Ref 100,101), osteostimulation or antibacterial activity (Ref 102–104).

It is clear that bioactive glasses have a promising role in the future of medicine. In recent years most of the research with these materials is going towards scaffolds, however the future as coating is encouraging and should not be neglected. Further research need to be developed to determine the applicability of the coated implants.

Acknowledgements

This work was supported by Generalitat de Catalunya (SGR-1777) and Spanish Government (MAT2016-76928-C2-1-R).

References

1. R.Z. LeGeros, Biodegradation and Bioresorption of Calcium Phosphate Ceramics, *Clin. Mater.*, 1993, **14**(1), p 65–88.
2. B.D. Ratner, A.S. Hoffman, F.J. Schoen, and J.E. Lemons, “An Introduction to Materials in Medicine,” *Biomaterials Science*, second ed., Academic Press, 2004.
3. W. Jin and P.K. Chu, Orthopedic Implants, *Encyclopedia of Biomedical Engineering*, R. Narayan, Ed., Elsevier Inc., 2019, p 425–439, doi:10.1016/B978-0-12-801238-3.10999-7.
4. S.M. Kurtz, K.L. Ong, E. Lau, and K.J. Bozic, Impact of the Economic Downturn on Total Joint Replacement Demand in the United States: Updated Projections to 2021, *J. Bone Jt. Surg. - Am. Vol.*, 2014, **96**(8), p 624–630.
5. S. Kurtz, K. Ong, E. Lau, F. Mowat, and M. Halpern, Projections of Primary and Revision Hip and Knee Arthroplasty in the United States from 2005 to 2030, *J. Bone Jt. Surg. - Ser. A*, 2007, **89**(4), p 780–785.
6. J. Cherry, T.Q. Tan, G.J. Demmler-Harrison, L.B. Mithal, S.L. Kaplan, W.J. Steinbach, and P. Hotez, Infectious Related to Prosthetic or Artificial Devices, *Feigin and Cherry Textbook of Pediatric Infectious Diseases, 8th edition*, Elsevier, 2018.
7. N.J. Eynon-Lewis, D. Ferry, and M.F. Pearse, Themistocles Gluck: An Unrecognised Genius, *Br. Med. J.*, 1992, **305**(6868), p 1534–1536.
8. W.A. Lane, Some Remarks on the Treatment of Fractures, *Br. Med. J.*, 1895, **1**(1790), p 861–863.
9. A.R. Lesić, S. Zagorac, V. Bumbasirević, and M.Z. Bumbasirević, The Development of Internal Fixation - Historical Overview., *Acta Chir. Iugosl.*, 2012, **59**(3), p 9–13.
10. M. Saini, Implant Biomaterials: A Comprehensive Review, *World J. Clin. Cases*, 2015, **3**(1), p 52–57.
11. K. Prasad, O. Bazaka, M. Chua, M. Rochford, L. Fedrick, J. Spoor, R. Symes, M. Tieppo, C. Collins, A. Cao, D. Markwell, K. Ostrikov, and K. Bazaka, “Metallic Biomaterials: Current Challenges and Opportunities,” *Materials*, 2017.
12. T.F. Moriarty, U. Schlegel, S. Perren, and R.G. Richards, Infection in Fracture Fixation: Can We Influence Infection Rates through Implant Design?, *J. Mater. Sci. Mater. Med.*, 2010, **21**(3), p 1031–1035, doi:10.1007/s10856-009-3907-x.
13. A.C. Marsh, N.P. Chamorro, and X. Chatzistavrou, Long-Term Performance and Failure of Orthopedic Devices, *Bone Repair Biomaterials*, 2019, p 379–410.
14. R.G.T. Geesink, K. De Groot, and C.P.A.T. Klein, Bonding of Bone to Apatite-Coated Implants, *J. Bone Jt. Surg. - Ser. B*, 1988, **70**(1), p 17–22.
15. R.G.T. Geesink, K. De Groot, and C.P.A.T. Klein, Chemical Implant Fixation Using Hydroxyl-Apatite Coatings: The Development of a Human Total Hip Prosthesis for Chemical Fixation to Bone Using Hydroxyl-Apatite Coatings on Titanium Substrates, *Clin. Orthop. Relat. Res.*, 1987, (225), p 147–170.
16. K. De Groot, R. Geesink, C.P.A.T. Klein, and P. Serekian, Plasma Sprayed Coatings of Hydroxylapatite, *J. Biomed. Mater. Res.*, 1987, **21**(12), p 1375–1381.
17. R.J. Furlong and J.F. Osborn, Fixation of Hip Prostheses by Hydroxyapatite Ceramic Coatings, *J. Bone Jt. Surg. - Ser. B*, 1991, **73**(5), p 741–745.
18. J.F. Osborn, Die Biologische Leistung Der Hydroxylapatitkeramik-Beschichtung Auf Dem Femurschaft Einer Titanendoprothese - Erste Histologische Auswertung Eines Humanexplantats, *Biomed. Tech.*, 1987, **32**(7–8), p 177–183.
19. R.G.T. Geesink, Experimental and Clinical Experience with Hydroxyapatitie-Coated Hip Implants, *Orthopedics*, 1989, **12**(9), p 1239–1242.
20. M.T. Manley and R. Koch, Clinical Results with the Hydroxyapatite-Coated Omnifit Hip Stem., *Dent. Clin. North Am.*, 1992, **36**(1), p 257–262.

21. R.G.T. Geesink and N.H.M. Hoefnagels, Six-Year Results of Hydroxyapatite-Coated Total Hip Replacement, *J. Bone Jt. Surg. - Ser. B*, 1995, **77**(4), p 534–547.

22. J.A. D'Antonio, W.N. Capello, and M.T. Manley, Remodeling of Bone around Hydroxyapatite-Coated Femoral Stems, *J. Bone Jt. Surg. - Ser. A*, 1996, **78**(8), p 1226–1234.

23. W.N. Capello, J.A. D'Antonio, M.T. Manley, and J.R. Feinberg, Hydroxyapatite in Total Hip Arthroplasty: Clinical Results and Critical Issues, *Clin. Orthop. Relat. Res.*, 1998, (355), p 200–211.

24. M.T. Manley, W.N. Capello, J.A. D'Antonio, A.A. Edidin, and R.G.T. Geesink, Fixation of Acetabular Cups without Cement in Total Hip Arthroplasty: A Comparison of Three Different Implant Surfaces at a Minimum Duration of Follow-up of Five Years, *J. Bone Jt. Surg. - Ser. A*, 1998, **80**(8), p 1175–1185.

25. D.D. D'Lima, R.H. Walker, and C.W. Colwell, Omnifit-HA Stem in Total Hip Arthroplasty: A 2- to 5-Year Followup, *Clin. Orthop. Relat. Res.*, Lippincott Williams and Wilkins, 1999, (363), p 163–169.

26. O. Reikerås and R.B. Gunderson, Excellent Results with Femoral Revision Surgery Using an Extensively Hydroxyapatite-Coated Stem: 59 Patients Followed for 10-16 Years, *Acta Orthop.*, 2006, **77**(1), p 98–103.

27. O. Reikerås and R.B. Gunderson, Excellent Results of HA Coating on a Grit-Blasted Stem: 245 Patients Followed for 8-12 Years, *Acta Orthop. Scand.*, 2003, **74**(2), p 140–145.

28. R.G.T. Geesink, Osteoconductive Coatings for Total Joint Arthroplasty, *Clin. Orthop. Relat. Res.*, 2002, (395), p 53–65.

29. J.M. Lee and C.W. Lee, Comparison of Hydroxyapatite-Coated and Non-Hydroxyapatite-Coated Noncemented Total Hip Arthroplasty in Same Patients, *J. Arthroplasty*, 2007, **22**(7), p 1019–1023.

30. E.W. Morscher, A. Hefti, and U. Aebi, Severe Osteolysis after Third-Body Wear Due to Hydroxyapatite Particles from Acetabular Cup Coating, *J. Bone Jt. Surg. - Ser. B*, 1998, **80**(2), p 267–272.

31. M. Røkkum, M. Brandt, K. Bye, K.R. Hetland, S. Waage, and A. Reigstad, Polyethylene Wear, Osteolysis and Acetabular Loosening with an HA-Coated Hip Prosthesis. A Follow-up of 94 Consecutive Arthroplasties, *J. Bone Jt. Surg. - Ser. B*, 1999, **81**(4), p 582–589.

32. E. Mohseni, E. Zalnezhad, and A.R. Bushroa, Comparative Investigation on the Adhesion of Hydroxyapatite Coating on Ti-6Al-4V Implant: A Review Paper, *Int. J. Adhes. Adhes.*, Elsevier, 2014, **48**, p 238–257, doi:10.1016/j.ijadhadh.2013.09.030.

33. L. Sun, Thermal Spray Coatings on Orthopedic Devices: When and How the FDA Reviews Your Coatings, *J. Therm. Spray Technol.*, Springer US, 2018, **27**(8), p 1280–1290, doi:10.1007/s11666-018-0759-2.

34. J.R. Jones, Review of Bioactive Glass: From Hench to Hybrids, *Acta Biomater.*, 2013, **9**(1), p 4457–4486, doi:10.1016/j.actbio.2012.08.023.

35. A. Oliva, A. Salerno, B. Locardi, V. Riccio, F. Della Ragione, P. Iardino, and V. Zappia, Behaviour of Human Osteoblasts Cultured on Bioactive Glass Coatings, *Biomaterials*, 1998, **19**(11–12), p 1019–1025.

36. S. Lopez-Esteban, E. Saiz, S. Fujino, T. Oku, K. Suganuma, and A.P. Tomsia, Bioactive Glass Coatings for Orthopedic Metallic Implants, *J. Eur. Ceram. Soc.*, 2003, **23**(15), p 2921–2930.

37. S.D. Newman, N. Lotfibakhshaiesh, M. O'Donnell, X.F. Walboomers, N. Horwood, J.A. Jansen, A.A. Amis, J.P. Cobb, and M.M. Stevens, Enhanced Osseous Implant Fixation with Strontium-Substituted Bioactive Glass Coating, *Tissue Eng. Part A*, 2014, **20**, p 1850–1857.

38. S. Kargozar, N. Lot, J. Ai, A. Samadikuchaksaraie, R.G. Hill, P.A. Shah, P. Brouki, M. Mozafari, M. Fathi, and M. Taghi, Synthesis, Physico-Chemical and Biological Characterization of Strontium and Cobalt Substituted Bioactive Glasses for Bone Tissue Engineering, *J. Non. Cryst. Solids*, 2016, **449**, p 133–140.

39. X. Liu, M.N. Rahaman, and Q. Fu, Bone Regeneration in Strong Porous Bioactive Glass (13-93) Scaffolds with an Oriented Microstructure Implanted in Rat Calvarial Defects, *Acta Biomater.*, 2013, **9**(1), p 4889–4898.

40. M. Miola, S. Ferraris, S. Di Nunzio, P.F. Robotti, G. Bianchi, G. Fucale, G. Maina, M. Cannas, S. Gatti, A.

Massé, C. Vitale Brovarone, and E. Verné, Surface Silver-Doping of Biocompatible Glasses to Induce Antibacterial Properties. Part II: Plasma Sprayed Glass-Coatings, *J. Mater. Sci. Mater. Med.*, 2009, **20**(3), p 741–749, doi:10.1007/s10856-008-3618-8.

41. X. Lu, J. Kolzow, R.R. Chen, and J. Du, Effect of Solution Condition on Hydroxyapatite Formation in Evaluating Bioactivity of B2O3 Containing 45S5 Bioactive Glasses, *Bioact. Mater.*, Elsevier, 2019, **4**, p 207–214, doi:10.1016/j.bioactmat.2019.05.002.

42. N.C. Lindfors, P. Hyvönen, M. Nyyssönen, M. Kirjavainen, J. Kankare, E. Gullichsen, and J. Salo, Bioactive Glass S53P4 as Bone Graft Substitute in Treatment of Osteomyelitis, *Bone*, 2010, **47**(2), p 212–218.

43. N.C. Lindfors, I. Koski, J.T. Heikkilä, K. Mattila, and A.J. Aho, A Prospective Randomized 14-Year Follow-up Study of Bioactive Glass and Autogenous Bone as Bone Graft Substitutes in Benign Bone Tumors, *J. Biomed. Mater. Res. - Part B Appl. Biomater.*, 2010, **94B**(1), p 157–164.

44. K. Pernaa, I. Koski, K. Mattila, E. Gullichsen, J. Heikkilä, A.J. Aho, and N.C. Lindfors, Bioactive Glass S53P4 and Autograft Bone in Treatment of Depressed Tibial Plateau Fractures: A Prospective Randomized 11-Year Follow-Up, *J. Long. Term. Eff. Med. Implants*, 2011, **21**(2), p 139–148.

45. T. Debnath, A. Chakraborty, and T. Pal, A Clinical Study on the Efficacy of Hydroxyapatite-Bioactive Glass Composite Granules in the Management of Periodontal Bony Defects, *J. Indian Soc. Periodontol.*, 2014, **18**(5), p 593–600.

46. M. Zhu, J. Li, B. Chen, L. Mei, L. Yao, J. Tian, and H. Li, The Effect of Calcium Sodium Phosphosilicate on Dentin Hypersensitivity: A Systematic Review and Meta-Analysis, *PLoS One*, 2015, **10**(11).

47. C.C. Martins, R.T. Firmino, J.J. Riva, L. Ge, A. Carrasco-Labra, R. Brignardello-Petersen, L.E. Colunga-Lozano, A.F. Granville-Garcia, F.O. Costa, J.J. Yepes-Nuñez, Y. Zhang, and H.J. Schünemann, "Desensitizing Toothpastes for Dentin Hypersensitivity: A Network Meta-Analysis," *Journal of Dental Research*, 2020, p 514–522.

48. R. Haghgoo, M. Ahmadvand, and S. Moshaverinia, Remineralizing Effect of Topical Novamin and Nanohydroxyapatite on Caries-like Lesions in Primary Teeth, *J. Contemp. Dent. Pract.*, 2016, **17**(8), p 645–649.

49. A.A. El-Rashidy, J.A. Roether, L. Harhaus, U. Kneser, and A.R. Boccaccini, Regenerating Bone with Bioactive Glass Scaffolds: A Review of in Vivo Studies in Bone Defect Models, *Acta Biomater.*, 2017, **62**, p 1–28, doi:10.1016/j.actbio.2017.08.030.

50. J.R. Davis, "Handbook of Thermal Spray Technology," J.R. Davis, Ed., 28th ed., (Portland), Ringgold Inc, 2004.

51. S. Dosta, M. Robotti, S. Garcia-Segura, E. Brillas, I.G. Cano, and J.M. Guilemany, Influence of Atmospheric Plasma Spraying on the Solar Photoelectro-Catalytic Properties of TiO2 Coatings, *Appl. Catal. B Environ.*, 2016, **189**, p 151–159.

52. I.G. Cano, S. Dosta, J.R. Miguel, and J.M. Guilemany, Production and Characterization of Metastable Al2O3–TiO2 Ceramic Materials, *J. Mater. Sci.*, 2007, **42**(22), p 9331–9335, doi:10.1007/s10853-007-1871-8.

53. L. Pawlowski, "The Science and Engineering of Thermal Spray Coatings," *The Science and Engineering of Thermal Spray Coatings: Second Edition*, second ed., John Wiley & Sons, 2008.

54. J.H. Chern Lin, M.L. Liu, and C.P. Ju, Structure and Properties of Hydroxyapatite-Bioactive Glass Composites Plasma Sprayed on Ti6Al4V, *J. Mater. Sci. Mater. Med.*, 1994, **5**(5), p 279–283.

55. B. Garrido, I.G. Cano, and S. Dosta, Adhesion Improvement and in Vitro Characterisation of 45S5 Bioactive Glass Coatings Obtained by Atmospheric Plasma Spraying, *Surf. Coatings Technol.*, 2021, **405**, p 126560.

56. G.M. Nelson, J.A. Nychka, and A.G. McDonald, "Flame Spray Deposition of Titanium Alloy-Bioactive Glass Composite Coatings," *Journal of Thermal Spray Technology*, 2011, p 1339–1351.

57. G.M. Nelson, J.A. Nychka, and A.G. McDonald, Structure, Phases, and Mechanical Response of Ti-Alloy Bioactive Glass Composite Coatings, *Mater. Sci. Eng. C*, 2014, **36**(1), p 261–276, doi:10.1016/j.msec.2013.12.017.

58. M. Aghasibeig, F. Tarasi, R.S. Lima, A. Dolatabadi, and C. Moreau, "A Review on Suspension Thermal Spray Patented Technology Evolution," *Journal of Thermal Spray Technology*, 2019.

59. L. Pawlowski, Suspension and Solution Thermal Spray Coatings, *Surf. Coatings Technol.*, Elsevier, 2009, **203**(19), p 2807–2829, doi:10.1016/j.surfcoat.2009.03.005.

60. G. Bolelli, D. Bellucci, V. Cannillo, R. Gadow, A. Killinger, L. Lusvarghi, P. Müller, and A. Sola, Comparison between Suspension Plasma Sprayed and High Velocity Suspension Flame Sprayed Bioactive Coatings, *Surf. Coatings Technol.*, Elsevier, 2015, **280**, p 232–249.

61. A. Killinger, R. Gadow, G. Mauer, A. Guignard, R. Vaen, and D. Stöver, "Review of New Developments in Suspension and Solution Precursor Thermal Spray Processes," *Journal of Thermal Spray Technology*, 2011, p 677–695.

62. E. Cañas, M. Vicent, E. Bannier, P. Carpio, M.J. Orts, and E. Sánchez, Effect of Particle Size on Processing of Bioactive Glass Powder for Atmospheric Plasma Spraying, *J. Eur. Ceram. Soc.*, 2016, **36**(3), p 837–845.

63. G. Goller, The Effect of Bond Coat on Mechanical Properties of Plasma Sprayed Bioglass-Titanium Coatings, *Ceram. Int.*, 2004, **30**(3), p 351–355, doi:10.1016/S0272-8842(03)00107-X.

64. T.M. Lee, E. Chang, B.C. Wang, and C.Y. Yang, Characteristics of Plasma-Sprayed Bioactive Glass Coatings on Ti-6Al-4V Alloy: An in Vitro Study, *Surf. Coatings Technol.*, 1996, **79**(1–3), p 170–177.

65. D. Bellucci, G. Bolelli, V. Cannillo, R. Gadow, A. Killinger, L. Lusvarghi, A. Sola, and N. Stiegler, High Velocity Suspension Flame Sprayed (HVSFS) Potassium-Based Bioactive Glass Coatings with and without TiO 2 Bond Coat, *Surf. Coatings Technol.*, 2012, **206**(19–20), p 3857–3868.

66. S.J. Ding, C.P. Ju, and J.H. Chern Lin, Morphology and Immersion Behavior of Plasma-Sprayed Hydroxyapatite/Bioactive Glass Coatings, *J. Mater. Sci. Mater. Med.*, 2000, **11**(3), p 183–190.

67. A. Cattini, D. Bellucci, A. Sola, L. Pawłowski, and V. Cannillo, Microstructural Design of Functionally Graded Coatings Composed of Suspension Plasma Sprayed Hydroxyapatite and Bioactive Glass, *J. Biomed. Mater. Res. - Part B Appl. Biomater.*, 2014, **102**(3), p 551–560.

68. A. Cattini, D. Bellucci, A. Sola, L. Pawłowski, and V. Cannillo, Suspension Plasma Spraying of Optimised Functionally Graded Coatings of Bioactive Glass/Hydroxyapatite, *Surf. Coatings Technol.*, 2013, **236**, p 118–126.

69. L. Altomare, D. Bellucci, G. Bolelli, B. Bonferroni, V. Cannillo, L. De Nardo, R. Gadow, A. Killinger, L. Lusvarghi, A. Sola, and N. Stiegler, Microstructure and in Vitro Behaviour of 45S5 Bioglass Coatings Deposited by High Velocity Suspension Flame Spraying (HVSFS), *J. Mater. Sci. Mater. Med.*, 2011, **22**(5), p 1303–1319.

70. G. Bolelli, N. Stiegler, D. Bellucci, V. Cannillo, R. Gadow, A. Killinger, L. Lusvarghi, and A. Sola, Deposition Mechanisms in High Velocity Suspension Spraying: Case Study for Two Bioactive Materials, *Surf. Coatings Technol.*, 2012, **210**, p 28–45.

71. L. Sun, C.C. Berndt, K.A. Gross, and A. Kucuk, Material Fundamentals and Clinical Performance of Plasma-Sprayed Hydroxyapatite Coatings: A Review., *J. Biomed. Mater. Res.*, (United States), 2001, **58**(5), p 570–592.

72. A. Bandyopadhyay, F. Espana, V.K. Balla, S. Bose, Y. Ohgami, and N.M. Davies, Influence of Porosity on Mechanical Properties and in Vivo Response of Ti6Al4V Implants, *Acta Biomater.*, 2010, **6**(4), p 1640–1648.

73. K.A. Hing, S.M. Best, and W. Bonfield, Characterization of Porous Hydroxyapatite, *J. Mater. Sci. Mater. Med.*, 1999, **10**(3), p 135–145.

74. F.M. Klenke, Y. Liu, H. Yuan, E.B. Hunziker, K.A. Siebenrock, and W. Hofstetter, Impact of Pore Size on the Vascularization and Osseointegration of Ceramic Bone Substitutes in Vivo, *J. Biomed. Mater. Res. - Part A*, 2008, **85**(3), p 777–786.

75. B. Annaz, K.A. Hing, M. Kayser, T. Buckland, and L.D.I. Silvio, Porosity Variation in Hydroxyapatite and Osteoblast Morphology: A Scanning Electron Microscopy Study, *J. Microsc.*, Blackwell Science Ltd, 2004, **215**(1), p 100–110, doi:10.1111/j.0022-2720.2004.01354.x.

76. J.P. Li, P. Habibovic, M. van den Doel, C.E. Wilson, J.R. de Wijn, C.A. van Blitterswijk, and K. de Groot, Bone Ingrowth in Porous Titanium Implants Produced by 3D Fiber Deposition, *Biomaterials*, 2007, **28**(18), p 2810–2820.

77. O. Rojas, M. Prudent, M.E. López, F. Vargas, and H. Ageorges, Influence of Atmospheric Plasma Spraying Parameters on Porosity Formation in Coatings Manufactured from 45S5 Bioglass® Powder, *J. Therm. Spray Technol.*, 2020, **29**(1–2), p 185–198.

78. C. Gabbi, A. Cacchioli, B. Locardi, and E. Guadagnino, Bioactive Glass Coating: Physicochemical Aspects and Biological Findings, *Biomaterials*, 1995, **16**(7), p 515–520, doi:10.1016/0142-9612(95)91123-G.

79. V.L. Calvo, M.V. Cabedo, E. Bannier, E.C. Recacha, A.R. Boccaccini, L.C. Arias, and E.S. Vilches, 45S5 Bioactive Glass Coatings by Atmospheric Plasma Spraying Obtained from Feedstocks Prepared by Different Routes, *J. Mater. Sci.*, 2014, **49**(23), p 7933–7942.

80. S. Bano, I. Ahmed, D.M. Grant, A. Nommeots-Nomm, and T. Hussain, Effect of Processing on Microstructure, Mechanical Properties and Dissolution Behaviour in SBF of Bioglass (45S5) Coatings Deposited by Suspension High Velocity Oxy Fuel (SHVOF) Thermal Spray, *Surf. Coatings Technol.*, 2019, **372**, p 229–238.

81. V. Cannillo and A. Sola, Different Approaches to Produce Coatings with Bioactive Glasses: Enamelling vs Plasma Spraying, *J. Eur. Ceram. Soc.*, Elsevier, 2010, **30**(10), p 2031–2039, doi:10.1016/j.jeurceramsoc.2010.04.021.

82. E. Verné, M. Miola, C. Vitale Brovarone, M. Cannas, S. Gatti, G. Fucale, G. Maina, A. Massé, and S. Di Nunzio, Surface Silver-Doping of Biocompatible Glass to Induce Antibacterial Properties. Part I: Massive Glass, *J. Mater. Sci. Mater. Med.*, 2009, **20**(3), p 733–740.

83. L.L. Hench, Biomaterials: A Forecast for the Future, *Biomaterials*, 1998, **19**(16), p 1419–1423.

84. L.L. Hench, Chronology of Bioactive Glass Development and Clinical Applications, *New J. Glas. Ceram.*, 2013, **3**(02), p 67–73.

85. P.N. De Aza, A.H. De Aza, P. Pena, and S. De Aza, Bioactive Glasses and Glass-Ceramics, *Bol. la Soc. Esp. Ceram. y Vidr.*, Sociedad Española de Cerámica y Vidrio, 2007, **46**(2), p 45–55, doi:10.13039/501100003359.

86. S.M. Rabiee, N. Nazparvar, M. Azizian, D. Vashaee, and L. Tayebi, Effect of Ion Substitution on Properties of Bioactive Glasses: A Review, *Ceram. Int.*, 2015, **41**, p 7241–7251.

87. T. Kokubo and H. Takadama, How Useful Is SBF in Predicting in Vivo Bone Bioactivity?, *Biomaterials*, 2006, **27**(15), p 2907–2915, doi:10.1016/j.biomaterials.2006.01.017.

88. L. Varila, S. Fagerlund, T. Lehtonen, J. Tuominen, and L. Hupa, Surface Reactions of Bioactive Glasses in Buffered Solutions, *J. Eur. Ceram. Soc.*, 2012, **32**(11), p 2757–2763.

89. B. Rolfe, J. Mooney, B. Zhang, S. Jahnke, S.-J. Le, Y.-Q. Chau, Q. Huang, H. Wang, G. Campbell, and J. Campbell, The Fibrotic Response to Implanted Biomaterials: Implications for Tissue Engineering, *Regenerative Medicine and Tissue Engineering - Cells and Biomaterials*, 2011.

90. S. Zhang, “Biological and Biomedical Coatings Handbook: Applications,” *Biological and Biomedical Coatings Handbook: Applications*, first ed., (Boca Raton), CRC Press, 2016.

91. U. Meyer, A. Büchter, H.P. Wiesmann, U. Joos, and D.B. Jones, “Basic Reactions of Osteoblasts on Structured Material Surfaces,” *European Cells and Materials*, 2005, p 39–49.

92. M. Jäger, C. Zilkens, K. Zanger, and R. Krauspe, Significance of Nano- and Microtopography for Cell-Surface Interactions in Orthopaedic Implants, *J. Biomed. Biotechnol.*, 2007, **2007**, p 1–19.

93. F.E. Ciraldo, E. Boccardi, V. Melli, F. Westhauser, and A.R. Boccaccini, "Tackling Bioactive Glass Excessive in Vitro Bioreactivity: Preconditioning Approaches for Cell Culture Tests," *Acta Biomaterialia*, 2018, p 3–10.

94. A. Lopez-Sastre, J.M. Gonzalo-Orden, J.R.A.R. Altónaga, J.R.A.R. Altónaga, and M.A. Orden, Coating Titanium Implants with Bioglass and with Hydroxyapatite. A Comparative Study in Sheep., *Int. Orthop.*, 1998, **22**(6), p 380–383, doi:10.1007/s002640050282.

95. B. Karakuzu-Ikizler, P. Terzioğlu, Y. Basaran-Elalmis, B.S. Tekerek, and S. Yücel, Role of Magnesium and Aluminum Substitution on the Structural Properties and Bioactivity of Bioglasses Synthesized from Biogenic Silica, *Bioact. Mater.*, KeAi Communications Co., 2020, **5**(1), p 66–73.

96. A.A. El-Kheshen, F.A. Khaliafa, E.A. Saad, and R.L. Elwan, Effect of Al2O3 Addition on Bioactivity, Thermal and Mechanical Properties of Some Bioactive Glasses, *Ceram. Int.*, Elsevier, 2008, **34**(7), p 1667–1673.

97. E. Bonnelye, A. Chabadel, F. Saltel, and P. Jurdic, Dual Effect of Strontium Ranelate: Stimulation of Osteoblast Differentiation and Inhibition of Osteoclast Formation and Resorption in Vitro, *Bone*, 2008, **42**(1), p 129–138.

98. S. O'Donnell, A. Cranney, G. Wells, J. Adachi, and J. Reginster, Strontium Ranelate for Preventing and Treating Postmenopausal Osteoporosis, *Cochrane Database Syst. Rev.*, John Wiley & Sons, 2006, (4).

99. L. Yu, M. Xia, X. Chen, C. Rong, J. Zhang, W. Zhou, S. Lian, and I. Introduction, Prepared By Hydrothermal Method, 2013, **2019**, p 2–9.

100. C. Stähli, M. James-Bhasin, A. Hoppe, A.R. Boccaccini, and S.N. Nazhat, Effect of Ion Release from Cu-Doped 45S5 Bioglass® on 3D Endothelial Cell Morphogenesis, *Acta Biomater.*, 2015, **19**, p 15–22.

101. G.F. Hu, Copper Stimulates Proliferation of Human Endothelial Cells under Culture, *J. Cell. Biochem.*, 1998, **69**(3), p 326–335.

102. M. Ottomeyer, A. Mohammadkah, D. Day, and D. Westenberg, Broad-Spectrum Antibacterial Characteristics of Four Novel Borate-Based Bioactive Glasses, *Adv. Microbiol.*, 2016, **06**(10), p 776–787.

103. M. Bellantone, H.D. Williams, and L.L. Hench, Broad-Spectrum Bactericidal Activity of Ag2O-Doped Bioactive Glass, *Antimicrob. Agents Chemother.*, 2002, **46**(6), p 1940–1945.

104. M. Bellantone, N.J. Coleman, and L.L. Hench, Bacteriostatic Action of a Novel Four-Component Bioactive Glass, *J. Biomed. Mater. Res.*, 2000, **51**(3), p 484–490.

105. A. Cattini, D. Bellucci, A. Sola, L. Pawłowski, and V. Cannillo, Functional Bioactive Glass Topcoats on Hydroxyapatite Coatings: Analysis of Microstructure and in-Vitro Bioactivity, *Surf. Coatings Technol.*, 2014, **240**, p 110–117.

106. E. Cañas, M.J. Orts, A.R. Boccaccini, and E. Sánchez, Solution Precursor Plasma Spraying (SPPS): A Novel and Simple Process to Obtain Bioactive Glass Coatings, *Mater. Lett.*, 2018, **223**, p 198–202.

2. Chapter: Scope of the work

2. Chapter: Scope of the work

The present thesis was developed in the context of surface modifications for materials used in hard tissue replacement implants. Thermal spraying techniques can be used to produce coatings with materials capable of replacing bone and stimulating its regeneration to promote more efficient osseointegration. The Thermal Spray Center has broad experience in thermal spraying to manufacture bioactive coatings. This trajectory is reflected in the development of different doctoral theses and the publications of the studies carried out (Ref 89,90,99–104,91–98). The **bibliographic study** presented in the review paper "Bioactive glass coatings obtained by thermal spray: Current status and future challenges" provided a starting point to determine the lines of study of this doctoral thesis.

This thesis focuses on improving the limitations of the use of bioactive glass coatings through different strategies: i) by modifying its physicochemical properties (by changing the composition or morphology of the feedstock material; post-treatments, use of composites) and ii) by using different thermal spray techniques (atmospheric plasma spray and cold gas spray). The developed coatings were analysed in terms of microstructure, bioactivity, and mechanical and biological response.

This general goal is divided into the following specific objectives:

Objective 1: Develop different **strategies to increase the tensile strength of bioactive glass coatings** obtained by atmospheric plasma spraying. Included in articles: "Adhesion improvement and in vitro characterisation of 45S5 bioactive glass coatings obtained by atmospheric plasma spraying" and "Improving the bond strength of bioactive glass coatings obtained by atmospheric plasma spraying".

- Develop and characterise bioactive glass coatings with **feedstock material with different morphology** to enhance the bonding with the substrate and asses the effect of the morphology regarding the degradation behaviour.
- **Design bioactive glass coatings in combination with hydroxyapatite** to diminish the thermal expansion mismatch of the bonded materials and characterisation of the modified surfaces.
- Use **temperature before or after the spraying process** to relieve tensions and improve cohesion at the interface with the substrate.

Objective 2: Study the adhesion and proliferation of osteoblasts on rough and smooth **bioactive glass surfaces with different compositions** by atmospheric plasma spraying and assessment of the effect of the composition on the physicochemical and mechanical properties of the coatings.

Objective 3: Strategies to **produce bioactive glass coatings by cold gas spraying**.

- Develop and characterise **composite bioactive glass/PEEK** onto polymer surfaces and evaluate the relationship of the mechanical and biological properties of the coatings with the glass content incorporated into the composite layer. This sub-objective is included in the papers: “Development of Bioglass/PEEK Composite Coating by Cold Gas Spray for Orthopedic Implants” and “45S5/PEEK coatings by Cold Gas Spray with in vitro bioactivity, degradation and cellular proliferation”.
- Design **novel glass formulations** to control its viscosity behaviour at relatively low temperatures and allow its deposition by cold gas spraying. Evaluation of bioactivity and degradation of the designed compositions under physiological conditions.

3. Chapter: Methodology

3. Chapter: Methodology

3.1. Raw materials and substrates

The coatings obtained by both APS and CGS have been obtained using powder as raw material. All coatings have been deposited on metallic and polymeric biomaterials substrates.

Powders

In this thesis, three different bioactive glass powders have been used for APS due to different causes during the evolution of the work. Initially, the **45S5** bioactive glass was chosen as the main object of study since it is the most studied composition and has a greater presence and acceptance in clinical use.

The 45S5 bioactive glass powder used in this thesis was bought from Denfotex Research (United Kingdom). The powder was produced by the traditional melt-quenching route. The theoretical compositions of the glasses employed are listed in Table 3.1.

The second bioactive glass composition used was **S53P4**. This composition was developed in the first stage of collaboration with the *Institute of Ceramics and Glass (ICV)* and served as an introduction to the methodology used to manufacture bioactive glasses. This composition was manufactured from a mixture of reagents: SiO_2, $(NH_4)_2HPO_4$, Na_2CO_3 and $CaCO_3$, following the procedure detailed in section 4.3. The S53P4 was chosen for being a composition accepted for commercial use and is commonly employed in some applications such as craniofacial reconstruction or for treating osteomyelitis.

The third bioactive glass used to produce APS coatings is a novel formulation named **62W** in the SiO_2-CaO-P_2O_5-MgO system. The 62W composition was designed and prepared by the *ICV* from a mixture of the following reagent grade: SiO_2, $Ca_3(PO_4)_2$, MgO and $CaCO_3$, following the indications of Rodrigo et al. (Ref 105). This composition incorporates magnesium oxide, which has stimulatory effects on the growth of new bone tissue, making it an interesting candidate for orthopaedic applications.

Table 3.1 Theoretical composition in molar percentage of the bioactive glasses used for APS

	SiO_2	**CaO**	**Na_2O**	**P_2O_5**	**MgO**
45S5	46.1	26.9	24.4	2.6	-
S53P4	53.9	21.8	22.7	1.7	-
62W	41.0	50.0	-	4.6	4.2

In addition to the bioactive glass compositions mentioned, other formulations were developed in collaboration with the *ICV*. With the idea of achieving a suitable composition for the CGS technique, a significant change in the structure of the developed glasses was sought, knowing

that this could compromise their bioactive capacity. Specifically, it was pursued that the glass had more capacity to deform at affordable temperatures for cold spraying. For this, different strategies were developed to reduce the glass transition temperature of the composition and a less viscous behaviour at low temperatures. The designed formulations are listed in Table 3.2.

Table 3.2 Theoretical composition in molar percentage of the glasses developed for CGS

Code	SiO_2	CaO	Na_2O	P_2O_5	CaF_2
CaF_17	31.37	21.31	24.36	5.21	17.76
CaF_25	28.4	19.29	22.06	4.71	25.54
CaF_25_Na	28.4	11.75	29.6	4.71	25.54
CaP_44	-	55.7	-	44.3	-
CaP_61	-	38.7	-	61.3	-
CaP_80	-	20	-	80	-
NaP_40	-	-	60	40	-
NaP_50	-	-	50	50	-
NaP_60	-	-	40	60	-
NaPCa_17	-	44.3	38.2	17.5	-
NaPCa_33	-	33.9	32.3	33.9	-
NaPCa_39	-	16.5	44.5	39	-
NaPCa_43	-	26.1	30.4	43.5	-
NaPCa_49	-	18	32.5	49.5	-
NaPCa_60	-	10	30	60	-
NaPCa_70	-	10	20	70	-
NaPCaF_40	-	-	46.7	40.9	12.4
NaPCaF_52	-	-	34.3	52.2	13.5
NaPCaF_60	-	-	30	60	10
NaPCaF_70	-	-	20	70	10

Another powder used was **hydroxyapatite** from Captal®30 (Plasma Biotal Limited, United Kingdom) with crystallinity above 95%. It is a medical-grade HA that follows the ISO 13779-6 (this part of ISO 13779 specifies requests for hydroxyapatite powders used as a raw material for the manufacturing surgical implants or coating of surgical implants).

Finally, PEEK has been chosen to facilitate the glass deposition on substrates of this same material. This powder has been used for producing composite coatings by CGS. The commercial PEEK powder used was from Victrex (United Kingdom).

Flowability of the powders

It was necessary to improve the flowability of the manufactured powders to make them capable of flowing during spraying. The angle of repose is the physical measure used to

analyse the flow behaviour of powder material. This parameter corresponds to the angle formed between the slope of a powder bed poured onto a flat and the horizontal surface. This method is used at an industrial level and also allows classifying the flow behaviour of powders. According to Carr (1965 & 1970) and Raymus (1985), it is considered that angles of repose below 30º indicate good flowability. Between 30º-45º there is some cohesiveness, between 45º-55º there is true cohesiveness, and above 55º the powder has very limited flowability (Ref 106).

There are different methods used to determine the angle of repose. In this thesis, the method used is illustrated in Figure 3.1. A representative sample of the powder (20 g) was poured into the funnel (10 mm internal diameter), which was held at a fixed height (150 mm) above the flat base. The angle of repose was measured from the slope formed by the powder accumulated at the flat base. In order to have reliable results, the measurements were made in triplicate for each powder. Moreover, to eliminate possible water absorption, the powders were dried for four h in a universal oven (UFE 400, Memmert, Schwabach, Germany) at 120 ºC before the test.

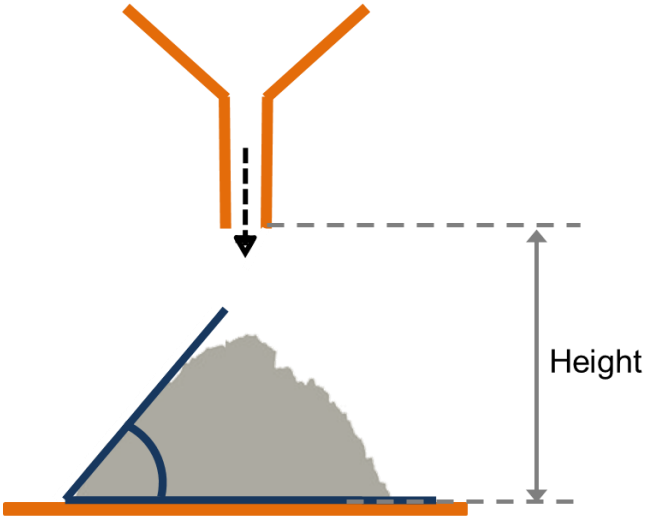

Figure 3.1 Schematic drawing of the method used for measuring the angle of repose of powders

The flowability of the powders was improved with the addition of aerosil, which is used as a fluidizing agent, an ultrafine hydrophilic silica powder with a very high specific surface area. As an example, Figure 3.2 represents the angle of repose measurements for different fractions of the S53P4 powder with and without a fluidizing agent. The addition of aerosil generates a significant reduction in the angle of repose, but more improvement in fluidity is no longer obtained from a certain amount of aerosil.

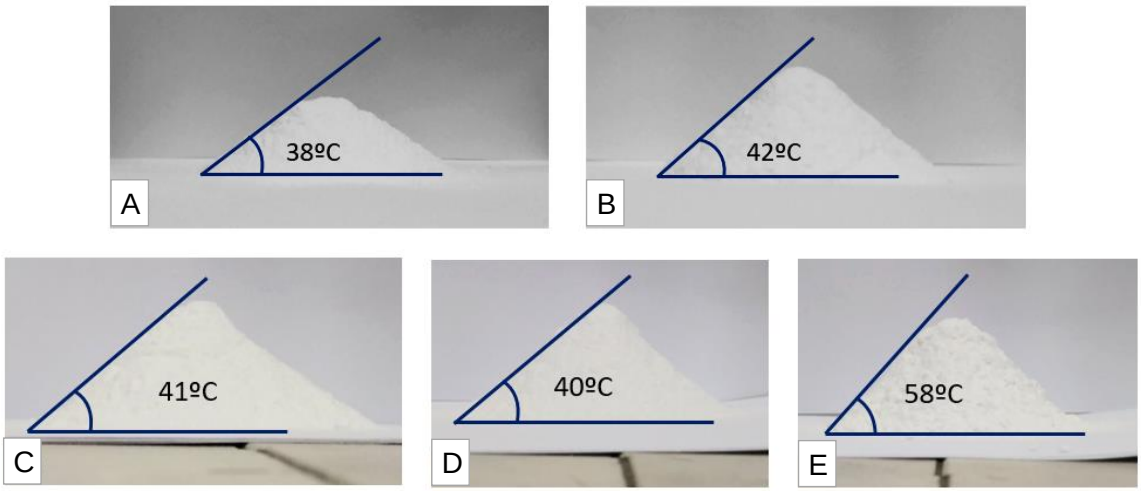

Figure 3.2 Sieved range between 80-63 µm: A) with 0.7 wt. % aerosil, B) without aerosil; sieved range between 63-40 µm: C) with 1.4 wt. % aerosil, D) with 0.7 wt. % aerosil and E) without aerosil

Commercial 45S5 glass also contains this anti-clogging agent. It was added by the company as an extra in the standard formulation, mixing directly 0.7 wt. % of aerosil with the milled powder.

Sieving of the powders

It is required to adjust the particle size of the powders to achieve a better homogeneity in the sprayed coatings. Therefore, a sieving process was carried out in the cases in which the particle size distribution of the powders was not adequate for the thermal spray technology to use. The sieving of the powders was carried out with a vibratory sieve shaker (AS200, Retsch, Germany), using the meshes of 80 µm, 63 µm and 40 µm. The powders were collected and classified as follows: range between 80 µm and 63 µm, range between 63 µm and 40 µm and range below 40 µm.

Substrates

The substrates used in the thesis have always been biocompatible materials available commercially for hard tissue replacement.

Titanium grade 5 (Ti6Al4V) has been used as substrate; this is the biomaterial most widely used in orthopedic implants. This alloy has been used in the studies included in sections 4.1, 4.2, and 4.4. Depending on the type of analysis or test to be carried out, samples with different geometry were used: 25 mm diameter disks cut from a bar (Ibermetal, Spain), samples measuring 50 mm × 100 mm × 5 mm (Ensinger, Spain) and disks of 2 mm thick and 9 mm diameter from a sheet (Ibermetal, Spain).

In section 4.3, PEEK has been used as substrate. Again, different geometries have been used to adapt to the requirements of each test. Coatings were deposited onto flat PEEK

substrates measuring 50 mm × 100 mm × 5 mm or with an area of 8 mm × 8 mm and 5 mm thick, obtained from PEEK sheets (Ensinger, Spain). Also, disks with a 25 mm diameter were cut from a PEEK bar (Vestakeep, Spain).

The details of the powders and substrates used in each test are reflected in the results chapter.

3.2. Methods of powder and coatings characterization

Powder characterization

The characteristics of the feedstock powders play a critical role in the properties of the coatings obtained, so it is important to characterise them to understand the results better. In this section, the details followed for each procedure and technique are not shown, more information can be found in the methodology included in corresponding section of Chapter 4.

The **shape and morphology of the materials** can be determined using scanning electron microscope (SEM). The equipment has a filament that generates a beam of electrons that scans the surface sample. The electrons generated from the interaction with the surface are collected with different detectors to provide topographic information of the sample (secondary electrons) or information about the surface composition (X-rays and backscattered electrons). In this study, an SEM (JSM-5310, JEOL, Tokyo, Japan) equipment with energy-dispersive X-ray spectrometry (EDS) and an SEM equipped with a backscattered electron detector (Phenom ProX, Phenom-World BV, Eindhoven, the Netherlands).

Most of the materials used in this work, polymers and ceramics, are non-conductive. For this reason, before observation, all the samples were coated with a gold layer to make them conductive using an SEM coating unit (E-5000, Polaron, Watford, England).

The different **particle size distributions** have been determined using a laser diffraction particle size analyser (LS 13 320, Beckman Coulter, California, USA). The powders were analysed with the tornado dry powder module capable of measuring particle sizes ranging from 0.40 µm to 2000 µm.

The **tapped density** (ρ_t) of the different powders used was also determined. The powder was tapped regularly in a graduated cylinder to settle the powder inside the cylinder. When the powder volume remained fixed at 5 mL, the tapped density was determined by weighing the sample.

X-ray diffraction (XRD) is a non-destructive technique that provides detailed information about the **crystallographic structure** of materials. The phases of the powders were evaluated using a diffractometer (X'Pert PRO MPD, PANalytical, Cambridge, UK). The patterns obtained from the analysis were processed with the PANalytical X'Pert HighScore Plus

software. Identifying the crystalline phases is possible by matching the acquired patterns with standard diffraction patterns contained in the software library.

Differential scanning calorimetry (DSC) is a technique that allows the identification of various physical properties by the correlation of heat flow associated with **thermal transitions** of the materials. In order to determine the thermal behaviour of some of the studied powders, DSC curves were obtained from the DSC equipment (DSC1, Mettler Toledo, Schwerzenbach, Switzerland).

The compositions developed for cold spraying, detailed in Table 1, were characterized by additional techniques that allow analyse their behaviour against temperature and their solubility.

Hot-stage microscopy (HSM) was performed using a microscope (EM201, Leica, Microsystems GmbH, Wetzlar, Germany). It allowed following the evolution of solid samples (cold-pressed powder) as a function of temperature through a camera coupled to a tubular oven that acquires the images. With the recorded results, the variation of the sample area and the variation of the shape factor as a function of temperature were determined through an image analysis program (Hesse Instruments). These data can be correlated with characteristic temperatures of the material and allow an indirect measurement of **glass viscosity** as a function of temperature. The measures were acquired from room temperature to 1200^{o}C at a heating rate of 10^{o}C/min.

Dissolution tests were conducted in deionized water. The amount of 150 mg of each powder, with particles between 100 µm and 710 µm, was hung in a mesh bag immersed in 4 mL of water. After 24h, the samples were taken out and rinsed with alcohol. Then, they were dried for 48h and weighed. Based on the weight difference before and after the test, the **dissolution percentage at 24h** was calculated.

Coating characterization

The characterization of the coatings has been done both at the surface level and at the cross-section. In this section, the details followed for perform each test and procedure are not shown, more information can be found in the methodology included in the corresponding section of the Chapter 4.

For the cross-section's characterization, samples were cut, then embedded in cold mounting resin and grinded with silicon carbide abrasive papers up to P4000 (grit size 5 µm). Finally, the samples were polished with 1 µm diamond solution. The **thickness** of the coatings was measured from the cross-sectional images using an optical microscope (DMI 5000 M, Leica, Wetzlar, Germany). The microstructure and the degree of porosity of the coatings are two fundamental characteristics of the mechanical and biological properties of the coatings. The

analysis of the **microstructure** of the coatings could be performed through an SEM. Before the observation, the samples were gold-coated to make them conductive.

The **surface roughness** is another factor related to the coatings dissolution and the interaction of the cells with the biomaterials. Therefore, characteristic roughness values (Ra and Rz) were recorded using a surface roughness measurement device (Surftest 301, Mitutoyo, Kawasaki, Japan).

XRD and DSC have been used to characterize the coatings. The **crystalline phases** related to the formation of the hydroxy-carbonate apatite layer and the patterns of the different coatings were analysed. In section 4.3, the DSC curves of the coatings were used to examine the **thermal transitions** that the materials underwent during the spraying process.

The **bonding strength** of a coating is a combination of adhesive strength (at the interface with the substrate) and cohesive strength (within the coating). The adhesive strength depends on the anchorage of the first layer of the coating, the residual stresses, and the roughness of the substrate material. In contrast, cohesive strength is influenced mainly by the microstructure of the coating.

The bonding strength of the coatings was measured according to the ASTM C633-13 standard using a universal testing machine (ME-402/10, Servosis, Madrid, Spain).

Orthopaedic implants are exposed to constant friction. For this reason, following the specifications of the ASTMG99-95, **the wear and friction behaviour** of coatings was characterized using a ball-on-disk test. After the test, the wear tracks were analysed employing a confocal microscope (PLu 2300, Sensofar, Barcelona, Spain) to calculate the volume of lost material due to wear and examined by SEM to analyze the effects of the wear mechanisms involved in the process. The **hardness** of the coatings was measured on polished cross-sections using a micro Vickers hardness tester (MXT-01, Matsuzawa Seiki, Tokio, Japan).

According to the biological properties of the coatings, different tests have been performed to assess their behaviour.

One key aspect of bioactive materials is the evaluation of in vitro degradation. It allows identifying the released elements from the coating and the degradation time, which should be suitable for supporting the regeneration process. Therefore, a **degradation study** was performed to evaluate the glass dissolution of the different coatings following the specifications of the ISO 10993 part 14: “Identification and quantification of degradation products of ceramic materials”.

The first parameter determined by the test is the weight loss percentage resulting from degradation. It was calculated with a high precision scale (CPA225D, Sartorius, Goettingen,

Germany). Next, the concentrations of elements released during the immersion were measured through inductively coupled plasma optical emission spectrometry (ICP-OES) (Optima 8300, PerkinElmer, Waltham, USA). This technique is commonly used to detect the chemical elements in a solution by the excitation of atoms or ions using argon plasma. Then, the intensity of the emissions from various wavelengths of light is measured, and the concentration of specific elements is calculated based on calibration. Finally, the pH of the solution was recorded using a universal pH meter (Hach, Spain).

Bioactive materials can bond to living bone through a layer of apatite. It has been shown that this apatite layer grows in simulated body fluids with ion concentrations nearly equal to those of human blood plasma. The apatite layer formed is very similar to that found in mineral bone. An in vitro test was performed following the ISO 23317 to evaluate the **bone-bonding ability** of the coatings. In the developed studies, the immersion time of the coatings varies from 1 day to 21 days.

An SEM observation of the samples analysed the process of the HCA layer formation. Furthermore, to assess the crystallization of the formed layer, a crystallographic structure analysis was performed by XRD.

In vitro methods for cell culture enable the study of the interaction of cells with a specific surface material in a controlled environment. The **behaviour of bone cells** onto some of the coatings developed has been studied. Human osteoblasts lines, obtained from knee trabecular bone after prosthesis replacement. The passage number of cell culture is the number of times it has been sub-cultured. For reliable results, cells cannot be sub-cultured many times, as high passages can cause alterations in gene expression and produce unusual results. For the in vitro tests, cultures in passage numbers between 3 and 6 were used. The ability of the samples to permit adhesion, growth, and proliferation of osteoblasts was evaluated by MTS assay (CellTiter 96® AQueous One Solution Cell Proliferation, Promega, USA). This colorimetric test quantifies viable cells by measuring the absorbance at 490 nm with a well plate reader (Infinite 200, Tecan, Männedorf, Switzerland). Moreover, cell attachment and morphology were analysed by SEM on samples previously dehydrated using a critical point dryer (CPD) (K850, Emitech, Lewes, UK) and carbon-coated using a high-vacuum carbon evaporator (K950X, Emitech, Lewes, UK).

3.3. Coating production

Equipment

The low-pressure cold gas spray (LP-CGS) equipment Dymet 423 (Dycomet Europe, Akkrum, The Netherlands) equipped with a CK-20 nozzle was used to spray PEEK and bioactive glass powders. In this technique, air is used as the propellant gas with a gas pressure of 0.6 MPa.

The gas temperature during the process was not very high; particularly, this equipment allowed us to work from room temperature to 500ºC.

For high-pressure cold gas spray (HP-CGS), two different types of equipments were used to spray bioactive glass powders. The first, Kinetiks 4000 (Impact Innovations Gmbh, Haun, Germany) fitted with a water-cooled WC nozzle. It operates with a maximum pressure of 40 bar and a temperature of 800ºC, respectively. The propellant gas can be nitrogen, helium or mixed. The WC based convergent-divergent nozzle (D24) used with this equipment has 41 mm of pre-chamber distance and a total length of 171 mm.

The second HP-CGS equipment, PCS-100 (Plasma Giken, Saitama, Japan) was used to spray bioactive glass powders. It can also be operated with nitrogen, helium or mixed, as propellant gas. It is limited to a maximum operating gas pressure of 50 bars and a maximum gas temperature of 1000ºC. Two nozzles were used, both WC-based convergent-divergent nozzles, one with a pre-chamber distance of 80 mm and a total length of 280 mm and another with a pre-chamber distance of 85 mm and a total length of 385 mm.

The plasma spray equipment used to deposit the bioactive powders was a Plasma-Technik A3000S (Sulzer Metco AG, Wohlen, Switzerland) equipped with a plasma torch (F4, Sulzer Metco AG, Wohlen, Switzerland). Argon was used as primary gas and hydrogen as secondary for the plasma plume formation. The powder carrier gas was also argon.

Optimization process

In general, thermal spray processes have numerous parameters that have a relationship among them and affect the final properties of the coatings. It is essential to determine the most suitable combination of the process parameters to obtain a coating with the desired quality. The procedure used to optimize the coatings is outlined below and shown in Figure 3.3.

Regardless of the spraying technique used (CGS or APS) it was necessary to **adjust parameters related to powder injection** (powder feed rate, carrier gas flow and injection angle). The material and the characteristics of the powder (particle size, morphology, fluidity, and specific temperatures) are determinants to set the proper parameters. The suitability of these parameters can be appreciated by the trajectory of the powder in the spray stream and also by the homogeneity in thickness of the coatings obtained.

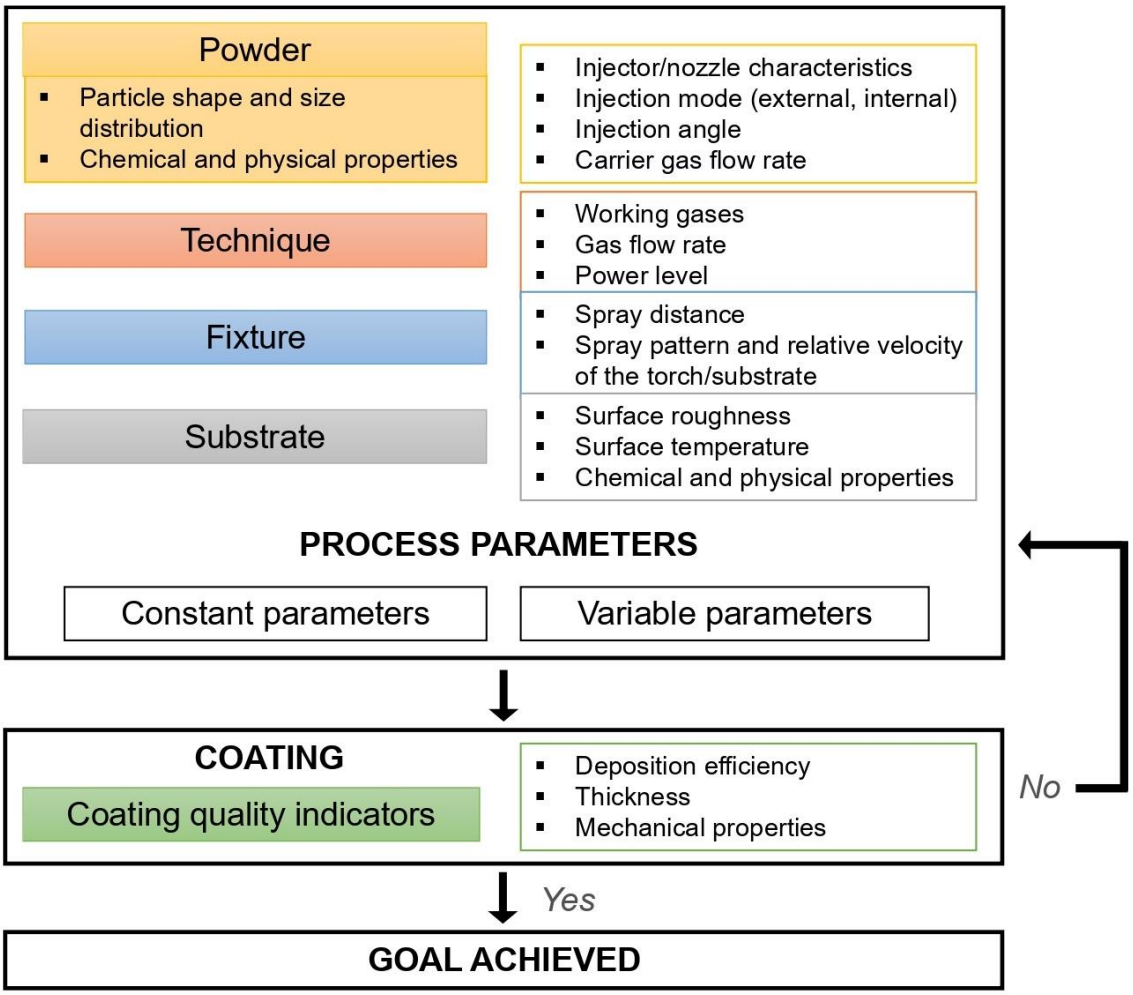

Figure 3.3 Optimization process for thermal spray coatings

In addition to the process parameters related to the injection of the powder, there are the parameters related to the specific spraying equipment and those that involve the substrate and the robot. Since there are many parameters involved in the formation of coatings by thermal spray techniques, it is important to **establish some parameters as fixed and others as variables** for the coating optimization process. Therefore, the classification of the parameters was done as follows:

- The parameters with less influence on the quality of the coatings, such as working gas, spray pattern and relative speed of the gun, the distance between passes, number of layers, and injection angle, were kept constant initially.
- The parameters with more influence on the quality of the coatings, such as stand-off distance between substrate and spraying gun and energy level (gas temperature and pressure in CGS and argon-hydrogen ratios in APS), were determined as variables.

Initial parameters were selected from the knowledge of the technique, considering the limits of the equipment, and with the information collected from literature to obtain **preliminary**

results. Then, to develop the coatings, wide ranges for each of the variable parameters (three different values per parameter) were established, while the rest were kept constant.

After spraying, the coatings were characterized to validate their quality. For this purpose, the **indicators of the quality** of the coating should be established. Usually, these are related to mechanical features (bond strength, hardness, and wear resistance), microstructural characteristics (degree of porosity, composition), or deposition efficiency. However, depending on the application, others can be more remarkable.

After analysing the sprayed coatings, the **variable parameters were readjusted**. The range of each of these parameters is narrowed around the values that have provided better results. Once the values with more significant influence provided the best results, the **parameters initially established as fixed could be adjusted** to optimize the coatings for acquiring the desired properties (high deposition efficiency, some mechanical property, specific microstructure). Furthermore, other external parameters, such as the surface roughness of the substrate, the pre-heating of the substrate or even post-treatments, can significantly affect the quality of the coating. These should also be considered, mainly when the desired properties are not easily achieved.

The desired **thickness** of the coating is a particular characteristic that can be adjusted easily by modifying the powder feed rate, the relative speed of the gun, or the number of layers. If an irregular thickness is observed in the sprayed area, it could be due to an overlapping problem. When this happens, a cyclical pattern of different thicknesses is usually observed, so it is necessary to adjust the distance between passes to obtain a satisfactory degree of overlapping.

When the coatings provide the desired results according to the quality indicators, **the goal is achieved**, and coatings optimization is finished.

It should be noticed that when any parameter with a significant effect on the properties of the coating is changed (the design of the nozzle, the working gases, or the feedstock powder), the values with more significant influence should be readjusted.

In this research study, the substrates have always been grit blasted and cleaned before depositing the coating. The mean **roughness** (Ra) was the value used as a reference for guaranteeing proper grit blasting. This parameter corresponds to the arithmetic measure of the absolute values of the roughness profile. Two different types of equipment were used for grit blasting (Formula 1400, Guyson International, Skipton, England) and (MAB-4, MAB industrial, Barcelona, Spain). Corundum G24 (grit size 800 µm) at a pressure of 0.5 MPa was used to provide the proper surface roughness to the substrates (Ra values between 4 µm and 7 µm).

Pre-heating the substrate immediately prior to deposition can reduce the residual stress and enhance the coating adhesion. In this study (section 4.1), this pre-treatment was accomplished by passing the torch over the surface of the substrate for one complete cycle with the same spraying conditions.

Post-treatments were performed to improve mechanical properties. Thermal treatments were applied to coatings in section 4.1. For this purpose, a high-temperature chamber furnace (CRN 4-18, Hobersal, Barcelona, Spain) was used.

4. Chapter: Results

4. Chapter: Results

4.1. Strategies for improving adhesion strength on bioactive glass coatings

As detailed in the literature review, the main problem why bioactive glass coatings are not a commercial substitute for hydroxyapatite coatings is the insufficient adhesion achieved by manufacturing these coatings. The different methods by which bioactive glass coatings can be manufactured do not meet the regulations for this type of medical device. This chapter addresses different strategies to improve the adhesion strength values of coatings obtained by atmospheric plasma spraying by:

- Using thermal post-treatments: this strategy is reported in the paper “Adhesion improvement and in vitro characterisation of 45S5 bioactive glass coatings obtained by atmospheric plasma spraying”, where the induced phases on the glass coating by the thermal treatment are shown. Moreover, the effect of the treatment on the bioactive capacity of the coatings was evaluated.
- Powder modifications: this strategy is approached from two different paths. One is based on incorporating a different powder into the bioactive glass coating, hydroxyapatite, to generate an increase in cohesion with the substrate. On the other hand, the morphology of the feedstock glass powders is modified to increase the specific surface area of the particles. Both are included in the paper “Improving the bond strength of bioactive glass coatings obtained by atmospheric plasma spraying” (still pendent of acceptance).

Surface & Coatings Technology 405 (2021) 126560

Contents lists available at ScienceDirect

Surface & Coatings Technology

journal homepage: www.elsevier.com/locate/surfcoat

Adhesion improvement and in vitro characterisation of 45S5 bioactive glass coatings obtained by atmospheric plasma spraying

B. Garrido, I.G. Cano, S. Dosta *

Thermal Spray Centre (CPT), Universitat de Barcelona (UB), 08028 Barcelona, Spain

Surface and Coatings Technology (January 2021), In Press

https://doi.org/10.1016/j.surfcoat.2020.126560

Abstract

Plasma sprayed bioactive glass coatings were studied using crushed 45S5 bioactive glass powder. It is widely accepted that plasma sprayed coating microstructure is highly affected by the characteristics of the powder and the parameters set on the spraying process. Once the coating deposition was optimized, two strategies were carried out to analyse their effect on the coating adhesion: cooling with carbon dioxide while spraying and a post heat treatment to the as-sprayed coatings.

Scanning electron microscopy and X-ray diffraction were used for analyse the obtained coatings. Additionally, coating adhesion to the substrate and degradation of the coatings in Tris buffer solution were evaluated for the different samples studied.

Coatings have been tested in vitro to evaluate their response by immersion in simulated body fluid, Hank's Balanced Salt Solution.

The results show an increase in the adhesion strength for the heat treated samples due to the stress relaxation achieved above glass transition temperature. Moreover, in the bioactivity test an apatite layer at the coatings surface was produced for all the strategies studied.

Keywords: Bioactive glass; Thermal spray; Bioactivity; Atmospheric plasma spray; Coatings; Biomaterials

1. Introduction

The global market for orthopaedic devices which include joint reconstructions, spinal devices, orthobiologics (substitutes and bone grafts) and trauma fixation among others reach every year higher values. Several factors are increasing the demand for orthopaedic implants. Mainly the ageing of the population that cause bone related diseases as osteoporosis and osteoarthritis. But also other diseases connected to lack of physical activity or poor diet intake and obesity have a growing trend in the last years that increment the requests of implants. Moreover, the increasing incidence of road traffic accidents and sports injuries have been an important factor for the market. The global orthopaedic device market is expected to rise in the following years.

Orthopaedic devices are very successful but there is a rate of implant failure that ends in revision surgery to correct. It is important to consider that revision surgery takes much longer, and is less successful than the primary procedure. Also the cost is higher than the primary intervention. For the patient it means more pain and the recovery takes weeks or months. In addition to the risk of a new surgery [1].

The main failures for orthopaedic devices are related to infections, being trauma devices more affected than joint replacements [2]. Other complications are associated to the implant-tissue interface due to a non-sufficient osteointegration or the stress shielding caused by the mismatch between the mechanical properties of bone tissue and the implanted materials.

Current biomaterials are reaching their limits and there is a need for study new opportunities that can satisfy biomechanical and biological requirements to improve the long-term success and to reduce the risk for revisions of artificial implants. One option is functionalizing current materials with bioactive glass coatings.

In the late 1960s Larry Hench developed the first composition of bioactive glass, named 45S5. It was composed of the following oxides wt.%: sodium oxide (24.5%), calcium oxide (24.5%), silicon dioxide (45.0%) and phosphorus pentoxide (6.0%). Takes its name because the glass has 45wt.% of SiO_2 and a calcium to phosphorus molar ratio of 5:1 [3,4].

Bioactive glass materials are different from conventional glasses. Their structure is quite more disrupted than the conventional ones. Bioactive glasses are characterized by their bioactivity and their unique bone bonding properties related to their surface reactivity when immersed in aqueous medium [1,4,5]. Depending on the composition, the glass can bond also to the soft tissue. The mechanism for bone bonding is in consequence of the formation of hydroxycarbonate apatite (HCA) layer on the surface of the glass, resulting from the initial glass dissolution. The biological apatite is partially replaced by the bone after long-term implantation. It is due because the ion release products from bioactive glasses stimulate

expressions of several genes of osteoblastic cells and promotes its proliferation [6–8]. Moreover, bioactive glasses show osteoconductive and osteoinductive capabilities [5].

The properties of each glass (e.g. the dissolution and the HCA layer formation rate) are a result of atomic structure. So by varying the content and the kind of the oxides in the glass, a full range of stability can be produced, from soluble to nonresorbable [1]. The 45S5 composition, in particular, is highly reactive.

When bioactive glasses come in contact with water, an ion exchange occurs at the glass/water interface. This ion exchange between modifier ions and protons from the solution results in a fast pH increase, mainly occurring in the first hours [9].

The release of ions from bioactive glasses is continuous over time [10], which suggest there is a release of ions from the bulk because the open silicate network allows the water molecules enter easy.

The excellent bioactive properties of bioactive glasses make them suitable for use to replace or repair damaged tissue. However, due to their poor mechanical properties, these glasses cannot be used as a bulk for load-bearing applications as other biomaterials such as titanium and cobalt-chrome alloys. [6,11]. Otherwise, they are able to be used as bone grafts, scaffolds and coating materials.

The first clinical bioactive glass product, the “Bioglass® Ossicular Reconstruction Prosthesis”, was a device used to treat conductive hearing loss by replacing the bones of the middle ear. It was a structure intended to conduct sound from the tympanic membrane to the cochlea. For this product was used the 45S5 composition [3,12].

Nowadays, most of the bioactive glass products available in the market are bone grafts [13–15]. But there are some other applications like an absorbable composite interference screw of bioactive glass and PLLA-PDLLA or a component for toothpaste [16,17].

The current biomaterials used for load bearing applications meet the necessary mechanical requirements. However, they have an inert behaviour when implanted. For this reason is necessary to apply a superficial modification to improve their interaction with the body. There are several methods (physical, chemical or combined strategies) used to improve the bioactivity of the surfaces keeping at the same time the bulk properties unaltered. One of the strategies used to convert bioinert materials into bioactive ones is depositing a biomaterial that stimulates the implant and host bond integration by thermal spray techniques.

Plasma-sprayed HA coatings have been used as surface coatings on metallic implants since the 1980s [18]. Moreover, it is possible to find in the literature several studies of ceramics or glass coatings produced by different thermal spray techniques such as a coating of a HA and TiO_2 mix (80-20% by weight) on Ti_6Al_4V by High-Speed Thermal Spray (HVOF) [19],

biomimetic nanocrystalline apatites deposited by low pressure cold sprayed (LP-CS) on Ti_6Al_4V [20], apatite and wollastonite coatings by APS on Ti_6Al_4V [21], 45S5 bioactive glass by APS on AISI 304 metallic substrate [22], etc.

Several researchers have proposed bioactive glasses as an alternative to HA coatings because of their ability to create a stable interface that bond to bone strongly. Moreover, their dissolution products promote cells to differentiate to bone cells [7].

It is possible to find studies developing bioactive glasses coatings by different thermal spray processes [23–29]. Some of these studies use just the glass powder, others use suspensions, others solution precursors and there are also works were mix the glasses with other compositions. In most of the studies glass coatings are very defective and are weakly bonded to the substrate [30].

One of the major challenges of using bioactive glass as coatings is improving the adhesion of the coating [11]. In this article, different strategies were studied to develop plasma sprayed 45S5 bioactive glass coatings with better adhesion. First step was varying the spraying parameters to achieve the best adhesion directly from the technique. Then two different approaches were studied: a cooling process with carbon dioxide while spraying the powder and a heat treating of the samples after spraying. Achieving good adhesion of the coating to the substrate is essential for bioactive glasses to be considered candidates to replace current hydroxyapatite coatings.

2. Experimental methods

2.1 Powder and substrate

The 45S5 bioactive glass powder was obtained from Denfotex research (United Kingdom). The powder was produced by the traditional melt-quenching route. To the milled powder 0.7 wt.% of aerosil was added, as an extra in the standard formulation, mixing directly with the powder. This fumed silica (aerosil) serves as a universal anticaking agent in powders, to make powders capable of flowing during spray process.

Titanium grade V disks of 2mm thick and 9mm diameter (Tamec, Spain) were used as substrates for physical and biological characterization. Specimens with 25mm diameter were used for measure the adhesion strength of the coatings.

2.2 Coating deposition

Bioactive glass coatings were deposited by Atmospheric Plasma Spraying (APS) onto titanium grade V substrates, previously grit blasted with corundum and then cleaned with ethanol before spraying.

The plasma spray equipment used was an APS A3000S system equipped with F4 Plasma torch. Argon was used as primary gas and hydrogen as secondary for the plasma plume formation. Powder carrier gas was also argon. The spraying parameters are listed in Table 1.

Spraying particles of brittle materials causes high stresses after solidification due to the rapid cooling. These stresses are relaxed through generating cracks, for this reason the coatings of glasses tend to present cracks and pores. Spraying parameters were studied to achieve a good melting of the particles to get homogeneous coatings. Stand-off distance was modified from 80 to 130mm, getting more controlled porosity for longer distances. Also the argon and hydrogen plasma gas flow rate has been changed from 30-35slpm and 12-6slpm, respectively. The carrier gas low rate was adjusted from 4 to 6l/min, being the lower the more appropriate. The injection angles used in these trials were whether 90º or 75º backwards.

Table 1. Plasma spraying parameters

Spraying parameters	**Bioactive glass coatings**
Argon plasma gas flow rate (slpm)*	35
Hydrogen plasma gas flow rate (slpm)*	12
Spray distance (mm)	125
Argon powder carrier gas (slpm)*	4
Injection angle (º)	90
Current (A)	600
Voltage (V)	66
Spray cycles	5

*Standard litre per minute

Trying to diminish the high stresses produced during solidification of the particles carbon dioxide was used in a cooling system fixed to the torch. Two nozzles on both sides of the spray torch emit a jet of carbon dioxide straight into the substrate during spraying. The idea is that particles arrive less heated to the substrate and diminish the amount of stresses that can affect the bond by the difference of temperature between the particles and the substrate. Carbon dioxide instead of air was chosen for cooling to ensure enough refrigeration and thus obtain glassy coatings. Afterwards we saw that cooling was not needed for obtain amorphous coatings.

In order to increase the bond adhesion a post heat treating was done to induce crystallinity and reduce the defects of the coating. The temperatures were selected in order to favour crystallization. At 610ºC a process of crystallization takes place for the 45S5 composition, and another one around 800ºC, these temperatures vary depending on the size particle or thickness of the coating and the heating conditions [31]. Besides, the chosen temperatures

were designated in a range were titanium alloy crystal structures remain unchanged [32]. The heating rate should be slow to avoid large temperature gradients and stresses which could result in cracking of the material. The as-sprayed coatings were heat treated at 725°C and 800°C for 5h and with a heating rate of 5°C/min in an air-circulated furnace, followed by slow cooling to room temperature.

2.3 Powder characterisation

The powder was sieved to get a narrow range before spraying. Laser diffraction particle size analyser Beckman Coulter LS 13320 was used to study the granulometry of the powder.

The shape and surface morphology of the glass powder was determined using a scanning electron microscope (SEM), JEOL JSM-5310 equipment. The samples were coated by a gold layer before microscopy study.

2.4 Coating characterisation

The crystal structure of the samples was determined by X-ray diffraction (XRD) using a PANalytical X'Pert PRO MPD Alpha1 powder diffractometer to define the structural changes caused by the processes.

The coatings and the formation of HCA layer on the surface of the samples after soaking in simulated body fluid were evaluated using SEM, JEOL JSM-5310 equipment.

The surface roughness of the final coatings was registered using a MITUTOYO SURFTEST 301. The Ra value corresponding to the arithmetical mean deviation of the assessed profile was recorded.

The adhesion strength of the coatings was measured according to ASTM C633-13 standard at atmospheric temperature. Coatings were glued using HTK ULTRA BOND 100® glue (HTK) to uncoated grit blasted samples. The tensile adhesion test was done using a Servosis ME-402/10 with self-aligning devices at 0.02mm/s of displacement rate and control of the position.

2.5 Bioactivity and degradation assessment

The in vitro ability to form apatite on the samples was studied following the ISO 23317:2014 using the simulated body fluid Hank's Balanced Salt Solution (HBSS) (Sigma-Aldrich, Germany). The composition of the HBSS is similar to the found in human blood plasma and some in vitro studies have been performed with this composition [33–35]. Coated samples were immersed in HBSS and exposed for 0, 1, 3, 6 and 14 days at 37^{o}C in a thermostatic bath with agitation. The solution was changed every 3 days to avoid ionic saturation of the medium. After the soaking time, the samples were rinsed three times with ultrapure water and dried for 24h at room temperature.

Before and after immersion the samples were characterized using SEM coupled with EDS to analyse the chemical and physical changes related to the bone-like apatite formation.

A degradation study was performed by immersing the samples for 120h in a buffered solution consisting of Tris-HCl with pH adjusted to 7.4±0.1 at 37±1ºC following the ISO 10993 standard, part 14: "Identification and quantification of degradation products of ceramic materials". The samples were placed in sterile polypropylene containers during the test. After degradation time, samples were rinsed thrice with ultrapure water and dried overnight at 120ºC until constant weight was recorded.

The weight loss percentage was calculated according to the equation: percentage of weight loss [%] = $100 \cdot (m_0 - m_f)/m_0$, where m_0 is the initial sample mass and m_f is the final sample mass after the sample drying. The weight results of the samples consider the whole of the mass including the substrate and the coating.

To study the dissolution process of the glass coatings, pH changes were recorded at different time periods using a universal pH meter (Hach, Spain).

3. Results and discussion

3.1. Powder characterisation

The size distribution used for spray was micron-sized with D_{10} = 52µm, D_{50} = 70µm and D_{90} = 110µm. The XRD pattern of the powder particles was the characteristic with amorphous structure.

The particles had irregular morphology as expected due to the route of fabrication. In addition, the cross section of the powders reveal full-dense particles (Fig. 1).

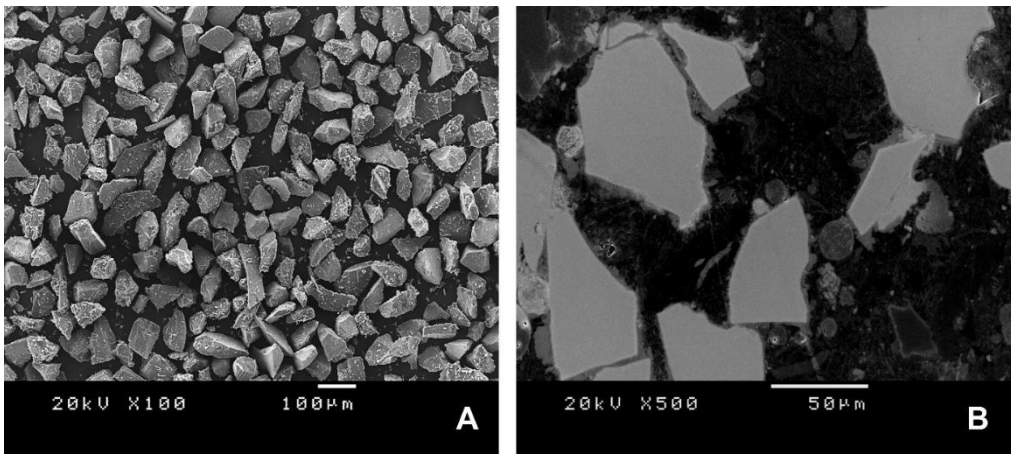

Figure 1. SEM micrographs of the free surface (A) and cross section (B) of the 45S5 powder

3.2. Coatings characterisation

Microstructure of the fabricated coatings can be observed in the cross-section micrographs showed in Fig 2. Due to the low thermal conductivity of the glass the particles are not completely molten during the spraying process even with the high temperatures of the plasma gas. Most of the particles are incompletely flattened when impacting the substrate providing this roughness to the substrate, which would be increased if the particle size of the powder is superior.

The cross sectional structure of the coatings reveals a significant amount of rounded cavities, this porosity is produced by volatilization of chemical components from the feedstock powder as reported previously for this glass composition [27].

The different coatings studied present a similar thickness, around 150µm. Also the value of the surface roughness is almost equal for the diverse coatings, about 13µm.

Particularly, the heat treated sample presents crystal structure and a major cohesion between the particles. However, the porosity and the thickness of the coating have not varied significantly.

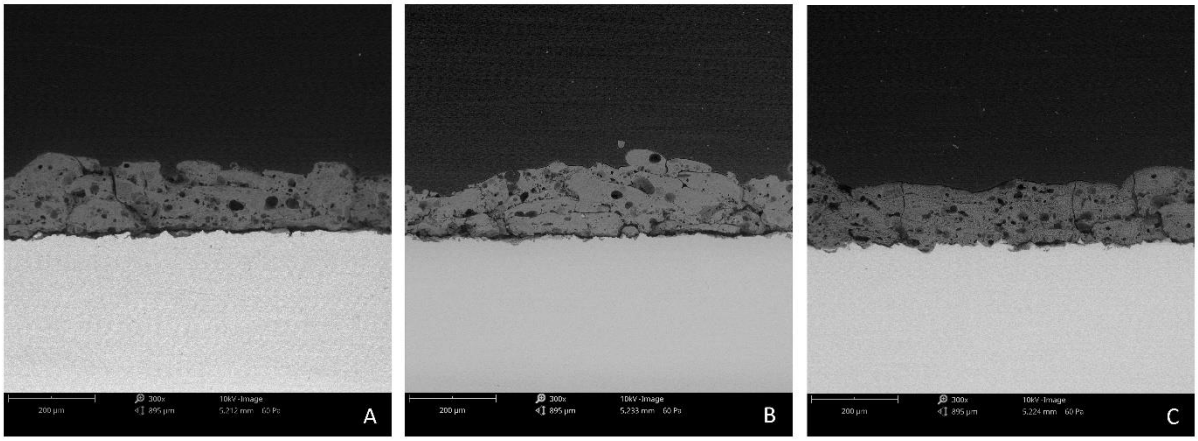

Figure 2. Cross section of the coatings: 45S5 as-sprayed (A), 45S5 with cooling (B) and with heat treatment to 725ºC

XRD results confirm that the as-sprayed coatings are amorphous due to the fast cooling of the melted particles. As expected the coatings performed with carbon dioxide cooling present also an amorphous pattern, attributed also to the fast cooling of the particles.

There are crystalline phases in the patterns corresponding to the coatings heated at 725ºC and 800ºC (Fig. 3(A)). Both patterns have peaks corresponding to sodium calcium silicate ($Na_6Ca_3Si_6O_{18}$, Ref. code: 01-079-1089) observed also by other authors working with 45S5 glass [30,31]. Particularly, the peaks corresponding to the sodium calcium silicate are more intense for the samples treated at 800ºC rather than 725ºC.

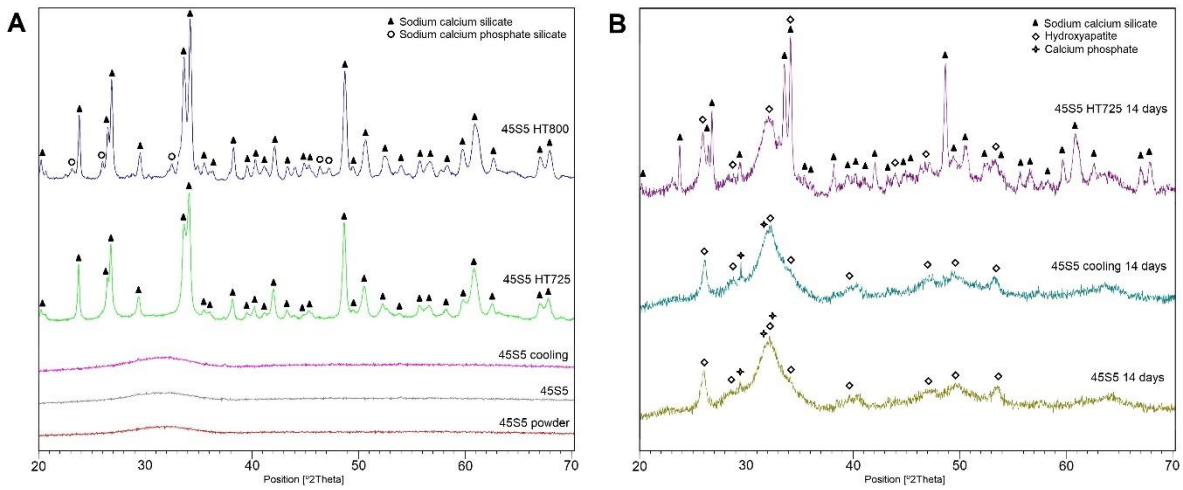

Figure 3. X-ray spectra of A) powder and coatings as-sprayed, with heat treatment to 725ºC and 800ºC and B) after being soaked in HBSS for 14 days

Furthermore, the spectrum of the coating treated at 800ºC reveals a secondary phase, corresponding to a sodium calcium phosphate silicate, identified as silicorhenanite ($Na_2Ca_4(PO_4)_2SiO_4$, Ref. code: 00-032-1053). Its crystallization starts at 800ºC as reported by other authors [31,36]. It can be concluded that higher temperature results in more crystallinity for the coatings.

The adhesion test results presented in Fig 4 indicate that cooling during the spraying process does not increase the bond strength of the coating. Then this strategy does not result in an improvement of the adhesion. Higher values of adhesion strength have been measured for coatings heat treated. Samples heat treated at 800ºC get a lower adhesion than the treated at 725ºC, achieving for the latter a value of 17.2±2.2MPa. With the heat treatment the coating stresses are reduced and crystallization is caused. As the glass is heated above the glass transition temperature a viscous state is achieved that produces better interparticle cohesion and a stress relaxation, which results in a stronger adhesion.

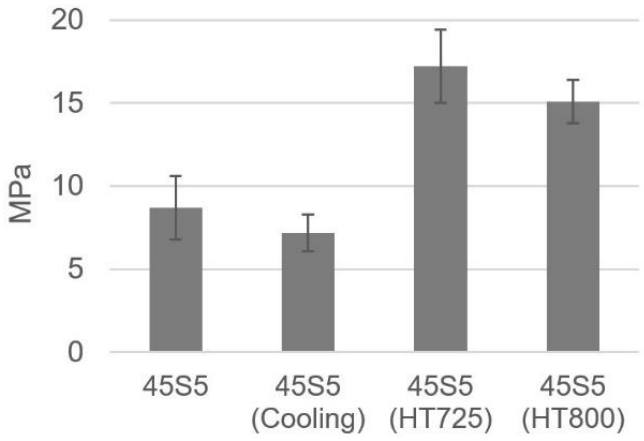

Figure 4. Tensile strength results of the different coatings

3.3. In vitro bioactivity study

In vitro tests were performed for 45S5 coatings, 45S5 with CO_2 cooling and 45S5 heat treated at 725ºC due to the better adhesion results.

The representative morphologies of the coatings before and after the exposure to HBSS during different periods are shown in Fig. 5. When bioactive glasses are in contact with simulated body fluids a HCA layer is developed, it starts with the formation of small spheres that grow and aggregate with the soaking time, generating a dense layer. After 1 day of exposure a few apatite particles can be observed over all the surfaces. After 6 days the surface of all the coatings is fully covered by the HCA layer, which indicates a good bioactivity for all the coatings.

The XRD patterns after exposure in HBSS for 14 days indicate that the surfaces of the coatings were covered by HCA. All the patterns have peaks corresponding to hydroxyapatite ($Ca_5(PO_4)_3(OH)$, Ref. code: 00-001-1008) (Fig. 3(B)). And the coatings without heat treatment present also peaks of calcium phosphate ($Ca_2O_7P_2$, Ref. code: 00-003-0605).

The bioactivity of a glass coating can be affected by many factors such as crystallinity, composition, porosity or specific surface area. Coatings obtained with cooling present less porosity, this fact could diminish the reactivity of the coating and diminish the degree of bioactivity. However, the difference is not enough to affect the formation of the apatite layer and the results reveal that CO_2 cooling during spraying does not alter the bioactivity of the coatings.

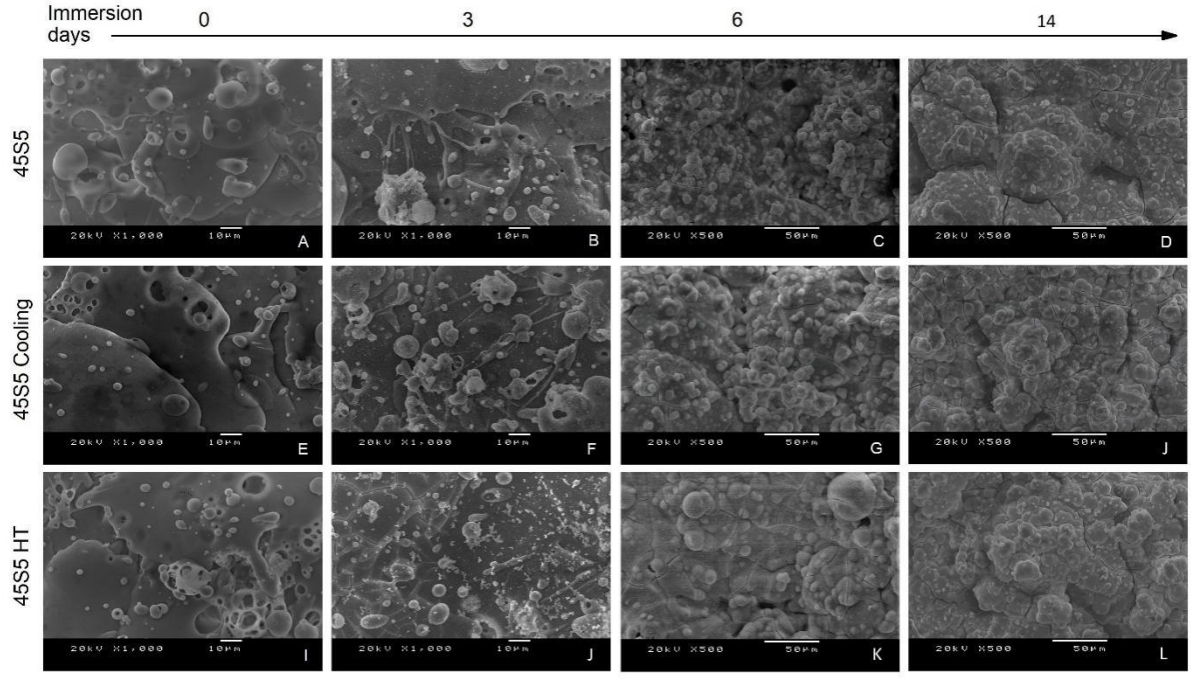

Figure 5. Morphology of samples as-sprayed (A,E,I), after 1 (B,F,J), 6 (C,G,K) and 14 (D,H,L) days of exposure to HBSS solution

Likewise the heat treatment does not affect the ability to form an apatite layer. It is expected that crystallinity can compromise the degree of bioactivity of the material, but partial crystallization not necessarily reduce it, depending on the formed phases [37]. Previous studies have reported that the $Na_6Ca_3Si_6O_{18}$ phase, detected in our coatings, is not affecting the HCA formation [38]. In our research, we have noticed that heat treated coatings allow the formation of the HCA layer, however a slight decrease in its formation rate can be seen. Particularly at 6 days (Fig. 5 (c,g,k)) less amount of apatite particles are present in heat treated coating.

The weight loss rate of coated samples after soaking in Tris-HCl solution is shown in Fig.6. The coatings obtained during cooling with carbon dioxide have similar degradation than the 45S5 coatings. It can be noticed that coatings heat treated at 725^{o}C have significantly less degradation than the other ones, it can be attributed to the crystallinity.

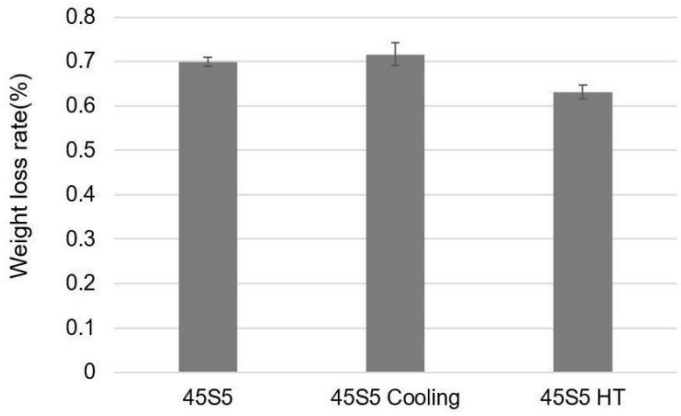

Figure 6. Weight loss rate of coated samples after soaking in Tris-HCl

In Fig.7 the results of the pH during soaking in Tris-HCl are shown. It help us to understand the ion exchange process between the coated samples and the Tris-HCl solution, the pH solution starts from 7.4 and increases to more than 7.8 for all the samples analysed. The increase of pH is higher the first hours, which indicates a fast ion exchange produced in the solution. However, there is less variation from 72h to 120h possibly indicating a stabilization value at this period.

The 45S5 and 45S5 Cooling samples present a similar variation of pH with time, consequently the ion release is almost equal for both coatings. The heat treated coatings start with a higher pH value than the other ones. However, for the rest of the periods the pH value is lower for these coatings than for the amorphous ones. Another time, this behaviour can be attributed to the acquired crystallinity of the heat treated samples, that present less ion release from the coatings, corroborating the weight loss rate results.

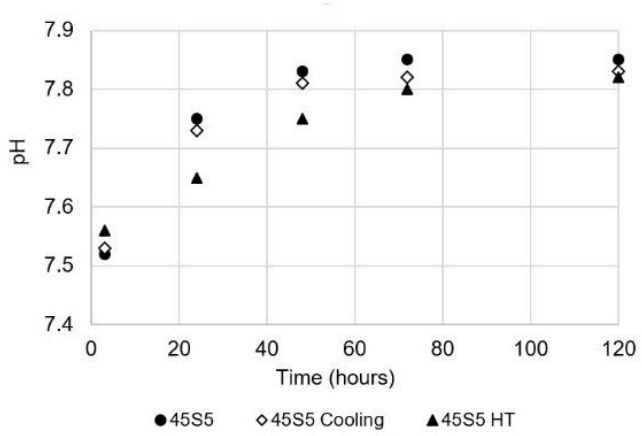

Figure 7. pH values of coated samples during soaking in Tris-HCl for different periods

4. Conclusions

The effect of cooling with CO_2 during spraying maintain the amorphous structure of the coating. Otherwise the post heat treatment generates sodium calcium silicate crystalline phase to the samples heated at 725ºC and 800ºC and sodium calcium phosphate silicate phase when heating at 800ºC.

The cooling process during spraying did not enhance the adhesion strength with the substrate, although with a post heat treatment high adhesion strengths were achieved due to the stress relaxation and the major cohesion achieved between particles. Higher values of adhesion strength were measured for coatings heat treated at 725ºC reaching a value of 17.2±2.2MPa.

The heat treatment provided a higher adhesion strength between the coating and the substrate, and preserved the bioactivity of the coatings in terms of HCA formation, but the kinetic of the HCA formation was slightly decreased. The development of a HCA layer in simulated body fluid solution is a positive indicator of the tendency of the coatings to support the mineralization process, however in terms of biological properties to prove the efficacy of the obtained coatings more studies should be developed, as cell tests.

Additionally, the degradation rate was lower for that coatings, due to the new arrangement of the glass structure. The results of the pH study in Tris-HCl solution corroborate that the ion release is higher for the amorphous coatings due to a more disrupted network.

Acknowledgements

This work was supported by Generalitat de Catalunya (SGR-1777) and Spanish Government (MAT2016-76928-C2-1-R).

References

[1] P. Ducheyne, K.E. Healy, D.W. Grainger, D.W. Hutmacher, C.J. Kirkpatrick, Comprehensive biomaterials, 2011. https://doi.org/10.1016/C2009-1-28384-5.

[2] M.G. Kaufman, J.D. Meaike, S.A. Izaddoost, Orthopedic Prosthetic Infections: Diagnosis and Orthopedic Salvage, Semin. Plast. Surg. 30 (2016) 66–72. https://doi.org/10.1055/s-0036-1580730.

[3] L.L. Hench, The story of Bioglass®, in: J. Mater. Sci. Mater. Med., 2006. https://doi.org/10.1007/s10856-006-0432-z.

[4] J.R. Jones, Review of bioactive glass: From Hench to hybrids, Acta Biomater. 9 (2013) 4457–4486. https://doi.org/10.1016/j.actbio.2012.08.023.

[5] M. Montazerian, E. Dutra Zanotto, History and trends of bioactive glass-ceramics, J. Biomed. Mater. Res. - Part A. 104 (2016) 1231–1249. https://doi.org/10.1002/jbm.a.35639.

[6] G. Kaur, V. Kumar, F. Baino, J.C. Mauro, G. Pickrell, I. Evans, O. Bretcanu, Mechanical properties of bioactive glasses, ceramics, glass-ceramics and composites: State-of-the-art review and future challenges, Mater. Sci. Eng. C. 104 (2019) 109895. https://doi.org/10.1016/j.msec.2019.109895.

[7] A. Hoppe, N.S. Güldal, A.R. Boccaccini, A review of the biological response to ionic dissolution products from bioactive glasses and glass-ceramics, Biomaterials. 32 (2011) 2757–2774. https://doi.org/10.1016/j.biomaterials.2011.01.004.

[8] I.D. Xynos, A.J. Edgar, L.D.K.K. Buttery, L.L. Hench, J.M. Polak, Gene-expression profiling of human osteoblasts following treatment with the ionic products of Bioglass® 45S5 dissolution, 2001. https://doi.org/10.1002/1097-4636(200105)55:2<151::AID-JBM1001>3.0.CO;2-D.

[9] D.S. Brauer, Bioactive glasses - Structure and properties, Angew. Chemie - Int. Ed. 54 (2015) 4160–4181. https://doi.org/10.1002/anie.201405310.

[10] S. Fagerlund, L. Hupa, M. Hupa, Dissolution patterns of biocompatible glasses in 2-Amino-2-hydroxymethyl- propane-1,3-diol (Tris) buffer, Acta Biomater. 9 (2013) 5400–5410. https://doi.org/10.1016/j.actbio.2012.08.051.

[11] S. Lopez-Esteban, E. Saiz, S. Fujino, T. Oku, K. Suganuma, A.P. Tomsia, Bioactive glass coatings for orthopedic metallic implants, J. Eur. Ceram. Soc. 23 (2003) 2921–2930. https://doi.org/10.1016/S0955-2219(03)00303-0.

[12] L.L. Hench, Chronology of Bioactive Glass Development and Clinical Applications, New J. Glas. Ceram. 03 (2013) 67–73. https://doi.org/10.4236/njgc.2013.32011.

[13] M. Peltola, K. Aitasalo, J. Suonpää, M. Varpula, A. Yli-Urpo, Bioactive glass S53P4 in frontal sinus obliteration: A long-term clinical experience, Head Neck. 28 (2006) 834–841. https://doi.org/10.1002/hed.20436.

[14] B. Ilharreborde, E. Morel, F. Fitoussi, A. Presedo, P. Souchet, G.F. Penneçot, K. Mazda, Bioactive glass as a bone substitute for spinal fusion in adolescent idiopathic scoliosis: A comparative study with iliac crest autograft, J. Pediatr. Orthop. 28 (2008) 347–351. https://doi.org/10.1097/BPO.0b013e318168d1d4.

[15] F. Carinci, A. Palmieri, M. Martinelli, V. Perrotti, A. Piattelli, G. Brunelli, M. Arlotti, F. Pezzetti, Genetic portrait of osteoblast-like cells cultured on PerioGlas, J. Oral Implantol. 33 (2007) 327–333. https://doi.org/10.1563/1548-1336(2007)33[327:GPOOCC]2.0.CO;2.

[16] J.R. Jones, D.S. Brauer, L. Hupa, D.C. Greenspan, Bioglass and Bioactive Glasses and Their Impact on Healthcare, Int. J. Appl. Glas. Sci. 7 (2016) 423–434. https://doi.org/10.1111/ijag.12252.

[17] B.J. Tai, Z. Bian, H. Jiang, D.C. Greenspan, J. Zhong, A.E. Clark, M.Q. Du, Anti-gingivitis effect of a dentifrice containing bioactive glass (NovaMin®) particulate, J. Clin. Periodontol. 33 (2006) 86–91. https://doi.org/10.1111/j.1600-051X.2005.00876.x.

[18] L. Sun, C.C. Berndt, K.A. Gross, A. Kucuk, Material fundamentals and clinical performance of plasma-sprayed hydroxyapatite coatings: a review., J. Biomed. Mater. Res. 58 (2001) 570–592. https://doi.org/10.1002/jbm.1056.

[19] H. Melero, J. Fernández, S. Dosta, J. Guilemany, Caracterización de nuevos recubrimientos biocompatibles de hidroxiapatita-TiO2 obtenidos mediante proyección térmica de alta velocidad, Bol. La Soc. Esp. Ceram. y Vidr. 50 (2011) 59–64. https://doi.org/10.3989/cyv.082011.

[20] E. Kergourlay, D. Grossin, N. Cinca, C. Josse, S. Dosta, G. Bertrand, I. Garcia, J.M. Guilemany, C. Rey, First Cold Spraying of Carbonated Biomimetic Nanocrystalline Apatite on Ti6Al4V: Physical-Chemical, Microstructural, and Preliminary Mechanical Characterizations, Adv. Eng. Mater. 18 (2016) 496–500. https://doi.org/10.1002/adem.201500409.

[21] V. Cannillo, F. Pierli, S. Sampath, C. Siligardi, Thermal and physical characterisation of apatite/wollastonite bioactive glass-ceramics, J. Eur. Ceram. Soc. 29 (2009) 611–619. https://doi.org/10.1016/j.jeurceramsoc.2008.06.034.

[22] V.L. Calvo, M.V. Cabedo, E. Bannier, E.C. Recacha, A.R. Boccaccini, L.C. Arias, E.S. Vilches, 45S5 bioactive glass coatings by atmospheric plasma spraying obtained from feedstocks prepared by different routes, J. Mater. Sci. 49 (2014) 7933–7942. https://doi.org/10.1007/s10853-014-8519-2.

[23] S. Bano, I. Ahmed, D.M. Grant, A. Nommeots-Nomm, T. Hussain, Effect of processing on microstructure, mechanical properties and dissolution behaviour in SBF of Bioglass (45S5) coatings deposited by Suspension High Velocity Oxy Fuel (SHVOF) thermal spray, Surf. Coatings Technol. 372 (2019) 229–238. https://doi.org/10.1016/j.surfcoat.2019.05.038.

[24] A. Cattini, D. Bellucci, A. Sola, L. Pawłowski, V. Cannillo, Functional bioactive glass topcoats on hydroxyapatite coatings: Analysis of microstructure and in-vitro bioactivity, Surf. Coatings Technol. 240 (2014) 110–117. https://doi.org/10.1016/j.surfcoat.2013.12.023.

[25] E. Cañas, M.J. Orts, A.R. Boccaccini, E. Sánchez, Solution Precursor Plasma Spraying (SPPS): A novel and simple process to obtain bioactive glass coatings, Mater. Lett. 223 (2018) 198–202. https://doi.org/10.1016/j.matlet.2018.04.031.

[26] G. Bolelli, D. Bellucci, V. Cannillo, R. Gadow, A. Killinger, L. Lusvarghi, P. Müller, A. Sola, Comparison between Suspension Plasma Sprayed and High Velocity Suspension Flame Sprayed bioactive coatings, Surf. Coatings Technol. 280 (2015) 232–249. https://doi.org/10.1016/j.surfcoat.2015.08.039.

[27] O. Rojas, M. Prudent, M.E. López, F. Vargas, H. Ageorges, Influence of Atmospheric Plasma Spraying Parameters on Porosity Formation in Coatings Manufactured from 45S5 Bioglass® powder, J. Therm. Spray Technol. 29 (2020) 185–198. https://doi.org/10.1007/s11666-019-00952-3.

[28] E. Verné, M. Miola, C. Vitale Brovarone, M. Cannas, S. Gatti, G. Fucale, G. Maina, A. Massé, S. Di Nunzio, Surface silver-doping of biocompatible glass to induce antibacterial properties. Part I: Massive glass, J. Mater. Sci. Mater. Med. 20 (2009) 733–740. https://doi.org/10.1007/s10856-008-3617-9.

[29] S.D. Newman, N. Lotfibakhshaiesh, M. O'Donnell, X.F. Walboomers, N. Horwood, J.A. Jansen, A.A. Amis, J.P. Cobb, M.M. Stevens, Enhanced Osseous Implant Fixation with Strontium-Substituted Bioactive Glass Coating, Tissue Eng. Part A. 20 (2014) 1850–1857. https://doi.org/10.1089/ten.tea.2013.0304.

[30] V. Cannillo, A. Sola, Different approaches to produce coatings with bioactive glasses: Enamelling vs plasma spraying, J. Eur. Ceram. Soc. 30 (2010) 2031–2039.

[31] D. Bellucci, V. Cannillo, A. Sola, An overview of the effects of thermal processing on bioactive glasses, Sci. Sinter. 42 (2010) 307–320. https://doi.org/10.2298/SOS1003307B.

[32] A. Ducato, L. Fratini, M. La Cascia, G. Mazzola, An automated visual inspection system for the classification of the phases of Ti-6Al-4V titanium alloy, in: Lect. Notes Comput. Sci. (Including Subser. Lect. Notes Artif. Intell. Lect. Notes Bioinformatics), 2013: pp. 362–369. https://doi.org/10.1007/978-3-642-40246-3_45.

[33] Q. Zhao, D. He, L. Zhao, X. Li, In-vitro study of microplasma sprayed hydroxyapatite coatings in Hanks balanced salt solution, Mater. Manuf. Process. 26 (2011) 175–180. https://doi.org/10.1080/10426914.2010.498071.

[34] J.A. Rincón-López, J.A. Hermann-Muñoz, N. Cinca-Luis, B. Garrido-Domiguez, I. García-Cano, J.M. Guilemany-Casadamon, J.M. Alvarado-Orozco, J. Muñoz-Saldaña, Preferred Growth Orientation of Apatite Crystals on Biological Hydroxyapatite Enriched with Bioactive Glass: A Biomimetic Behavior, Cryst. Growth Des. 19 (2019) 5005–5018. https://doi.org/10.1021/acs.cgd.9b00268.

[35] S.A. Omar, J. Ballarre, Y. Castro, E. Martinez Campos, W. Schreiner, A. Durán, S.M. Cere, 58S and 68S sol-gel glass-like bioactive coatings for enhancing the implant performance of AZ91D magnesium alloy, Surf. Coatings Technol. 400 (2020). https://doi.org/10.1016/j.surfcoat.2020.126224.

[36] L. Lefebvre, J. Chevalier, L. Gremillard, R. Zenati, G. Thollet, D. Bernache-Assolant, A. Govin, Structural transformations of bioactive glass 45S5 with thermal treatments, Acta Mater. 55 (2007) 3305–3313. https://doi.org/10.1016/j.actamat.2007.01.029.

[37] J. Chevalier, L. Gremillard, Ceramics for medical applications: A picture for the next 20 years, J. Eur. Ceram. Soc. 29 (2009) 1245–1255. https://doi.org/10.1016/j.jeurceramsoc.2008.08.025.

[38] S. Grasso, R.K. Chinnam, H. Porwal, A.R. Boccaccini, M.J. Reece, Low temperature spark plasma sintering of 45S5 Bioglass®, J. Non. Cryst. Solids. 362 (2013) 25–29. https://doi.org/10.1016/j.jnoncrysol.2012.11.009.

Improving the bond strength of bioactive glass coatings obtained by atmospheric plasma spraying

B. Garrido, A. Martín-Morata, I.G. Cano, S.Dosta

Surface and Coatings Technology (May 2022), Submitted

Abstract

Osseointegration is a necessary process for the successful bonding of implants. Modification of biomaterials surface is a possible strategy in order to improve the bioactive response of the implanted materials. Bioactive glasses are materials resembling the mineral part of the bone and can be used as coating material onto metallic implants. However, the significant difference in the coefficient of thermal expansion (CTE) between the metallic substrate and the bioactive glass material makes difficult to obtain enough coating adhesion.

In order to achieve adequate coatings to be used in orthopaedic implants, some strategies were studied to improve the bond strength of bioactive glass coatings. The different approaches were considered: first, producing agglomerated bioactive glass powders; the second strategy was based on designing different coatings combining hydroxyapatite (HA) with bioactive glass; other strategies involved the pre-heating of the substrate and the application of a post-thermal treatment.

Bioactive coatings were produced by atmospheric plasma spray (APS) onto titanium alloy substrates. The studied coatings were characterized in microstructure, adhesion strength, and bioactivity. It was found that a significant improvement in adhesion strength was obtained for the developed coatings. However, this improvement involved a reduction in the bioactive response of the coatings.

Keywords: Bioactive glass; Thermal spray; Bioactivity; Atmospheric plasma spray; Coatings; Bond strength

1. Introduction

Implant modification by developing coatings on its surface is considered one of the most effective techniques to enhance the osseointegration of implanted biomaterials [1]. However, effective improvement is only possible if the coating stays well adhered to the substrate until a good bonding with the bone tissue is obtained [2]. Nowadays, thermal spraying, particularly atmospheric plasma spraying (APS) is one of the most common methods employed to produce bioactive ceramic coatings [3].

APS is a deposition technique where the powder is injected into the flame by a carrier gas, usually argon. The powder particles are melted and accelerated to the substrate forming the coating during the process. A modulated mixture of argon and hydrogen is used to produce the proper plasma jet that enables the melting and acceleration of the particles, considering the feedstock powder features [4]. The high temperatures of the plasma allow the spraying of materials with high melting temperatures and low thermal conductivity, such as ceramics [3,5,6].

Hydroxyapatite (HA) coatings produced by APS have been widely used and widely accepted in medicine in the last decades [3,7]. However, the failure rate of implants, either due to insufficient osseointegration or infection, leaves room for improvement [8–11]. Increasing the lifetime of implants and their success rate is one of the major challenges in orthopaedic implant technology. Developing new bioactive coatings is an interesting approach to address that issue.

Bioactive glasses are a family of glasses with a similar composition to the inorganic component of the bone's mineral phase. These biomaterials have unique properties due to a more open structure than conventional glasses [12]. Bioactive glasses were discovered in 1969 by L.L. Hench [13] and arrived in medicine as a promising material capable of bonding to both hard and soft tissues. Furthermore, these reactive glasses exhibit an encouraging cellular response compared to other biomaterials [14].

Bioactive glass coatings have been developed in recent years using different techniques, such as electrophoretic deposition, sol-gel, enamelling, laser cladding, or thermal spraying. However, the large difference in thermal expansion coefficient (CTE) between metallic biomaterials and the bioactive glass coatings makes it challenging to obtain enough coating adhesion to commercialize them. In order to use these coating materials, an improvement in their adhesion strength becomes a necessity. Minimum bond strength of 22 MPa can ensure the mechanical integrity of the coatings according to international regulations. In a previous study [15], the authors applied heat treatment to a bioactive coating to improve the bonding with the metallic substrate. The coating obtained doubled the adhesion value with the heat treatment, reaching a bond strength of 17.2 MPa.

The present work aims to deeply evaluate strategies to overcome the low adhesion of bioactive glass coatings deposited by APS. During the present investigation, different approaches were considered: changing the morphology of the feedstock powders, with this new arrangement of the material could favour the adhesion with the substrate compared to the quartered particles; incorporating HA as support material, taking advantage of the excellent adhesion of HA with the metallic substrate; applying heat before or after the spraying process to reduce internal stresses in the coating that could affect the bond to the substrate. The developed coatings were studied, analysing, in particular, their mechanical and biological properties. The overall objective was to create a coating with suitable mechanical properties while ensuring its bioactivity.

2. Experimental methods

2.1. Powder and substrate

Two commercial powders were used to produce the designed coatings: a sintered HA Captal®30 powder (Plasma Biotal Limited, United Kingdom) with crystallinity above 95% and a bioactive glass powder 45S5 (Denfotex Research, United Kingdom) manufactured by the usual melt-quenching method. In addition, the same bioactive glass powder was used to produce the agglomerated glass powders.

Titanium G5 (Ibermetal, Spain) was used as substrate material. Particularly, discs with 25 mm of diameter and 10 mm of height were used for tensile strength tests. For the metallographic characterization of the coatings, rectangular substrates measuring 100 × 20 × 5 mm were used. Finally, for the in vitro studies, coatings were deposited onto discs with a diameter of 9 mm and thickness of 1 mm.

2.2. Agglomeration of powder

The agglomeration of bioactive glass powders was performed in a conventional method, where a binder was used to join the powder particles, which was later removed by heating [16].

Firstly, the 45S5 commercial powder was milled using planetary ball mill equipment (PM 400, Retsch, Haan, Germany), with Y-ZrO_2 balls of 5 and 10 mm diameter and grinding jars of the same material. The revolution speed was fixed at 400 rpm and grinding was done for two hours, since no further particle size reduction was observed for longer processes. The friction and the high impact that particles suffer during the process produced the particle size reduction.

Once the powder was milled, a sieving step was done to remove the large particles. The collected fraction below 40 μm was combined with a PVA solution (10 g of PVA 87-90% hydrolysed in 150 mL of Milli-Q water) until a semi-wet state of the powder was reached. The

amount of PVA solution added to the milled powders was adjusted to achieve proper agglomerates; the best results were observed when adding 0.2 mL of solution per gram of milled powder.

After incorporating the binding agent, powders were spread on an aluminium foil and let dry at room temperature for 24 hours. Subsequently, a sieving step was done, and a fraction between 20 and 80 µm was collected. This way, agglomerates with a proper size for APS were obtained [17,18].

The final step consisted in removing the binder agent. For this purpose, agglomerated particles were heated using a high-temperature chamber furnace (CRN 4-18, Hobersal, Barcelona, Spain). The heating rate was 10ºC/min up to 500ºC, followed by a dwell step of 1h and finally cooling to room temperature at 10ºC/min. Burnout of the binder was done at 500ºC, below glass transition temperature of the 45S5 (550ºC) [19] to avoid phase transformations and above degradation temperature of PVA, which occurs between 200ºC and 300ºC [16].

2.3. Design of coatings

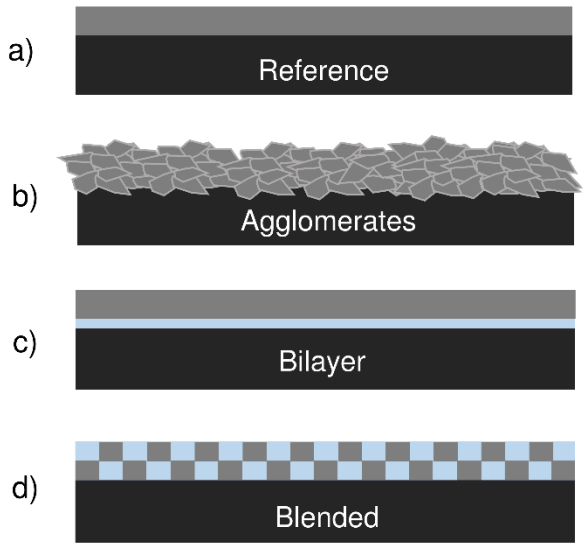

Figure 1. Designed coatings: a) Reference, b) Agglomerates, c) Bilayer and d) Blended

The different strategies addressed to enhance the bond strength of the bioactive glass coatings are represented in Figure 1. (i) The first coating designed involved agglomerated 45S5 particles, produced as described previously (agglomeration of powder). This coating was named “Agglomerates”. (ii) The second coating consisted of an anchor layer of HA between the glass and the titanium alloy to mitigate the large difference in CTE between these materials. This coating was called “Bilayer”. (iii) Another coating consisted of a manual blend of HA and 45S5 powders in a 1:1 ratio by weight. This coating was named “Blended”. (iv)

Finally, a coating produced with the bioactive glass powder was used for comparison purposes. This coating was called “Reference”.

Furthermore, two approaches were considered for the developed coatings to reduce the residual stress and enhance the coating adhesion of the bioactive glasses with the substrate. First, the effect of pre-heating the substrate immediately prior to deposition was assessed. The heating was applied by scanning the torch over the surface of the substrate for one entire cycle and maintaining the same spraying conditions. The pre-heating temperature (218ºC ± 2ºC) was measured with a digital thermometer (PCE-T390, PCE Instruments, Durham, United Kingdom). The second approach consisted of asses the effect of applying a post-thermal treatment at 725ºC for five hours to the coatings, following the process described in our previous research [15]. The different coatings performed are detailed in Table 1.

Table 1. References of the different coatings developed

Reference name	Pre-treatment	Post-treatment
Reference	-	-
Reference SH	Surface heating	-
Reference TT	-	Thermal treatment
Agglomerates	-	-
Agglomerates SH	Surface heating	-
Agglomerates TT	-	Thermal treatment
Bilayer	-	-
Bilayer SH	Surface heating	-
Bilayer TT	-	Thermal treatment
Blended	-	-
Blended SH	Surface heating	-
Blended TT	-	Thermal treatment

2.4. Coating deposition

For the coating deposition, APS equipment (Plasma-Technik A3000S, Sulzer Metco AG, Wohlen, Switzerland) with an F4 plasma torch was used with argon as the primary carrier gas and hydrogen as secondary gas for the plume formation. The powders were deposited onto titanium alloy substrates previously grit-blasted (MAB-4, MAB industrial, Barcelona, Spain) with corundum G24 (grit size 800 µm) at 0.5 MPa. Before the spraying process, the substrates were cleaned with ethanol. As a result, the surface roughness after the grit-blasting process was Ra = 5.7 ± 1.1 µm and Rz = 37.8 ± 3.3 µm.

The parameters used for coating deposition were selected according to the powder characteristics. For the glass powder, the chosen parameters provided quite energetic conditions to make able the melting of the glass powder; these parameters are referred to as type A in Table 2. The parameters selected for the HA powder were determined by the results found in a study developed in our group included in the thesis of Mireia Gaona (University of Barcelona, 2007). The influence of some spraying parameters on different properties such as crystallinity, adhesion strength, and thickness was analysed. These parameters are determined as type B in Table 2.

The Reference and Agglomerates coatings and the top layer of Bilayer coating were produced using type A spraying conditions. Next, the Blended coating was sprayed using type B conditions because the high plasma energy involved in type A caused severe phase changes in HA. Moreover, the coatings containing HA using type A were unsatisfactory. Then, the Blended coating and the lower layer of the Bilayer coating were deposited using type B conditions.

Table 2. Plasma spraying parameters used to produce the coatings

	Type A	**Type B**
Primary gas (Ar), flow rate (slpm)	35	50
Secondary gas (H_2), flow rate (slpm)	12	1
Arc Current (A)	600	500
Stand-off distance (mm)	80	80

2.5. Characterisation of the powder and coating

The morphology and microstructure of the powders and coatings were determined using a scanning electron microscope (SEM) (Phenom ProX, Phenom-World BV, Eindhoven, The Netherlands) equipped with energy-dispersive X-ray diffraction. To analyse the cross-sections of the powders and coatings, samples were prepared by cold mounting resin and abraded with silicon carbide abrasive papers up to P4000 (grit size 5 µm). The polishing of the samples was carried out with 1 µm diamond slurry. Before the microscopy studies, the samples were coated with a gold layer to make them conductive using an SEM coating unit (E-5000, Polaron, Watford, England).

The tapped density of the different powders was measured. Each powder was tapped regularly in a graduated cylinder to settle the powder inside the cylinder. The filling and tapping process was repeated until the powder volume remained fixed at 5 mL. When this occurred, the amount of powder used was weighted.

The particle size distribution of the sieved powders was determined through a laser diffraction particle size analyser (LS 13 320, Beckman Coulter, California, USA).

To determine the bond strength of the coatings, a mechanical testing machine (ME-402/10, Servosis, Madrid, Spain) was used following the ASTM C633-13 (Standard test method for adhesion or cohesion strength of thermal spray coatings). Three coated samples of each type were glued using HTK ULTRA BOND 100® glue (HTK, Germany) to grit blasted counter-test pieces. Then, normal tensile stress was applied to the coating with the displacement rate set at 0.02 mm/s until fracture took place. In addition to performing the test on the developed coatings, it was also done on the coatings after one day of immersion in hank's balanced salt solution (HBSS) (Sigma-Aldrich, Germany) at 37ºC.

2.6. Ability to form apatite and degradation assessment

The bone-bonding ability of the coatings was evaluated by an in vitro test following the ISO 23317 (Implants for surgery - In vitro evaluation for the apatite-forming ability of implant materials). Three samples of each coating type were immersed, in vertical position, in HBSS solution inside polypropylene containers placed in a thermostatic bath with agitation at 37oC. The HCA formation was evaluated at different periods (0, 3, 7, and 14 days). The solution was refreshed twice a week to avoid ionic saturation. After each period, samples were rinsed with ultra-pure water and dried for 24h at room temperature.

The formation of the HCA layer on the coatings was assessed at different periods by the surface inspection of the samples using SEM equipment. All the samples were coated with a gold layer to increase their conductivity prior to this observation. Furthermore, the cross-section of the formed layer was analysed for the samples immersed during the most extended period. For this examination, the cross-sections were prepared as described previously. Finally, the samples were gold coated and examined by SEM after drying in a desiccator for 48h.

The degradation behaviour of the different bioactive coatings was evaluated following the specifications of the ISO 10993-14 (Biological evaluation of medical devices - Part 14: Identification and quantification of degradation products from ceramics). Samples were immersed in a buffered solution of Tris-HCl with pH adjusted to 7.4 ± 0.1 at 37 ± 1ºC for 120h. After the test, the samples were rinsed with ultra-pure water and dried overnight at 120ºC. The loss of weight suffered by the samples was determined by measuring their weight before and after the test with a high precision scale (CPA225D, Sartorius, Gottingen, Germany). Moreover, pH variation caused by the dissolution process was analysed by recording the pH values after the test using a universal pH meter (Hach, Spain). Finally, the concentration of elements released from the coatings (silicon, calcium, phosphorus, and sodium) was

determined using inductively coupled plasma optical emission spectrometry (ICP-OES) (Optima 8300, PerkinElmer, Waltham, USA).

3. Results and discussion

3.1. Powder characterisation

The SEM analysis performed on the powders allowed us to establish the difference in their morphology and size, as shown in Figure 2. Particularly, the particles of HA powders show a spherical morphology composed of small particles forming aggregates. This microstructure is typical for agglomerated and sintered powder, where small particles are compacted and bonded together by applying heat and pressure. Furthermore, the cross-section of the HA powders also reveals some porosity. On the contrary, the 45S5 glass particles are dense and irregular, with the presence of corners and sharp edges. This shape is consistent with the manufacturing process where the material is crushed after the melt-quenching. Moreover, the particles observed are quite similar in size to each other. Finally, the agglomerated powders produced are composed of small particles, between 1 and 20 µm approximately. These aggregated particles present an irregular and porous morphology.

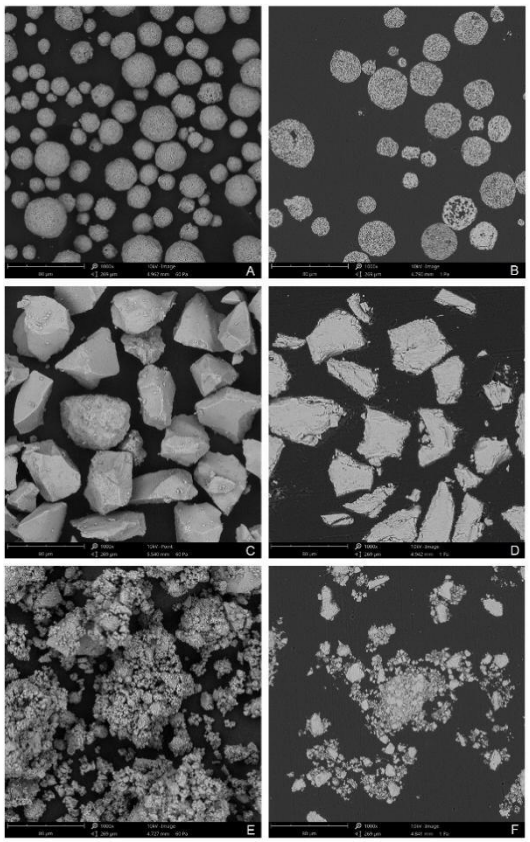

Figure 2. Free surface and cross-section of powders: (A,B) HA, (C,D), 45S5 bioactive glass and (E,F) 45S5 agglomerated

The particle size distribution of the powders measured by laser diffraction can be observed in Figure 3, and the characteristic values related to their size distribution are found in Table 3. HA powder, represented by a dotted line, exhibits a narrow distribution, and most of the particles are in the range of 20 to 40 µm. For glass particles, the distribution is also in a narrow range, represented by a dashed line, but in that case, most of the particles have a size between 10 and 80 µm. By contrast, the manufacturing process of the agglomerated powder has resulted in a broader particle size distribution with a bimodal nature, represented by the solid line in the graph. The values obtained with this technique are consistent with the observations by microscopy.

The values of the tapped density are shown in Table 3. It can be seen how the change in morphology of the glass particles has caused a notable reduction in the density of the agglomerated powders when compared to the original glass powder.

Table 3. Tapped density and particle size distribution in volume of the powders

	Tapped density (g/cm^3)	**d_{10} (µm)**	**d_{50} (µm)**	**d_{90} (µm)**
HA	1.39	18.0	28.5	42.2
45S5	1.38	10.7	55.1	78.4
45S5 Agglomerated	0.92	7.1	28.5	82.7

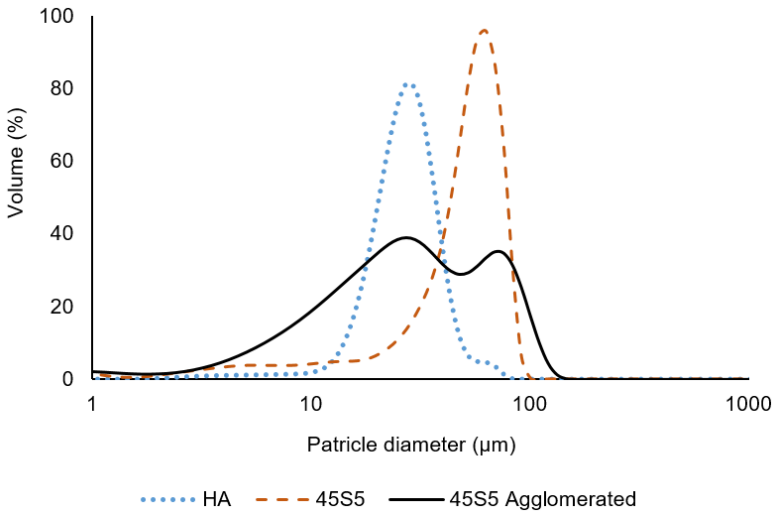

Figure 3. Particle size distribution in volume of the powders

3.2. Bond strength tests

When the osseointegration process starts, the interface must remain immobile for the bond to form. For this purpose, the coating should stay well adhered when the device is implanted and thus facilitate a good bonding with the bone tissue. During the osseointegration process, the stability of the implant-bone fixation depends on the initial mechanical stability that

decreases over time while biological stability increases. It should be noticed that when osseointegration is accomplished, the strength of the bioactive bond formed is equal or higher than that of the host bone.

In the first part of the study, the bond of the coatings listed in Table 1 was evaluated. The bond strength results of the coatings without immersion and after 1 day of immersion in physiological solution are detailed in Table 4, Figure 4, and Figure 5.

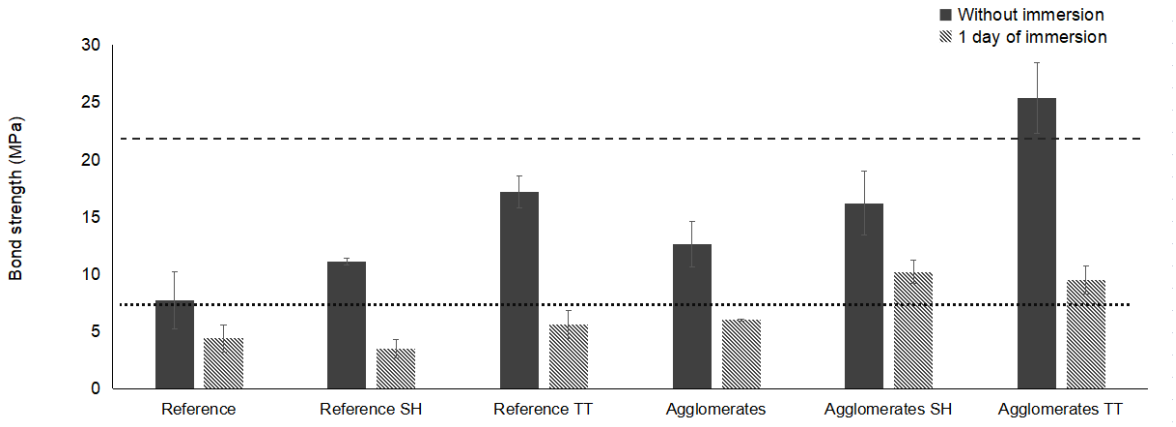

Figure 4. Bond strength of the bioactive glass pure coatings without immersion and after 1 day of immersion in HBSS solution (slashed line: minimum value required for non-immersed coatings according to regulations; dotted line: the value of HA after immersion)

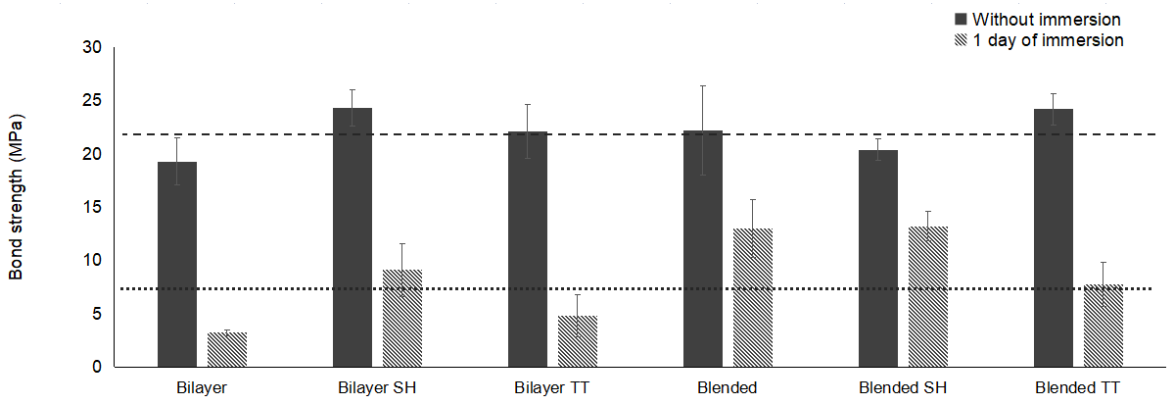

Figure 5. Bond strength of the coatings incorporating HA without immersion and after 1 day of immersion in HBSS solution (slashed line: minimum value required for non-immersed coatings according to regulations; dotted line: the value of HA after immersion)

The first design to improve the bonding of the coating with the substrate consisted of modifying the morphology of the feedstock powder. Through the agglomeration process, powders with lower density and higher porosity and specific surface were obtained compared to the commercial one. A notable increase in bond strength was observed when comparing Agglomerates coatings to the Reference coatings for the same spraying conditions (12.6 ±

2.0 MPa to 7.7 ± 2.5 MPa). The results may suggest that agglomerated powders melt more easily than the commercial particles as the agglomerated powder has high porosity and is composed of smaller particles that cause faster heating of the material [20]. The proper melting of the particles can favour the bond with the substrate and, therefore, increase the bond strength.

Table 4. Bond strength of the designed coatings before and after 1 day of immersion

Coating type	Bond strength (MPa)		Bond strength loss after one day of immersion (%)
	Without immersion	After one day of immersion	
Reference	7.7 ± 2.5	4.4 ± 1.2	43
Reference SH	11.1 ± 0.3	3.5 ± 0.8	68
Reference TT	17.2 ± 1.4	5.6 ± 1.2	67
Agglomerates	12.6 ± 2.0	6.0 ± 0.1	52
Agglomerates SH	16.2 ± 2.8	10.2 ± 1.0	37
Agglomerates TT	25.4 ± 3.1	9.5 ± 1.2	63
Bilayer	19.3 ± 2.2	3.2 ± 0.3	83
Bilayer SH	24.3 ± 1.7	9.1 ± 2.5	63
Bilayer TT	22.1 ± 2.5	4.8 ± 2.0	78
Blended	22.2 ± 4.2	13.0 ± 2.7	41
Blended SH	20.4 ± 1.0	13.2 ± 1.4	35
Blended TT	24.2 ± 1.5	7.7 ± 2.1	68
HA	≈ 39.0 ± 5.0	≈ 7.5 ± 2.5	81

Table 5: Percentage of bond strength increase with pre and post treatments when compared to the same coating type

Coating type	Bond strength increase coating type (%)	
	SH	TT
Reference	44	123
Agglomerates	29	102
Bilayer	26	15
Blended	-8	9

Another of the strategies developed to improve the bonding of bioactive glass coatings involved the incorporation of HA because of its greater affinity with titanium alloy. HA has a high acceptance and commercialization in orthopaedic and dental implants; however, it has a lower bioactive capacity than bioactive glasses. In this line, two types of coating were

considered: Bilayer that included an intermediate layer of HA between the substrate and the glass layer and Blended, formed by the mixture of HA and glass powders. In both cases, the presence of HA caused a significant improvement (more than twice) in the bond strength of the coatings compared to the Reference coating. This enhancement can be explained by the minor mismatch of the CTE of HA (13.9×10^{-6} ºC [21]) and Ti6Al4V ($9.5\text{-}10.5 \times 10^{-6}$ ºC [22]) than 45S5 (15.1×10^{-6} ºC [23]) and the substrate. The primary mechanism related to the residual stresses, which affect the integrity of the coatings, occurs after deposition, during the cooling process to room temperature. A significant mismatch of the CTEs of different materials is why large residual stresses result after cooling [24]**.** Moreover, it is appreciated that the failure of Bilayer coating is cohesive between HA and bioactive glass layer and not in the interface with the substrate.

In general, the influence of surface heating resulted in a substantial increase in bond strength, as can be seen in Table 5. The large temperature difference between the impinging particles onto the unheated substrate gives rise to high interface stresses. Thus, by pre-heating the substrate, the stress generated in the deposited particles can be reduced [25]. For the Blended coating, this pre-heating of the surface did not cause an enhancement in adhesion.

The application of the thermal treatment resulted in greater adherence to the coatings. This increase was exceptionally high for coatings containing only bioactive glass, increasing adhesion by 123% for the Reference coatings and 102% for the Agglomerates. The enhancement of mechanical properties of glass materials by a thermal treatment has been demonstrated in previous studies [15,26,27]. When heating is done above the glass transition temperature of the glass, a viscous state is achieved that allows for better inter-particle cohesion and stress relaxation. Moreover, the crystallization of some phases occurs during the post-treatment, which improves the mechanical properties of the material.

In line with the regulations (ASTM F1147-05 Standard Test Method for Tension Testing of Calcium Phosphate and Metallic Coatings), calcium phosphate and metallic coatings adhered to dense metal substrates require a minimum adhesion strength of 22 MPa to be suitable for orthopaedic applications. The coatings that meet this requirement were: Agglomerates TT, Bilayer SH, Bilayer TT, Blended and Blended TT.

It is important that when the coatings are in contact with physiological fluid, as occurs when they are implanted, the impact on tensile strength is moderate since a good fixation promotes the stability and success of the implants. In addition to measuring the adherence of the coatings, this assessment was also analysed after 1 day of immersion in physiological solution. The bond strength value corresponding to pure HA coating is 39.0 ± 5.0 MPa. This coating was produced with the spraying conditions type B (Table 2) in Gaona's thesis

(University of Barcelona, 2007). After one day of immersion, the HA coating suffered a severe loss of bond strength (7.0 ± 2.5 MPa), as shown in Table 4.

Regarding the developed coatings in this study, the percentage of bond strength loss after one day of immersion was lower than in the HA coating, except for the Bilayer coating, which presented a similar value.

Moreover, it should be noted that Agglomerates SH, Agglomerates TT, Bilayer SH, Blended, Blended SH, and Blended TT coatings had a greater bond strength after one day of immersion than HA coating.

Therefore, concerning the whole bond strength study, the coatings that reached bond strength values that meet the requirements for implants and at the same time achieved an adherence value after immersion in physiological solution greater than HA were Agglomerates TT, Bilayer SH, Blended, and Blended TT.

3.3. In vitro bioactivity study - Ability to form apatite

In addition to having a good bond strength, it is important that the coatings also can stimulate bone regeneration. Therefore, bioactivity and degradation tests were performed to evaluate their biological response to physiological solutions. This part of the study was carried out on some of the coatings developed. Since this part of the study mainly affects the upper part of the coating, SH coatings were dismissed, due to the similarity with their analogues. Regarding the thermally treated samples, only the Agglomerates TT were selected since the adhesion improvement for the coatings containing HA was very slight, and the Reference TT was already analysed in our previous study [15]. Thus, the coatings considered most relevant for this part of the study were: Reference, Agglomerates, Agglomerates TT, Bilayer and Blended.

The biomaterials forming the coatings, bioactive glass and HA, are expected to provide bioactive capacity to the samples. Due to the great importance of the HCA layer formation in the osseointegration process, the coatings were immersed in physiological solution for fourteen days. The surface of the coatings was periodically evaluated to analyse the kinetics in the formation of an HCA layer on their surfaces.

In Figure 6, the surface of the coatings before the test and after three and fourteen days of immersion in HBSS are shown. The surfaces of the coatings without immersion formed by agglomerated particles (Agglomerates and Agglomerates TT) showed high porosity, particularly coatings that were not heat treated, since heating can reduce the porosity [28]. In addition, fingered splats corresponding to molten glass particles were observed on the surface of Reference and Bilayer coatings. While on the surface of the Blended coatings, it is possible to appreciate the presence of HA particles in combination with glass particles.

The formation of the HCA layer begins with the nucleation of small apatite spheres, which grow and form aggregated deposits. The continuous formation and growth of apatite deposits lead to a layer covering the bioactive material. After three days of immersion, Reference, Agglomerates and Bilayer coatings showed a continuous layer of HCA on their surface, revealing the rapid growth of the apatite layer on these surfaces. On the surface of the Blended and Agglomerates TT coatings, it is possible to appreciate the presence of small spheres of apatite since these coatings are still in an early stage of the HCA layer formation. In addition, it can be seen how in the Blended coating, the deposits of apatite were formed on the top of glass particles, which are more reactive than HA areas. In the final period, the surface of all the coatings was fully covered by a continuous HCA layer.

The tests results suggest that Reference, Agglomerates, and Bilayer coatings promote a fast HCA layer growth.

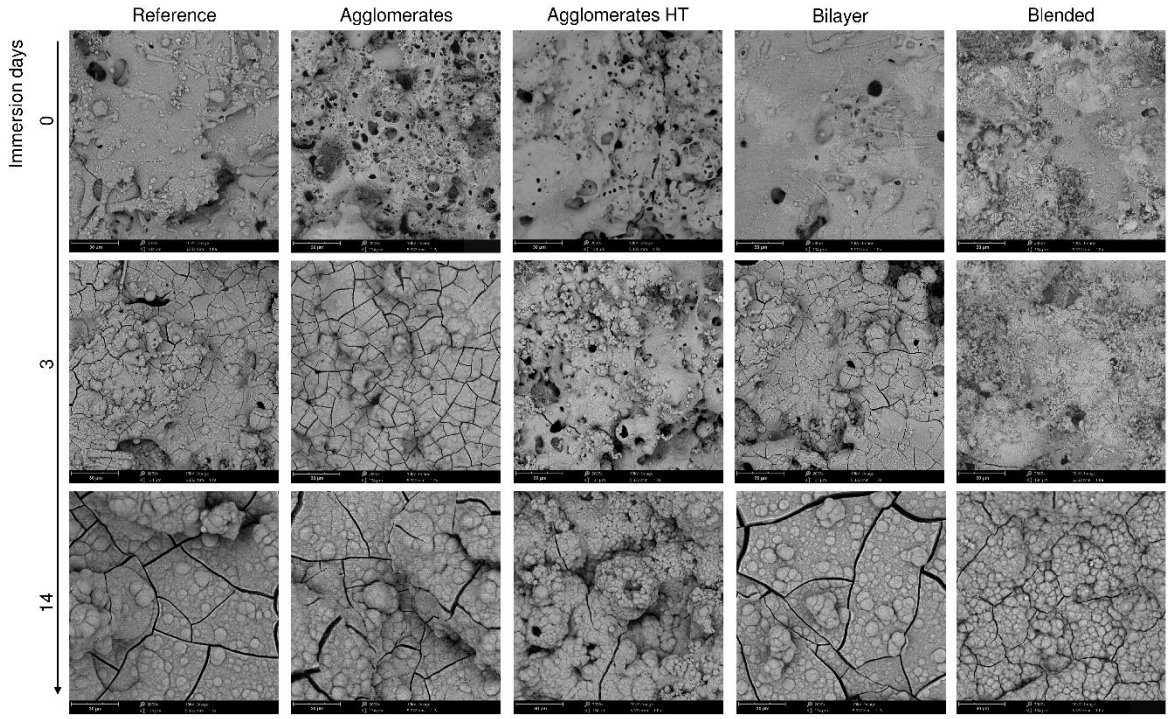

Figure 6. SEM images of the samples without immersion and after soaking in HBSS for different times: after 3 and 14 days

The cross-section of the HCA layer formed after 14 days of immersion can be observed in Figure 7. It is possible to see that a continuous layer (light grey) is formed throughout all the surfaces of the coatings after this period. For the Reference, Agglomerates and Bilayer coatings, a thicker HCA layer was formed, with a thickness of 9.9 ± 2.1 µm, 9.7 ± 1.5 µm and 8.8 ± 0.7 µm, respectively. The thickness of the HCA layer formed onto the surfaces of the Agglomerates TT and Blended coatings reached lower values, 6.7 ± 1.1 µm and 6.7 ± 1.7 µm.

The results of the cross-sections are in agreement with the SEM images in Figure 5. The fast HCA layer growth for the Reference, Agglomerates, and Bilayer coatings is corroborated. Furthermore, in these cross-sections, it is also possible to appreciate a significant internal porosity in the Reference, Agglomerates, Agglomerates TT coatings, and the upper layer of the Bilayer coating, which is entirely made of glass. In contrast, the HA layer of the Bilayer coating and the Blended coating present a dense microstructure after deposition.

As expected, the different strategies studied give rise to bioactive coatings due to the materials composing the coatings. However, a great difference has been noted in the kinetics of formation of the HCA layer among these coatings.

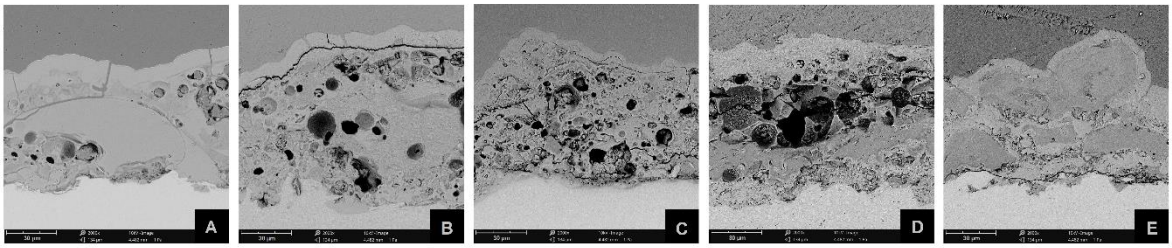

Figure 7. Cross-section micrographs showing the HCA layer after 14 days of immersion in HBSS

3.4. Degradation assessment

The degradation rate and the ion release of bioactive materials are strongly linked to their osseointegration ability. Therefore, the degradation behaviour of the designed coatings was evaluated to a further understanding of their biological capabilities.

The coatings degradation was characterized by the weight loss and ionic dissolution at different periods after immersion in physiological fluid and by the pH values recorded in the solution after the test. The percentages of samples weight loss are illustrated in Figure 8.

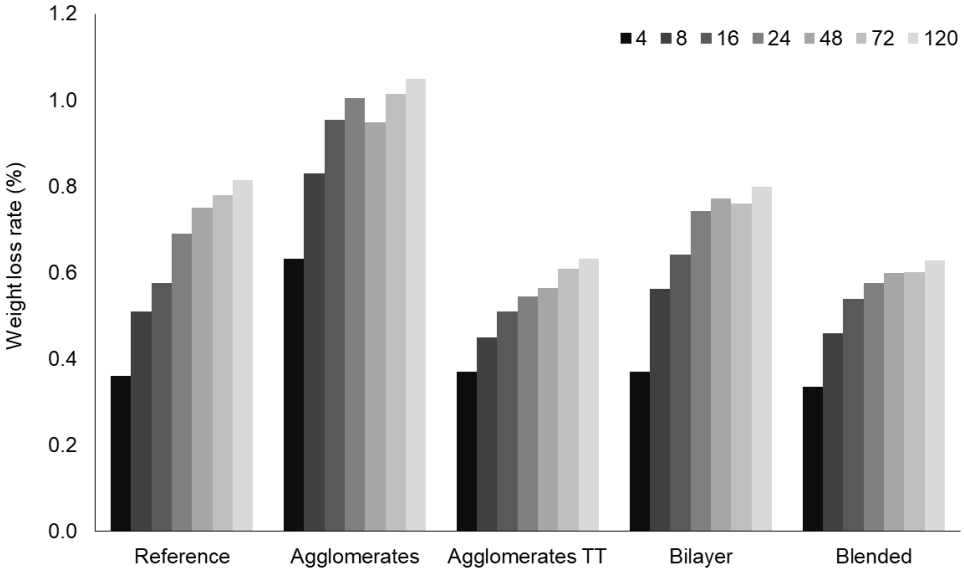

Figure 8. Weight loss rate of coated samples after soaking in Tris-HCl solution for different time periods (4, 8, 16, 24, 48, 72 and 120h)

For all the analysed coatings, an increase in weight loss was observed over time, with a rise in the shorter periods and a slight tendency to stabilize in the latter. Agglomerates coatings reveal the highest weight loss rate. The authors suggest that it can be explained by the large surface area of the coating exposed to the solution and the high surface porosity, as shown in Figure 6. In particular, the Agglomerates TT coatings show a great reduction in weight loss compared to the Agglomerates coatings that were not thermally treated. This result can be explained by the presence of the crystalline phase generated as a result of the heat treatment, giving rise to a more ordered and less reactive structure in the coating. This behaviour was observed previously in our study [15], where bioactive glass coatings, formed by non-agglomerated powders, suffered less weight loss when they were thermally treated. Reference and Bilayer coatings exhibited an intermediate result. Similar behaviour was expected for these coating types since the top surface of both coatings had the same characteristics. In both cases, the surface was less rough and porous compared Agglomerates, which may explain the lower reactivity observed. Finally, Blended coatings had less reactivity, with a result very similar to the Agglomerates TT. In the case of Blended coatings, the lower weight loss can be explained by the presence of both HA and glass on the surface. In particular, HA regions are less reactive and cause less material release than a surface where only glass is exposed.

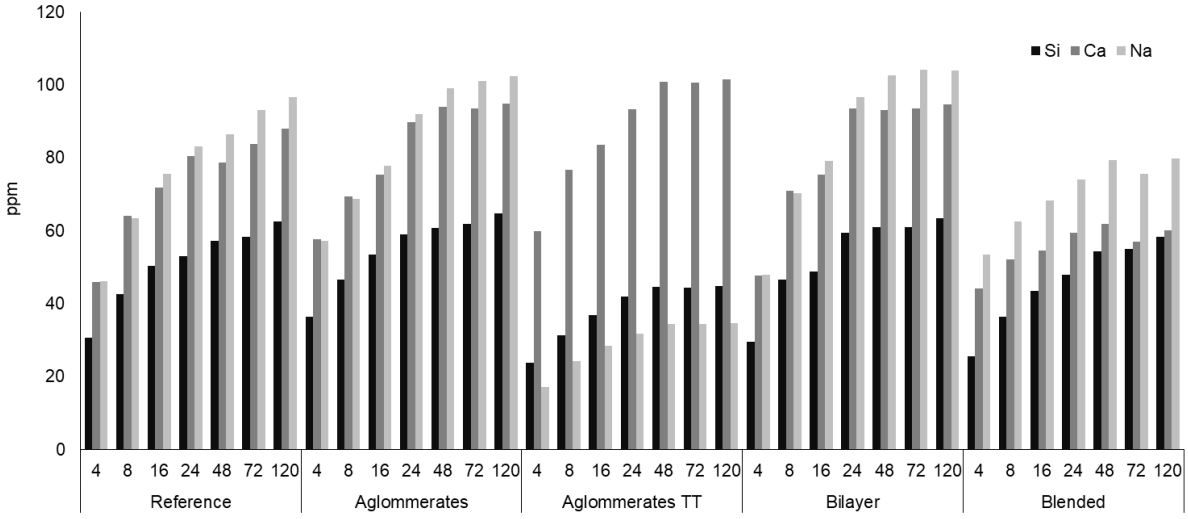

Figure 9. Ion release after immersion in Tris-HCl solution at different time periods (4, 8, 16, 24, 48, 72 and 120h)

To further corroborate these findings, the analysis of ion release over time contributed to a better understanding of the degradation process that different coatings undergo. The results of the concentration of ions released during the degradation study are shown in Figure 9.

For all the examined coatings, the release of silicon, calcium and sodium ions increased with time, with the same trend that was observed in the weight loss analysis of the samples. However, differences were observed in the type of ions released on each occasion. The first

step in the dissolution of bioactive glass is realising modifying cations [29]. It was clearly observed in the case of Reference, Agglomerates and Bilayer, where more calcium and sodium ions than silicon ions were detected in the solutions. These coatings showed the same behaviour regarding the release of ions. A similar amount of calcium and sodium ions were released in the first periods. In the last periods, the sodium released was slightly higher than that of calcium. The release of network-forming elements was lower and particularly only silicon ions were detected in the solution, due to the high contribution of silicon oxide (45.0% by weight) in this glass composition. The amount of phosphorus detected was very low due to the few phosphorous pentoxide (6.0% by weight) in the 45S5 glass composition; these values were not represented in Figure 9. As expected, the change in the morphology of the feedstock powder did not affect the type of ions released. The performance of the thermal treatment in the Agglomerates TT coating resulted in a decrease in the number of ions released during the test. In addition, a change in trend was observed in terms of the elements released. Approximately three times more calcium ions than sodium ions were released for this specific coating, unlike the other coatings. This change was due to the crystalline phase $Na_6Ca_3Si_6O_{18}$ formed by the thermal treatment, where many of the sodium ions became part of this new phase. In this new structure, composed of an amorphous and a crystalline part, the release of ions occurs initially in the amorphous area, since these elements are loosely bound in the structure. Furthermore, the incorporation of HA in the Blended coating resulted in a minor release of elements, but with an initial tendency similar to that of the Reference, Agglomerates and Bilayer. In particular, more sodium than calcium ions were released, and the difference increased for longer periods suggesting that some of the calcium ions released may be reabsorbed by the HA of the surface.

The results obtained by ICP analysis reflected different results for the different coatings studied. The amount of elements released was consistent with the weight loss measured, where Reference, Agglomerates and Blended Coatings suffered the greatest weight loss and ion release.

After the period of 120h, the ions released from the coatings caused a variation in the pH of the solution, which was initially 7.4; these results are shown in Figure 10.

The recorded pH values revealed an increase after the test caused by the release of ions. In particular, the release of sodium and calcium ions causes an increase in the pH of the solution, while the release of silicon tends to reduce it. The pH results were consistent with the trend observed for the weight loss and the ion release of the coatings.

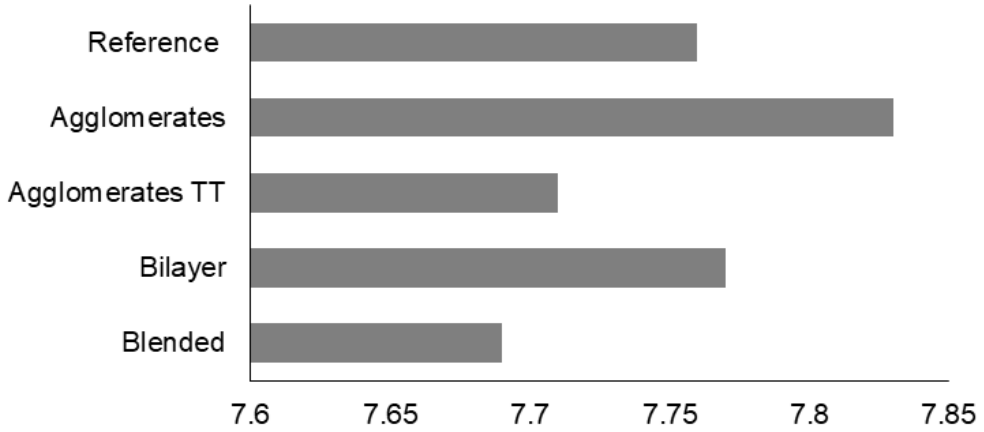

Figure 10. pH value after immersion of samples into Tris-HCl solution for 120h

The results of the degradation study corroborated the findings related to the ability of the coatings to form an apatite layer, which occurs faster for the more reactive coatings. Among the coatings evaluated in this part of the study, the ones with the strongest adhesion presented the slowest bioactive behaviour. Indeed, the characteristics that provide a greater bond strength are the same ones that cause a delay in the reactivity and consequently in the kinetic of HCA layer formation. Even so, all coatings can promote a bioactive response.

Analysing mechanical and biological properties, the more interesting candidates for use in implants are Agglomerates TT, Bilayer SH and Blended. Considering the manufacture process, Agglomerated TT coatings require a longer process, having to adapt the morphology of the powder and performing a post-treatment after the deposition process. Thus, Bilayer SH and Blended coatings are easier to develop. Bilayer SH requires three steps in the plasma equipment, an initial stage of heating the substrate and the subsequent deposition of two different powders. The Blended coating is formed by manually mixing the raw material powders in the same weight ratio.

4. Conclusions

Bioactive glass coatings with enhanced mechanical properties were produced using APS. The bond strength study showed that by a change in the morphology of the original glass particles, an improvement in the bond with the substrate can be obtained. Furthermore, incorporating HA as a bond coat and as a blend with the feedstock powder helped achieve better-adhered coatings. Pre-heating of the substrate produced an increase in the bond strength of the pure glass coatings, around 30 to 45%, compared to the original type of coating. While applying a post-thermal treatment at 725°C caused a greater increase for pure glass coatings, between 100 to 125%, compared to the original ones. The analysis of the bond strength of the coatings after one day of immersion in physiological solution revealed a pronounced decrease in that property compared to the coatings without immersion. In general, the loss of adherence for the designed coatings is lower than the experimented for

HA. Regarding the requirements of bond strength for coating implants Agglomerates TT, Bilayer SH and Blended coatings presented the more interesting results for samples with and without immersion in physiological solution.

The coating composition at the surface is a key aspect for the bioactive behavior of the coatings, as was demonstrated by the studies of the HCA layer formation and the degradation of the coatings. The formation of the HCA layer occurred at a higher rate for the Reference, Agglomerates and Bilayer coatings, while Agglomerates TT and Blended coatings showed slower kinetic reaction for HCA layer formation. After two weeks of immersion, a continuous HCA layer could be seen in all the coatings, with a greater thickness for the coatings in which it formed faster. The bioactivity results were also supported by the weight loss, the ion release and the pH values after the 120h immersion in physiologic solution. The microstructure characteristics that favour the good bonding of the coatings caused, at the same time less reactive coatings and, consequently, presented lower kinetics of HCA layer formation. This study verified that bioactive glass coatings with good adherence can be obtained, regardless of a certain reactivity.

After analysing the set of results, the Blended coatings would be the most interesting candidate to provide an improvement in the osseointegration process of current implants.

Acknowledgements

This work was supported by Generalitat de Catalunya (SGR-1777) and Spanish Government (MAT2016-76928-C2-1-R).

References

[1] H. Dong, H. Liu, N. Zhou, Q. Li, G. Yang, L. Chen, Y. Mou, Surface modified techniques and emerging functional coating of dental implants, Coatings. 10 (2020) 1–25. https://doi.org/10.3390/coatings10111012.

[2] A.F. Mavrogenis, R. Dimitriou, J. Parvizi, G.C. Babis, Biology of implant osseointegration, 9 (2009) 61–71.

[3] E. Mohseni, E. Zalnezhad, A.R. Bushroa, Comparative investigation on the adhesion of hydroxyapatite coating on Ti-6Al-4V implant: A review paper, Int. J. Adhes. Adhes. 48 (2014) 238–257. https://doi.org/10.1016/j.ijadhadh.2013.09.030.

[4] S. Sampath, H. Herman, Rapid solidification and microstructure development during plasma spray deposition, J. Therm. Spray Technol. 5 (1996) 445–456. https://doi.org/10.1007/BF02645275.

[5] J.R. Davis, Handbook of thermal spray technology, 28th ed., Ringgold Inc, Portland, 2004.

[6] L. Pawlowski, The Science and Engineering of Thermal Spray Coatings, second ed., John Wiley & Sons, 2008.

[7] Y. Liu, B. Rath, M. Tingart, J. Eschweiler, Role of implants surface modification in osseointegration: A systematic review, J. Biomed. Mater. Res. - Part A. 108 (2020) 470–484. https://doi.org/10.1002/jbm.a.36829.

[8] B.D. Ratner, A.S. Hoffman, F.J. Schoen, J.E. Lemons, An Introduction to Materials in Medicine, second ed., Academic Press, 2004.

[9] W. Jin, P.K. Chu, Orthopedic implants, in: R. Narayan (Ed.), Encycl. Biomed. Eng., Elsevier Inc., 2019: pp. 425–439. https://doi.org/10.1016/B978-0-12-801238-3.10999-7.

[10] S. Kurtz, K. Ong, E. Lau, F. Mowat, M. Halpern, Projections of primary and revision hip and knee arthroplasty in the United States from 2005 to 2030, J. Bone Jt. Surg. - Ser. A. 89 (2007) 780–785. https://doi.org/10.2106/JBJS.F.00222.

[11] T.F. Moriarty, U. Schlegel, S. Perren, R.G. Richards, Infection in fracture fixation: Can we influence infection rates through implant design?, J. Mater. Sci. Mater. Med. 21 (2010) 1031–1035. https://doi.org/10.1007/s10856-009-3907-x.

[12] D.S. Brauer, Bioactive glasses - Structure and properties, Angew. Chemie - Int. Ed. 54 (2015) 4160–4181. https://doi.org/10.1002/anie.201405310.

[13] J.R. Jones, Review of bioactive glass: From Hench to hybrids, Acta Biomater. 9 (2013) 4457–4486. https://doi.org/10.1016/j.actbio.2012.08.023.

[14] A. Oliva, A. Salerno, B. Locardi, V. Riccio, F. Della Ragione, P. Iardino, V. Zappia, Behaviour of human osteoblasts cultured on bioactive glass coatings, Biomaterials. 19 (1998) 1019–1025. https://doi.org/10.1016/S0142-9612(97)00249-4.

[15] B. Garrido, I.G. Cano, S. Dosta, Adhesion improvement and in vitro characterisation of 45S5 bioactive glass coatings obtained by atmospheric plasma spraying, Surf. Coatings Technol. 405 (2021) 126560. https://doi.org/10.1016/j.surfcoat.2020.126560.

[16] M.C. Pantilimon, T.S. Kang, S.J. Lee, Synthesis of nano-sized indium oxide (In2O3) powder by a polymer solution route, Ceram. Int. 42 (2016) 3762–3768. https://doi.org/10.1016/j.ceramint.2015.11.006.

[17] P. Vuoristo, Thermal Spray Coating Processes, in: S. Hashmi (Ed.), Compr. Mater. Process., Elsevier, 2014: pp. 229–276. https://doi.org/10.1016/B978-0-08-096532-1.00407-6.

[18] M. Wang, Composite coatings for implants and tissue engineering scaffolds, in: Biomed. Compos., 2009: pp. 127–177. https://doi.org/10.1533/9781845697372.2.127.

[19] L. Lefebvre, J. Chevalier, L. Gremillard, R. Zenati, G. Thollet, D. Bernache-Assolant, A. Govin, Structural

transformations of bioactive glass 45S5 with thermal treatments, Acta Mater. 55 (2007) 3305–3313. https://doi.org/10.1016/j.actamat.2007.01.029.

[20] A. Nouri, A. Sola, Powder morphology in thermal spraying, J. Adv. Manuf. Process. 1 (2019). https://doi.org/10.1002/amp2.10020.

[21] H. Miyazaki, I. Ushiroda, D. Itomura, T. Hirashita, N. Adachi, T. Ota, Thermal expansion of hydroxyapatite between - 100 °C and 50 °C, Mater. Sci. Eng. C. 29 (2009). https://doi.org/10.1016/j.msec.2008.12.001.

[22] S. Lopez-Esteban, E. Saiz, S. Fujino, T. Oku, K. Suganuma, A.P. Tomsia, Bioactive glass coatings for orthopedic metallic implants, J. Eur. Ceram. Soc. 23 (2003) 2921–2930. https://doi.org/10.1016/S0955-2219(03)00303-0.

[23] D. Bellucci, V. Cannillo, A. Sola, Coefficient of thermal expansion of bioactive glasses: Available literature data and analytical equation estimates, Ceram. Int. 37 (2011) 2963–2972. https://doi.org/10.1016/j.ceramint.2011.05.048.

[24] G. Qian, T. Nakamura, C.C. Berndt, Effects of thermal gradient and residual stresses on thermal barrier coating fracture, Mech. Mater. 27 (1998) 91–110. https://doi.org/10.1016/S0167-6636(97)00042-2.

[25] M. Mellali, P. Fauchais, A. Grimaud, Influence of substrate roughness and temperature on the adhesion/cohesion of alumina coatings, Surf. Coatings Technol. 81 (1996). https://doi.org/10.1016/0257-8972(95)02540-5.

[26] S. Prasad, V. Kumar Vyas, Ershad, R. Pyare, Crystallization and mechanical properties of (45S5-HA) biocomposite for biomedical implantation, Ceram. - Silikaty. 61 (2017) 378–384. https://doi.org/10.13168/cs.2017.0039.

[27] V. Cannillo, A. Sola, Different approaches to produce coatings with bioactive glasses: Enamelling vs plasma spraying, J. Eur. Ceram. Soc. 30 (2010) 2031–2039. https://doi.org/10.1016/j.jeurceramsoc.2010.04.021.

[28] E. Cañas, V. Sanz, M.J. Orts, E. Sánchez, Post-deposition heat treatment effect on microstructure of suspension plasma sprayed bioactive glass coatings, Surf. Coatings Technol. 371 (2019). https://doi.org/10.1016/j.surfcoat.2018.11.003.

[29] L.L. Hench, Ö. Andersson, Bioactive Glasses, in: An Introd. to Bioceram., 1993: pp. 41–62. https://doi.org/10.1142/9789814317351_0003.

4.2. Biological response of different compositions of bioactive glasses

There is no material matching the remodelling rates of natural bone. Hydroxyapatite, which is frequently used as a bioactive coating material for implants, has a low degree of resorption. In comparison, bioactive glass materials can be designed by tailoring their dissolution rate and degree of bioactivity. Depending on the oxides composing the glass and the proportions, each glass acquires a particular structure and, consequently, specific properties. In addition, the ions released as a result of dissolution can have other attractive effects on the application. Therefore, bioactive glasses have become an interesting alternative to be used as coating material.

The following section aims to evaluate the biological response of various bioactive glass coatings and the extent to which the composition can modulate their physicochemical and biological properties. In vitro tests using osteoblasts were performed to validate the biological potential of each composition. In addition, the bioactive and degradable behaviour of the coatings were studied and their resistance to tensile strength.

1. Introduction

Hydroxyapatite (HA) has been used as a bone substitute because of its close composition with the natural bone. The first use of this biomaterial was in the 1950s as a filler for repairing bone defects (Ref 1). A few decades later, specifically in the 1980s, HA was introduced in bioactive coatings to improve dental implants. Later, its next appearance was in the stems of hip prostheses (Ref 2,3). These first HA coatings were applied using atmospheric plasma spraying (APS) technique. Among the many techniques currently available for HA deposition, APS remains the method of choice for most medical manufacturers (Ref 4,5).

Despite the great success of HA-coated titanium implants, their long-term stability continues to be a point of improvement on which many researchers are focused. Combining the mechanical properties of titanium with the bioactive capacity provided by ceramic coatings is a very interesting strategy. However, it is necessary to improve the stability of the coating.

In this study, different bioactive glasses have been evaluated in order to improve the initial stability of the coating, which can be closely linked to the long-term stability of ceramic coatings and promote a suitable biological response to inert substrates.

45S5 and S53P4 are two commercial compositions of bioactive glasses formed by the same oxides but in different proportions. In particular, S53P4 has more network-forming oxide content, so its structure is less disrupted than 45S5. The other bioactive glass used, the 62W, is a composition free of sodium oxide that includes magnesium oxide, a common element for the human body that can also stimulate the growth of bone tissue (Ref 6,7). In previous studies, the role of magnesium oxide in silicate-based bioactive glasses has been studied. Karakuzu-Ikizler et al. demonstrated that incorporating magnesium oxide (1% wt.) on the commercial 45S5 composition enhanced its bioactivity and biodegradability (Ref 8). Bellucci et al. studied the incorporation of magnesium oxide (10% mol.) in a CaO-rich silicate bioactive glass and confirmed its beneficial effect on bioactivity (Ref 9).

The main objective of this study is to examine the effectiveness of the bioactive glasses deposited by APS on the Ti6Al4V substrate by evaluating their mechanical and biological properties. In addition, since the type and proportions of oxides present in each glass composition can affect the physical-chemical and biological properties, the role of the different glass components is also investigated. HA coatings were used as comparative material, as most commercial implants are HA-coated.

2. Materials and methods

2.1. Powder and substrate

Four different powders were used for producing the bioactive coatings. In particular, two bioactive glasses from the SiO_2-CaO-Na_2O-P_2O_5 system were selected: a commercial 45S5 powder (Denfotex Research, United Kingdom) and an S53P4 powder manufactured at the *Instituto de Cerámica y Vidrio (ICV)* from a mixture of reagent grade: SiO_2, $(NH_4)_2HPO_4$, Na_2CO_3 and $CaCO_3$. In addition, the bioactive glass powder 62W, in the SiO_2-CaO-P_2O_5-MgO system was also selected. It was produced in collaboration with *ICV* by using the following reagents: SiO_2, $Ca_3(PO_4)_2$, MgO and $CaCO_3$. The specific composition in molar percentage of the bioactive glasses can be seen in Table 1.

Bioactive glass powders were produced by the traditional melt-quenching route. The different compositions were prepared from the mixture of the reagents mentioned above. Each mixture was melted using a platinum crucible at high temperature (1450 ºC for S53P4 and 1500 ºC for 62W) in an electric furnace for 2h, with a heating rate of 5 ºC/min. After that, the melt material was poured over cold water to prevent its crystallization and to get a glass frit. The fritted glass was milled using a tungsten-carbide vibrating cup mill to obtain the glass powder. The resulting powder was sieved using meshes of 63 and 100 µm with a vibratory sieve shaker (AS200, Retsch, Germany). The powders in the range between 63 and 100 µm were collected and used for producing the coatings. The amount of 0.7% wt. of aerosil was added to the final powder to improve its ability to flow and be sprayed.

Furthermore, HA powder was used as comparative material, in particular, a commercial sintered HA powder Captal®30 (Plasma Biotal Limited, United Kingdom) with phase purity higher than 95% and crystallinity above 95%.

Table 1. Theoretical composition of the bioactive glasses in molar percentage

	SiO_2	**CaO**	**Na_2O**	**P_2O_5**	**MgO**	**Network-forming oxides**
45S5	46.1	26.9	24.4	2.6	-	48.7
S53P4	53.9	21.8	22.7	1.7	-	55.6
62W	41.0	50.0	-	4.6	4.2	45.6

Ti6Al4V discs of 2 mm thick and 9 mm diameter (Tamec, Spain) were used as substrates for the in vitro tests. The samples used for the bond strength test (Ibermetal, Spain) had 25 mm and 5 mm in diameter and height, respectively. For the metallographic characterization of the coatings, rectangular substrates measuring 100 × 20 × 5 mm were used (Ibermetal, Spain).

2.2. Coating deposition

The coatings were developed using APS equipment (Plasma-Technik A3000S, Sulzer Metco AG, Wohlen, Switzerland) with a F4 plasma torch. Argon was used as the primary carrier gas and hydrogen as the secondary gas for the plume formation. The powders were deposited onto substrates, previously grit-blasted (MAB-4, MAB industrial, Barcelona, Spain) with corundum G24 (grit size 800 µm) at 0.5 MPa. This process generated the proper surface roughness for a good adhesion (Ra = 4.4 ± 0.6 µm and Rz = 31.2 ± 3.8 µm). Before the spraying process, the substrates were cleaned with ethanol.

The parameters used for coating deposition are detailed in Table 2. These conditions were selected after optimizing the coating formation for each powder by varying the spray distance, the current, and the gas flow rate of argon and hydrogen.

Table 2. Plasma spraying parameters

	HA	**45S5**	**S53P4**	**62W**
Argon plasma gas flow rate (slpm)	50	35	35	30
Hydrogen plasma gas flow rate (slpm)	1	12	12	15
Spray distance (mm)	80	125	90	125
Current (A)	500	600	600	650
Spray cycles	5	5	5	5

2.3. Powder and coating characterization

To characterize the initial powders and the developed coatings, an analysis was performed using a scanning electron microscope (SEM), (Phenom ProX, Phenom-World BV, Eindhoven, The Netherlands) equipped with an energy-dispersive X-ray diffraction. Before the observation, the materials were coated with a gold layer to make them conductive using a sputtering coating system (E-5000, Polaron, Watford, England).

A grinding and polishing process was done to analyse the cross-section of the coatings. First, samples were cold mounted in resin and then abraded with silicon carbide papers up to P4000 (grit size 5 µm). Finally, these samples were polished using 1 µm diamond slurry.

The bond strength of the coatings was determined using a mechanical test machine (ME-402/10, Servosis, Madrid, Spain) following the ASTM C633-13 (Standard test method for adhesion or cohesion strength of thermal spray coatings). Three coated samples of each composition were glued using HTK ULTRA BOND 100® glue (HTK, Germany) to grit blasted counter-test pieces. Then, normal tensile stress was applied to the coating with the displacement rate set at 0.02 mm/s until a fracture occurred. In addition, to perform the test

on the developed coatings, we tested the coatings after one day of immersion in hank's balanced salt solution (HBSS) (Sigma-Aldrich, Germany) at 37ºC.

2.4. Bioactivity and degradation assessment

ISO 23317 (Implants for Surgery - In Vitro Evaluation for Apatite-Forming Ability of Implant Materials) was followed to evaluate the ability of the coatings to form an HCA layer. Coated samples were vertically immersed in HBSS in a thermostatic bath with agitation at 37ºC. To avoid ionic saturation of the medium the solution was refreshed twice a week. Three samples of each coating type were tested for different times: 0, 3, 7, 14 and 21 days. After each period, coated samples were rinsed with ultra-pure water and dried at room temperature for 24h. To assess the kinetic of the HCA layer formation, the surface of the samples was analysed by SEM for the different periods. In addition, to determine the thickness of the formed layer, it was analysed from cross-sectional images of the samples immersed 14 days. The crystallographic structure of as-sprayed coatings and samples immersed for 14 days in HBSS was analysed using X-ray diffraction (XRD) using a diffractometer (X'Pert PRO MPD, PANalytical, Cambridge, UK).

To evaluate the glass dissolution of the different compositions studied a degradation test was performed following the ISO 10993-14 (Biological Evaluation of Medical Devices - Part 14: Identification and Quantification of Degradation Products from Ceramics). Samples were immersed at 37 ± 1ºC for 120h in a Tris-HCl solution with pH adjusted to 7.4 ± 0.1. After the immersion time, samples were rinsed with ultra-pure water and dried overnight at 120ºC. To determine the degradation behaviour, the weight of dried samples was measured before and after the test with a high precision scale (CPA225D, Sartorius, Goettingen, Germany). Moreover, the pH measurement of the solution at the end of the test was recorded using a universal pH meter (Hach, Spain). The detail of the material released in the solution was determined by measuring the change in the ion concentration (silicon, calcium, sodium, magnesium and phosphorus) using inductively coupled plasma optical emission spectrometry (ICP-OES) (Optima 8300, PerkinElmer, Waltham, USA).

2.5. Cell culture studies

Osteoblasts were seeded onto three developed coatings of each series in each experiment to study the ability of the different compositions to allow adhesion, growth and proliferation of the cells. The tests were done in triplicate with different human osteoblast lines (obtained from knee trabecular bone after prosthesis replacement (Ref 10)) in the passage from 3 to 6 to ensure reliable results. Parc de Salut Mar Ethics Committee approved the study. In order to avoid the inter-experiment variability, results were normalized to the tissue culture plastic (TCP) at three days within each experiment, which was included as a control.

Before the cellular tests, samples were sterilized in ethanol 70% for three hours to avoid contamination during the test. Then a preconditioning step was done for 24h immersing all samples in Dulbecco's modified eagle's medium (DMEM) (Invitrogen, USA) supplemented with 10% fetal bovine serum. This step was required to avoid cell death caused by the rapid increase in the pH due to the release of ions from the glass (Ref 11,12). A cell suspension was prepared and seeded at a density of 6.5×10^3 cells/sample with supplemented DMEM onto the coated samples and TCPs placed in a 48-well polystyrene plate. The incubation was done at 37ºC in a humidified atmosphere of 5% CO_2, changing the media every 3 days.

Cell proliferation was analysed using MTS assay (CellTiter 96® AQueous One Solution Cell Proliferation, Promega, USA). This colorimetric test quantifies viable cells based on reducing MTS tetrazolium by cells into a coloured formazan product soluble in cell culture medium. After each period (3, 7 and 14 days), the medium was removed, and samples were transferred to new wells. Then, the samples were incubated for 1h and 30 minutes in a solution containing 50 µL of MTS reagent and 250 µL of the supplemented medium. Afterward, the absorbance was recorded at 490 nm through a well plate reader (Infinite 200, Tecan, Männedorf, Switzerland).

The quantitative results from the MTS assay were analysed using one-way analysis of variance (ANOVA) followed by Tukey's post hoc test to determine differences among groups. Where $p<0.05$ was considered to be statistically significant.

SEM was used to analyse the attachment and morphology of the cells after one week of incubation. Osteoblasts were seeded onto the coatings at the same density as for MTS assay. After the immersion time, the samples were washed twice with phosphate-buffered saline (PBS) buffer (pH 7.4) to remove non-bounded cells. The remaining cells were fixed with 2.5 % glutaraldehyde in PBS for 3h. After that step, the samples were rinsed again with PBS. The dehydration of the cells was performed with ethanol baths of 15 minutes each, increasing its concentration in the following sequence: 50, 65, 70, 80, 90, 95, and 100%. Finally, the samples were dried using a critical point dryer (CPD) (K850, Emitech, Lewes, UK) and carbon-coated for the SEM observation using a high-vacuum carbon evaporator (K950X, Emitech, Lewes, UK).

Cell response can be affected by surface roughness (Ref 13). So, to ensure that the differences in cell response correspond to the effect of composition and not to the roughness factor, we performed additional tests on smooth samples. The coatings were abraded until a surface roughness $Ra < 5$ µm was achieved to obtain surfaces with no relevant topographical features.

3. Results

3.1. Powder and coating characterization

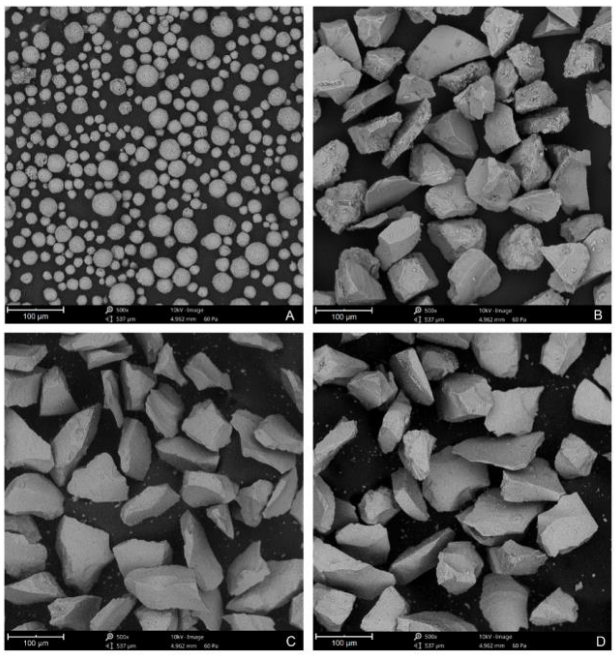

Figure 3. SEM micrographs of the HA (A) and bioactive glasses: 45S5 (B), S53P4 (C) and 62W (D) powders

The HA powder consists of micrometric spherical particles below 60 μm) composed of small particles forming aggregates (Figure 3A). In contrast, the three bioactive glass powders present the typical morphology of crushed powders, irregular and sharp particles (Figure 3B-3C-3D). The size distribution of particles is similar for all the glass powders, and these are significantly larger and denser than HA particles.

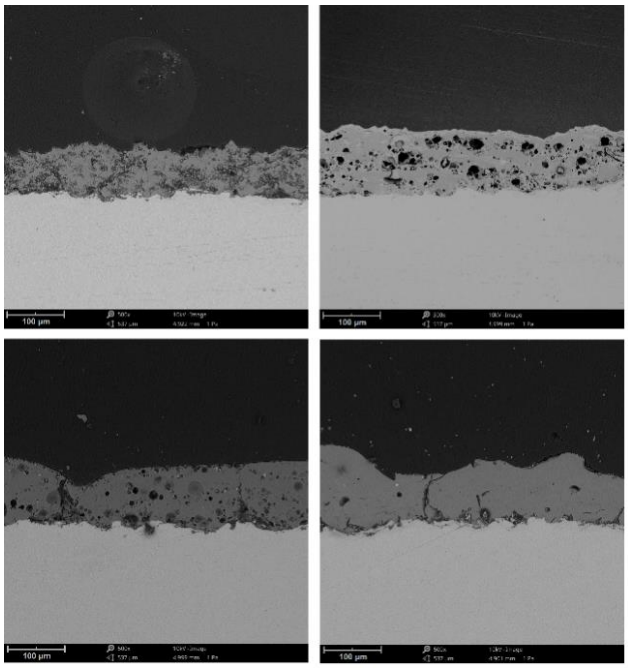

Figure 4. Cross-sectional SEM micrographs: (A) HA, (B) 45S5, (C) S53P4 and (D) 62W

Table 3. Roughness parameters of the as-sprayed coatings

	HA	45S5	S53P4	62W
Ra (µm)	5.4 ± 0.3	13.1 ± 1.4	13.4 ± 1.0	11.8 ± 1.1
Rz (µm)	31.0 ± 2.3	63.2 ± 3.8	71.7 ± 6.0	57.9 ± 7.4

The cross-sectional images of the as-sprayed coatings using different feedstock powders are shown in Figure 4. As can be seen, thick and well-adhered coatings were obtained for all the materials. Some cracks caused due to thermal stresses were also observed in the glass coatings. The microstructure of the coatings obtained spraying 45S5, and S53P4 revealed certain porosity, with the presence of larger pores for the 45S5. The porosity can occur due to the volatilization of sodium and phosphorus oxide at high temperatures. Some pores can form between particles that did not completely melt and consequently did not fully flatten, creating cavities between them during the build-up of the coating. As the 62W composition has no sodium in the composition, no porosity was observed for this coating. The roughness results obtained are given in Table 3, which shows an increase in values when glass powders were used instead of HA.

3.2. Bond strength study

In order to explore the quality of the deposited coatings, bond strength tests were carried out for the as-sprayed coatings and the coatings after one day of immersion in physiological solution, Figure 5 shows the results corresponding to each coating type. The study showed that HA-coated samples without immersion have larger bond strength, followed by 62W, S53P4 and 45S5, respectively. The high bond strength of 62W glass can be related to the absence of pores in its microstructure, which are responsible for cohesive failure.

To favor the osseointegration process between the implant and the bone, it is important that the coating has good stability in the initial stage. The HA coating suffered the highest percentage of bond strength loss after one day of immersion (81%). Thus HA coatings do not adequately meet this characteristic. The 45S5 glass had the lowest adhesion value without immersion and it also had the lowest value after one day of immersion, which corresponded to 50% of adherence loss. Therefore, considering the mechanical properties, this coating does not meet the requirements. The most interesting results were shown by the S53P4 and 62W coatings, for which the bond strength was reduced after the immersion test by 67% and 40%, respectively. In particular, the 62W coating reached a value of 19.1 MPa after immersion, being a significantly higher value compared to the other coatings.

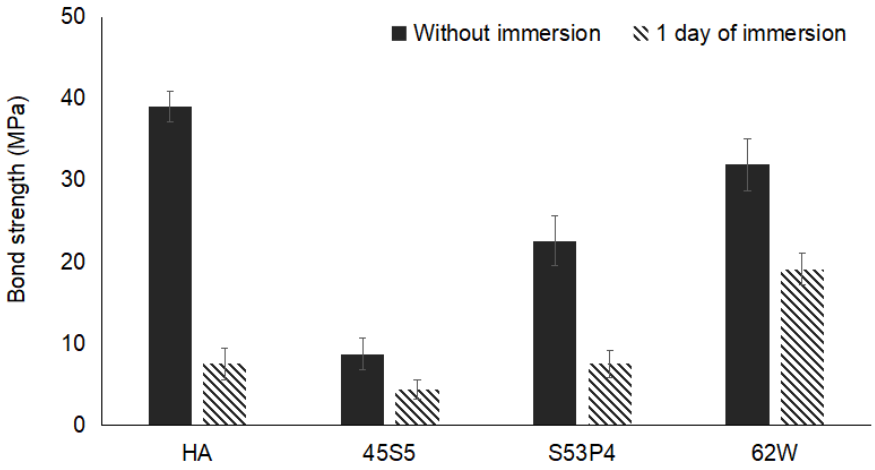

Figure 5. Bond strength of the different coatings developed before and after immersion in HBSS

3.3. In vitro bioactivity study - Ability to form apatite

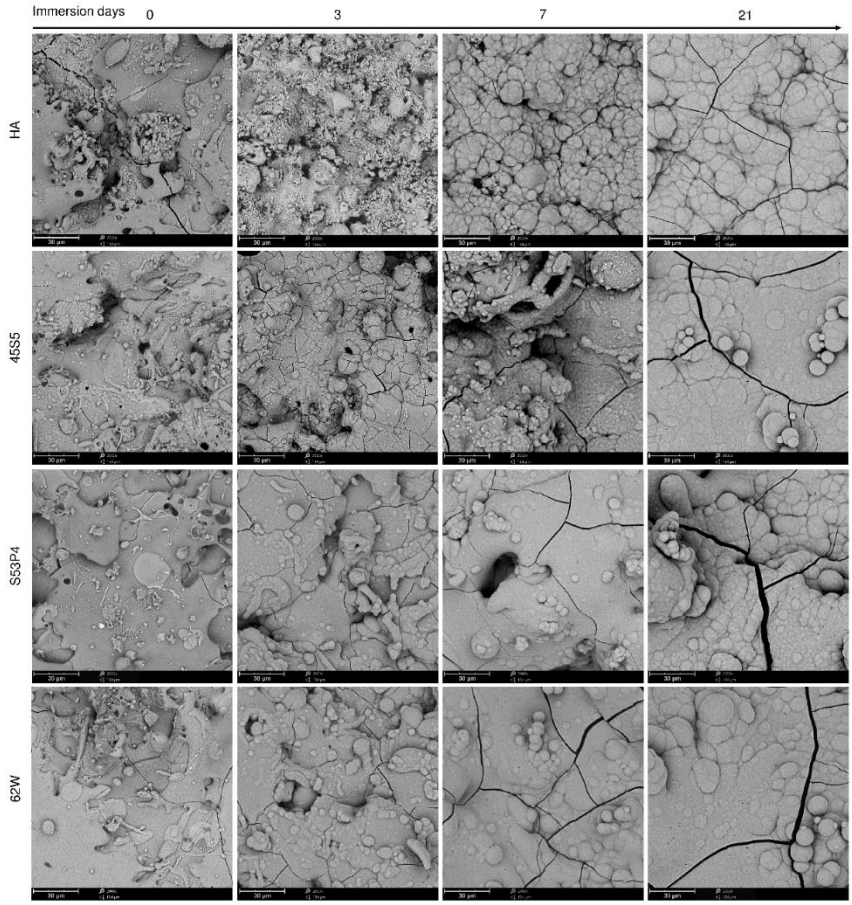

Figure 6. SEM images of the samples surface after soaking in HBSS for different times: after 3, 7 and 14 days

The ability of the coatings to promote the bonding with bone tissue was evaluated for all the coatings. The results of the test were displayed in Figure 6, Figure 7 and Figure 8, corresponding to the top surface of the samples, XRD patterns, and the cross-sectional images, respectively.

After three days of immersion in HBSS, the surface of the coated samples revealed that all the glass coatings were uniformly covered with apatite. However, the HA-coated samples only presented isolated apatite deposits after three days of immersion. At seven and twenty-one days, all the coatings revealed the dome-like morphology of precipitated apatite over the entire surface, suggesting growth of the formed HCA layer. XRD patterns represented in Figure 7 revealed that the structure of the bioactive glass as-sprayed coatings is entirely amorphous. The rapid cooling that the glass undergoes after the fusion of the particles prevents the formation of crystalline phases as a consequence of the spraying process. After two weeks of immersion, peaks related to the hydroxyapatite layer (Ref. 00-024-0033) were detected for all the coating types corroborating the bioactive ability of the coatings studied.

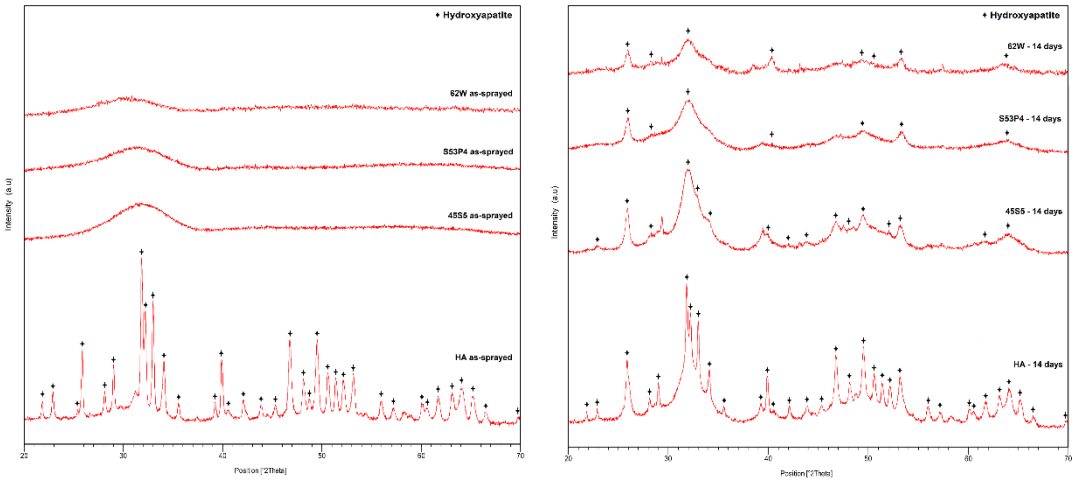

Figure 7. X-ray spectra acquired on the samples before and after immersion in HBSS for 14 days

After three weeks of immersion, the cross-sectional images verified the formation of a continuous HCA layer throughout the surface of the coatings. It was also observed that a coating thickness reduction of the sprayed coatings due to the HCA layer formation and the dissolution occurred. The measured thickness for the HCA layer formed was thinner for HA coatings (see Table 4), and this coating type suffered a minor coating reduction than glass ones during the test. Thick HCA layers were observed on the surface of the 45S5, S53P4, and 62W coatings, which experienced greater than 60% coating reduction. Specifically, the 62W composition had more pronounced results, with an HCA layer thickness of 15.8 µm and a severe thickness reduction from 105.3 µm to 37.1 µm, suggesting that elements in this glass can promote rapid osseointegration.

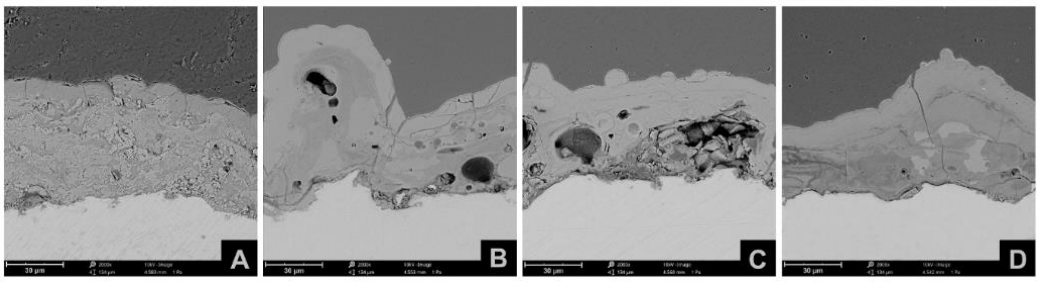

Figure 8. Cross-section micrographs showing the HCA layer after 21 days of immersion in HBSS

Table 4. Thickness of the coatings before and after three weeks of immersion in HBSS

	HA	45S5	S53P4	62W
As-sprayed coating (μm)	81.1 ± 9.0	100.6 ± 11.8	99.9 ± 17.5	105.3 ± 17.9
Residual coating (μm)	50.4 ± 6.0	39.7 ± 7.7	38.2 ± 6.4	37.1 ± 6.8
HCA layer (μm)	7.3 ± 1.3	11.0 ± 2.6	12.3 ± 2.1	15.8 ± 3.2
Coating reduction (%)	37.9	60.5	61.8	64.8

3.4. Degradation study

The degradation rate and the ion release of bioactive glasses are related to the network's structure and are tightly linked with the bioactive behaviour of the coatings. Therefore, it should be considered that the pH variation of the solution is caused by the ion exchange produced between protons from the solution and modifier cations from the glass. Water molecules can enter the structure more easily when the silicate network is disrupted (fewer network formers and, consequently, lower network connectivity). Therefore, the ion exchange occurs more quickly, causing a higher increase in pH. Consequently, the weight loss is related to the ions released from the coatings to the solution.

In the degradation test, the coated samples were immersed for 120h in Tris-HCl solution. The percentage of weight loss of the samples at different periods and the pH values recorded at the end of the test are illustrated in Figures 9 and 10, respectively.

All the glass compositions gradually increased weight loss over time, with a more pronounced rise in the initial stage. It was possible to observe a different degree of degradation among the compositions. In particular, 45S5 glass showed the highest dissolution of all glasses investigated here. For this composition, the rise in pH (Figure 10) and weight loss (Figure 9) was considerably higher than that of all other glasses, as 45S5 has fewer network-forming oxides and, therefore, a more disrupted structure. Otherwise, the S53P4 is composed of the same oxides as 45S5 but contains fewer modifier oxides and more network formers.

As a consequence of its more connected structure, the dissolution rate was markedly lower, and less degradation was measured than in the 45S5 (Figure 9). Regarding the 62W

coatings, these showed a higher weight loss rate at the initial periods, indicating that this glass composition suffered a rapid release of ions when it is in contact with the physiological solution and tended to stabilize at more prolonged periods. At the end of the test, the 62W glass presented a higher weight loss rate than the S53P4 glass and lower than 45S5 glass. The 62W glass is characterized by having a similar content of network-forming oxides with respect 45S5 (see Table 1), but it does not contain alkaline oxides in the structure. Instead, it contains a higher amount of alkaline earth oxides (CaO and MgO). Since alkaline oxides favour solubility, it is consistent that 62W composition suffered less degradation than 45S5. Finally, the HA coatings experimented the slightest dissolution due to the low degradation rate of this biomaterial (Ref 14). As expected, the variation in the pH of the solution was minimal for this coating type.

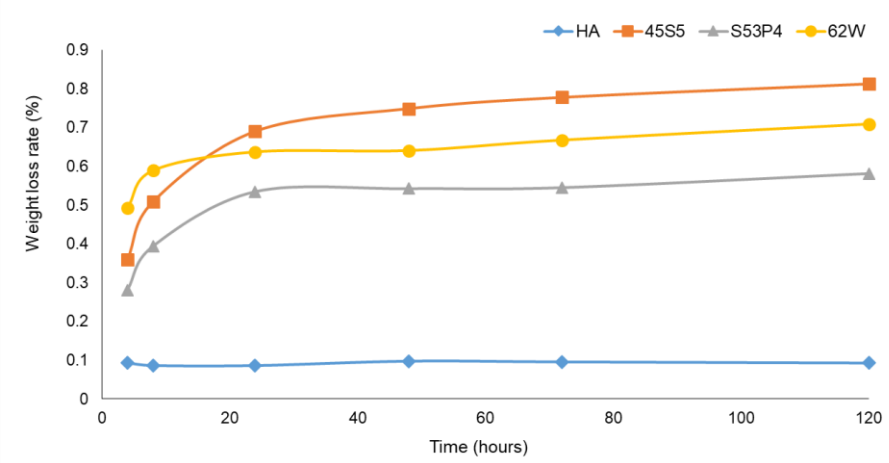

Figure 9. Weight loss rate of coated samples after soaking in Tris-HCl solution for different time periods

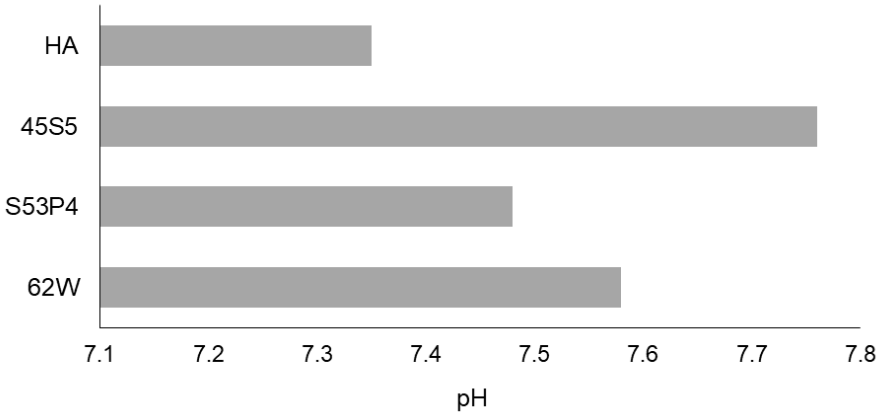

Figure 10. Value of pH recorded after soaking the different coatings for 120h in Tris-HCl solution

ICP analysis helped to clarify the ion release experimented by each biomaterial during the degradation test. The concentration of elements (silicon, phosphorus, calcium, sodium, and magnesium) present in the solution is represented in Figure 11.

For all the glass compositions, less network former elements (silicon and phosphorus) were detected than modifier elements (calcium, sodium, and magnesium) in the solution. This is because the detachment of elements from the structure is more difficult for the network formers, as these are covalently bonded. It also explains the relatively low amount of silicon release, despite the high content of this element in the glass compositions.

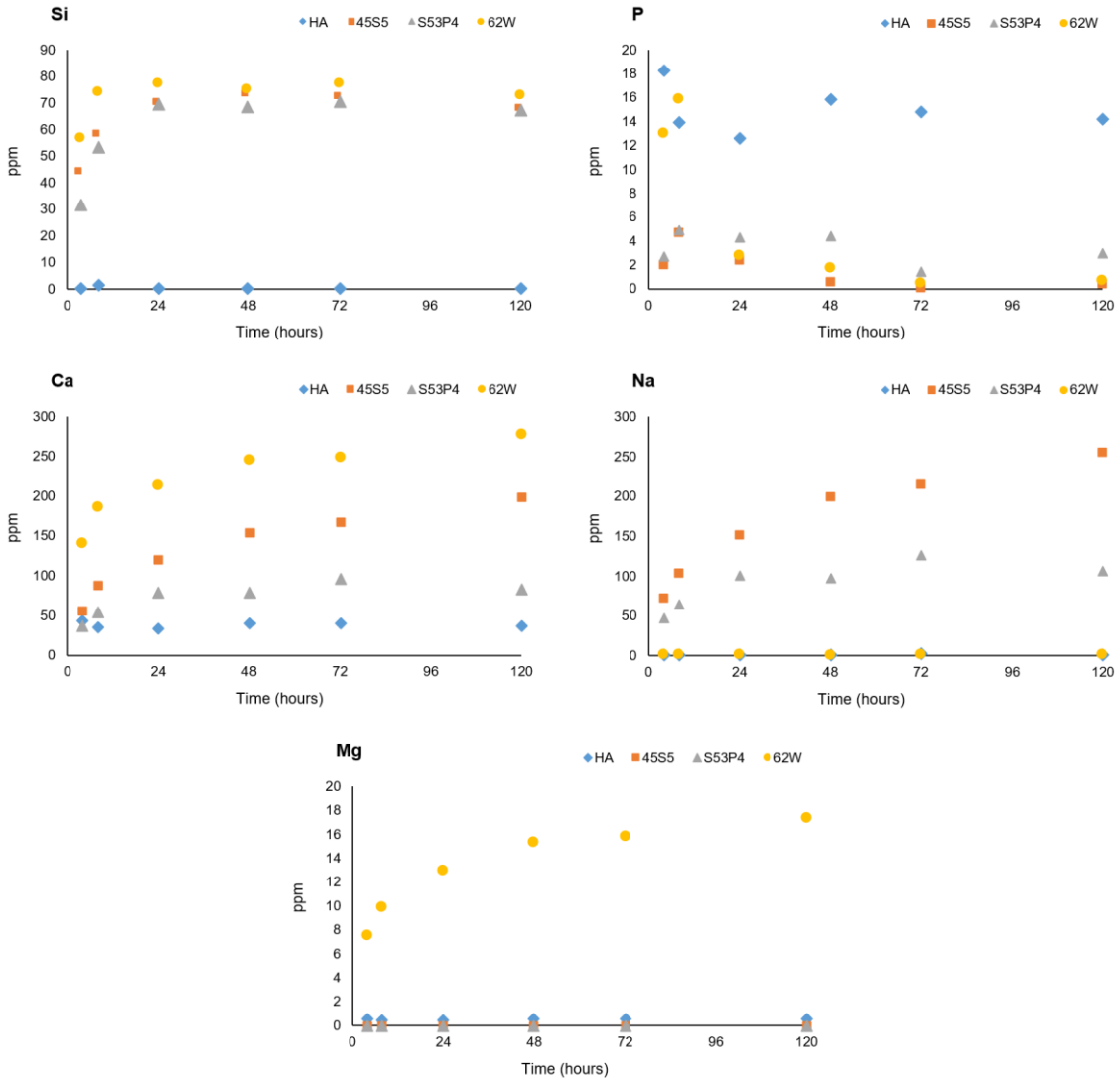

Figure 11. Ion release into Tris-HCl solution after immersion of the developed coatings for 120h

Regarding the HA samples, only calcium and phosphorus were found in the corresponding solutions, which remained practically constant throughout the test, as this biomaterial has low degree of solubility in physiological solution. 45S5 composition suffered high dissolution, especially related to the modifier ions. Even though the amount of calcium and sodium oxides in the composition was similar for this glass, a higher release of sodium was detected as these ions were weakly bonded to the structure. For the S53P4, the release of calcium and sodium presented a similar trend and has happened for the 45S5 composition, more amount of sodium than calcium was identified by ICP. The silicon measured after the test was similar for all the glass compositions. However, it can be noticed that less silicon was detached from

the S53P4 coatings, despite it is the composition with more silica in the network. This behaviour could be attributed to the higher network formers in this glass. Finally, the 62W coatings revealed a fast silicon release for the initial periods. This trend was also observed for the same composition in the weight loss rate observed for the first periods. The amount of calcium detected for 62W glass was remarkably high compared to the others since the calcium oxide content is higher for this composition as it is sodium-free. In the 62W solutions the presence of magnesium was also detected, as this is present on the composition at a low proportion (see Table 1). The role of magnesia in silicate glasses has not been entirely clarified and could be different depending on the proportion of this oxide in the composition. In some studies it has been seen to act as an intermediate oxide (Ref 15,16), while in others as a modifier oxide (Ref 17). In 62W composition, by the amount of magnesium detached from the structure during the degradation test, it seems that it could be acting as a modifier.

3.5. Cell culture study

The different compositions affect the cellular response of the coatings obtained by APS. The results obtained in the study of the formation of the HCA layer and the degradation test have already shown different behaviours for the studied materials. Osteoblasts were seeded on the different coatings and TCP as a positive control. Regarding the ability of osteoblasts to proliferate, MTS results at different periods are displayed in Figure 12.

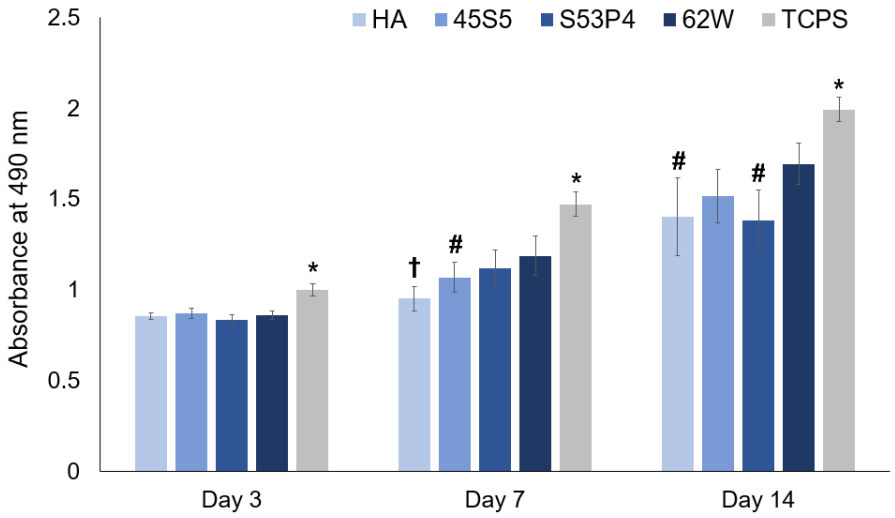

Figure 12. MTS activity analysis for human osteoblasts after incubation onto the different bioactive coatings developed at 3, 7 and 14 days. (n = 9; p-values < 0.01)

*Significantly more cells in the indicated group compared to the other groups at the same time point. † Significantly fewer cells in the indicated group than in the other groups at the same time point. #Significantly fewer cells than 62W at the same time point.

At three days, no significant differences were observed between the bioactive coatings studied, so the initial adhesion of the osteoblasts was similar to the different coatings studied. After seven days, it was possible to see a significant increase in the cellular activity of the

glass coatings concerning HA. After fourteen days of testing, the 45S5 and 62W glasses could promote greater cell proliferation than the other bioactive coatings. Other studies have reported a stimulating effect in osteoblasts proliferation for compositions containing few amounts of magnesia (Ref 9,18). According to the MTS results, it can be concluded that the glass composition affects the growth and proliferation of osteoblasts.

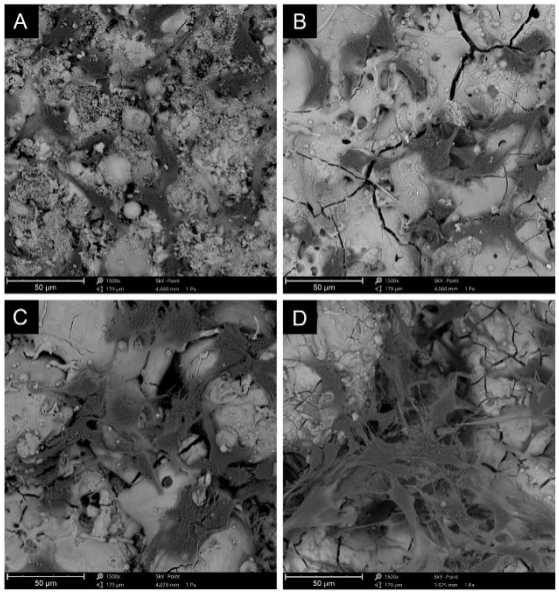

Figure 13. SEM observation of as-sprayed surface after 7 days of osteoblasts incubation: (A) HA, (B) 45S5, (C) S53P4 and (D) 62W

The morphology of cells attached to the surface of bioactive coatings after seven days in HBSS are shown in Figure 13. For the different coatings, well-adhered and spread cells with long filopodia were observed, with the typical morphology. Moreover, since the coating roughness can affect the interaction of the osteoblasts with the surface, additional tests on smooth samples (Ra < 5 µm) were developed. Thus, it is possible to clarify if the differences in cell response correspond only to the effect of the composition. Cells incubated onto smooth bioactive coatings after seven days in HBSS are shown in Figure 14. From these images can be concluded that cell response is not affected by the roughness of our coatings. Well adhered and spread cells were observed on rough surfaces. In addition, regardless of the surface roughness, more cells can be noticed in the 62W coating in this period, suggesting that the cells show some preference for this glass composition, as seen in the MTS analysis.

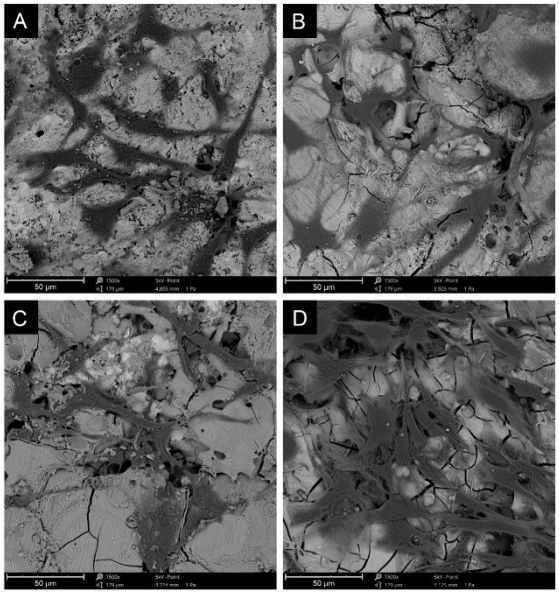

Figure 14. SEM observation of the surface of smooth coatings after 7 days of osteoblasts incubation: (A) HA, (B) 45S5, (C) S53P4 and (D) 62W

4. Conclusions

In this work, we have produced bioactive glass coatings with enhanced mechanical and biological properties using APS. The effect of the different oxides forming the glasses was studied, by analysing the quality of the coatings in terms of microstructure, bond strength, and in vitro response, with results that show significant differences in the properties of the coatings because of the different compositions.

The microstructure analysis revealed that 45S5 and S53P4 present certain porosity, while 62W coating has a dense microstructure since it is a composition free of sodium. The absence of pores in this coating provides strong adhesion to the coating, with values as high as 31.9 MPa as-sprayed coating and 19.1 MPa after one day of immersion in HBSS. In addition, S53P4 and 62W are the coatings that suffered less reduction in bond strength concerning as-sprayed coatings after one day in a physiological fluid.

The composition is a key aspect of the bioactive behaviour of the coatings, as was demonstrated by the studies of the HCA layer formation and the degradation of the coatings. In particular, the HCA layer formation occurs rapidly for the different glass coatings, while HA showed a slower kinetic reaction for HCA layer formation. After three weeks of immersion, a continuous HCA layer could be seen in all the coatings studied, with higher thickness for the 62W composition (15.8 µm). In addition, the degradation rate of the different coatings was proven to be influenced by the glass composition, as demonstrated by the results of weight loss, the ion release, and the pH values after the 120h immersion in Tris-HCl solution. The 62W coating suffered rapid release in the first stage of the test.

In vitro studies showed that human osteoblasts can adhere and proliferate on the evaluated compositions, with a stimulating effect on osteoblasts proliferation caused by the elements that form the coating. The growth and proliferation of osteoblasts are higher at fourteen days for the 45S5 and 62W coatings.

The 62W glass, characterized by a sodium-free composition that includes magnesium oxide, provides a pore-free coating with good mechanical properties and can stimulate bone tissue growth, becoming an interesting candidate for bone repair applications.

Funding

This work was supported by the Spanish Government (MCIN/AEI/ 10.13039/501100011033) through grant MAT2016-76928-C2-1-R, Generalitat de Catalunya (SGR-1777) and the Centro de Investigación Biomédica en Red de Fragilidad y Envejecimiento Saludable-CIBERFES (CB16/10/00245) from Instituto de Salud Carlos III, and FEDER funds.

References

1. V.S. Kattimani, S. Kondaka, and K.P. Lingamaneni, Hydroxyapatite - Past, Present, and Future in Bone Regeneration, *Bone Tissue Regen. Insights*, 2016, **7**, p 9–19, doi:10.4137/btri.s36138.
2. L. Sun, C.C. Berndt, K.A. Gross, and A. Kucuk, Material Fundamentals and Clinical Performance of Plasma-Sprayed Hydroxyapatite Coatings: A Review., *J. Biomed. Mater. Res.*, (United States), 2001, **58**(5), p 570–592.
3. A. McCabe, M. Pickford, and J. Shawcross, The History, Technical Specifications and Efficacy of Plasma Spray Coatings Applied to Joint Replacement Prostheses, *Reconstr. Rev.*, 2016, **6**(4), p 19–26.
4. R. Azari, H.R. Rezaie, and A. Khavandi, Effect of Titanium Dioxide Intermediate Layer on Scratch and Corrosion Resistance of Sol–Gel-Derived HA Coating Applied on Ti-6Al-4V Substrate, *Prog. Biomater.*, 2021, **10**(4), p 259–269.
5. R.B. Heimann, Plasma-Sprayed Hydroxylapatite Coatings as Biocompatible Intermediaries Between Inorganic Implant Surfaces and Living Tissue, *J. Therm. Spray Technol.*, 2018, **27**(8), p 1212–1237.
6. H. Zhou, B. Liang, H. Jiang, Z. Deng, and K. Yu, Magnesium-Based Biomaterials as Emerging Agents for Bone Repair and Regeneration: From Mechanism to Application, *J. Magnes. Alloy.*, Elsevier, 2021, **9**(3), p 779–804.
7. S. Castiglioni, A. Cazzaniga, W. Albisetti, and J.A.M. Maier, “Magnesium and Osteoporosis: Current State of Knowledge and Future Research Directions,” *Nutrients*, 2013.
8. B. Karakuzu-Ikizler, P. Terzioğlu, Y. Basaran-Elalmis, B.S. Tekerek, and S. Yücel, Role of Magnesium and Aluminum Substitution on the Structural Properties and Bioactivity of Bioglasses Synthesized from Biogenic Silica, *Bioact. Mater.*, KeAi Communications Co., 2020, **5**(1), p 66–73.
9. D. Bellucci, A. Sola, R. Salvatori, A. Anesi, L. Chiarini, and V. Cannillo, Role of Magnesium Oxide and Strontium Oxide as Modifiers in Silicate-Based Bioactive Glasses: Effects on Thermal Behaviour, Mechanical Properties and in-Vitro Bioactivity, *Mater. Sci. Eng. C*, 2017, **72**, p 566–575.
10. A.M. Vilardell, N. Cinca, N. Garcia-Giralt, S. Dosta, I.G. Cano, X. Nogués, and J.M. Guilemany, In-Vitro Comparison of Hydroxyapatite Coatings Obtained by Cold Spray and Conventional Thermal Spray Technologies, *Mater. Sci. Eng. C*, 2020, **107**, p 110306, doi:10.1016/j.msec.2019.110306.
11. F.E. Ciraldo, E. Boccardi, V. Melli, F. Westhauser, and A.R. Boccaccini, “Tackling Bioactive Glass Excessive in Vitro Bioreactivity: Preconditioning Approaches for Cell Culture Tests,” *Acta Biomaterialia*, 2018, p 3–10.
12. F. Hohenbild, M. Arango-Ospina, A. Moghaddam, A.R. Boccaccini, and F. Westhauser, Preconditioning of Bioactive Glasses before Introduction to Static Cell Culture: What Is Really Necessary?, *Methods Protoc.*, 2020, **3**(2).
13. J.E. Gough, I. Notingher, and L.L. Hench, Osteoblast Attachment and Mineralized Nodule Formation on Rough and Smooth 45S5 Bioactive Glass Monoliths, *J. Biomed. Mater. Res. - Part A*, 2004, **68**(4), p 640–650.
14. J.M. Lane, J.E. Mait, A. Unnanuntana, B.P. Hirsch, A.D. Shaffer, and O.A. Shonuga, Materials in Fracture Fixation, *Comprehensive Biomaterials*, Elsevier, 2011, p 219–235.
15. S.J. Watts, R.G. Hill, M.D. O’Donnell, and R. V. Law, Influence of Magnesia on the Structure and Properties of Bioactive Glasses, *J. Non. Cryst. Solids*, North-Holland, 2010, **356**(9–10), p 517–524.
16. K. Shimoda, Y. Tobu, M. Hatakeyama, T. Nemoto, and K. Saito, Structural Investigation of Mg Local Environments in Silicate Glasses by Ultra-High Field 25Mg 3QMAS NMR Spectroscopy, *Am. Mineral.*, 2007, **92**(4), p 695–698.
17. J.F. Stebbins, Structure and Dynamics of Magnesium in Silicate Melts: A High-Temperature 25Mg NMR Study, *Am. Mineral.*, 1998, **83**(9–10), p 1022–1029.
18. R. Sergi, V. Cannillo, A.R. Boccaccini, and L. Liverani, Incorporation of Bioactive Glasses Containing Mg, Sr, and Zn in Electrospun PCL Fibers by Using Benign Solvents, *Appl. Sci.*, 2020, **10**(16), p 5530, doi:10.3390/app10165530.

4.3. Production and characterization of bioactive glass/PEEK coatings

As detailed in the literature review, different thermal spray technologies have been employed to produce bioactive glass coatings, with powder as feedstock material (APS and FS) and with suspensions (HVSFS, SPS and SPPS).

However, no studies were found using cold spray, being a technique of particular interest due to the low gas temperatures involved in the coating manufacturing. Deposit coatings by CGS allow the powder characteristics of the raw material to be preserved and favour spraying on polymeric materials without degrading them.

For the first time, we have obtained a coating of bioactive glass material deposited by CGS. It consists of a composite coating formed by a bioactive glass embedded in a PEEK matrix. PEEK was selected because it is largely used in hard tissue replacement, and the glass presence should improve the bioactive capacity of the coating and its mechanical resistance.

The first publication of this section, “Development of Bioglass/PEEK Composite Coating by Cold Gas Spray for Orthopedic Implants” is focused on obtaining the composite coating and a study of its mechanical properties depending on the glass content. The second paper, “45S5/PEEK coatings by Cold Gas Spray with in vitro bioactivity, degradation and cellular proliferation” (still pendent of acceptance) is focused on the biological response of the composite coating; this addresses bioactivity test, degradation study and cell assessment with osteoblasts to verify the promoting effect of the presence of glass particles.

J Therm Spray Tech
https://doi.org/10.1007/s11666-021-01312-w

PEER REVIEWED

Development of Bioglass/PEEK Composite Coating by Cold Gas Spray for Orthopedic Implants

B. Garrido[1] · V. Albaladejo-Fuentes[1] · I. G. Cano[1] · S. Dosta[1]

Submitted: 17 May 2021 / in revised form: 15 December 2021 / Accepted: 16 December 2021

Journal of Thermal Spray Technology (January 2022), In Press

https://doi.org/10.1007/s11666-021-01312-w

Abstract

Cold gas spray (CGS) technology has allowed the development of biofunctional coatings composed of 45S5 and polyetheretherketone (PEEK). The combination of a bioactive glass material embedded in a polymeric matrix makes this composite an interesting material for orthopedic applications since this composite meets the biomechanical and biological requirements of an implant. In the present study, blends of bioactive glass 45S5 and PEEK powder with different granulometry and 45S5/PEEK ratio have been prepared. These mixtures of powders have been deposited onto PEEK substrates by CGS with the goal of incorporating a bioactive additive to the biocompatible polymer, which can improve the bone-implant interaction of PEEK. The deposition efficiency (DE) of the coatings has been evaluated, and from the results obtained, it was possible to conclude that DE is significantly affected by the granulometry and by the 45S5/PEEK ratio of the blends. By scanning electron microscopy (SEM) inspection, it was observed that the use of blends with high 45S5/PEEK ratio lead to the deposition of coatings with high content of 45S5. Finally, the friction behavior of the coatings was analyzed performing ball-on-disk tests and these experiments showed that the presence of glass particles has a beneficial role in the wear resistance.

Keywords: Bioactive glass; Biomaterials; Cold Spray; Mixtures; PEEK; Wear testing

1. Introduction

The replacement of damaged bone tissue with an implant is currently used widely to manage numerous diseases, with the implementation of this strategy increasing every year (Ref 1,2). Its success is a consequence of the research performed over the years on new materials that meet the biomechanical and biological requirements of an artificial implant in order to reduce the number of rejections in patients (Ref 3,4). This field continues to evolve and some materials have already been consolidated for certain applications, such as stainless steel in temporary fixation devices and titanium in dental implants (Ref 5,6). Currently, the improvement of implants to extend their durability and increase their success rate after implantation focuses on three different aspects: (i) the use of composite material, (ii) doping of conventional materials and (iii) surface modification. It should be noted though that the development and search of new biomaterials that have better properties than current ones are not being fully neglected.

Polyetheretherketone (PEEK) is a promising biomaterial for orthopedic applications. This biomaterial is a thermoplastic polymer in the polyaryletherketone (PAEK) family (Ref 7), which emerged in the late 1990s as an ideal candidate to replace metal implant components. PEEK is a biocompatible material that is chemically and physically stable and exhibits a similar elastic modulus to that of cortical bone, which makes it suitable for some orthopedic applications (Ref 8). However, PEEK is biologically inert and prevents good bonding when implanted in vivo. This drawback makes it fundamental to modify the biomaterial in order to improve its lack of bioactivity. For this purpose, surface modification (chemical treatment, physical treatment or surface coating) and composites with bioactive materials are the preferred strategies (Ref 9–18).

Bioactive glasses, discovered in 1969 at the University of Florida, are a group of reactive materials that can bond to bone tissue (Ref 19). These glasses are degradable in the body and stimulate bone cells to produce new bone, therefore being suitable for applications involving direct contact with the bone (Ref 20–23). 45S5 was the first bioactive glass to be developed and has the following composition: 45.0 SiO_2, 24.5 CaO, 24.5 Na_2O and 6.0 P_2O_5 (wt%). Due to its biological properties, this biomaterial is commercially available for specific clinical applications (Ref 23). However, their poor mechanical properties prevent these ceramic materials from being used in bulk and their application is restricted to the production of coatings, graft bone or scaffolds (Ref 20,24–29).

Thus, a correct combination of PEEK and bioactive glasses may lead to the production of very promising PEEK composite biomaterials that combine the biocompatibility and bioactivity of both materials.

Cold gas spray (CGS) is a novel coating deposition technique that can be used at lower gas temperatures and high particle velocities (Ref 30,31) when compared to conventional thermal spray technologies. During the deposition process, the substrate does not reach significantly high temperatures, which is very important when developing coatings on polymeric surfaces. In this specific technique, the particles deform and adhere to the substrate or to other particles and the coating is formed in a solid-state method (Ref 32,33).

There are a few studies on the development of bioactive glass coatings by different thermal spray techniques in the literature (Ref 34–37); however, there is no study on the use of CGS in the deposition of bioactive glasses. The glass transition temperature of bioactive glasses makes it difficult to produce glass coatings using this technique. Taking into account the adhesion mechanism of the coatings in the CGS process, the combination of a polymer (PEEK) and glass (45S5) can help to deposit this new composite functional material. Sanpo et al. demonstrated in 2009, the feasibility of deposit a ceramic material combined with PEEK polymer using CGS technology (Ref 38). In particular, they observed that the polymer formed a continuous matrix in which the silver ion-doped HA was embedded.

Other studies have reported the manufacturing of PEEK/45S5 coatings on metallic substrates using the electrophoretic deposition technique (Ref 13,18). However, the development of PEEK/45S5 coatings on a PEEK substrate has not been studied to date. This blend of PEEK and 45S5 will be the first time that a bioactive glass has been deposited by the CGS technique.

The aim of the present work was to develop functional materials by depositing a composite PEEK/45S5 coating on PEEK samples to improve their response when implanted in the body. During the present investigation, the development of the abovementioned coatings by the CGS technique was studied, analyzing in particular the effects of the glass content. A study of the wear behavior was also carried out. The overall objective was to create a coating that can maintain appropriate mechanical properties while ensuring bioactivity and a good bone cell response.

2. Materials and Methods

2.1. Powders and substrates

To provide the bioactive capacity, a commercial 45S5 bioactive glass powder (Denfotex Research, United Kingdom) was selected, which was produced by the traditional melt-quenching route. A commercial PEEK powder (Victrex, United Kingdom) was used as the polymeric matrix of the coating. The coatings were deposited onto flat PEEK substrates measuring 50 mm × 100 mm × 5 mm (Ensinger, Spain) for the deposition efficiency studies.

PEEK disks with a 25 mm diameter, cut from a PEEK bar (Vestakeep, Spain), were used to determine the wear behavior of the coatings and to evaluate the cross-section of the coatings.

2.2. Powder characterization

The morphology of the powders was determined using a scanning electron microscope (SEM) equipped with a backscattered electron detector (Phenom ProX, Phenom-World BV, Eindhoven, the Netherlands). Before the microscopy studies, all the samples were coated by a gold layer to make them conductive using a SEM coating unit (E-5000, Polaron, Watford, England).

A laser diffraction particle size analyzer (LS 13320, Beckman Coulter, California, USA) was used to measure the granulometry of the powders. Commercial PEEK and 45S5 powders were sieved to obtain two powder fractions of each material using a 63 µm and a 40 µm mesh sieve (Retsch, Germany). In this way, it was possible to assess the effect of the granulometry on the deposition efficiency (DE) and the thickness of the coatings. Since powders of small particles on the micrometric scale (between 1 and 50 µm) (Ref 39) are recommended for the CGS technique, the ranges selected were those between 40 and 63 µm, called the “coarse range”, and those below 40 µm, called the “fine range”.

The tapped density (ρt) of the different powders was measured using a graduated cylinder. The powder was tapped regularly to settle the powder inside the cylinder. The filling and tapping process was repeated until the volume of the powder remained fixed at 5 ml.

2.3. Coating deposition

For the coating deposition, the low-pressure cold gas spray (LPCGS) equipment (Dymet 423, Dycomet Europe, Akkrum, the Netherlands) was used with air as the propellant gas. The blends were deposited onto PEEK substrates previously grit blasted (Formula 1400, Guyson International, Skipton, England) with corundum G24 (grit size 800 µm) at a pressure of 0.5 MPa. Afterwards, the substrates were cleaned with ethanol. The surface roughness after the grit blasting process was Ra = 4.9 ± 0.4 µm and Rz = 27.3 ± 2.8 µm. The spraying parameters are listed in Table 1.

In this study, coatings with two different thickness were produced by varying the traverse gun speed. The thick coatings, which allow a better observation, were sprayed using low traverse gun speed (80 mm/s) and were used for characterize the materials deposition, microstructure and distribution of the elements. Using a high traverse gun speed (240 mm/s) thin coatings were obtained. These coatings, with a suitable thickness for the final application, were used to study the wear and hardness of the coatings.

The LPCGS is a thermal spray technique that involves relatively low temperatures. The equipment used allowed us to work with gas temperatures ranging from room temperature to

500ºC. This enabled us to spray polymers without decomposing them. The glass transition temperature of PEEK starts at 143ºC, with melting achieved at 343ºC and the decomposition starting at 575ºC (Ref 40). Moreover, the amorphous structure of the bioactive glass is not affected at the studied temperatures (300-350ºC). The glass transition temperature of the 45S5 bioactive glass starts at 550ºC and melting occurs at 1070ºC (Ref 41).

Table 1. Cold gas spraying parameters

Spraying parameters	
Pressure (bar)	5-6
Gas temperature (ºC)	300-350
Spray distance (mm)	10
Layers	1
Gun traverse speed (mm/s)	80-240

The DE is the ratio in percentage of the mass of the material deposited on the specimen to the mass of the sprayed material.

$$\boldsymbol{DE}\ (\%) = \frac{\Delta \boldsymbol{m}_{\boldsymbol{specimen}}}{\Delta \boldsymbol{m}_{\boldsymbol{sprayed\ material}}}\ \boldsymbol{x}\ \mathbf{100}$$

As mentioned before, the granulometry of the powders can affect the DE and the thickness of the coatings. A preliminary study was conducted to choose the optimal size distribution of the powders to develop subsequent tests. Hence, three blends of fine and coarse powders were sprayed, with the amount of glass powder kept at 10% in volume in all the cases. These blends corresponded to: PEEK/45S5 (fine/fine), using the fine range of both powders; PEEK/45S5 (coarse/fine), using the coarse and fine range of PEEK and 45S5, respectively; and PEEK/45S5 (coarse/coarse), using the coarse range of both powders. In addition, PEEK powders corresponding to the fine and coarse range were also sprayed to determine the DE of the polymeric material with a different particle size distribution.

After the preliminary study, the effect of glass content on the blends was evaluated using the selected granulometry of the powders. For this purpose, the blends of PEEK and the bioactive glass were prepared by manually mixing: 0, 10, 25, 35 and 50 volume percentages of 45S5.

2.4. Coating characterization

The thickness of the coating was measured from the cross-sectional images of each coating using an optical microscope (DMI 5000 M, Leica, Wetzlar, Germany). The calculation of the thickness involved measuring the width of the cross-section at eight points distributed along the length of each microsection and calculating the arithmetic mean of the measurements. For each coating, five cross-sectional images were taken at a magnification of 50x.

The cross-sections of the coatings were prepared by cold mounting resin and grinding them with silicon carbide abrasive papers up to P4000 (grit size 5 µm). Finally, the samples were polished with 1 µm diamond solution.

To confirm the influence of the glass powder on the thickness of the samples, coatings with significantly different thicknesses were analyzed. Depending on the gun traverse speed used, different thicknesses were obtained. Thicknesses of approximately 900-700 µm were obtained at a traverse speed of 80 mm/s, whereas thicknesses of 300-200 µm were obtained when applying a traverse speed of 240 mm/s.

To analyze the distribution of the elements of the blend in the cross-section, an elemental mapping was performed on the gold-covered cross-sections. The main element of the glass, silicon, was chosen to identify the presence of 45S5 in the coating. An SEM (JSM-5310, JEOL, Tokyo, Japan) equipment with energy-dispersive X-ray spectroscopy (EDS) was used for this analysis.

The glass content within the coating was analyzed on large areas of the coatings sprayed with a lower gun traverse speed that allowed a better observation of the particle distribution.

Image analysis of the micrographs was done to quantify the area percentage of glass material by means of ImageJ program. The area percentage was measured by an average of 5 images for each coating, taken at a magnification of 200x. It should be noted that the glass quantity on the coatings calculated correspond to an area percentage and cannot be compared with the volumetric percentages of the blends.

2.5. Tribological behavior of the coatings

A ball-on-disk test under dry conditions was developed to characterize the wear and friction behavior of the coatings. Four tests were performed for each coating, applying a load of 5 N at a constant velocity of 133 rpm for a total sliding distance of 1000 m. Alumina balls with a diameter of 9 mm were used and the track radius developed on the samples was 13 mm. The surfaces were prepared to obtain an Ra value under 0.8 µm to meet the specifications of the ASTMG99-95 (Ref 42). All the tests were performed at room temperature with a relative humidity of about 30%.

After the tests, the wear track of each sample was analyzed at four different points employing a confocal microscope (PLu 2300, Sensofar, Barcelona, Spain) to calculate the volume of lost material due to wear. For this evaluation, the track cross-section area was multiplied by the track length to obtain the wear volume.

In addition, the wear scars and the alumina balls were examined by SEM to analyze the effects of the wear mechanisms involved in the process.

Finally, hardness was measured on polished cross-sections, using a micro vickers hardness tester (MXT-01, Matsuzawa Seiki, Tokio, Japan). For each coating, ten indentations were done along the cross-section under a load of 50 gf.

3. Results and Discussion

3.1. Powder characterization

The morphology of the powders can be seen in Figure 1. The 45S5 powder shows an irregular morphology with angular-shaped particles, as expected due to the route of fabrication. The free surface of the PEEK powder presents a spherical and porous morphology of the agglomerated powder, with agglomerated particles measuring between 5 and 40 µm.

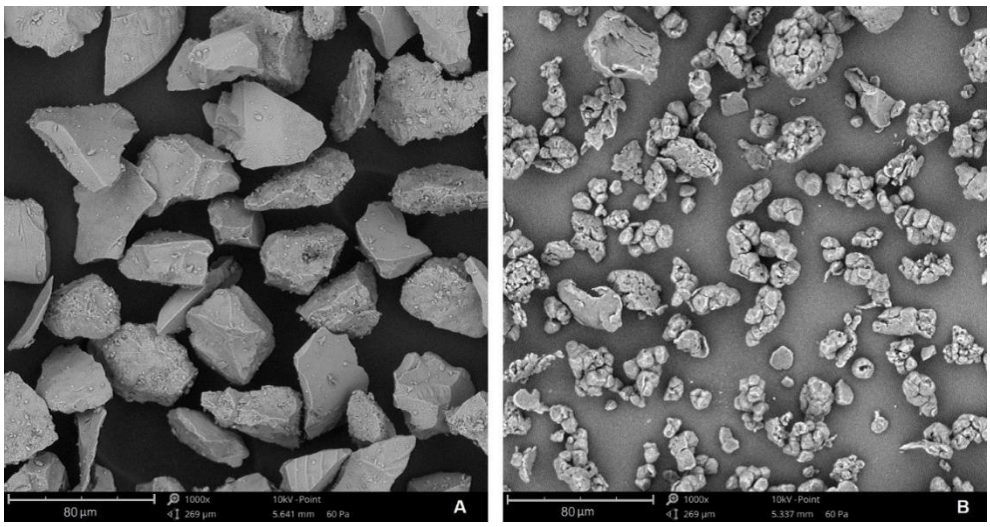

Figure 1. SEM micrographs of the free surface of bioactive glass (a) and PEEK (b) powders

The characteristic values of the size distribution of the powders and their density are listed in Table 2.

Table 2. Particle size distribution in volume and tapped density of the 45S5 and PEEK powders

	Mean (µm)	d_{10} (µm)	d_{50} (µm)	d_{90} (µm)	ρ_t (g/cm^3)
PEEK - coarse range	48.6	19.8	49.4	73.2	0.48
PEEK - fine range	22.5	10.2	21.2	37.6	0.42
45S5 - coarse range	56.5	20.6	57.9	84.9	1.38
45S5 - fine range	40.5	28.1	41.1	53.2	1.33

The glass particles were larger than the PEEK ones, as can be seen when comparing the same sieved ranges. This difference can be explained by: firstly, the size of the particles of the initial powder, where the PEEK powder had a larger quantity of fine particles; secondly, the angular morphology of the glass powder that allowed the narrow and elongated particles

to pass through the sieve on their narrowest side; and finally, the higher density of the glass powders that facilitated the passage of the particles through the sieve.

3.2. Coating deposition

A preliminary study was carried out to determine the most suitable granulometry of the powders to produce the coatings. Taking into account the DE results of the PEEK powders (presented in Figure 2), a higher efficiency was obtained when the fine range was used, with an increase of almost 10% of the DE compared to that obtained with the coarse range. For the blended powders, a higher DE was achieved when the PEEK/45S5 (fine/fine) blend was used. These results are in agreement with those of other studies showing that smaller polymeric particles reach higher values of DE with the CGS technique, which might be associated with a greater impact velocity (Ref 43). Furthermore, the lowest DE value was obtained with the PEEK/45S5 (coarse/coarse) blend.

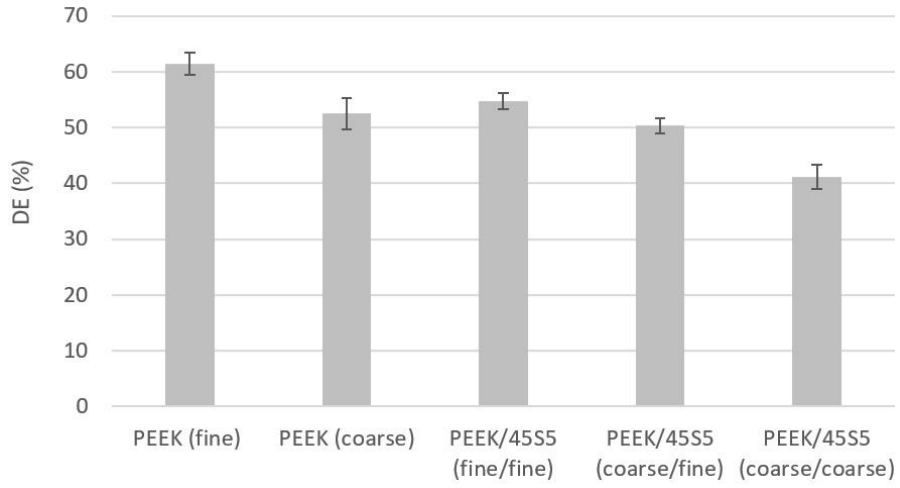

Figure 2. Deposition efficiency of blends with 90 vol.% of PEEK and 10 vol.% of 45S5 in the feedstock and different granulometry

Based on the results of this initial study, coatings were produced with the fine range of each material.

The influence of the glass content on the DE was analyzed using the PEEK/45S5 (fine/fine) blend. The results are presented in Figure 3, which shows a clear tendency of the efficiencies decreasing with an increasing glass content in the feedstock. This effect can be attributed to the difficulty of depositing glass particles, which are brittle, with this technique. It has been widely demonstrated that in the CGS technique, plastic deformation of the particle that is impinging onto the substrate surface is required for particle adhesion. However, in this specific case (in polymers), thermal softening of the powder and proper substrate roughness play a major role in the adhesion to the substrate.

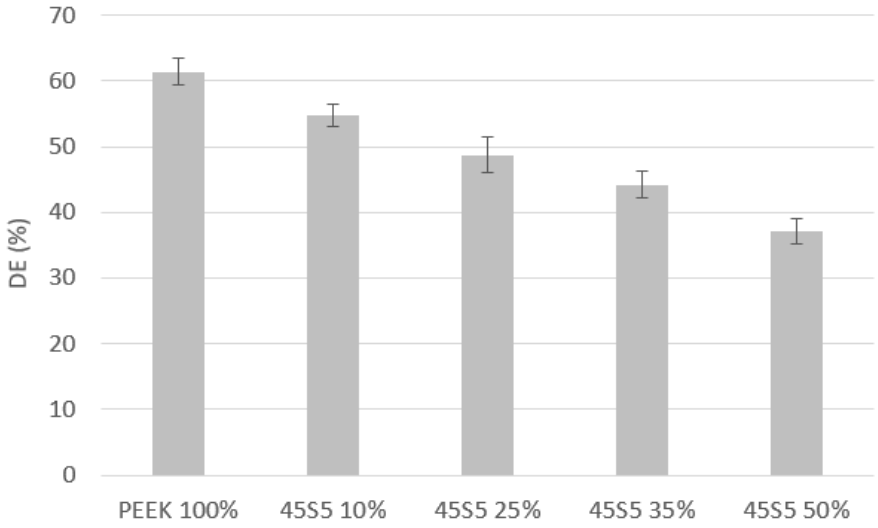

Figure 3. Deposition efficiency of mixtures PEEK/45S5 with different volume ratio in the feedstock

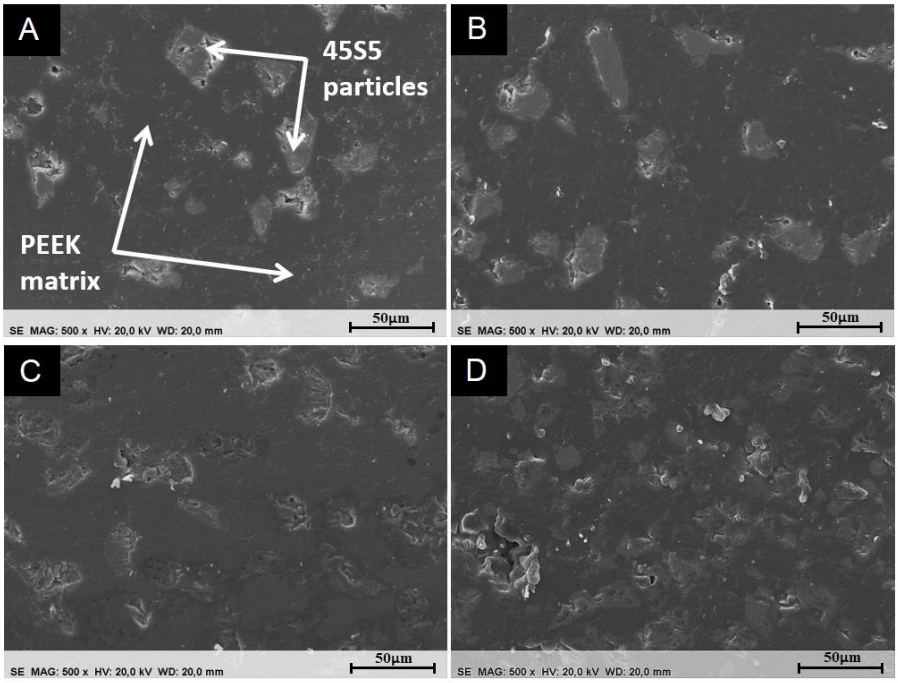

Figure 4. Cross-sectional SEM images: (a) 45S5 10%, (b) 45S5 25%, (c) 45S5 35% and (d) 45S5 50%

Considering the differences in the physical properties of the two feedstock materials, it can be assumed that it is easier for the polymers to reach deformation by thermal softening. Glass particles are more difficult to deform without melting and they impinge onto the substrate in a brittle state when sprayed. Glass particles are not deformed during the process and are embedded in a polymer matrix composed of the PEEK particles (Figure 4). In addition, it is assumed that in blends with a lower PEEK content, the glass particles find fewer areas to adhere to and the impact between the glass particles results in abrasive behavior. Therefore, the PEEK coating without glass showed the highest efficiency value of 61%, with the DE gradually decreasing with the increasing presence of glass.

3.3. Coating characterization

The effect of the glass content on the thickness of the coatings was determined by visual inspection of the cross-sections of the coatings. This analysis was carried out on coatings obtained with different gun traverse speeds (80 mm/s and 240 mm/s). The results are displayed in Figure 5.

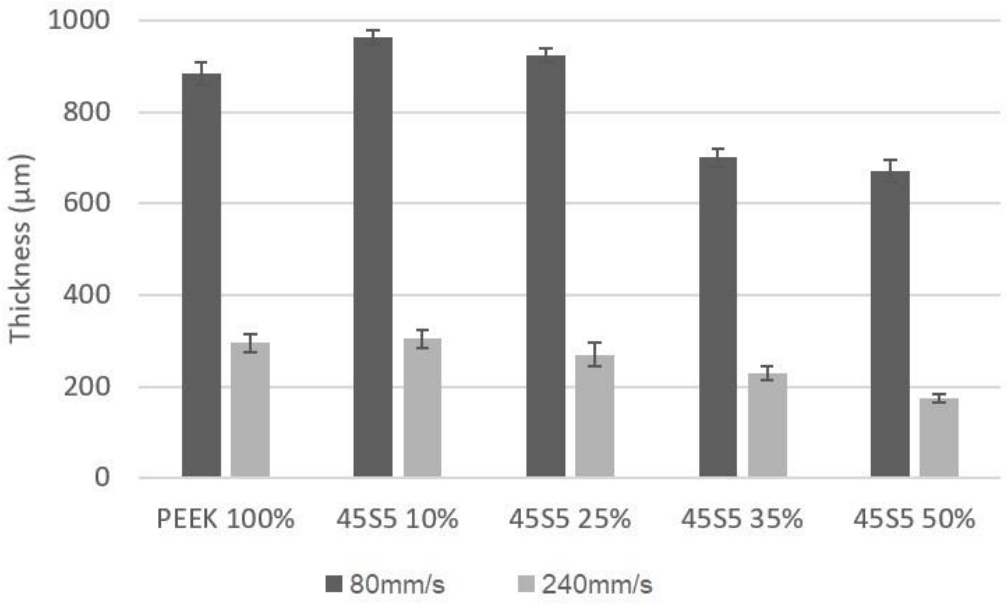

Figure 5. Coating thickness of PEEK/45S5 blends sprayed at low and high traverse speed

A slight increase in thickness was observed when the blend with 10 vol % of glass was used for both, the low and high speed, while the DE decreased slightly, as can be seen in Figure 3 (low speed). This difference in tendency could be explained because the glass particles embedded into the coating are larger than the PEEK particles and did not deform during the spraying process. This could have caused the slight increase in the thickness of the coating produced with 10 vol % of glass.

The blends with glass content starting from 35 vol % resulted in a gradual decrease in the thickness, showing the same tendency as the DE. In the coatings with more glass, it is expected that the glass particles find fewer areas rich in PEEK particles to help in their adhesion when they reach the surface, resulting in thinner coatings.

In particular, the 25 vol% coatings, showed an intermediate result. The thickness of the coating sprayed at low traverse speed was higher than the PEEK 100% coating while the DE decreased. On the contrary, when this blend was sprayed at high traverse speed, the thickness of the coating decreased respect the pure PEEK coating, as well as the DE. This result could be explained because in the thicker coating, where more material is forming the coating, the effect of the size of the glass particles has a greater relevance.

The results corroborated that the presence of PEEK in the blend allows the deposition of the glass, which by itself cannot build up a coating.

The thickness of the pure PEEK coatings was exactly three times lower when the speed was increased by up to three times (Figure 5). This indicated that PEEK particles can adhere to the substrate and to other particles with the same ease. On the contrary, in coatings containing glass, the thickness was reduced by more than 3 times when the speed was increased by up to three times. This may be due to the poor adhesion of the glass directly to the substrate.

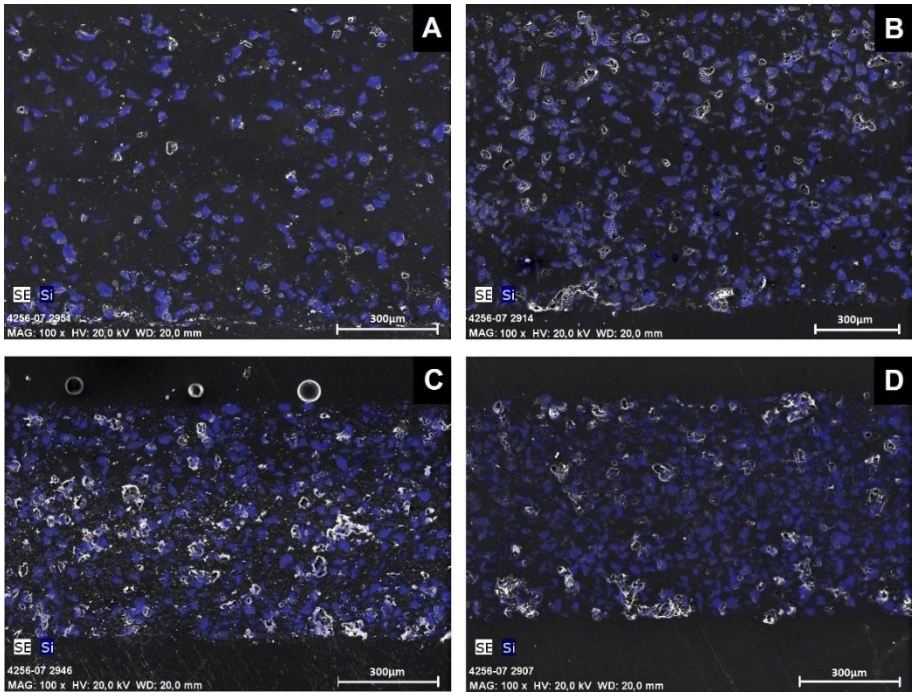

Figure 6. EDS maps showing the distribution of silicon (representing glass) in the cross section: (a) 45S5 10%, (b) 45S5 25%, (c) 45S5 35% and (d) 45S5 50%

For the coatings to be bioactive, it is important that the glass particles are well distributed throughout the coating, especially at its surface. For this purpose, the glass content was analyzed on the coatings sprayed with a lower gun traverse speed that allowed a better observation of the particle distribution. However, to validate this analysis, it was verified (analyzing one of the coatings sprayed at 240mm/s) that the glass concentration in the coating is not affected by the gun traverse speed.

A mapping of silicon, corresponding to the main element of the 45S5 glass, is shown in Figure 6 and the results of area percentage, from the image analysis are displayed in Table 3. The low standard deviation verifies the homogeneity of the distribution of the glass particles throughout the coating. In addition, it has been seen that the polymer matrix allows the deposition of a large amount of glass in the coating, producing a coating with up to an area of 32% of glass when the blend with 50 vol % of glass was used. Moreover, as can be seen

in Figure 5, glass particles were also found on the surface of the coating, thus indicating its potential bioactive capacity.

3.4. Wear friction study

The mean value of the wear coefficient calculated in the last 200 m is shown in Table 3. Furthermore, the volume of lost material was determined by confocal microscopy. The test was carried out on the coatings obtained by spraying blends with different glass contents at 240 mm/s, which provided sufficiently thick coatings for the test.

Table 3. Properties of the coatings obtained using PEEK/45S5 (fine/fine) blends

	Glass quantity on coating (area %)	Coefficient of friction, μ	Volume of lost material (mm^3)	Volume loss respect pure PEEK coating (%)
PEEK 100%	-	0.51 ± 0.04	0.790 ± 0.236	-
45S5 10%	6.9 ± 0.1	0.50 ± 0.02	0.181 ± 0.018	23
45S5 25%	14.2 ± 0.2	0.40 ± 0.03	0.226 ± 0.080	29
45S5 35%	27.9 ± 1.1	0.41 ± 0.02	0.200 ± 0.070	25
45S5 50%	32.6 ± 1.9	0.37 ± 0.04	0.147 ± 0.033	19

When analyzing the coatings without any glass content, some holes could be observed, which corresponded to PEEK particles that had been pulled out from the coating matrix (Figure 7A, B). Furthermore, clear ploughing was observed, where PEEK particles from the coating had been pushed and displaced to form ridges adjacent to the grooves found in the sliding track (Figure 7A).

It is assumed that some of the PEEK particles that had detached during the test were deposited again onto the track, while others adhered to the alumina ball and some appeared as debris on the surface of the coatings after the test.

A different mechanism was observed when glass particles were present in the coatings. There were several cracks on the glass particles (clear particles in Figure 7D, F, H, J). It seems that the detached glass fragments caused parallel grooves on the sliding track (Figure 7D, F, H, J) before being re-encrusted onto the PEEK-rich areas of the track. This was assumed because no holes related to the PEEK particles were observed in the sliding track, while small glass particles were seen on the track that were smaller in size than the feedstock glass particles.

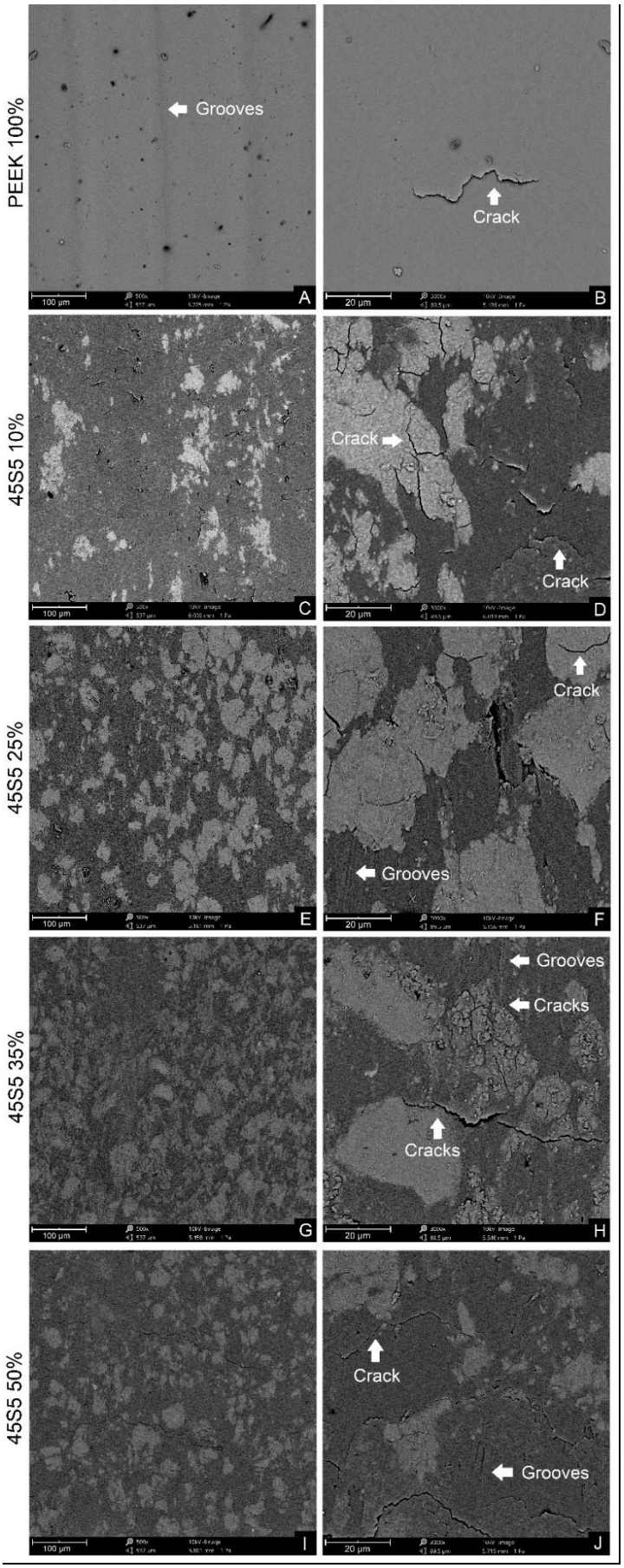

Figure 7. SEM images of the wear track at low and high magnifications

From the results obtained, it is assumed that a path with a progressively higher glass content was generated during the test. It was noticed that glass particles prevented the detachment of the polymer particles, resulting in a significant decrease in wear that was reflected by a remarkable reduction in the volume of lost material and a decrease in the coefficient of friction.

In the samples with a low glass content (10 vol % of 45S5), the volume of lost material was significantly reduced when compared to the coatings with no glass (from 0.790 mm^3 to 0.181 mm^3). However, the coefficient of friction decreased only slightly (from 0.51 to 0.50).

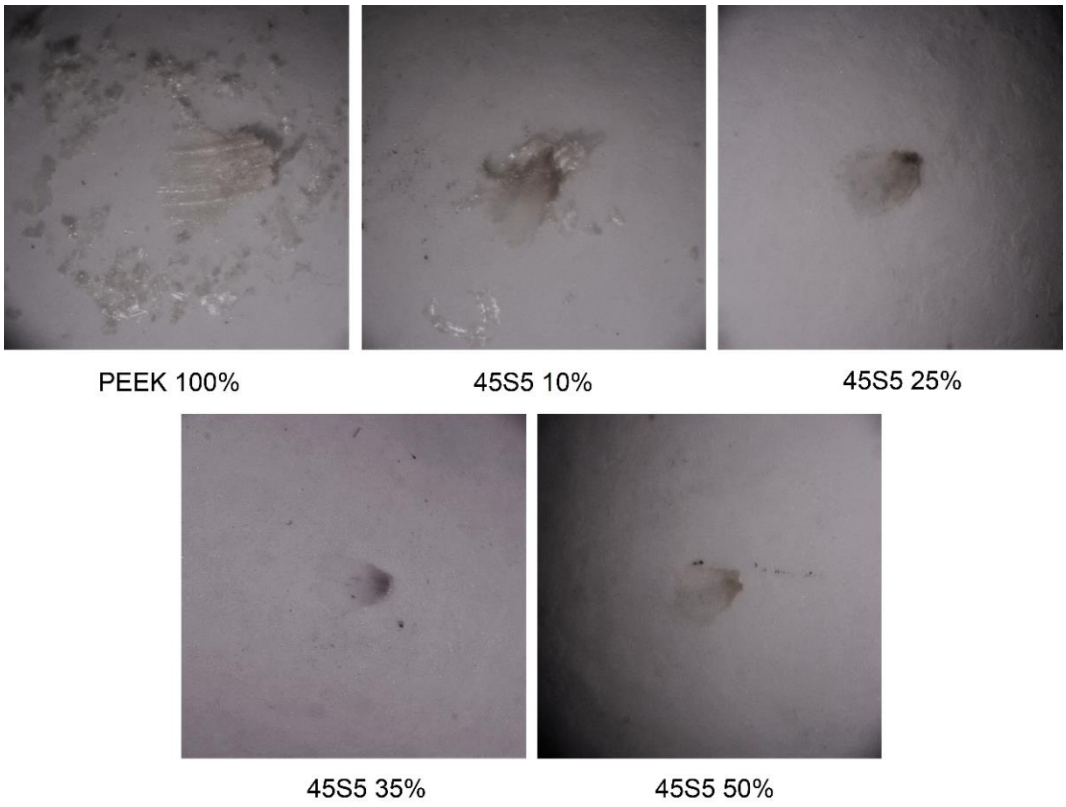

Figure 8. Alumina balls after the ball-on-disk test

On the surfaces of these coatings, debris related to the PEEK particles appeared after the test and PEEK particles also adhered to the alumina balls, as can be seen in Figure 8. Both events occurred to a lesser degree in the coatings with glass. The amount of glass in the coatings with 10 vol % of 45S5 was not enough to provide a clear protection against wear.

Finally, in the coatings containing 25 vol % or more of glass, no debris was observed on the surface after the test and fewer PEEK particles adhered to the alumina balls (Figure 8). The fragments of glass particles were re-encrusted onto the sliding track, producing a path with a high amount of glass that meant better resistance against wear and generating lower coefficient of friction values for these coatings, particularly those containing 50 vol % of 45S5.

The hardness results obtained can be seen in Figure 9. Coatings containing glass show higher values of hardness when compared to pure PEEK coatings. The glass particles

provide less deformability to the composite coating, for this reason the hardness increases slightly with the presence of glass.

The higher hardness of coatings containing glass causes the wear resistance increase and the reduction in the volume of lost material evaluated in the wear friction study.

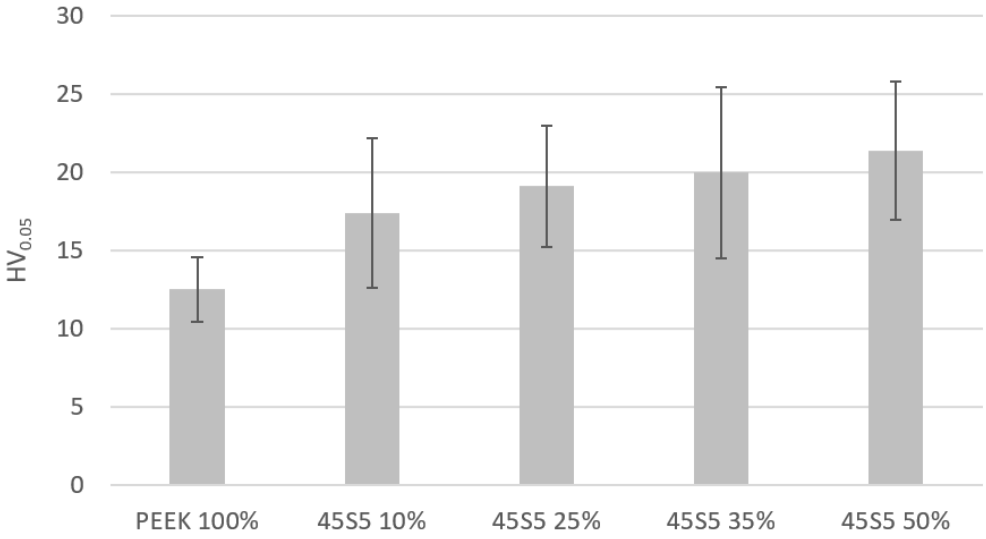

Figure 9. Vickers hardness values of PEEK/45S5 composite coatings

4. Conclusions

This study demonstrated that the LPCGS technology can easily produce 45S5/PEEK bioactive coatings with improved wear resistance.

The use of PEEK in the blend material facilitated the deposition of bioactive glass particles by the CGS technique. In this way, a bioactive component could be incorporated into the coatings. Further studies should be conducted to validate the bioactivity of the developed composite coatings.

The highest DE values were obtained when mixtures of fine particles were used. Decreases in the DE and the coating thickness were observed with an increasing glass content in the blend. This was probably due to the glass particles not being deformed during the process, but only being embedded into a polymer matrix composed of PEEK particles. In addition, the cross-sections revealed that the glass particles were homogeneously distributed throughout the coatings.

The high degree of wear caused on the pure PEEK coatings can be explained by the plastic deformation of the PEEK particles. The presence of glass in the coatings increased wear resistance, as reflected by a decrease in the coefficient of friction and a reduction in the volume of lost material (more than 70% when compared to the pure PEEK coatings). In this case, glass particles prevented the polymeric particles from detaching. The coating containing 50 vol % of 45S5 showed the highest wear resistance and hardness.

References

1. S. Kurtz, K. Ong, E. Lau, F. Mowat, and M. Halpern, Projections of Primary and Revision Hip and Knee Arthroplasty in the United States from 2005 to 2030, *J. Bone Jt. Surg. - Ser. A*, 2007, **89**(4), p 780–785

2. B.D. Ratner, A.S. Hoffman, F.J. Schoen, and J. Lemons, Biomaterials Science: A Multidisciplinary Endeavor, *Biomaterials Science*, 2nd ed., B.D. Ratner, A.S. Hoffman, F.J. Schoen, and J. Lemons, Eds., Academic Press, 2004, p 1–20

3. N. Patel and P. Gohil, A Review on Biomaterials: Scope, Applications & Human Anatomy Significance, *Int. J. Emerg. Technol. Adv. Eng.*, 2012, **2**(4), p 91–101

4. B. Dhandayuthapani and D.K. Sakthi, Biomaterials for Biomedical Applications, *Biomedical Applications of Polymeric Materials and Composites*, R. Francis and D.K. Sakthi, Eds., Wiley-VCH Verlag, 2016, p 1–20

5. M. Saini, Implant Biomaterials: A Comprehensive Review, *World J. Clin. Cases*, 2015, **3**(1), p 52–57

6. W. Jin and P.K. Chu, Orthopedic Implants, *Encyclopedia of Biomedical Engineering*, R. Narayan, Ed., Elsevier Inc., 2019, p 425–439

7. S.M. Kurtz and J.N. Devine, PEEK Biomaterials in Trauma, Orthopedic, and Spinal Implants, *Biomaterials*, 2007, **28**(32), p 4845–4869

8. D. Almasi, N. Iqbal, M. Sadeghi, I. Sudin, M.R. Abdul Kadir, and T. Kamarul, Preparation Methods for Improving PEEK's Bioactivity for Orthopedic and Dental Application: A Review, *International Journal of Biomaterials*, 2016, **2016**, 1-12

9. M.A. Ur Rehman, F.E. Bastan, A. Nawaz, Q. Nawaz, and A. Wadood, Electrophoretic Deposition of PEEK/Bioactive Glass Composite Coatings on Stainless Steel for Orthopedic Applications: An Optimization for in Vitro Bioactivity and Adhesion Strength, *Int. J. Adv. Manuf. Technol.*, 2020, **108**(5–6), p 1849–1862

10. A. Nawaz, S. Bano, M. Yasir, A. Wadood, and M.A. Ur Rehman, Ag and Mn-Doped Mesoporous Bioactive Glass Nanoparticles Incorporated into the Chitosan/Gelatin Coatings Deposited on PEEK/Bioactive Glass Layers for Favorable Osteogenic Differentiation and Antibacterial Activity, *Mater. Adv.*, 2020, **1**(5), p 1273–1284

11. S.W. Ha, M. Kirch, F. Birchler, K.L. Eckert, J. Mayer, E. Wintermantel, C. Sittig, I. Pfund-Klingenfuss, M. Textor, N.D. Spencer, M. Guecheva, and H. Vonmont, Surface Activation of Polyetheretherketone (PEEK) and Formation of Calcium Phosphate Coatings by Precipitation, *J. Mater. Sci. Mater. Med.*, 1997, **8**(11), p 683–690

12. J.P. Fan, C.P. Tsui, C.Y. Tang, and C.L. Chow, Influence of Interphase Layer on the Overall Elasto-Plastic Behaviors of HA/PEEK Biocomposite, *Biomaterials*, 2004, **25**(23), p 5363–5373

13. M.A. Ur Rehman, F.E. Bastan, Q. Nawaz, W.H. Goldmann, M. Maqbool, S. Virtanen, and A.R. Boccaccini, Electrophoretic Deposition of Lawsone Loaded Bioactive Glass (BG)/Chitosan Composite on Polyetheretherketone (PEEK)/BG Layers as Antibacterial and Bioactive Coating, *J. Biomed. Mater. Res. - Part A*, 2018, **106**(12), p 3111–3122

14. Y. Torres, C. Romero, Q. Chen, G. Pérez, J.A. Rodríguez-Ortiz, J.J. Pavón, L. Álvarez, C. Arévalo, and A.R. Boccaccini, Electrophoretic Deposition of PEEK/45S5 Bioactive Glass Coating on Porous Titanium Substrate: Influence of Processing Conditions and Porosity Parameters, *Key Eng. Mater.*, T. Ebel and F. Pyczak, Eds., Aug 31 - Sept 3, 2015 (Lüneburg, Germany), Trans Tech Publications, 2016, p 343–350

15. M. Miola, E. Verné, A. Piredda, S. Seuss, S. Cabanas-Polo, and A.R. Boccaccini, Development and Characterization of PEEK/B_2O_3-Doped 45S5 Bioactive Glass Composite Coatings Obtained by Electrophoretic Deposition, *Key Eng. Mater.*, A.R. Boccaccini, J.H. Dickerson, B. Ferrari, O. Van der Biest, and T. Uchikoshi, Eds., Oct 5-10, 2014 (Hernstein, Austria), Trans Tech Publications, 2015, **654**, p 165–169

16. S. Yu, K. Prakash, R. Kumar, and P. Cheang, In Vitro Apatite Formation and Its Growth Kinetics on Hydroxyapatite / Polyetheretherketone Biocomposites, 2005, **26**, p 2343–2352

17. W. Hong, F. Guo, J. Chen, X. Wang, X. Zhao, and P. Xiao, Bioactive Glass–Chitosan Composite Coatings on PEEK: Effects of Surface Wettability and Roughness on the Interfacial Fracture Resistance and in Vitro Cell Response, *Appl. Surf. Sci.*, 2018, **440**, p 514–523

18. S. Seuss, M. Heinloth, and A.R. Boccaccini, Surface & Coatings Technology Development of Bioactive Composite Coatings Based on Combination of PEEK , Bioactive Glass and Ag Nanoparticles with Antibacterial Properties, *Surf. Coat. Technol.*, 2016, **301**, p 100–105

19. L.L. Hench and J.R. Jones, Bioactive Glasses: Frontiers and Challenges, *Front. Bioeng. Biotechnol.*, 2015, **3**

20. G. Kaur, V. Kumar, F. Baino, J.C. Mauro, G. Pickrell, I. Evans, and O. Bretcanu, Mechanical Properties of Bioactive Glasses, Ceramics, Glass-Ceramics and Composites: State-of-the-Art Review and Future Challenges, *Mater. Sci. Eng. C*, 2019, **104**

21. A. Hoppe, N.S. Güldal, and A.R. Boccaccini, A Review of the Biological Response to Ionic Dissolution Products from Bioactive Glasses and Glass-Ceramics, *Biomaterials*, 2011, **32**(11), p 2757–2774

22. D.S. Brauer, Bioactive Glasses - Structure and Properties, *Angew. Chemie - Int. Ed.*, 2015, **54**(14), p 4160–4181

23. J.R. Jones, Review of Bioactive Glass: From Hench to Hybrids, *Acta Biomater.*, 2013, **9**(1), p 4457–4486

24. S. Lopez-Esteban, E. Saiz, S. Fujino, T. Oku, K. Suganuma, and A.P. Tomsia, Bioactive Glass Coatings for Orthopedic Metallic Implants, *J. Eur. Ceram. Soc.*, 2003, **23**(15), p 2921–2930

25. N.C. Lindfors, I. Koski, J.T. Heikkilä, K. Mattila, and A.J. Aho, A Prospective Randomized 14-Year Follow-up Study of Bioactive Glass and Autogenous Bone as Bone Graft Substitutes in Benign Bone Tumors, *J. Biomed. Mater. Res. - Part B Appl. Biomater.*, 2010, **94B**(1), p 157–164

26. N.C. Lindfors, P. Hyvönen, M. Nyyssönen, M. Kirjavainen, J. Kankare, E. Gullichsen, and J. Salo, Bioactive Glass S53P4 as Bone Graft Substitute in Treatment of Osteomyelitis, *Bone*, 2010, **47**(2), p 212–218

27. K. Pernaa, I. Koski, K. Mattila, E. Gullichsen, J. Heikkilä, A.J. Aho, and N.C. Lindfors, Bioactive Glass S53P4 and Autograft Bone in Treatment of Depressed Tibial Plateau Fractures: A Prospective Randomized 11-Year Follow-Up, *J. Long. Term. Eff. Med. Implants*, 2011, **21**(2), p 139–148

28. T. Debnath, A. Chakraborty, and T. Pal, A Clinical Study on the Efficacy of Hydroxyapatite-Bioactive Glass Composite Granules in the Management of Periodontal Bony Defects, *J. Indian Soc. Periodontol.*, 2014, **18**(5), p 593–600

29. A.A. El-Rashidy, J.A. Roether, L. Harhaus, U. Kneser, and A.R. Boccaccini, Regenerating Bone with Bioactive Glass Scaffolds: A Review of in Vivo Studies in Bone Defect Models, *Acta Biomater.*, Acta Materialia Inc, 2017, **62**, p 1–28

30. E. Irissou, J.G. Legoux, A.N. Ryabinin, B. Jodoin, and C. Moreau, Review on Cold Spray Process and Technology: Part I - Intellectual Property, *J. Therm. Spray Technol.*, 2008, **17**(4), p 495–516

31. A.M. Vilardell, N. Cinca, A. Concustell, S. Dosta, I.G. Cano, and J.M. Guilemany, Cold Spray as an Emerging Technology for Biocompatible and Antibacterial Coatings: State of Art, *J. Mater. Sci.*, Springer US, 2015, **50**(13), p 4441–4462

32. V.K. Champagne, Introduction, *The Cold Spray Materials Deposition Process*, V.K. Champagne, Ed., Elsevier, 2007, p 1–7

33. R. Kromer, R.N. Raoelison, C. Langlade, Y. Xie, M.P. Planche, T. Sapanathan, and S. Costil, Cold Gas Dynamic Spray Technology: A Comprehensive Review of Processing Conditions for Various Technological Developments till to Date, *Addit. Manuf.*, Elsevier B.V., 2017, **19**, p 134–159

34. O. Rojas, M. Prudent, M.E. López, F. Vargas, and H. Ageorges, Influence of Atmospheric Plasma Spraying Parameters on Porosity Formation in Coatings Manufactured from 45S5 Bioglass® Powder, *J. Therm. Spray Technol.*, 2020, **29**(1–2), p 185–198

35. V.L. Calvo, M.V. Cabedo, E. Bannier, E.C. Recacha, A.R. Boccaccini, L.C. Arias, and E.S. Vilches, 45S5 Bioactive Glass Coatings by Atmospheric Plasma Spraying Obtained from Feedstocks Prepared by Different Routes, *J. Mater. Sci.*, 2014, **49**(23), p 7933–7942

36. B. Garrido, I.G. Cano, and S. Dosta, Adhesion Improvement and in Vitro Characterisation of 45S5 Bioactive Glass Coatings Obtained by Atmospheric Plasma Spraying, *Surf. Coatings Technol.*, 2021, **405**

37. G. Bolelli, N. Stiegler, D. Bellucci, V. Cannillo, R. Gadow, A. Killinger, L. Lusvarghi, and A. Sola, Deposition Mechanisms in High Velocity Suspension Spraying: Case Study for Two Bioactive Materials, *Surf. Coatings Technol.*, 2012, **210**, p 28–45

38. N. Sanpo, M.L. Tan, P. Cheang, and K.A. Khor, Antibacterial Property of Cold-Sprayed HA-Ag/PEEK Coating, *J. Therm. Spray Technol.*, 2009, **18**(1), p 10–15

39. P. Vuoristo, Thermal Spray Coating Processes, *Comprehensive Materials Processing*, S. Hashmi, Ed., Elsevier, 2014, p 229–276

40. P. Patel, T.R. Hull, R.W. McCabe, D. Flath, J. Grasmeder, and M. Percy, Mechanism of Thermal Decomposition of Poly(Ether Ether Ketone) (PEEK) from a Review of Decomposition Studies, *Polym. Degrad. Stab.*, 2010, **95**(5), p 709–718

41. L. Lefebvre, J. Chevalier, L. Gremillard, R. Zenati, G. Thollet, D. Bernache-Assolant, and A. Govin, Structural Transformations of Bioactive Glass 45S5 with Thermal Treatments, *Acta Mater.*, 2007, **55**(10), p 3305–3313

42. “Test Method for Wear Testing with a Pin-on-Disk Apparatus,” G99-17, *Annual Book of ASTM Standards*, Part 17, ASTM, 2017, p 1–6

43. Y. Xu and I.M. Hutchings, Cold Spray Deposition of Thermoplastic Powder, *Surf. Coatings Technol.*, 2006, **201**(6), p 3044–3050

45S5/PEEK coatings by Cold Gas Spray with in vitro bioactivity, degradation and cellular proliferation

B. Garrido, V. Albaladejo-Fuentes, S.Dosta, N. Garcia-Giralt, I.G. Cano

Surfaces and Interfaces (February 2022), Submitted

Abstract

In this study, the biological response of cold sprayed coatings composed of bioactive glass 45S5 and polyetheretherketone (PEEK) was evaluated. The functional coatings were produced by cold gas spray (CGS) technology a technique that allows the deposition of powders at significant low temperatures, avoiding heat damage to polymeric surfaces. By CGS, blends with different ratio of bioactive glass and PEEK powder have been deposited onto PEEK substrates in order to improve the bone-implant interface of this inert polymer.

The ability of the coatings to form a hydroxy-carbonate apatite layer when immersed in a simulated body fluid solution was evaluated by observation with scanning electron microscopy (SEM) and X-ray diffraction (XRD). Results verify that bioactive glass particles in the composite coatings enhance their bioactivity. A degradation test was performed with Tris-HCl solution. From the results obtained by inductively coupled plasma optical emission spectroscopy (ICP-OES) and the weight loss of the samples, it was noticed that the degradation of the coatings was directly related to the amount of glass in the coatings.

Finally, the ability of bone-forming cells to adhere and proliferate on the coatings was evaluated. These experiments showed that the presence of glass particles produces an increase in cell proliferation in the long term.

Keywords: bioactive glass, PEEK, bioactivity, CGS, cell proliferation, degradation behavior

1. Introduction

Polyetheretherketone (PEEK) is a thermoplastic polymer with suitable mechanical properties for specific medical applications since this biomaterial is non-toxic and has an inert behavior when implanted in the body. PEEK products have reached the market with a good acceptance, mainly in spinal applications, and particularly for implantation of intervertebral body fusion devices (IBFDs) and vertebral body replacements (VBRs) [1]. The radiolucency and stiffness of PEEK, close to that of the cortical bone, has made this polymeric biomaterial very popular in the manufacture of these kind of devices, even replacing titanium alloys for this specific field. For instance, in 2005, a PEEK implant was used for the first time in cranioplasty, after a failed reconstruction of a large left orbito-fronto-temporal bony defect with a titanium mesh that had to be removed. A specific PEEK implant, that perfectly matched the dimensions of the bone defect was designed and manufactured, providing a solution with excellent results for the patient [2]. Nowadays, in cranial reconstruction application, the successful implantation rate of this material is over 90% with a complication rate around 15% [3].

Nevertheless, the use of polymeric materials for biomedical application is not only restricted to PEEK components. Since the late 1960s, ultra-high molecular weight polyethylene (UHMWPE) has been used in knee joint implants due to its great wear resistance and high fracture toughness. However, improving implant longevity still remains as a goal to increase the life's quality of patients. In this respect, current research suggests that PEEK could be an alternative, providing better creep resistance and fatigue limit than conventional UHMWPE implants [4–6] and the use of PEEK in this type of implant could be considered in the coming years.

Despite of the advantages shown by this biomaterial, for some specific applications PEEK is not economically competitive when compared to traditional solutions and this is limiting the progress in the implantation of this solution as alternative to some metal-based solution. Thus, in the fixation of bone fractures, stainless steels, cobalt–chrome alloys and titanium alloys are still preferentially used not only because of their mechanical properties and resistance compared to polymers.

A key aspect in the success of implants is the biological response of the material inserted, which is directly related to its bioactivity. In this sense, the main problem of PEEK as biomaterial is its hydrophobicity and the lack of bioactivity, absolutely necessary to reach a good bonding between the implant and bone tissue [7]. To the date, several research studies have been performed to enhance this feature of PEEK material; with most of the strategies focused either on the surface modification of the polymer (physical treatment, chemical

treatment or surface coating) or the preparation of a composite material with a bioactive element [8].

This second solution, that implies the combination of a bioactive material with PEEK, leads to the formation of a final component that provides adequate bioactivity to the final implant. Bioactive glasses exhibit a similar chemical composition to that of natural bone, which make them suitable for some biomedical applications. These biomaterials are highly reactive and degradable in body fluids. Depending on the glass composition, different dissolution rates are obtained, being more degradable those glasses with a more open network [9]. These glasses are able to bond to bone tissue by the formation of a biomimetic layer of hydroxy-carbonate apatite (HCA) in its surface. The presence of this HCA layer, with a composition similar to that of the bone, favors the good osteintegration of the implant to the bone matrix [10,11].

However, when used as main material of an implant device, the drawbacks of these bioactive glasses are very clear and related to their mechanical brittleness and very low fracture toughness. For this reason their potential use is limited to non-load-bearing applications, such as coatings, graft bone or scaffolds [12–14].

A variety of processing techniques are available to deposit bioactive glasses onto materials with inert behavior. Enameling is a method that involves high temperatures to coat materials [15,16], and sol-gel process needs a post heat treatment [17,18]. To prepare the coatings by these methods, a high temperature is required and bioactive glasses have a tendency to crystallize, which can result in a reduction of bioactivity [19,20]. Moreover, electrophoretic deposition is a common method to deposit bioactive glass coatings [21–23], but for this technique the substrate must be conductive and cannot be applied for coat polymers. Among the thermal spray methods, atmospheric plasma spraying and solution precursor plasma spraying has been used for produce bioactive glass coatings [24,25]. However, these methods also involve high temperatures, which is a problem for coating polymeric surfaces.

Cold gas spray (CGS) emerged in the 1980s as a new thermal spray technique, it was developed by A. Papyrin and coworkers [26]. CGS is a technique that offers the advantage of a fast coating deposition, low cost and high deposition efficiency. The deposition mechanism by CGS is based on supplying high kinetic energy to the coating feedstock particles. With this, deposition is achieved in two steps, a first step of particles adhesion to the substrate and the subsequent build-up of the deposit which involve the plastic deformation of the particles due to the transformation of their kinetic energy into localized thermal energy when they impinge onto the substrate surface [27]. The low processing temperatures necessary in CGS for this increase in the kinetic energy of the particles avoid the melting of the particles, as occurs in the conventional thermal spray techniques [28–30]. This feature

can favor the deposition of glass materials, without crystallizing them, and polymers without decomposing them.

Considering the clear advantages that this thermal spray technique brings to the deposition of glass materials, without crystallizing them, and polymers without decomposing them. In the current work, we want to demonstrate the capabilities of CGS for the production of a composite biomaterial that combines the mechanical properties of PEEK and the biological properties of bioactive glasses, with the ultimate aim of finally generating a functionalized biomaterial with an improved tissue response compared to PEEK implants

For this, PEEK/45S5 composite coatings were developed on PEEK substrates by CGS. This bioactive glass shows the following composition: 45.0 SiO2, 24.5 CaO, 24.5 Na2O and 6.0 P2O5 (wt%). It was the first bioactive glass, discovered by Larry Hench and coworkers in the late 1960s [31] and although it has been used as composite material in combination with PEEK to produce coatings [32,33], these never have been previously deposited by LP-CGS. For the goal of demonstrating the functionality of the new solution, coatings with different amount of glass were studied (analyzing the coating build-up and the microstructure of the coatings) and the biological properties of the developed composite coatings were also evaluated, particularly, studying the ability to form an HCA layer, the degradation and the cellular proliferation of osteoblasts on the coatings.

2. Material and methods

2.1. Powder and substrate

Two different powders were used for producing the composite coatings. A commercial PEEK powder (Victrex, United Kingdom) was chosen for this study and a commercial 45S5 bioactive glass powder (Denfotex Research, United Kingdom) produced by the traditional melt-quenching route was used.

The blends were prepared by manually mixing of the powders. The blend ratios selected for spraying are listed in Table 1.

Table 1. Sprayed blends of PEEK and bioactive glass (v/v)

Blend/coating code	Volume of PEEK	Volume of 45S5
PEEK 100%	100%	0%
45S5 10%	90%	10%
45S5 25%	75%	25%
45S5 35%	65%	35%
45S5 50%	50%	50%

As the coatings were addressed to improve PEEK implants, the substrates used in all cases were of this material. To evaluate the cross-section of the coatings and the formation of an HCA layer PEEK disks with a 25 mm diameter, cut from a PEEK bar (Vestakeep, Spain), were used. PEEK specimens obtained from a PEEK sheet (Ensinger, Spain), with an area of 8 mm × 8 mm and 5 mm thick, were used for degradation test and biological characterization.

2.2. Powder and coating characterization

A scanning electron microscope (SEM) (Phenom ProX, Phenom-World BV, Eindhoven, The Netherlands) was used to characterize the morphology of the feedstock powders. Before the observation, both materials were coated with a gold layer to make them conductive using a sputtering coating system (E-5000, Polaron, Watford, England).

Both commercial powders were sieved using a 40 µm mesh sieve (Restch, Germany) and the fraction below this mesh was collected for producing the blends. The granulometry of the sieved powders was determined by a laser diffraction particle size analyzer (LS 13320, Beckman Coulter, California, USA).

Coatings were deposited using a low-pressure cold gas spray (LP-CGS) equipment (Dymet 423, Dycomet Europe, Akkrum, The Netherlands). The gun was equipped with a CK-20 nozzle. Air was used as the propellant gas with a gas pressure of 0.6 MPa. In this technique, the gas temperature is not very high. Particularly, this equipment allowed us to work from room temperature to 500ºC. The stand-off distance was 10 mm and all coatings were deposited by performing a single torch cycle.

Prior to the blend's deposition, PEEK substrates were grit blasted (Formula 1400, Guyson International, Skipton, England) with corundum G24 (grit size 800 µm) at a pressure of 0.5 MPa and afterwards, ethanol cleaned. Generating the proper surface roughness is essential to favor the particles adhesion to the substrate. In this study, grit blasted PEEK roughness was Ra = 4.9 ± 0.4 µm and Rz = 27.3 ± 2.8 µm.

In this study, coatings with two different thickness were produced by varying the traverse gun speed. For characterize the deposition and distribution of elements, thick coatings (around 800 µm) were sprayed using low traverse gun speed (80 mm/s). These coatings allowed a well observation of the particle distribution. By the other hand, thinner coatings (around 250 µm), were deposited increasing the traverse gun speed to 240 mm/s. These thinner coatings present a suitable thickness for the real application, to achieve a long-term stability of the implants and were used for the biological characterization. It its worth indicating that this decision was taken since its widely accepted that higher thickness can promote delamination and fragmentation before reach a good bonding with bone tissue [34,35].

The microstructure and the distribution of the elements, in the cross-section and the top surface of the coatings, was observed by an SEM (JSM-5310, JEOL, Tokyo, Japan) equipment with energy-dispersive X-ray spectrometry (EDS). For the chemical analysis, an elemental mapping was done by EDS. The main element of this bioactive glass, silicon, was selected to identify the glass particles in the coating.

To analyze the distribution of the glass particles, cross-sections were prepared by cold mounting resin, grinding them with silicon carbide abrasive papers up to P4000 (grit size 5 µm) and polishing with 1 µm diamond slurry. Cross-sections and surface coatings were gold-covered prior to the observation.

In order to determine the thermal behavior of the studied powders and coatings, differential scanning calorimetry (DSC) (DSC1, Mettler Toledo, Schwerzenbach, Switzerland) measurements were carried under a nitrogen atmosphere, using aluminum crucibles. For the test, 3-5 mg of each powder were heated from 0ºC to 450ºC at 10ºC/min rate. Then the powder was cooled to 0ºC at -30ºC/min and a second heating was applied to 450ºC at 10ºC/min. DSC analysis was performed for PEEK and 45S5 feedstock powders, also for the different blends and for the obtained coatings.

Image analysis of the EDS micrographs was done to quantify the area percentage of glass material either incorporated into the composite coating or exposed to the media on the coating surface. For each coating, an average of five images, taken at a magnification of 200x, was done to quantify the area percentage. This analysis was carried out on cross-sections and surface coatings using ImageJ program. The stages of image processing were as follows: first the acquisition of the image, second the selection of the channel of interest (blue channel corresponding to silicon), then the adjustment of the threshold level to eliminate noise and finally the identification and quantification of the area. An example of the process in the surface of a 45S5 10% coating can be seen in Figure 1. The authors know that the area percentage value measured and calculated by this method do not represent the actual content of 45S5 in the composite but an estimation of this value. However, because of the inertness of both material, image analysis may provide a correlation between feedstock blend and coating compositions, and as a result, with biological response of the composite.

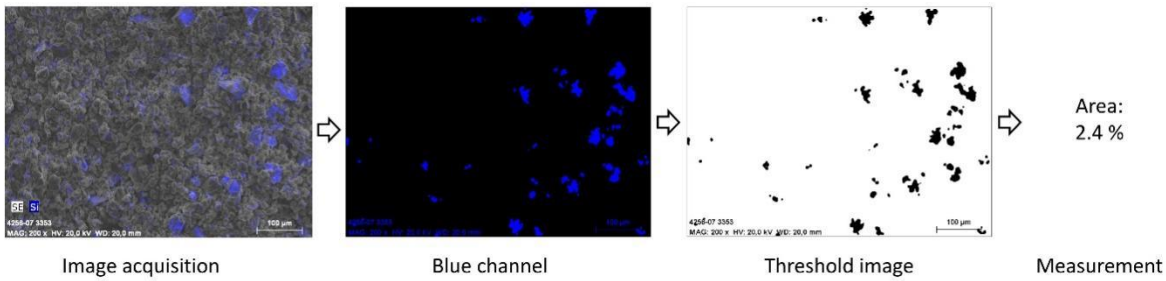

Figure 1. Stages of image processing

2.3. Bioactivity and degradation assessment

To evaluate the ability of the coatings to form an HCA layer an in vitro test was performed following the ISO 23317 [36]. Samples were immersed, in vertical position, in hank's balanced salt solution (HBSS) (Sigma-Aldrich, Germany) in a thermostatic bath with agitation at 37ºC. The solution was refreshed twice a week to avoid ionic saturation of the medium. The evaluation of the HCA formation was studied at different periods: 0, 3, 7, 14 and 21 days. Three samples of each coating type were immersed for each exposure time. After the immersion period, samples were rinsed with ultrapure water and dried 24h at room temperature.

To evaluate the process of formation of the HCA layer at each period, the surface of the samples was observed using an SEM (JSM-5310). For this observation, all the specimens were gold-covered to allow them to be conductive.

Furthermore, the formed layer was analyzed from the cross-sectional images of the samples immersed 7 and 21 days. For this examination, the cross-sections were prepared as described previously. After being dried in a desiccator for 48h, the samples were gold coated and examined by SEM (JSM-5310).

To assess the crystallization of the formed layer of HCA, a crystallographic structure analysis of the samples immersed 14 days in HBSS was performed by means of X-ray diffraction (XRD) using a diffractometer (X'Pert PRO MPD, PANalytical, Cambridge, UK).

A degradation study was performed to evaluate the glass dissolution of the different coatings. Following the specifications of the ISO 10993-14 [37], the samples were immersed in a buffered solution consisting of Tris-HCl with pH adjusted to 7.4 ± 0.1, at 37 ± 1ºC for 120h.

To determine the weight loss percentage due to degradation, the samples were weighted, before and after the test, with a high precision scale (CPA225D, Sartorius, Goettingen, Germany). After the time exposure, the samples were rinsed thrice with ultrapure water and dried overnight at 120ºC before being weighted. At the end of the test, pH was recorded using a universal pH meter (Hach, Spain). The concentrations of silicon, calcium and sodium were measured by means of inductively coupled plasma optical emission spectrometry (ICP-OES) (Optima 8300, PerkinElmer, Waltham, USA).

2.4. Cell culture studies

Osteoblasts were seeded onto different coatings to study the ability of the samples to allow adhesion, growth and proliferation of this cellular type. The tests were repeated in triplicate with different human osteoblasts lines (obtained from knee trabecular bone after prosthesis replacement [38]) in passage from 3 to 6 to obtain reliable results. The study was approved by Parc de Salut Mar Ethics Committee. Three different biomaterials of each series were

evaluated in each experiment and controls of tissue culture plastic (TCP) were also included. In order to avoid the inter-experiment variability, results were normalized with respect to the TCP at 3 days within each experiment.

Before the cellular tests, samples were sterilized in ethanol 70% for 3h to avoid contamination during the test. After the sterilization step, samples were immersed in Dulbecco's modified eagle's medium (DMEM) (Invitrogen, USA) supplemented with 10% fetal bovine serum for 24h. This precondition step is necessary to avoid cell death caused by the increase in the pH due to rapid release of ions from the glass [39]. A cell suspension was prepared and seeded at a density of 6.5×10^3 cells/sample with supplemented DMEM onto the PEEK coated samples placed in a 48-well polystyrene plate. The incubation was done at 37ºC in a humidified atmosphere of 5% CO_2, changing the media every 3 days.

After 3, 7 and 14 days of incubation, cell proliferation was analyzed using MTS assay (CellTiter 96® AQueous One Solution Cell Proliferation, Promega, USA). This colorimetric test allows quantification of viable cells, based on the reduction of MTS tetrazolium by cells into a colored formazan product soluble in cell culture medium. After each period, the medium was removed from the wells and the samples were transferred to new wells. Then, the samples were incubated with 50 µl of MTS reagent and 250 µl of supplemented medium for 1 hour and a half. Afterwards, the absorbance was recorded at 490 nm by means of a well plate reader (Infinite 200, Tecan, Männedorf, Switzerland).

The quantitative results from the MTS assay were analyzed using one-way analysis of variance (ANOVA) followed by Tukey's post hoc test to determine differences among groups. Where $p<0.05$ was considered to be statistically significant.

SEM (Phenom ProX) was used to analyze attachment and morphology of the cells. Osteoblasts were seeded onto the coatings at the same density than for MTS assay. After 24h of incubation, the samples were washed twice with phosphate buffered saline (PBS) buffer (pH 7.4) to remove non-bounded cells. The remaining cells were fixed with 2.5 % glutaraldehyde in PBS for 3h. After that step, the samples were rinsed twice with PBS. The dehydration of the cells was performed with ethanol baths of 15 minutes each one, increasing the ethanol concentration: 50, 65, 70, 80, 90, 95 and 100%, respectively. Finally, the samples were dried using critical point dryer (CPD) (K850, Emitech, Lewes, UK) and carbon-coated for the SEM observation using a high-vacuum carbon evaporator (K950X, Emitech, Lewes, UK).

3. Results and discussion

3.1. Powder and coating characterization

In CGS, the particle size of the powder has a significant influence on the coating achieved. Xu et al [40] studied cold spray deposition of thermoplastic coatings at different particle sizes and found that higher final velocities and a greater mass deposit were achieved for the smaller particles, which experienced a greater acceleration for the same air pressure. For this reason, commercial powders were sieved to work with an appropriate particle size, and then characterize to corroborate the correct processing of the feedstock materials.

The SEM analysis performed on the powders allowed us to establish the difference in their morphology and size, as shown in Figure 2. Particularly, the 45S5 glass particles are dense and irregular, with presence of corners and sharp edges, common result for crushed particles after the melt-quenching process. In addition, it is here observed that the particles are quite similar in size to each other. On the contrary, PEEK powder is composed of small aggregated particles that form agglomerated particles more rounded and less compact than the glass ones. In general, it is appreciated by SEM inspection that the PEEK particles are smaller than glass ones, and also a greater variation in particle size.

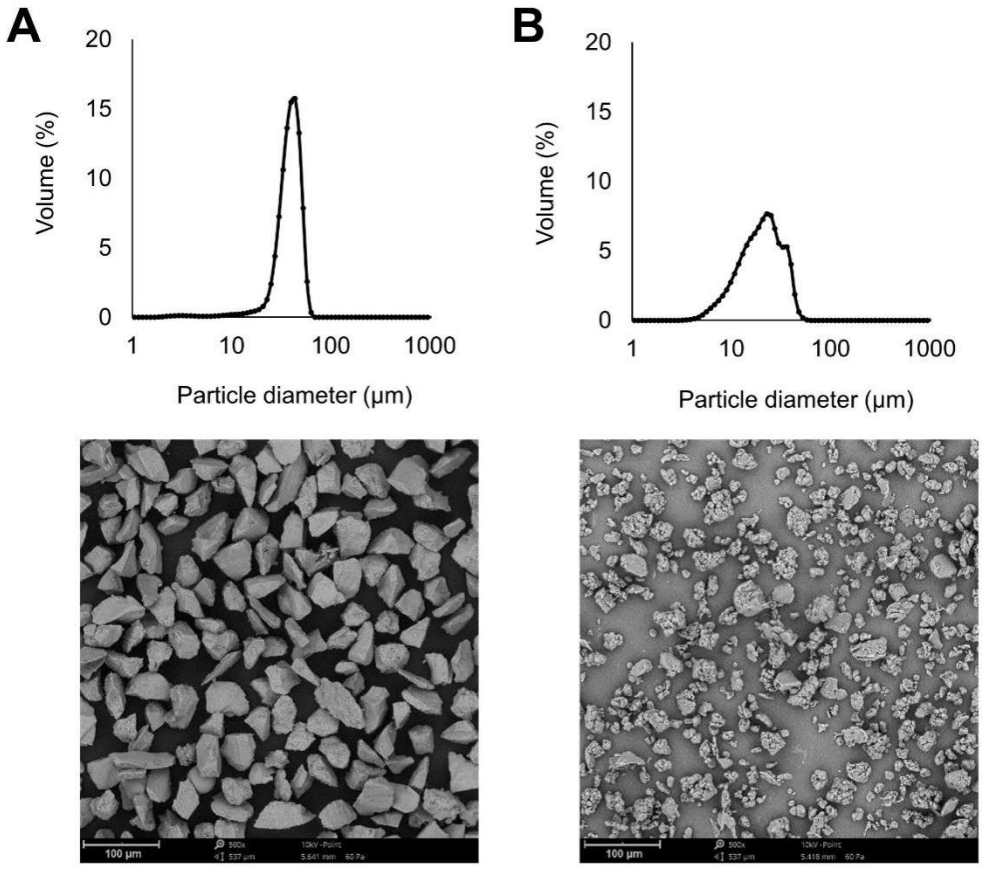

Figure 2. Particle size distribution in volume and SEM micrographs of the bioactive glass (A) and PEEK (B) powders

The particle size distribution of both powders measured by laser diffraction can be observed in Figure 2. For the glass particles, it exhibits a narrow distribution, achieved with the sieving process with the following characteristic values related to size distribution: d_{10} = 28.1 µm, d_{50} = 41.1 µm, d_{90} = 53.2 µm. Even though both powders were 40 µm mesh sieve, glass particles above that size are detected which can be associated to the irregular morphology of the particles, that allows them to pass through the mesh by its thinner side during the sieving process. By contrast, the PEEK powder exhibits a slightly bimodal nature. The size distribution of PEEK powder is characterized by d_{10} = 10.2 µm, d_{50} = 21.2 µm, d_{90} = 37.6 µm. The values obtained with this technique are consistent with the observations by microscopy.

Blends of the sieved 45S5 and PEEK powders with the compositions listed on Table 1 were sprayed by LPCGS using spraying parameters detailed in Table 2. The microstructure of the deposited coatings is shown in Figure 3. The observation of their cross section reveals that the deposit shows two clearly distinguishable regions. Thus, the PEEK particles are forming a dense and continuous matrix (dark gray region in Figure 3), suggesting that the PEEK particles reach a temperature above its glass transition temperature and therefore have been plastically deformed during the process or even have been able to melt. Otherwise the glass particles (light gray in Figure 3) are embedded in the polymeric matrix. The bioactive particles are perfectly surrounded and retained by the polymeric matrix and maintain their initial morphology, which indicates that glass particles have not been plastically deformed during the spraying process. In the coatings with a greater amount of glass, some porosity between particles can be observed.

The analysis of the cross-sections corroborates the success in the production of a composite coating, which includes bioactive glass particles embedded in a polymeric matrix. Furthermore, the deposition of the coatings has been achieved without altering the composition of the bioactive particles by means of CGS.

During the spraying process with LPCGS, the gas temperature was set at a maximum of 350ºC. However, due to the speed at which the process occurs, we can consider that the sprayed blends were in contact with the hot flow of gas only for a very short period of time. Furthermore, both polymeric and ceramic materials are known as materials with low thermal conductivity. Under these conditions, it may be expected that the particles did not reach the temperature of the gas. However, in order to confirm that neither the particles nor the substrates reached very high temperatures during the composite coating production and then permitted us to deposit polymeric materials without decomposing them, the thermal behavior of the blends and coatings by DSC was evaluated.

As it is well known, the glass transition temperature of PEEK starts at 143ºC, the melting is achieved at 343ºC and decomposition occurs at 575ºC [41,42]. When the PEEK particles

impinge onto the substrate, particles should be between glass transition and melting temperature; in this range of temperature the thermoplastics can be deformed plastically. This can explain the dense polymeric matrix observed in the cross-sections, in which the separation between PEEK particles is not appreciated.

By the other hand, the glass transition temperature of the 45S5 occurs at 550ºC and melting is evidenced at 1070ºC [43,44]. Consequently, to undergo plastic deformation the glass particles require higher temperatures than the reached during the process.

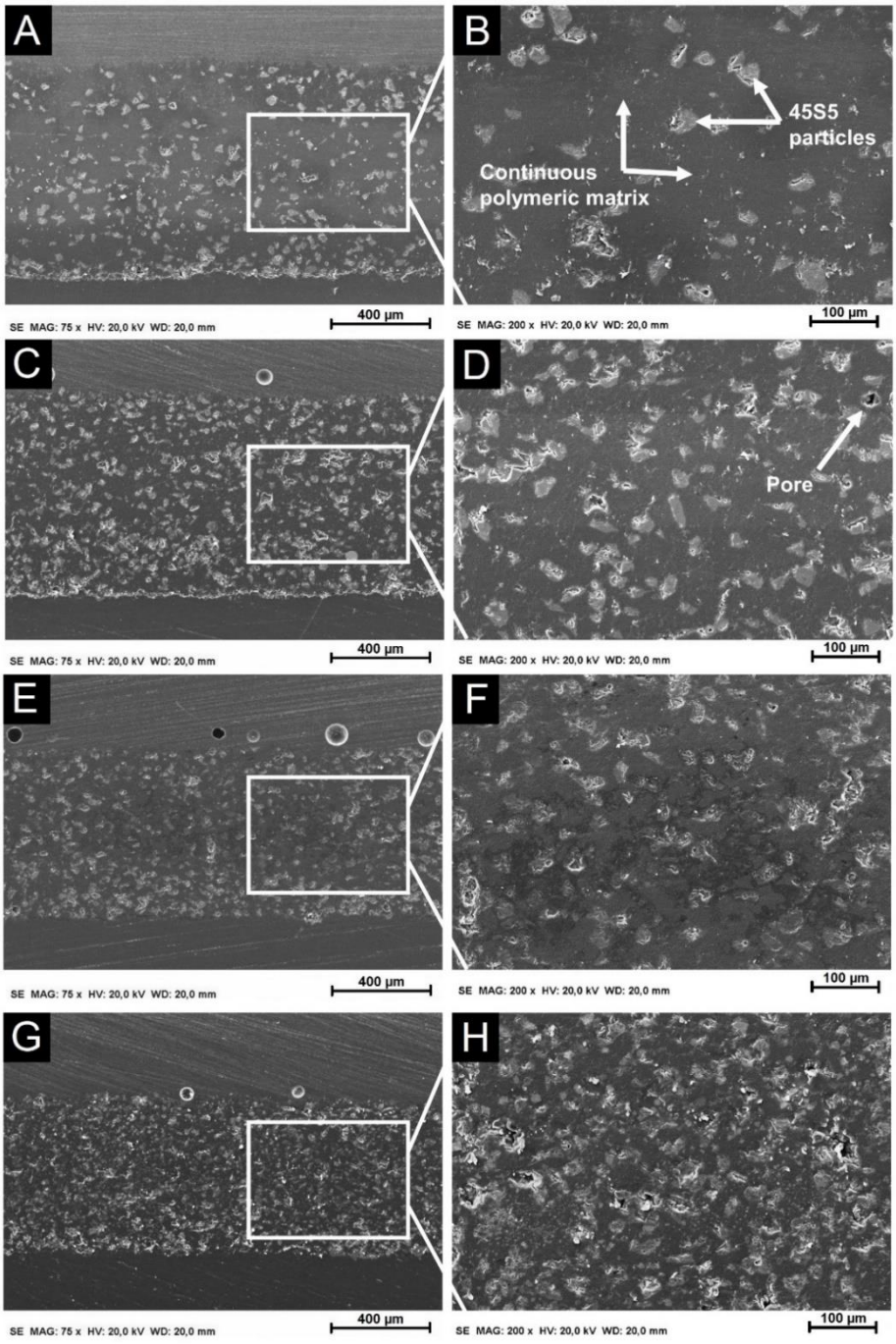

Figure 3. Cross-sectional SEM micrographs: (A) and (B) 45S5 10%, (C) and (D) 45S5 25%, (E) and (F) 45S5 35%, (G) and (H) 45S5 50%

For these test, parameters of the analysis were selected in order to simulate the processes that materials undergo during the cold spraying deposition. Thus, the materials were subjected to a first heating step that simulates the fast acceleration of the particles in a stream of preheated gas, followed by a rapid cooling corresponding to the cool down of the gas stream as it expands in the diverging section of the nozzle [45] and the rapid cool down that particles undergo once deposited onto the substrate. Finally, we carry out a second heating step to validate the thermal changes experienced by the particles in this heating-cooling down cycle.

The DSC curves of the feedstock powders (bioactive glass and PEEK) are represented in Figure 4A-B. For each material the first heating step is represented by a solid line, and the second heating step is represented by a dashed line. During the first heating step, two endothermic peaks were detected below 200ºC for the 45S5 powder, which disappeared during the second heating and can be related to the desorption of water retained in the glass particles [44,46–48]. The heating curves associated to the PEEK powder revealed an endothermic peak at 344ºC corresponding to the melting temperature of the thermoplastic polymer, no more peaks were detected for this powder.

For comparison purposes, in Figure 4C, D, E, F, G the curves of the first heating of both, the blends before spraying (solid line) and the coatings (discontinuous line) are shown. It is important noticed that the coatings have already experienced a thermal treatment during the spraying process, thus the discontinuous line provide information about the state of the material after the coating production. The curves of the blends revealed a first endothermic peak (90ºC) corresponding to the release of water retained in the glass particles. As this endothermic peak belongs to the glass particles, it is possible to see this peak with greater intensity for the blends with more glass content, and it is not identified in the PEEK 100% ones. The curves related to the coatings do not present this endothermic peak, due to the elimination of the water during the spraying process. The exothermic peak at 344ºC that corresponds to the melting of PEEK is evidenced in all the heating curves. The intensity of the peak is higher for the blends and coatings with more polymer content. Furthermore, the peak intensity in the blends is lower than in its respective coatings; this can be explained by the greater difficulty of the glass to be deposited by this technique, most of the sprayed polymeric particles end up as part of the coating, while many of the glass particles fail to be retained.

The results of the DSC analysis corroborate that no melting of the PEEK particles has occurred during the coating deposition. Therefore, the dense and continuous polymeric matrix, observed in the cross-section of the coatings (Figure 3), was obtained by the plastic

deformation of PEEK particles below its melting temperature, this data could not be affirmed only with the observation of the cross section.

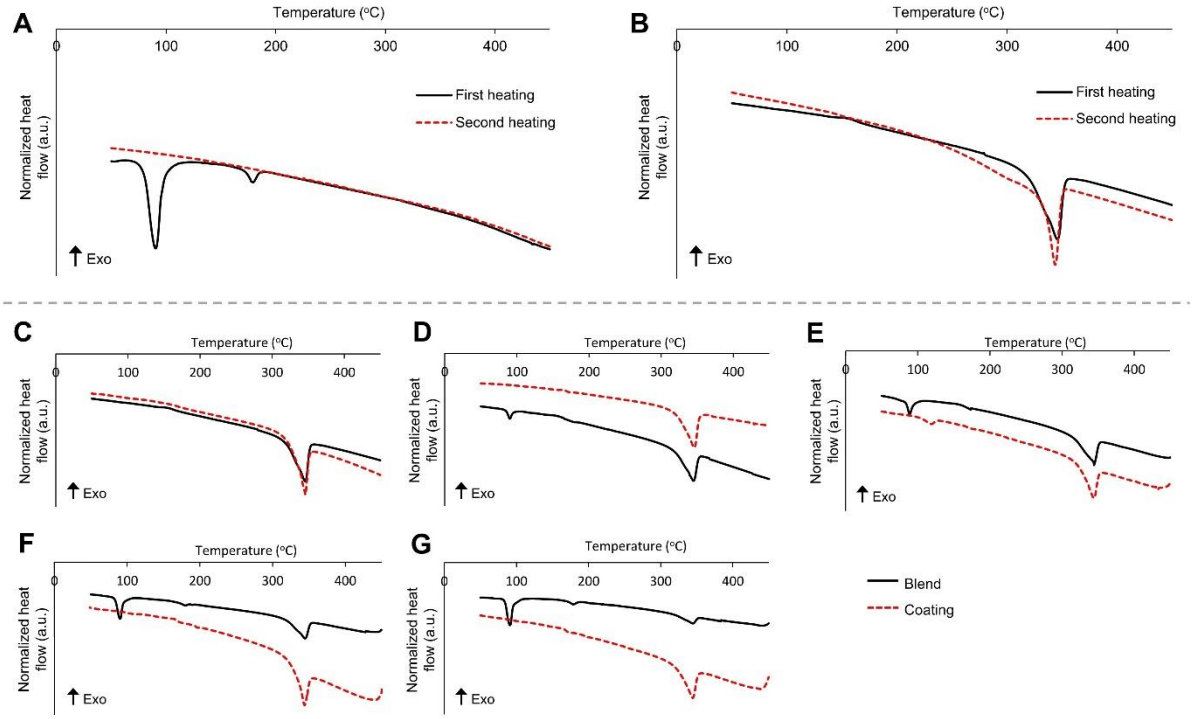

Figure 4. DSC curves of first and second heating: (A) 45S5 glass powder, (B) PEEK powder; and first heating of blends vs coatings: (C) PEEK 100%, (D) 45S5 10%, (E) 45S5 25%, (F) 45S5 35% and (G) 45S5 50%

For a good bioactive response of the coating it is important that the glass particles are well distributed throughout the coating, and especially these must be present on the surface of the composite that, at the end, is the part of the component that will be in direct contact with body fluids.

To validate the amount of glass particles retained in the coatings, an image analysis quantification was performed on the top surface and cross-sections of the different coatings, following the procedure described in section 2.2; (an example of the analysis can be seen in the Figure 1). By this method, it was possible to compare the amount of bioactive glass particles retained with the blend composition sprayed. Thus, the percentage of area corresponding to glass material in the coating cross section and top coating surface are represented versus the volumetric percentage of glass on the sprayed blends Figure 5. It should be noted that the values shown cannot be compared with the volumetric percentages of the blends.

For both the cross sections and the surfaces, a gradual increase in the glass area can be observed related to the amount of glass in the sprayed blends up to a glass content of 25%.

In addition, from 35% glass in the blend, the increase in glass retained in the cross-section and in the surface is less significant. For these coatings with the highest glass content, the

glass particles are rebounding when impinge onto other glass particles that are already part of the coating, having a lower ability to remain retained by the polymeric matrix but generating kind of erosion on the top of the coating.

The results corroborate that the glass particles are present not only inside the coating as could be seen in Figure 3, but also on the surface. As a consequence of the presence of bioactive particles on the surface of the coatings, these composite materials could promote the bioactive response of PEEK coatings.

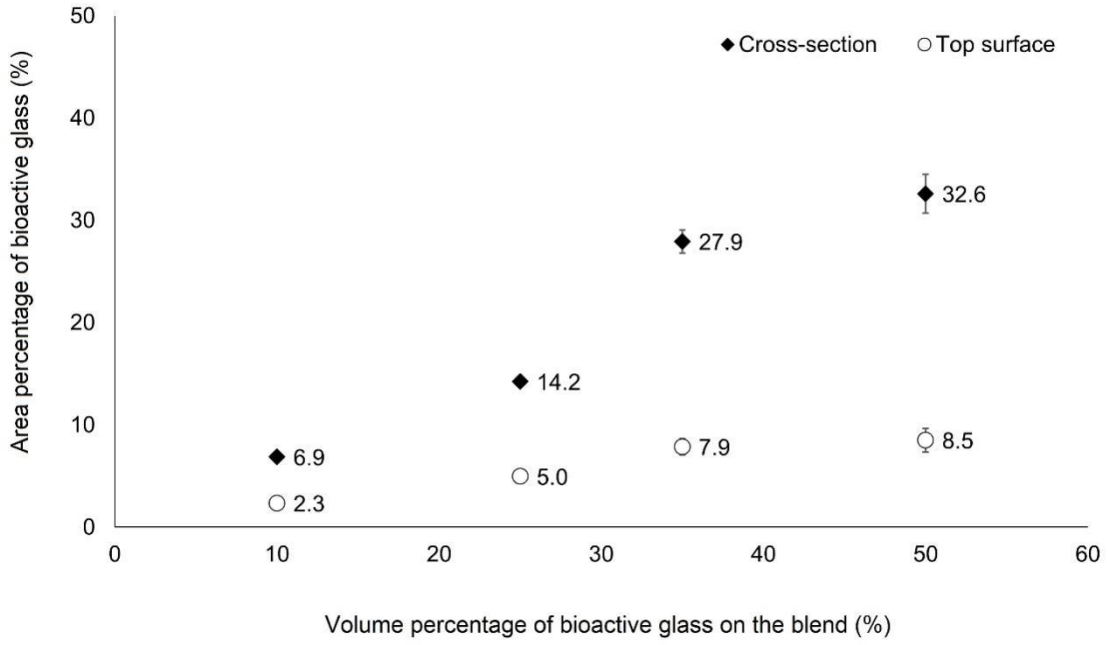

Figure 5. Area percentage of bioactive glass quantified vs volume percentage of bioactive glass on the blend

3.2. In vitro bioactivity study - Ability to form apatite

The presence of glass in the coatings is expected to provide bioactive capacity to the samples since the ionic dissolution of glass stimulates the formation of the HCA, which promotes the osteointegration between bone and implant.

The formation of the apatite layer follows a sequence of rapid reactions described by Hench: (i) ion exchange between glass and solution, (ii) formation of silanols at the glass solution interface, (iii) formation of a silica-gel layer by condensation and re-polymerization of silanols, (iv) formation of a $CaO\text{-}P_2O_5$ rich layer by incorporation of calcium and phosphate from solution and (v) crystallization of the amorphous $CaO\text{-}P_2O_5$ rich layer to form crystalline HCA layer [49,50].

Due to the great importance of this HCA layer in implant osteointegration, all the composite coatings were immersed in HBSS solution for twenty-one days, and the surface of the

coatings was periodically evaluated to analyze the progress achieved for a HCA layer formation onto their surfaces. Three-dimensional surface SEM micrographs of the PEEK 100% coating (Figure 6) after fourteen days of immersion in HBSS, revealed that PEEK coatings are not able to form a HCA layer as expected if we consider that this material is not bioactive. In this Figure, it can be observed the key role that 45S5 has as bioactive component of the coating even at low content; since all the coatings containing glass particles are able to form the HCA layer. The coatings with a glass content higher than 10% followed similar behavior regarding the formation of the HCA layer. In them, the incorporation of 45S5 glass in the composite coating promoted quicker development of the HCA layer compared to 45S5 10% coating. For these coatings, it is possible to appreciate higher presence of small apatite spheres at three days and, in particular, the deposits of apatite have begun to be formed on the top of glass particles. On the contrary, in the 45S5 10% coatings small apatite spheres were clearly identified in the early stages of the experiment (at three days of immersion), which grown and formed aggregated deposits after seven days of immersion, until finally, fully cover the surface of the coating by a continuous HCA layer after two weeks of test. At twenty-one days of exposure the HCA layers of all coatings with glass content continued growing. However, the micrographs corresponding to that period were not showed in Figure 6 due to the similarity with the previous period.

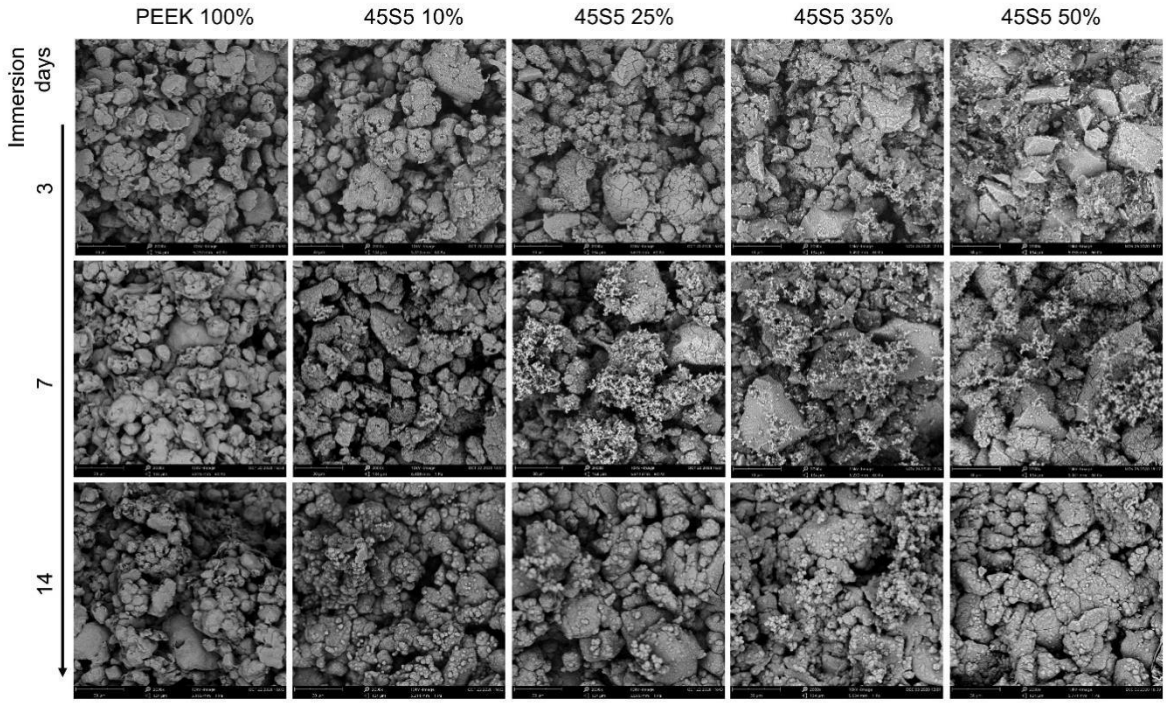

Figure 6. SEM images of the samples surface after soaking in HBSS for different times: after 3, 7 and 14 days

These images allow to validate the bioactive capacity of the coatings containing glass particles. The results may suggest that coatings obtained by cold spraying 45S5-PEEK blends with at least 25% of glass can promote a fast HCA layer growth which can lead to a

successful implant osteointegration. The coatings obtained with the 45S5 10% blend present also bioactivity but with a considerable decrease on the kinetic of HCA formation respect the other coatings containing glass. Whereas PEEK 100% coatings could not form an HCA layer after twenty-one days in the solution.

The few amount of bioactive glass found on the top surface of the coatings (Figure 5) has been shown to be able to promote the formation of the HCA layer. However, the composite coatings needs 14 days of immersion to be fully covered by a layer of bone-like apatite, while in other studies with more presence of bioactive materials on the top surface the HCA layer covers completely the coatings in shorter periods: Ur Rehman et al [51] at 3 days, Garrido et al [24] at 6 day or Yu et al [52] at 7 days.

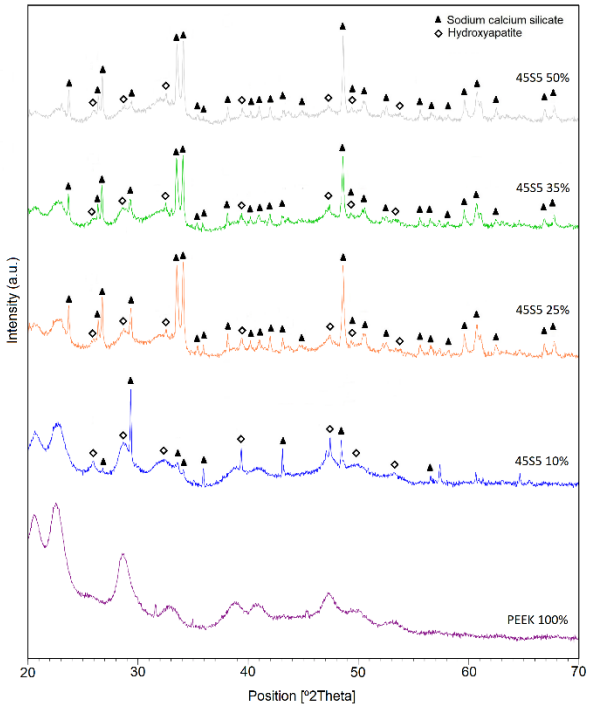

Figure 7. X-ray spectra acquired on the samples after immersion in HBSS for 14 days

X-Ray diffraction analysis was used for confirming the formation of HCA layers on the surface of the coatings immersed for 2 weeks in HBSS. XRD patterns of the rinsed and dried coatings after these 14 days are illustrated in Figure 7. The pattern of the pure PEEK coating revealed broad peaks corresponding to the crystalline phase of the PEEK polymer. The absence of peaks related to the formation of HCA layer corroborates the lack of bioactivity of the inert coating, according to the SEM images of Figure 6 where no change in the surface of these coatings can be detected. In the pattern of the 45S5 10% coating, the detected peaks are consistent with sodium calcium silicate ($Na_6Ca_3Si_6O_{18}$; code: 01–079-1089) and hydroxyapatite ($Ca_5(PO_4)_3(OH)$; code: 00–001-1008), related to the presence of bioactive glass particles and the HCA layer formation. Moreover, the peaks corresponding to the PEEK phases are observed with great intensity. Regarding the XRD profiles of the coatings with

more glass content (45S5 25%, 35% and 50%) some observations can be done. The peaks corresponding to the phases involved in the development of the HCA layer are similar for the different coatings. Besides, it is possible to appreciate the broad peaks associated to PEEK with a trend of less intensity as the amount of glass in the coating increases, due to the lower amount of PEEK in these coatings.

These results suggest that the kinetic of formation and growth of the apatite layer in the coatings with at least 25% of glass in the sprayed blend is significantly higher than for the coating with less amount of glass.

The cross-section of the HCA layer formed after 7 and 21 days of exposure can be observed in Figure 8. It seems that after one week a thin layer (light grey) has been formed on the different composite coatings. However, this HCA layer is not continuous along all the coatings, particularly in the 45S5 10% there are some parts without apatite deposition. These results are in agreement with the SEM images observation in Figure 6 at 7 days, where 45S5 10% coatings showed a slower rate of apatite formation respect the other glass coatings. At 3 weeks the HCA layer has grown for all the samples, becoming clearly continuous throughout all the surface coating and reaching a thickness between 2 and 4 µm. In addition, after 21 days of exposure, the absence of glass particles (light grey) in the coatings could be observed. This corroborates the process described in the literature, in which the formation of the apatite layer is related to the degradation of bioactive glass.

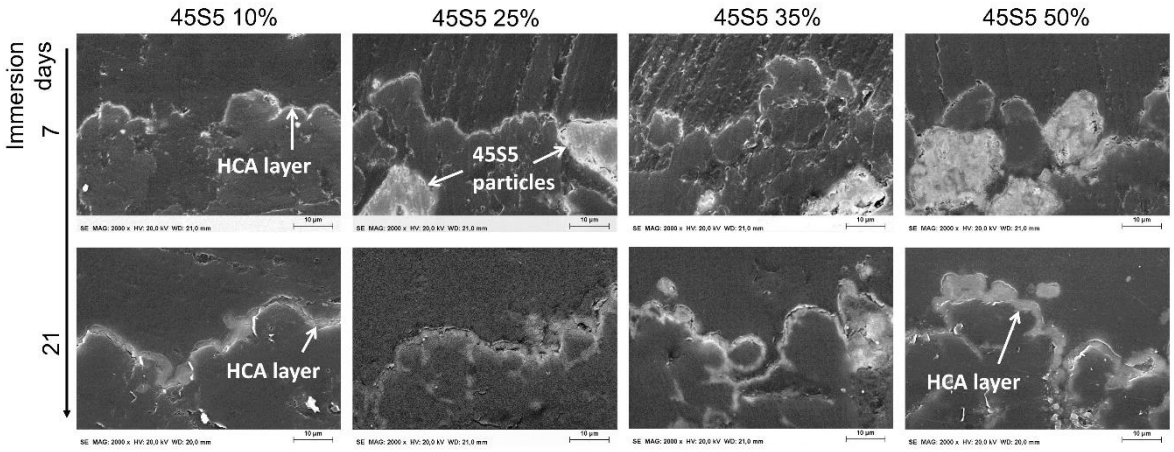

Figure 8. Cross-section micrographs showing the HCA layer after 7 and 21 days of immersion in HBSS

3.3. Degradation study

The degradation rate and the ion release of bioactive glasses can strongly affect the biocompatibility of the coatings. Furthermore, the capacity of bioactive glass particles to be replaced by bone is tightly linked to their dissolution. For this reason, a degradation study of the developed coatings can provide valuable data on their biological capabilities.

In the degradation test, the weight loss associated with the degradation of the glass retained on the coatings was studied. The coated samples were immersed for 120h in Tris-HCl solution. The percentages of weight loss of the samples and the pH values after the test are illustrated in Figure 9.

The incorporation of bioactive glass in the coatings resulted in a remarkable increase in degradation, compared to the pure PEEK coating, which is non-degradable in physiological fluids. The increase in weight loss observed can be clearly connected with the area percentage of bioactive glass quantified on the surface of the coatings showed in Figure 5. Particularly, the two coatings with more glass content (45S5 35% and 50%) achieved same values of weight loss (1.00 and 0.99%), suggesting that the glass found in the surface was not significantly different in both cases. Furthermore, the ions release from the glass particles of the coatings cause an increase in the pH solution, proportional also with the amount of glass in contact with the solution.

These results are consistent with the lower bioactive capacity of the 45S5 10% coatings to form an apatite layer as discussed previously in section 3.2. The dissolution products of the bioactive glass of the coatings are promoting the formation of the HCA layer, as evidenced in the cross sections after 21 days of immersion in HBSS, where the glass particles near the surface were completely dissolved (Figure 8).

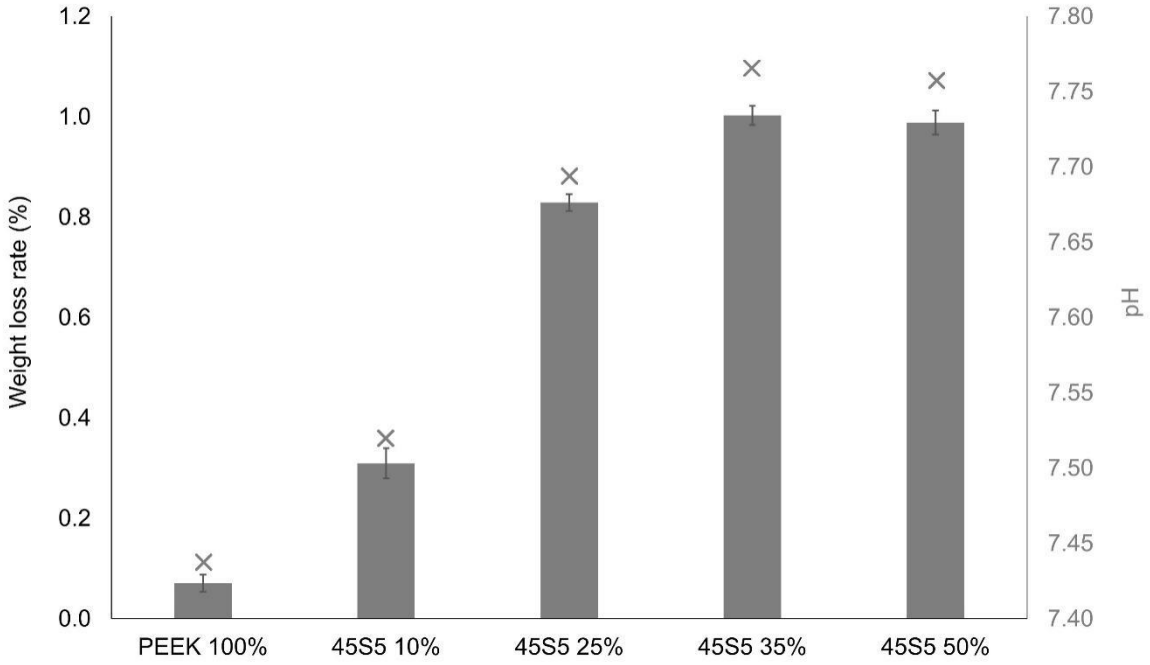

Figure 9. Weight loss rate of coated samples after soaking in Tris-HCl solution (bars) and pH value recorded after the test (×)

The chemical contents of the solutions after the degradation test were measured using ICP-OES. The ions corresponding to the dissolution of the glass were detected, which are associated with the loss of weight of the coatings studied. The concentration of elements released (silicon, calcium and sodium) at 5 days are shown in Figure 10.

According to Hench [53], the first step in bioactive glass dissolution is the release of alkali modifier cations (Na^+ in 45S5). This is consistent with our results, where sodium ions are the most released, followed by the calcium ions. Both are the modifying elements of the network, consequently the most susceptible to be released. In addition, the release of network-forming elements (silicon and phosphorus) was lower and particularly only silicon ions were detected in the solution, due to the high contribution of silicon oxide (45.0 wt%) on this specific glass composition. Phosphorous was not detected due to the low content in the original glass (6.0% wt.).

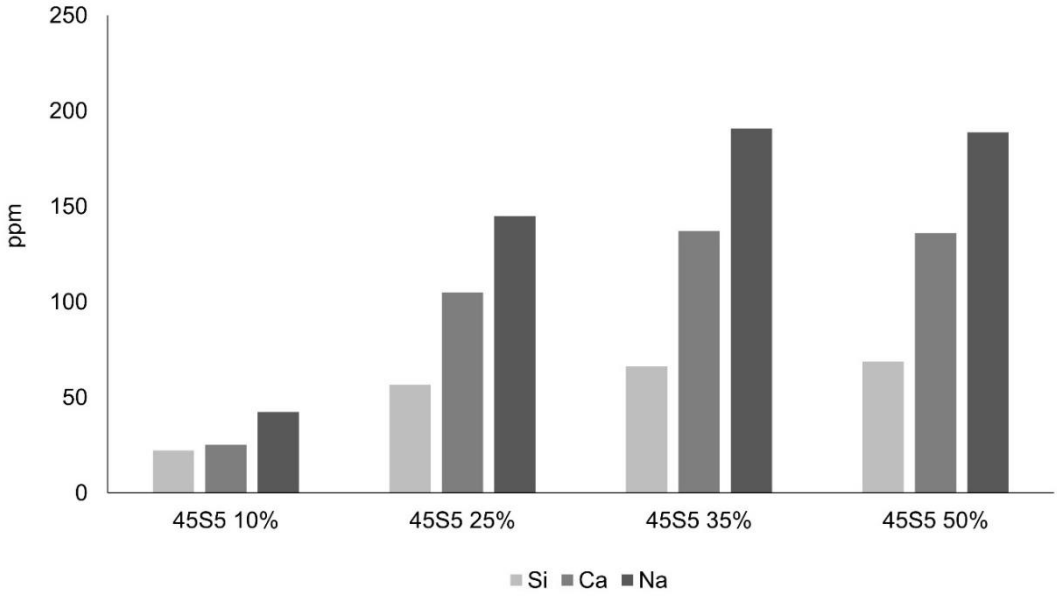

Figure 10. Ion release into Tris-HCl solution after immersion of samples for 120h.

This ion exchange process caused by the glass particles results in an increase in the pH of the solution and the dissolution of the glass particles. The results from this analysis perfectly match the results of weight loss and pH values discussed previously and validate the discussed bioactive response of the coatings.

By combining the results from the different techniques employed to study the bioactivity and degradation of the coatings, we could conclude that the presence of glass in the composite coatings is key to acquire bioactive behavior. Moreover, the bioactive capacity of the 45S5 10% coatings is considerably lower than the other ones. While the coatings with 35 and 50% of glass on the blend provide comparable bioactive capacity, due to the similarity of the amount of glass retained in the sprayed coatings, particularly on the surface.

3.4. Cell culture study

The integrity of the coatings obtained by LPCGS is related to the glass content in the blend. As the amount of glass increases, erosion begins to occur and the ability of the polymeric matrix to retain the glass particles decreases. In addition, the results obtained in the apatite layer formation and degradation tests are correlated with the amount of glass exposed on the surface, where no significant differences were obtained for the coatings with higher glass content. Therefore, cell assays were performed only on the following coatings: PEEK 100%, 45S5 10%, 25% and 35%. The cells were seeded on the mentioned composite coatings and also on TCP as a positive control.

Regarding the ability of osteoblasts to proliferate, MTS results at different periods are plotted in Figure 11. A similar cellular activity was observed between the different coatings studied for short periods, thus, at 3 and 7 days there were no significant differences between the coatings with different glass content. However, after 14 days, a slight increase in cellular activity was recorded for the coatings with higher glass content. According to this, it might be concluded that glass presence may be promoting osteoblast proliferation at long-term. Other studies have already reported that, in short-term periods, in which no differences were observed on cellular response between pure PEEK samples and composite PEEK/bioactive-ceramic samples [54–56].

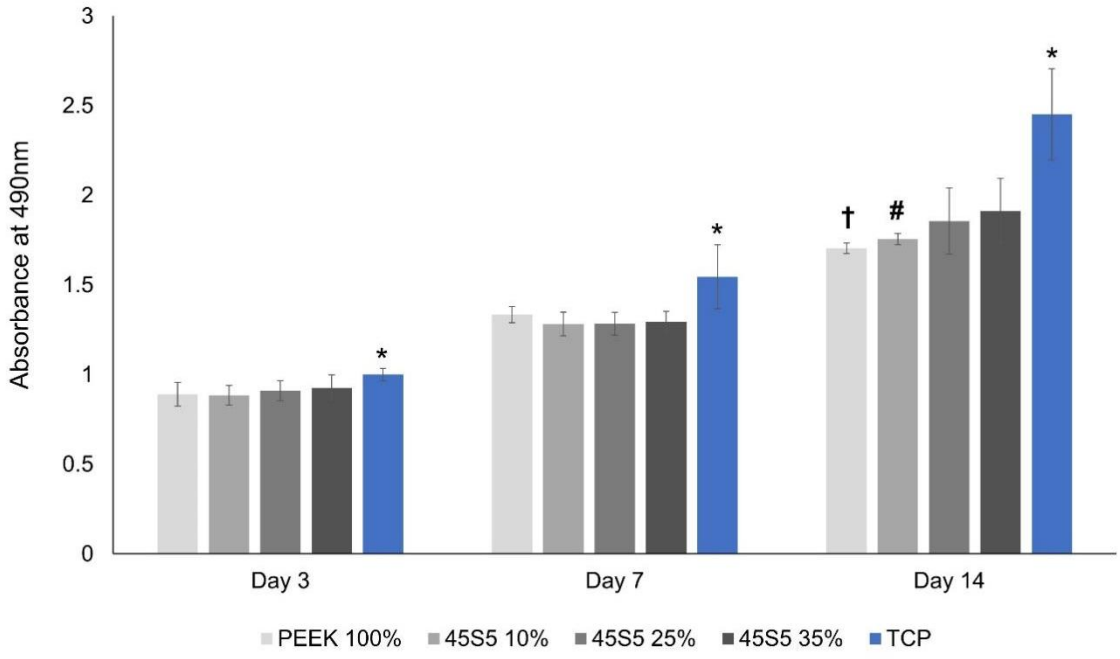

Figure 11. MTS activity analysis for human osteoblasts after incubation onto PEEK 100%, 45S5 10%, 45S5 25% and 45S5 35% at 3, 7 and 14 days. (n = 9; p-values < 0.01)

*Significantly more cells in the indicated group compared to the other groups at the same time point. †Significantly fewer cells than 45S5 25% and 45S5 35% at the same time point. #Significantly fewer cells than 45S5 35% at the same time point.

Morphological aspect of cells onto the coating surfaces were observed by SEM; micrographs after 24 hours of culture are shown in Figure 12. The darkest particles correspond to PEEK, while the lighter ones are glass particles. In general, osteoblasts seeded onto the coatings with and without glass content showed the same morphology; the cells spread and adhered to the coatings with long filopodia, showing a common cell morphology for this type of cells. From these images can be concluded that cells can be adhered on the top of both materials that form the coatings (PEEK and 45S5). Despite of these, the images of the composite coatings (10%, 25% and 35% 45S5 coatings) may suggest that the cells show some preference to adhere to the glass particles, since all cells identified in these coatings are clearly attached to the exposed glass particles. However, since the PEEK area was notably majority in the coatings, a difference in that way could not be appreciated.

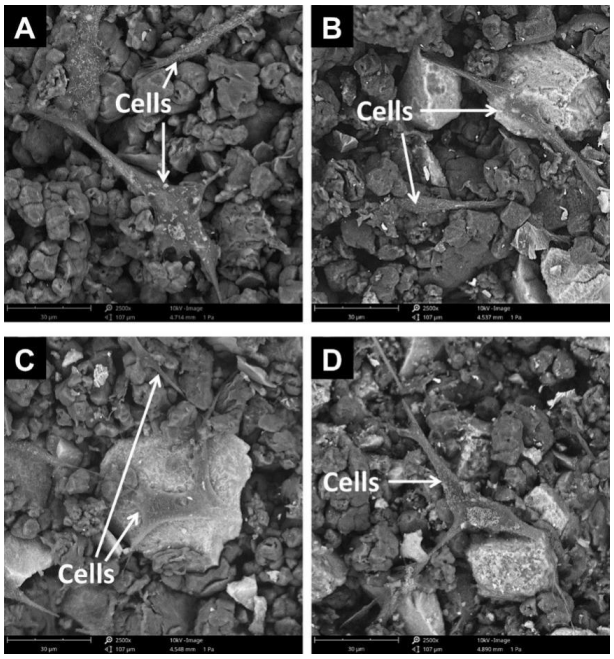

Figure 12. SEM observation of osteoblasts after 24h incubation (x1500). (A) PEEK 100%, (B) 45S5 10%, (C) 45S5 25% and (D) 45S5 35%

4. Conclusions

In this work we have produced 45S5/PEEK composite coatings with enhanced biological properties, by means of LPCGS. The ratio of glass in the sprayed blends was studied, by analyzing the quality of the coatings in terms of microstructure and in vitro response, with results that show an improvement in the properties of the coatings due to the presence of glass. However, interesting differences among coatings were observed.

The produced coatings were composed of a dense and continuous polymeric matrix, where the glass particles were embedded without being altered during the deposition process. The analysis of the microstructure revealed that the capacity of the polymeric matrix to retain glass

was limited; since by increasing the amount of glass in the blends reaches a maximum of glass incorporation for a 35% of glass content.

The amount of glass in the surface is a key aspect for the bioactive behavior of composite coatings as was demonstrated by the studies of the HCA layer formation and the coatings degradation. In particular, the formation of the HCA layer occurs at a similar rate for the coatings with 25, 35 and 50% of glass content in the blends, whilst coatings containing only 10% of glass in the blend showed slower kinetic reaction for HCA layer formation. After three weeks of immersion, a continuous HCA layer could be seen in all the coatings containing glass, with a thickness between 2 and 4 μm. In addition, the degradation rate of the different composite coatings was proven to be mainly related to the glass content in its surface, with an increase proportional to the identified glass area and reaching a top at 35% of glass in the sprayed blend. The bioactivity results were also supported by the weight loss, the ion release and the pH values after the 120h immersion in Tris-HCl solution.

Cellular *in vitro* studies showed that human osteoblasts were able to adhere and proliferate on the evaluated surfaces, with a slight increase of the proliferation at 14 days of incubation for the samples with higher glass content. After 24h of culture, osteoblasts were attached and completely spread onto the different materials forming the composite coatings.

Acknowledgements

This work was supported by the Spanish Government (MCIN/AEI/ 10.13039/501100011033) through grant MAT2016-76928-C2-1-R, Generalitat de Catalunya (SGR-1777) and the Centro de Investigación Biomédica en Red de Fragilidad y Envejecimiento Saludable-CIBERFES (CB16/10/00245) from Instituto de Salud Carlos III, and FEDER funds.

References

[1] J. Graham, J. Peck, FDA Regulation of Polyaryletheretherketone Implants, in: S. Kurtz (Ed.), PEEK Biomater. Handb., 1st ed., William Andrew, 2012: pp. 277–292. https://doi.org/10.1016/B978-1-4377-4463-7.10017-X.

[2] P. Scolozzi, A. Martinez, B. Jaques, Complex orbito-fronto-temporal reconstruction using computer-designed PEEK implant, J. Craniofac. Surg. 18 (2007) 224–228. https://doi.org/10.1097/01.scs.0000249359.56417.7e.

[3] J. Zhang, W. Tian, J. Chen, J. Yu, J. Zhang, J. Chen, The application of polyetheretherketone (PEEK) implants in cranioplasty, Brain Res. Bull. 153 (2019) 143–149. https://doi.org/10.1016/j.brainresbull.2019.08.010.

[4] L. de Ruiter, K. Rankin, M. Browne, A. Briscoe, D. Janssen, N. Verdonschot, Decreased stress shielding with a PEEK femoral total knee prosthesis measured in validated computational models, J. Biomech. 118 (2021) 110270. https://doi.org/10.1016/j.jbiomech.2021.110270.

[5] Y.G. Koh, J.A. Lee, K.T. Kang, Prediction of wear on tibial inserts made of UHMWPE, PEEK, and CFR-PEEK in total knee arthroplasty using finite-element analysis, Lubricants. 7 (2019) 30. https://doi.org/10.3390/lubricants7040030.

[6] S. Verma, N. Sharma, S. Kango, S. Sharma, Developments of PEEK (Polyetheretherketone) as a biomedical material: A focused review, Eur. Polym. J. 147 (2021) 110295. https://doi.org/10.1016/j.eurpolymj.2021.110295.

[7] S. Najeeb, Z. Khurshid, S. Zohaib, M.S. Zafar, Bioactivity and osseointegration of PEEK are inferior to those of titanium: A systematic review, J. Oral Implantol. 42 (2016) 512–516. https://doi.org/10.1563/aaid-joi-D-16-00072.

[8] D. Almasi, N. Iqbal, M. Sadeghi, I. Sudin, M.R. Abdul Kadir, T. Kamarul, Preparation Methods for Improving PEEK's Bioactivity for Orthopedic and Dental Application: A Review, Int. J. Biomater. 2016 (2016) 1–12. https://doi.org/10.1155/2016/8202653.

[9] D.S. Brauer, Bioactive glasses - Structure and properties, Angew. Chemie - Int. Ed. 54 (2015) 4160–4181. https://doi.org/10.1002/anie.201405310.

[10] L.L. Hench, H.A. Paschall, Direct chemical bond of bioactive glass-ceramic materials to bone and muscle, J. Biomed. Mater. Res. 7 (1973) 25–42. https://doi.org/10.1002/jbm.820070304.

[11] J.R. Jones, D.S. Brauer, L. Hupa, D.C. Greenspan, Bioglass and Bioactive Glasses and Their Impact on Healthcare, Int. J. Appl. Glas. Sci. 7 (2016) 423–434. https://doi.org/10.1111/ijag.12252.

[12] C. Gabbi, A. Cacchioli, B. Locardi, E. Guadagnino, Bioactive glass coating: physicochemical aspects and biological findings, Biomaterials. 16 (1995) 515–520. https://doi.org/10.1016/0142-9612(95)91123-G.

[13] N.C. Lindfors, P. Hyvönen, M. Nyyssönen, M. Kirjavainen, J. Kankare, E. Gullichsen, J. Salo, Bioactive glass S53P4 as bone graft substitute in treatment of osteomyelitis, Bone. 47 (2010) 212–218. https://doi.org/10.1016/j.bone.2010.05.030.

[14] A.A. El-Rashidy, J.A. Roether, L. Harhaus, U. Kneser, A.R. Boccaccini, Regenerating bone with bioactive glass scaffolds: A review of in vivo studies in bone defect models, Acta Biomater. 62 (2017) 1–28. https://doi.org/10.1016/j.actbio.2017.08.030.

[15] V. Cannillo, A. Sola, Different approaches to produce coatings with bioactive glasses: Enamelling vs plasma spraying, J. Eur. Ceram. Soc. 30 (2010) 2031–2039. https://doi.org/10.1016/j.jeurceramsoc.2010.04.021.

[16] J. Chang, Y.L. Zhou, Surface modification of bioactive glasses, in: Bioact. Glas., Elsevier, 2018: pp. 119–143. https://doi.org/10.1016/B978-0-08-100936-9.00008-3.

[17] M.H. Fathi, A. Doost Mohammadi, Preparation and characterization of sol-gel bioactive glass coating for

improvement of biocompatibility of human body implant, Mater. Sci. Eng. A. 474 (2008) 128–133. https://doi.org/10.1016/j.msea.2007.05.041.

[18] S.A. Omar, J. Ballarre, Y. Castro, E. Martinez Campos, W. Schreiner, A. Durán, S.M. Cere, 58S and 68S sol-gel glass-like bioactive coatings for enhancing the implant performance of AZ91D magnesium alloy, Surf. Coatings Technol. 400 (2020) 126224. https://doi.org/10.1016/j.surfcoat.2020.126224.

[19] M. Fabert, N. Ojha, E. Erasmus, M. Hannula, M. Hokka, J. Hyttinen, J. Rocherullé, I. Sigalas, J. Massera, Crystallization and sintering of borosilicate bioactive glasses for application in tissue engineering, J. Mater. Chem. B. 5 (2017) 4514–4525. https://doi.org/10.1039/c7tb00106a.

[20] O.P. Filho, G.P. Latorre, L.L. Hench, Effect of crystallization on apatite-layer formation of bioactive glass 45S5, J. Biomed. Mater. Res. 30 (1996) 509–514. https://doi.org/10.1002/(SICI)1097-4636(199604)30:4<509::AID-JBM9>3.0.CO;2-T.

[21] S. Heise, M. Höhlinger, Y.T. Hernández, J.J.P. Palacio, J.A. Rodriquez Ortiz, V. Wagener, S. Virtanen, A.R. Boccaccini, Electrophoretic deposition and characterization of chitosan/bioactive glass composite coatings on Mg alloy substrates, Electrochim. Acta. 232 (2017) 456–464. https://doi.org/10.1016/j.electacta.2017.02.081.

[22] K. Kawaguchi, M. Iijima, T. Muguruma, K. Endo, I. Mizoguchi, Effects of bioactive glass coating by electrophoretic deposition on esthetical, bending, and frictional performance of orthodontic stainless steel wire, Dent. Mater. J. 39 (2020) 593–600. https://doi.org/10.4012/dmj.2019-085.

[23] M. Alaei, M. Atapour, S. Labbaf, Electrophoretic deposition of chitosan-bioactive glass nanocomposite coatings on AZ91 Mg alloy for biomedical applications, Prog. Org. Coatings. 147 (2020) 105803. https://doi.org/10.1016/j.porgcoat.2020.105803.

[24] B. Garrido, I.G. Cano, S. Dosta, Adhesion improvement and in vitro characterisation of 45S5 bioactive glass coatings obtained by atmospheric plasma spraying, Surf. Coatings Technol. 405 (2021) 126560. https://doi.org/10.1016/j.surfcoat.2020.126560.

[25] E. Cañas, M.J. Orts, A.R. Boccaccini, E. Sánchez, Solution Precursor Plasma Spraying (SPPS): A novel and simple process to obtain bioactive glass coatings, Mater. Lett. 223 (2018) 198–202. https://doi.org/10.1016/j.matlet.2018.04.031.

[26] A. Papyrin, V. Kosarev, S. Klinkov, A. Alkimov, V. Fomin, Discovery of the cold spray phenomenon and its basic features, in: Cold Spray Technol., 2007: pp. 1–32. https://doi.org/10.1016/b978-008045155-8/50001-6.

[27] S.T. Oyinbo, T.C. Jen, A comparative review on cold gas dynamic spraying processes and technologies, Manuf. Rev. 6 (2019) 25. https://doi.org/10.1051/mfreview/2019023.

[28] P. Vuoristo, Thermal Spray Coating Processes, in: S. Hashmi (Ed.), Compr. Mater. Process., Elsevier, 2014: pp. 229–276. https://doi.org/10.1016/B978-0-08-096532-1.00407-6.

[29] R.N. Raoelison, Y. Xie, T. Sapanathan, M.P. Planche, R. Kromer, S. Costil, C. Langlade, Cold gas dynamic spray technology: A comprehensive review of processing conditions for various technological developments till to date, Addit. Manuf. 19 (2018) 134–159. https://doi.org/10.1016/j.addma.2017.07.001.

[30] V.K. Champagne, The cold spray materials deposition process, Woodhead Publishing Limited, 2007. https://doi.org/10.1533/9781845693787.

[31] L.L. Hench, The story of Bioglass®, in: J. Mater. Sci. Mater. Med., 2006. https://doi.org/10.1007/s10856-006-0432-z.

[32] Y. Torres, C. Romero, Q. Chen, G. Pérez, J.A. Rodríguez-Ortiz, J.J. Pavón, L. Álvarez, C. Arévalo, A.R. Boccaccini, Electrophoretic deposition of PEEK/45S5 bioactive glass coating on porous titanium substrate: Influence of processing conditions and porosity parameters, in: T. Ebel, F. Pyczak (Eds.), Key Eng. Mater., Trans Tech Publications, Lüneburg, Germany, 2016: pp. 343–350. https://doi.org/10.4028/www.scientific.net/KEM.704.343.

[33] S. Seuss, M. Heinloth, A.R. Boccaccini, Development of bioactive composite coatings based on combination of PEEK, bioactive glass and Ag nanoparticles with antibacterial properties, Surf. Coatings Technol. 301 (2016) 100–105.

[34] Y.C. Yang, E. Chang, Influence of residual stress on bonding strength and fracture of plasma-sprayed hydroxyapatite coatings on Ti-6Al-4V substrate, Biomaterials. 22 (2001) 1827–1836. https://doi.org/10.1016/S0142-9612(00)00364-1.

[35] H.S. Hedia, Effect of coating thickness and its material on the stress distribution for dental implants, J. Med. Eng. Technol. 31 (2007) 280–287. https://doi.org/10.1080/03091900600861616.

[36] ISO 23317: 2007, Implants for surgery —In vitro evaluation for apatite-forming ability of implant materials, Geneva Int. Organ. Stand. (2007).

[37] ISO, ISO 10993-14:2001 Biological evaluation of medical devices — Part 14: Identification and quantification of degradation products from ceramics, Int. Organ. Stand. (2001).

[38] A.M. Vilardell, N. Cinca, N. Garcia-Giralt, S. Dosta, I.G. Cano, X. Nogués, J.M. Guilemany, In-vitro comparison of hydroxyapatite coatings obtained by cold spray and conventional thermal spray technologies, Mater. Sci. Eng. C. 107 (2020). https://doi.org/10.1016/j.msec.2019.110306.

[39] F.E. Ciraldo, E. Boccardi, V. Melli, F. Westhauser, A.R. Boccaccini, Tackling bioactive glass excessive in vitro bioreactivity: Preconditioning approaches for cell culture tests, Acta Biomater. 75 (2018) 3–10. https://doi.org/10.1016/j.actbio.2018.05.019.

[40] Y. Xu, I.M. Hutchings, Cold spray deposition of thermoplastic powder, Surf. Coatings Technol. 201 (2006) 3044–3050. https://doi.org/10.1016/j.surfcoat.2006.06.016.

[41] S.M. Kurtz, J.N. Devine, PEEK biomaterials in trauma, orthopedic, and spinal implants, Biomaterials. 28 (2007) 4845–4869. https://doi.org/10.1016/j.biomaterials.2007.07.013.

[42] P. Patel, T.R. Hull, R.W. McCabe, D. Flath, J. Grasmeder, M. Percy, Mechanism of thermal decomposition of poly(ether ether ketone) (PEEK) from a review of decomposition studies, Polym. Degrad. Stab. 95 (2010) 709–718. https://doi.org/10.1016/j.polymdegradstab.2010.01.024.

[43] D. Bellucci, V. Cannillo, A. Sola, An overview of the effects of thermal processing on bioactive glasses, Sci. Sinter. 42 (2010) 307–320. https://doi.org/10.2298/SOS1003307B.

[44] L. Lefebvre, J. Chevalier, L. Gremillard, R. Zenati, G. Thollet, D. Bernache-Assolant, A. Govin, Structural transformations of bioactive glass 45S5 with thermal treatments, Acta Mater. 55 (2007) 3305–3313. https://doi.org/10.1016/j.actamat.2007.01.029.

[45] T. Schmidt, H. Assadi, F. Gärtner, H. Richter, T. Stoltenhoff, H. Kreye, T. Klassen, From particle acceleration to impact and bonding in cold spraying, J. Therm. Spray Technol. 18 (2009) 794–808. https://doi.org/10.1007/s11666-009-9357-7.

[46] B.T. Hoa, H.T.T. Hoa, N.A. Tien, N.H.D. Khang, E. V. Guseva, T.A. Tuan, B.X. Vuong, Green synthesis of bioactive glass 70SiO2-30CaO by hydrothermal method, Mater. Lett. 274 (2020). https://doi.org/10.1016/j.matlet.2020.128032.

[47] A. Saboori, M. Rabiee, F. Moztarzadeh, M. Sheikhi, M. Tahriri, M. Karimi, Synthesis, characterization and in vitro bioactivity of sol-gel-derived SiO2-CaO-P2O5-MgO bioglass, Mater. Sci. Eng. C. 29 (2009). https://doi.org/10.1016/j.msec.2008.07.004.

[48] A.M. El-Kady, A.F. Ali, Fabrication and characterization of ZnO modified bioactive glass nanoparticles, Ceram. Int. 38 (2012). https://doi.org/10.1016/j.ceramint.2011.07.069.

[49] L.L. Hench, Chronology of Bioactive Glass Development and Clinical Applications, New J. Glas. Ceram. 3 (2013) 67–73. https://doi.org/10.4236/njgc.2013.32011.

[50] O. Peitl, E. Dutra Zanotto, L.L. Hench, Highly bioactive P2O5-Na2O-CaO-SiO2glass-ceramics, J. Non. Cryst. Solids. 292 (2001) 115–126. https://doi.org/10.1016/S0022-3093(01)00822-5.

[51] M.A. Ur Rehman, F.E. Bastan, Q. Nawaz, W.H. Goldmann, M. Maqbool, S. Virtanen, A.R. Boccaccini, Electrophoretic deposition of lawsone loaded bioactive glass (BG)/chitosan composite on polyetheretherketone (PEEK)/BG layers as antibacterial and bioactive coating, J. Biomed. Mater. Res. - Part A. 106 (2018) 3111–3122. https://doi.org/10.1002/jbm.a.36506.

[52] S. Yu, K.P. Hariram, R. Kumar, P. Cheang, K.K. Aik, In vitro apatite formation and its growth kinetics on hydroxyapatite/ polyetheretherketone biocomposites, Biomaterials. 26 (2005) 2343–2352. https://doi.org/10.1016/j.biomaterials.2004.07.028.

[53] L.L. Hench, Ö. Andersson, Bioactive Glasses, in: An Introd. to Bioceram., 1993: pp. 41–62. https://doi.org/10.1142/9789814317351_0003.

[54] W. Hong, F. Guo, J. Chen, X. Wang, X. Zhao, P. Xiao, Bioactive glass–chitosan composite coatings on PEEK: Effects of surface wettability and roughness on the interfacial fracture resistance and in vitro cell response, Appl. Surf. Sci. 440 (2018) 514–523. https://doi.org/10.1016/j.apsusc.2018.01.183.

[55] M.B. da Cruz, J.F. Marques, G.M. Peñarrieta-Juanito, M. Costa, J.C.M. Souza, R.S. Magini, G. Miranda, F.S. Silva, J.M.M. Caramês, A.D.S.P. da Mata, Bioactive-Enhanced Polyetheretherketone Dental Implant Materials: Mechanical Characterization and Cellular Responses, J. Oral Implantol. 47 (2021) 9–17. https://doi.org/10.1563/aaid-joi-D-19-00172.

[56] Y. Deng, P. Zhou, X. Liu, L. Wang, X. Xiong, Z. Tang, J. Wei, S. Wei, Preparation, characterization, cellular response and in vivo osseointegration of polyetheretherketone/nano-hydroxyapatite/carbon fiber ternary biocomposite, Colloids Surfaces B Biointerfaces. 136 (2015) 64–73. https://doi.org/10.1016/j.colsurfb.2015.09.001.

4.4. Development of bioactive glass powders for cold gas spray

When brittle materials, such as bioactive glasses, are deposited by cold gas spray, the dense ceramic particles break into fragments that are adhered to the surface as a fragmented block. As brittle materials are not easily deformed, and the temperatures involved in the process are not enough to reach the thermal softening of the whole particles, the impact results in particle fracture. Thus, generating a coating with this material is challenging, and with dense particles, only a thin monolayer could be formed.

A change in the viscosity behaviour of the material can be obtained by varying the oxides forming the glass. Thus, novel glass compositions can get the deposition of the brittle material. The following section details the design of silica-based and phosphate-based glasses with features adjusted to CGS requirements. In addition, the bioactive and degradable behaviour of the glasses developed was evaluated.

1. Introduction

The present study seeks to design glass formulations with lower viscosity, adjusted to the CGS working temperature so that a softening of the material can be achieved at the time of deposition to form a glass coating. Different glass compositions were produced and evaluated to achieve this behavior in the powder.

One of the strategies consisted of incorporating CaF_2 into the SiO_2-CaO-$N_{a2}O$-P_2O_5 system. In this way, we have a silicate-based bioactive glass to which we add CaF_2 that acts as a fluidizing element (Ref 1–4). In previous studies (Ref 5) demonstrated that the addition of CaF_2 keeps the bioactivity of the glass and also promotes osteoblast differentiation and bone mineralization.

The addition of CaF_2 was done by replacing mainly CaO and SiO_2. This way, the elements which disrupt the network are kept. The glasses used are listed in Table 1.

Table 1. Silica glass compositions with CaF_2 in molar percentage

Code	System	SiO_2	CaO	Na_2O	P_2O_5	CaF_2
CaF_17	SiO_2-CaO-$N_{a2}O$-P_2O_5-CaF_2	31.37	21.31	24.36	5.21	17.76
CaF_25	SiO_2-CaO-$N_{a2}O$-P_2O_5-CaF_2	28.4	19.29	22.06	4.71	25.54
CaF_25_Na	SiO_2-CaO-$N_{a2}O$-P_2O_5-CaF_2	28.4	11.75	29.6	4.71	25.54

In addition to silica glasses, we can find phosphate-based glasses, which contain phosphorus oxide, as glass former, although its use is quite unusual. P_2O_5 forms glass based on the phosphate tetrahedron PO_4, covalently bonded with other tetrahedrons forming the glassy network (Ref 6,7). The main problem with the structure of phosphate-based glasses is their solubility, which is caused by the phosphorus tetrahedron having a double bond with one of the oxygens, so oxygen cannot bond with other tetrahedra, which results in a very open network. In phosphate glasses, the oxide modifiers and stabilizers play an essential role in slowing down the dissolution rate of these glasses. In particles, alkaline earth metals such as CaO improve solubility. Furthermore, alkalis like Na_2O make the network even more soluble.

In this study phosphate-based glasses in two different binary systems (P_2O_5-CaO and P_2O_5-Na_2O) and in two different ternary systems (P_2O_5-Na_2O-CaO and P_2O_5-Na_2O-CaF_2) were designed, the compositions are detailed in Table 2 and represented in Figure 1.

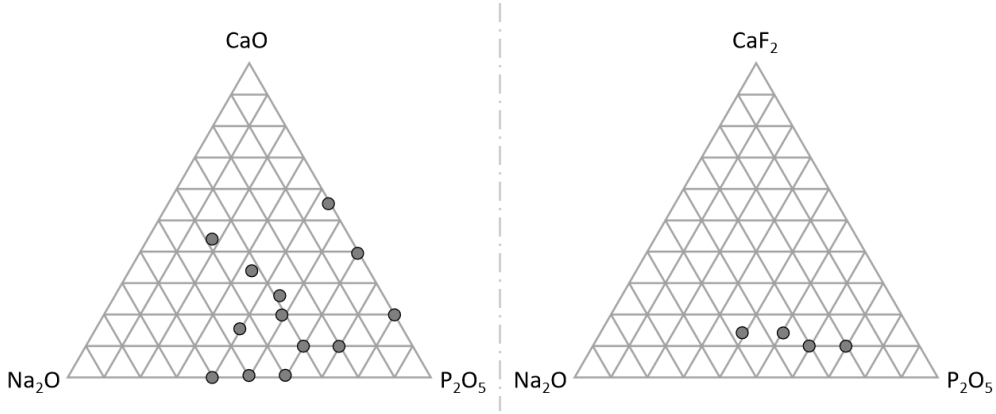

Figure 1. Ternary phosphate glass diagrams of P_2O_5-Na_2O-CaO and P_2O_5-Na_2O-CaF_2

Table 2. Phosphate-based glass compositions in molar percentage

Code	System	CaO	Na_2O	P_2O_5	CaF_2
CaP_44	P_2O_5-CaO	55.7	-	44.3	-
CaP_61	P_2O_5-CaO	38.7	-	61.3	-
CaP_80	P_2O_5-CaO	20	-	80	-
NaP_40	P_2O_5-Na_2O	-	60	40	-
NaP_50	P_2O_5-Na_2O	-	50	50	-
NaP_60	P_2O_5-Na_2O	-	40	60	-
NaPCa_17	P_2O_5-Na_2O-CaO	44.3	38.2	17.5	-
NaPCa_33	P_2O_5-Na_2O-CaO	33.9	32.3	33.9	-
NaPCa_39	P_2O_5-Na_2O-CaO	16.5	44.5	39	-
NaPCa_43	P_2O_5-Na_2O-CaO	26.1	30.4	43.5	-
NaPCa_49	P_2O_5-Na_2O-CaO	18	32.5	49.5	-
NaPCa_60	P_2O_5-Na_2O-CaO	10	30	60	-
NaPCa_70	P_2O_5-Na_2O-CaO	10	20	70	-
NaPCaF_40	P_2O_5-Na_2O-CaF_2	-	46.7	40.9	12.4
NaPCaF_52	P_2O_5-Na_2O-CaF_2	-	34.3	52.2	13.5
NaPCaF_60	P_2O_5-Na_2O-CaF_2	-	30	60	10
NaPCaF_70	P_2O_5-Na_2O-CaF_2	-	20	70	10

To evaluate the viability of the developed glasses to be sprayed by CGS, the different compositions were prepared and characterised in terms of dissolution behaviour, bioactivity and viscosity.

2. Materials and methods

2.1. Glass preparation

Glasses were prepared using the chemical reagents detailed in Table 3. The weighted batches were homogeneously mixed before melting in a platinum crucible at the temperature detailed in Table 3 by using an electric furnace. The heating rate was 5 ºC/min and the melting was done for 2 h. The melt material was poured on a brass plate and then milled in an agate mortar with a pestle to obtain the powder.

Table 3. Reagents and melting temperature for each glass system.

System	Reagents	T (ºC)
SiO_2-CaO-$N_{a2}O$-P_2O_5-CaF_2	Na_2CO_3 + $(NH_4)_2{\cdot}HPO_4$ + $CaCO_3$ + SiO_2+ CaF_2	1430
P_2O_5-CaO	$(NH_4)_2{\cdot}HPO_4$ + $CaCO_3$	1100
P_2O_5-Na_2O	$(NH_4)_2{\cdot}HPO_4$ + $Na_2HPO_4{\cdot}2H_2O$	1100
P_2O_5-Na_2O-CaO	$CaHPO_4$ + $NaH_2PO_4{\cdot}H_2O$ + $CaCO_3$ or $CaHPO_4$ +$NaH_2PO_4{\cdot}H_2O$ + Na_2CO_3	1200
P_2O_5-Na_2O-CaF_2	$Na_2HPO_4{\cdot}2H_2O$ + $(NH_4)_2{\cdot}HPO_4$ + CaF_2	1100

2.2. Hot-stage microscopy

The determination of the characteristic viscosity points using hot-stage microscopy was carried out with a heating microscope (Hesse Instruments) equipped with a camera Leica (EM201, Leica, Microsystems GmbH, Wetzlar, Germany) incorporating automatic image analysis. Fine powder samples were shaped by cold pressing to obtain samples with correct shape for analysis. The analysis was performed from room temperature till 1200ºC with a heating rate of 10 ºC /min.

2.3. Chemical dissolution of glasses in deionized water

Powders were sieved between 100 and 710 µm and placed in a desiccator 48h before the test. Then, 150 mg of each powder was placed in a mesh bag immersed in 4 mL of deionized water at 37ºC for 24h. After the test, samples were rinsed with alcohol and dried in an electric oven for 24h. The dissolution rate was measured based on the weight difference of each glass before and after the test.

2.4. Apatite forming ability of the glasses in physiological solution

The in vitro ability of the glasses to form apatite was studied following the ISO 23317:2014 using the simulated body fluid Hank's Balanced Salt Solution (HBSS) (Sigma-Aldrich, Germany). Glass samples were immersed in HBSS and exposed for 3 and 14 days at 37ºC in a thermostatic bath with agitation. The solution was changed every 3 days to avoid ionic saturation of the medium. After the soaking time, the samples were characterised using SEM

coupled with EDS to analyse the chemical and physical changes related to the bone-like apatite formation.

2.5. Coating deposition

For the coating deposition, two CGS equipments were used: the low-pressure cold gas spray (LPCGS) equipment (Dymet 423, Dycomet Europe, Akkrum, the Netherlands) was used with air as the propellant gas and the high-pressure cold-spray (HPCGS) (PCS-100 (Plasma Giken, Saitama, Japan). The glases were deposited onto titanium alloy substrates previously grit-blasted (Formula 1400, Guyson International, Skipton, England) with corundum G24 (grit size 800 µm) at 0.5 MPa. Furthermore, splats were deposited onto polished titanium alloy substrates.

3. Results and discussion

3.1. Glass forming ability and viscosity

We tried to synthesize 3 silicate-based glasses and 17 phosphate-based glasses. However, it did not succeed for some compositions, as the melt was highly prone to phase crystallization, resulting in white coloured samples. In Figure 2, the compositions of phosphate-based that present amorphous structures are marked in white circles, while the compositions that suffered devitrification are marked in grey, these results are also summarized in Table 3. In particular, the samples corresponding to the ternary system P_2O_5-Na_2O-CaO suffered greater vitrifiability on cooling. The silicate-based glasses presented an amorphous structure.

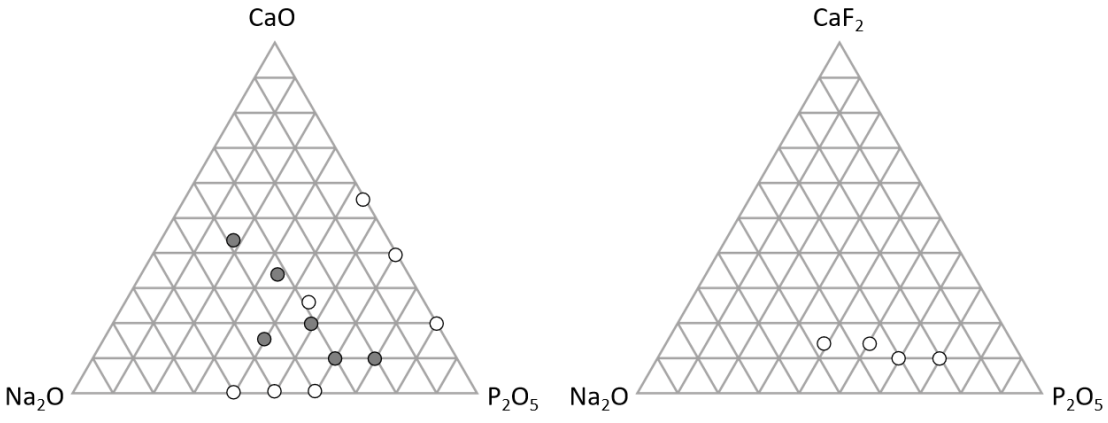

Figure 2. Structure of the glass prepared of P_2O_5-Na_2O-CaO and P_2O_5-Na_2O-CaF_2, in white glassy structure and in grey devitrification

A heating microscope with an in-situ observation during the whole thermal process is a unique tool for understanding material's behaviour. In the present study, heating microscopy was employed to evaluate the viscosity points during thermal treatment of the different glass developed.

The changes in the shape of the samples can be related to thermal events, which can be correlated to viscosity points (Ref 8). According to the values found by Pascual et al. (Ref 9), the following points are considered softening point ($\eta=10^{6.3}$), half ball ($\eta=10^{4.1}$) and flow point ($\eta=10^{3.4}$). The heating microscope curves (sample cross-section area changes versus temperature) for different groups of glasses and the thermal events related to viscosity points are represented in Figures 3-7.

According to the results obtained by this analysis, the glasses produced in the P_2O_5-Na_2O system have a viscosity (softening point 339-452ºC) more adequate for their use in CGS, as these glasses could be able to deform when the powder is heated at the operating temperatures of the equipment. The effect of incorporating CaF_2 into the silicate-based glasses resulted in a low variation in the viscosity concerning the 45S5 glass, which is not enough for the CGS technique.

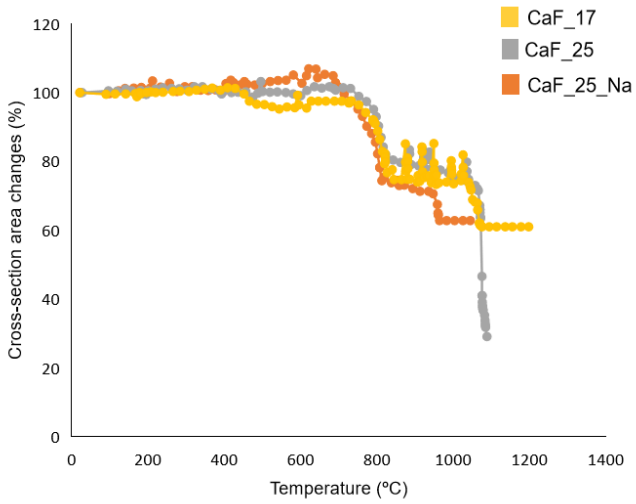

Figure 3. Heating microscope curves of glasses on the silicate-bases glass with fluorite

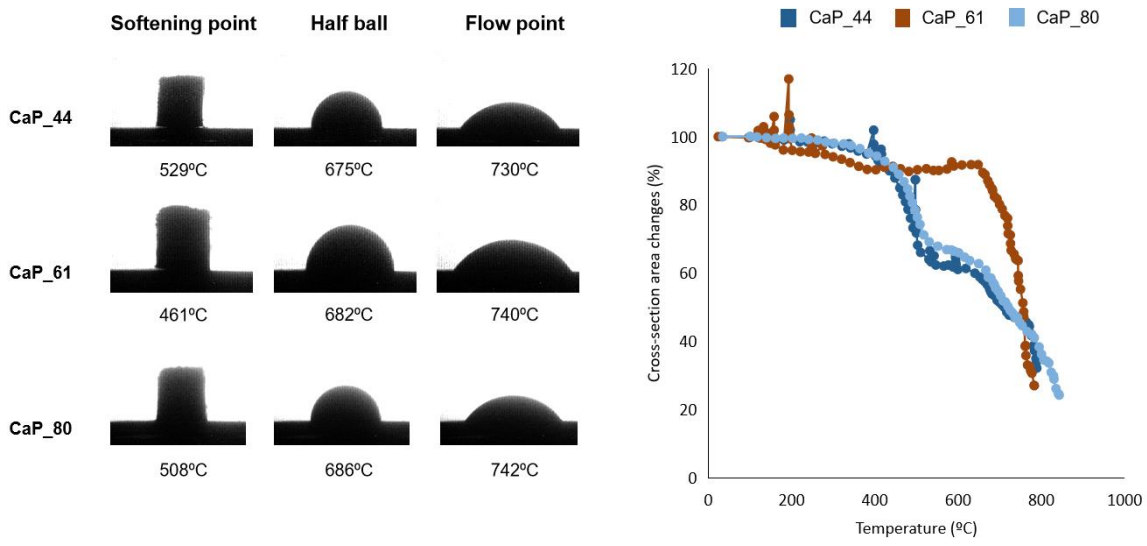

Figure 4. Micrographs of the characteristic points of viscosity and heating microscope curves of glasses on the system P_2O_5-CaO

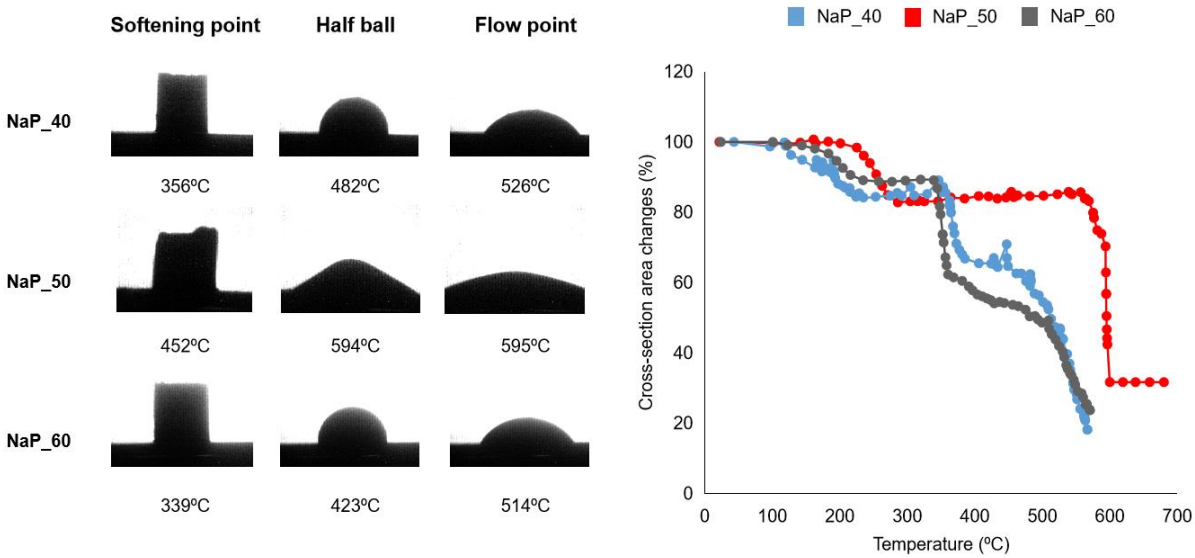

Figure 5. Micrographs of the characteristic points of viscosity and heating microscope curves of glasses on the system P_2O_5-Na_2O

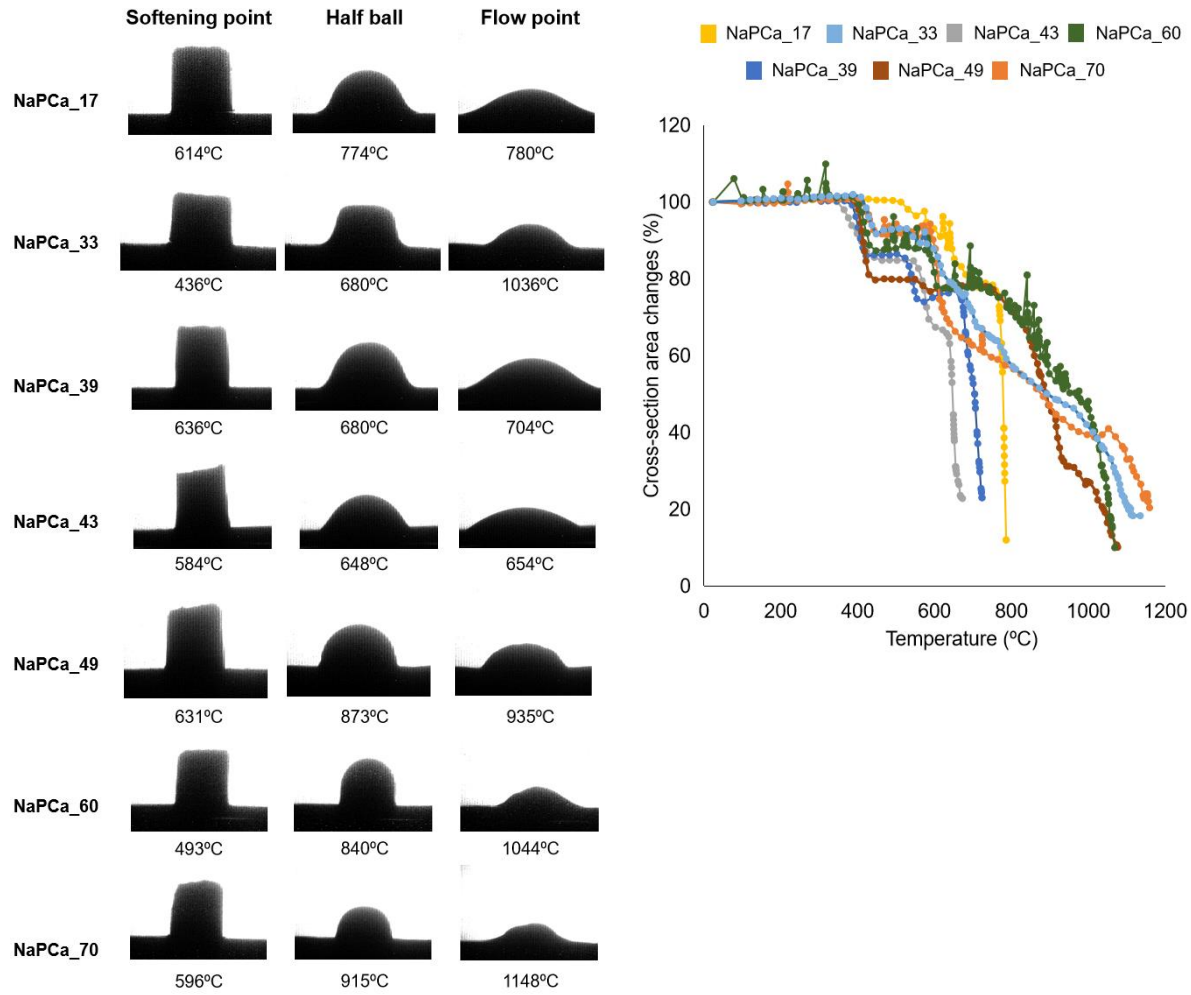

Figure 6. Micrographs of the characteristic points of viscosity and heating microscope curves of glasses on the system P_2O_5-Na_2O-CaO

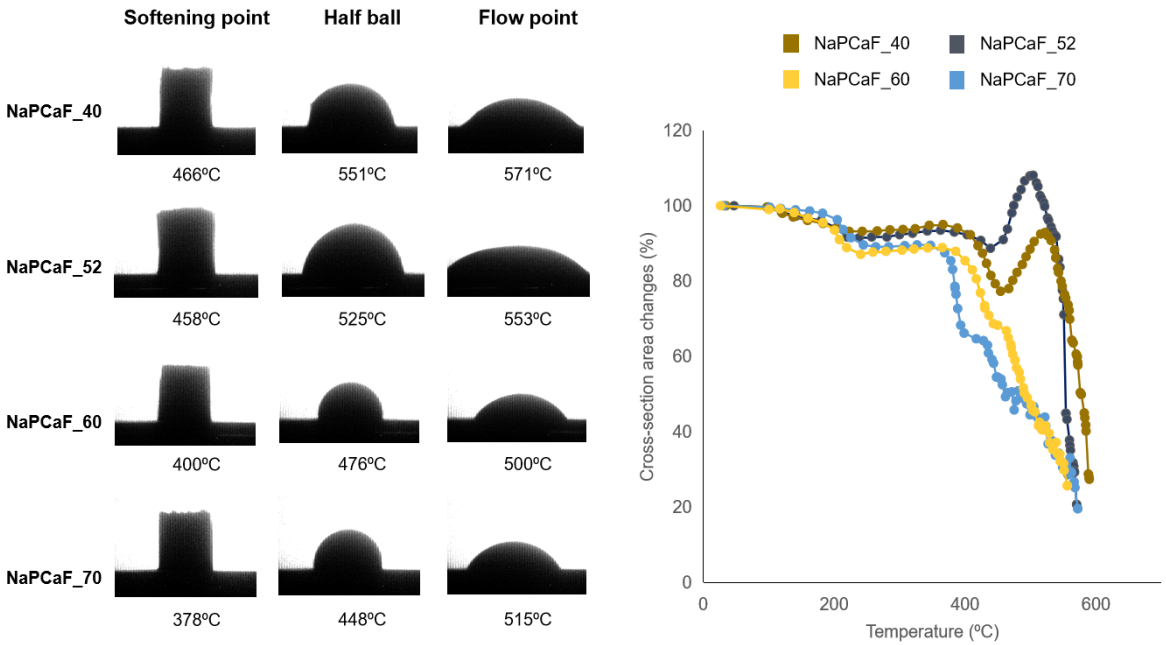

Figure 7. Micrographs of the characteristic points of viscosity and heating microscope curves of glasses on the system P_2O_5-Na_2O-CaF_2

Table 3. Structure formed and dissolution of the phosphate glass compositions

Code	Structure	Weight loss percentage
CaP_44	Glassy	12
CaP_61	Glassy	21
CaP_80	Glassy	21
NaP_40	Glassy	94
NaP_50	Glassy	92
NaP_60	Glassy	87
NaPCa_17	Devitrification	4
NaPCa_33	Devitrification	8
NaPCa_39	Devitrification	2
NaPCa_43	Glassy	43
NaPCa_49	Devitrification	2
NaPCa_60	Devitrification	8
NaPCa_70	Devitrification	11
NaPCaF_40	Glassy	68
NaPCaF_52	Glassy	60
NaPCaF_60	Glassy	74
NaPCaF_70	Glassy	78

3.2. Dissolution behaviour of glasses in deionized water

The dissolution of the phosphate-based glasses was analysed by the weight loss percentage of the samples after 24h of immersion and the results are detailed in Table 3. It is possible to appreciate a great dissolution for the compositions of the binary system P_2O_5-Na_2O followed by the ones in the ternary system P_2O_5-Na_2O-CaF_2. By comparing the two binary systems, it is clearly seen that introducing CaO instead of Na_2O provides a notable effect on the durability of the phosphate, as was reported in the literature (Ref 10). When CaF_2 is replacing CaO in the ternary system, the degradation of the glass is severely affected. The less soluble samples among the phosphate-based glasses developed correspond to the ternary system P_2O_5-Na_2O-CaO, which suffered devitrification. It should be noted that the glasses with higher dissolution correspond to the glasses with lower viscosity at the softening point. These results are consistent since the glasses with a network more disrupted can deform and flow more easily than the ones with a more interconnected network.

3.3. Apatite forming ability of the glasses in physiological solution

The ability of the phosphate-based glasses to form an apatite layer was assessed at 3 and 7 days. However, the high dissolution rate of all the designed compositions did not allow the formation of the layer.

3.4. Single particle and coating deposition

In Figure 8, it is possible to see the free surface of the 45S5 bioactive glass powder at the left and the right, a single 45S5 glass particle deposited by cold gas technology.

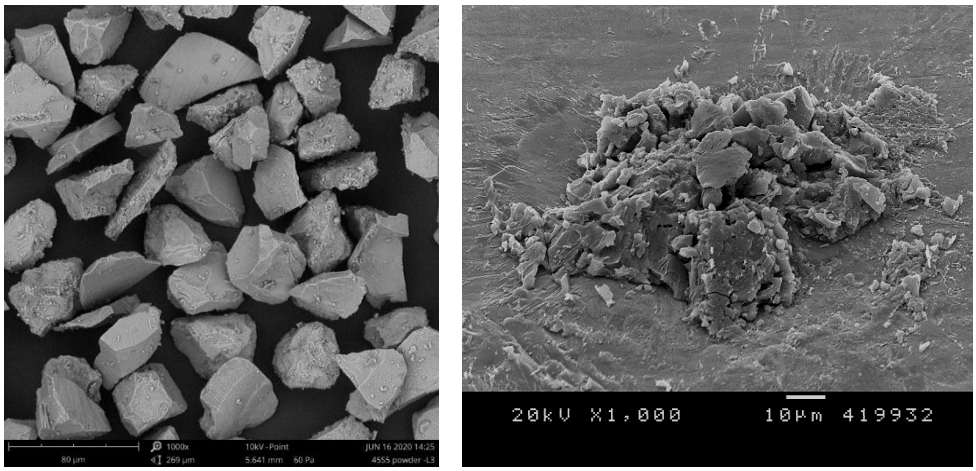

Figure 8. Free surface of 45S5 powder and single particle deposition of bioactive glass 45S5 by cold gas spray (gas pressure 1000ºC and pressure 45 bar)

When brittle materials, such as bioactive glasses, are deposited by cold gas spray, the dense ceramic particles break into fragments that are adhered to the surface as a fragmented block. As brittle materials cannot deform, and the temperatures involved in the process are not enough to reach the thermal softening of the whole particles, the impact results in particle fracture. Thus, generating a coating with this material is a challenge, and only a thin monolayer can be formed. However, with the change in the composition of the designed glasses, a drastic variation of viscosity has been achieved, as can be seen in the heating microscopy curves Figure 9.

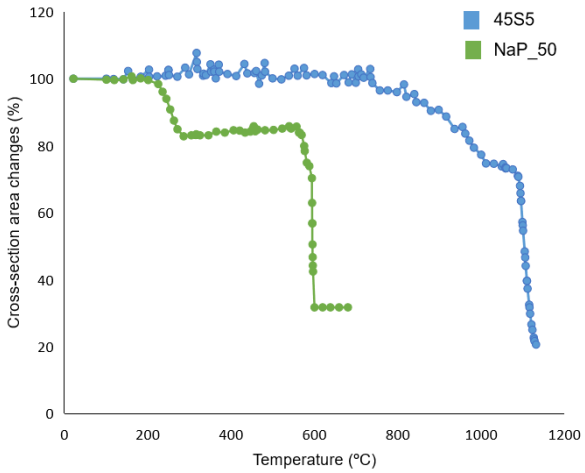

Figure 9. Comparison of heating microscope curves of a glass designed in the P_2O_5-Na_2O system versus the 45S5 glass

The splats of NaP_50 glass deposited by LPCGS and HPCGS are represented in Figure 10 and Figure 11, respectively.

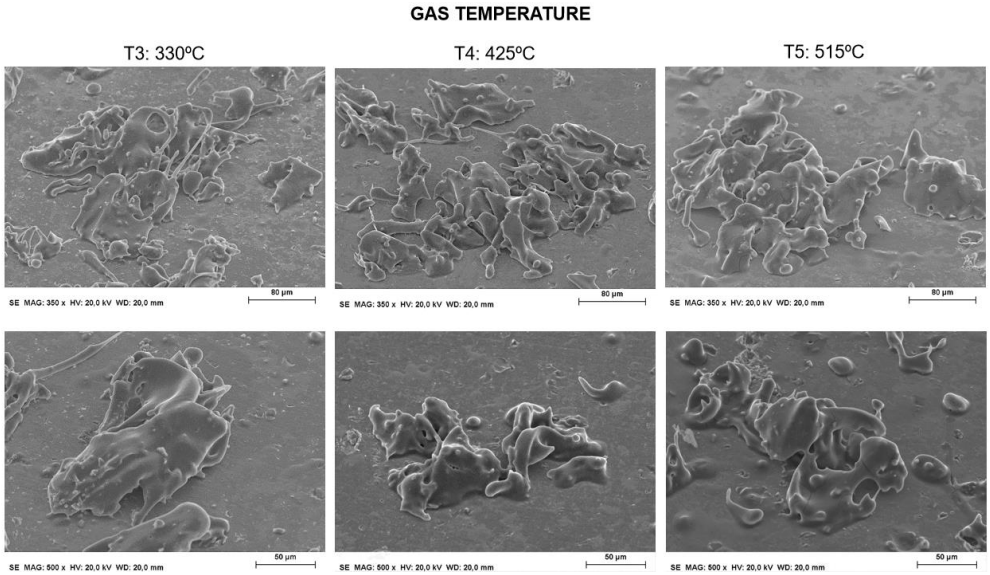

Figure 10. Single particle deposition of NaP_50 glass by low-pressure cold gas spray

For the splats deposited by low-pressure, three different gas temperatures were employed, and the particles deposited onto the polished substrates, in contrast with the 45S5, are deformed and well adhered. The deposited particles have not suffered fragmentation and no cracks are observed in them. Furthermore, it is possible to observe long fingers in some of the particles caused by the deformation arose.

For the splats deposited by high-pressure, it is possible to see that particles are in a more fragile state since some cracks are appreciated in the adhered particles. Moreover, several cracks related to rebounded particles can be appreciated in the polished substrate.

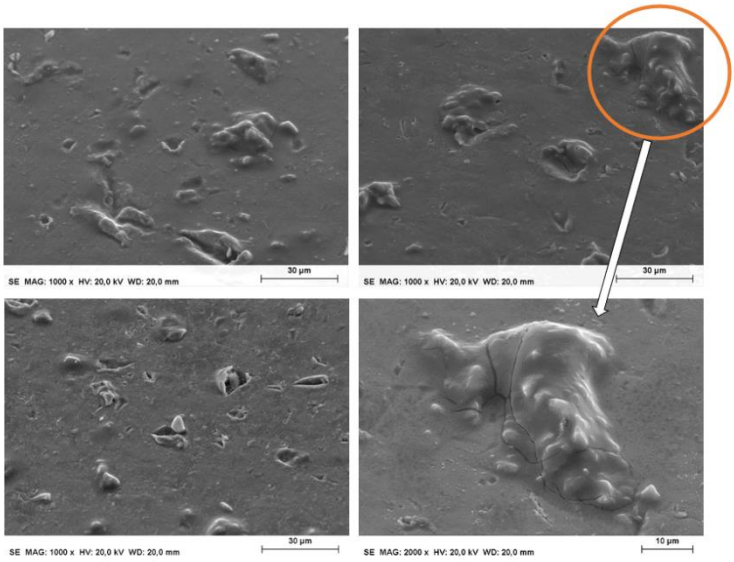

Figure 11. Single particle deposition of NaP_50 glass by high-pressure cold gas spray (gas temperature 1000ºC and pressure 45 bar)

As explained before, the coating deposition was not achieved for 45S5 dense glass powders, neither for LPCGS nor HPCGS. However, with the NaP_50 glass a coating was achieved only by LPCGS, as shown in Figure 12.

The coating adhesion was achieved when gas temperatures were 425ºC and 515ºC. Even the single particle deposition was also achieved at 330ºC, the coating was not reached at this gas temperature. The deposition was done onto grit-blasted substrates, and pre-heating of the substrate notably enhanced the deposition of the coating. The observation of the free surface showed no cracks and good cohesion among particles.

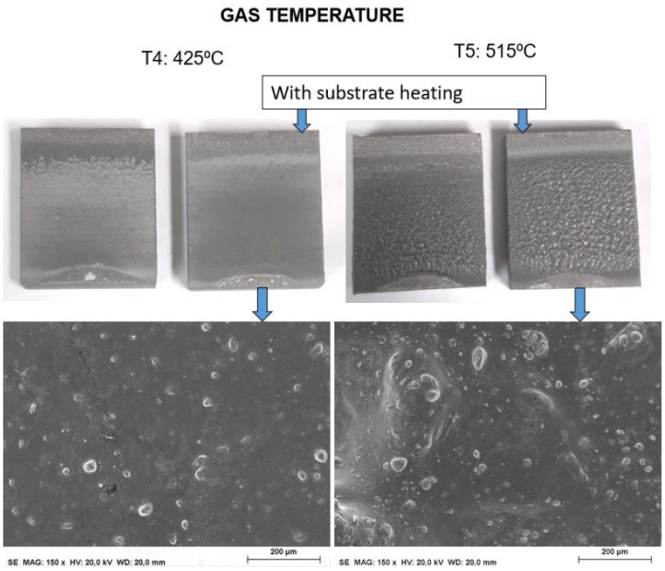

Figure 12. Substrates coated with NaP_50 glass by LPCGS at different conditions

4. Conclusions

In this study, different compositions have been formulated with lower viscosity at the working temperature of cold spraying. It has been found that phosphate-based compositions can achieve significantly lower viscosity than silicate-based ones.

With glasses in the P_2O_5-Na_2O system, it has been possible to deposit coatings using cold gas spray. The splats, deposited by high-pressure and low-pressure, revealed that the particles achieve greater deformation and do not fragment compared to 45S5. In particular, when low-pressure is used, the deformation of the particles is greater since the impact speed and energy is more favourable for brittle materials that need time to heat up and that suffer from difficult deformation if arrive in a rigid state to the substrate. Furthermore, pre-heating the substrate favoured the coating deposition of the glass in the P_2O5-Na_2O system.

Glasses have been deposited by cold spraying, however these glasses cannot be used to coat implants, since their dissolution is high, and are not capable to promote bioactivity.

References

1. D.S. Brauer, A. Al-Noaman, R.G. Hill, and H. Doweidar, Density-Structure Correlations in Fluoride-Containing Bioactive Glasses, *Mater. Chem. Phys.*, Elsevier B.V., 2011, **130**(1–2), p 121–125, doi:10.1016/j.matchemphys.2011.06.015.

2. D.S. Brauer, M.N. Anjum, M. Mneimne, R.M. Wilson, H. Doweidar, and R.G. Hill, Fluoride-Containing Bioactive Glass-Ceramics, *J. Non. Cryst. Solids*, Elsevier B.V., 2012, **358**(12–13), p 1438–1442, doi:10.1016/j.jnoncrysol.2012.03.014.

3. D.S. Brauer, N. Karpukhina, M.D. O'Donnell, R. V. Law, and R.G. Hill, Fluoride-Containing Bioactive Glasses: Effect of Glass Design and Structure on Degradation, PH and Apatite Formation in Simulated Body Fluid, *Acta Biomater.*, 2010, **6**(8), p 3275–3282, doi:10.1016/j.actbio.2010.01.043.

4. F.A. Shah, Fluoride-Containing Bioactive Glasses: Glass Design, Structure, Bioactivity, Cellular Interactions, and Recent Developments, *Mater. Sci. Eng. C*, Elsevier B.V., 2016, **58**, p 1279–1289, doi:10.1016/j.msec.2015.08.064.

5. E. Gentleman, M.M. Stevens, R.G. Hill, and D.S. Brauer, Surface Properties and Ion Release from Fluoride-Containing Bioactive Glasses Promote Osteoblast Differentiation and Mineralization in Vitro, *Acta Biomater.*, Acta Materialia Inc., 2013, **9**(3), p 5771–5779, doi:10.1016/j.actbio.2012.10.043.

6. M.T. Islam, R.M. Felfel, E.A. Abou Neel, D.M. Grant, I. Ahmed, and K.M.Z. Hossain, Bioactive Calcium Phosphate–Based Glasses and Ceramics and Their Biomedical Applications: A Review, *J. Tissue Eng.*, 2017, **8**.

7. U. Hoppe, A Structural Model for Phosphate Glasses, *J. Non. Cryst. Solids*, 1996, **195**(1–2), p 138–147.

8. M.J. Pascual, L. Pascual, and A. Durán, Determination of the Viscosity-Temperature Curve for Glasses on the Basis of Fixed Viscosity Points Determined by Hot Stage Microscopy, *Phys. Chem. Glas.*, 2001, **42**(1), p 61–66.

9. M.J. Pascual, A. Durán, and M.O. Prado, A New Method for Determining Fixed Viscosity Points of Glasses, *Phys. Chem. Glas.*, 2005, **46**(5), p 512–520.

10. H. Gao, T. Tan, and D. Wang, Effect of Composition on the Release Kinetics of Phosphate Controlled Release Glasses in Aqueous Medium, *J. Control. Release*, 2004, **96**(1), p 21–28.

5. Chapter: Global discussion of the results

5. Chapter: Global discussion of the results

After presenting the results obtained, a global discussion of the most relevant results is carried out. The current thesis studied surface modifications by incorporating bioactive glass coatings using thermal spray. In Figure 5.1, the different thermal spray techniques according to the literature used to deposit bioactive glass coatings are represented and highlighted the ones used in this work.

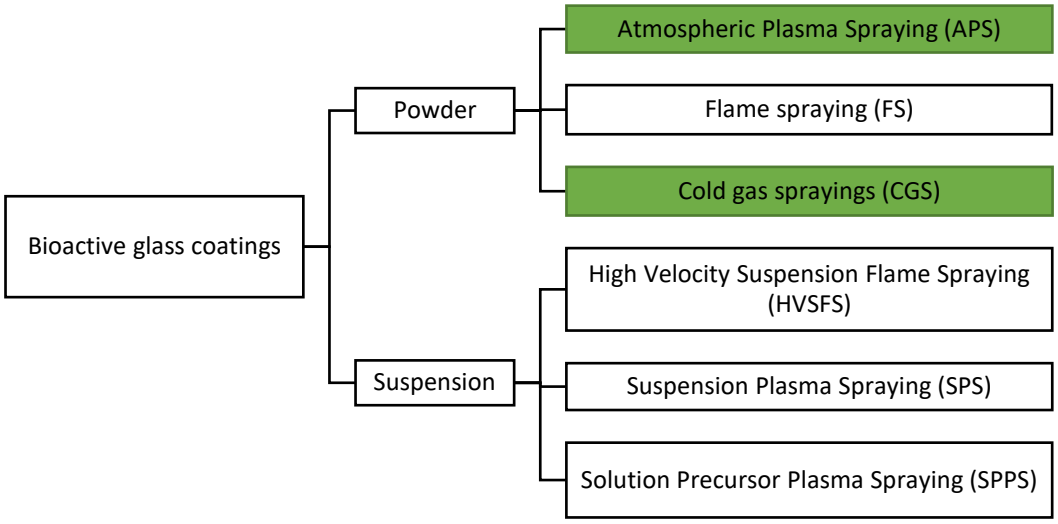

Figure 5.1 Thermal spray techniques used for developing bioactive glass coatings

Part of the study has focused on understanding and developing improved bioactive glass coatings by APS since most manufacturers use this technology to produce HA-coated implants.

Strategies to improve the adhesion of bioactive glass coatings

With the application of the post-thermal treatment, an improvement in the adherence of the bioactive glass coatings is achieved. By heating the glass above its glass transition temperature, it results in a more fluid state that facilitates the reorganization of the atoms that form it, allowing greater cohesion between the particles that make up the coating and relaxation of the tensions present in the coating. Also, at the temperature at which the treatment is performed, the crystallization of the sodium-calcium silicate crystalline phase occurs, providing stronger bonds in the structure that favor greater coating adherence.

The modification of the morphology of the feedstock powder also causes an improvement in coating adhesion. During the spraying process, the heating of the agglomerated particles is more effective than in the dense glass particles. As the agglomerates are composed of smaller particles, these melt quickly. In addition, the structure of the agglomerates is porous and has a great specific surface. This set of characteristics allows faster heating of the agglomerated particles, especially when dealing with a material with low thermal conductivity and a short heating period during the deposition process. So when the agglomerated particles

reach the surface of the substrate, they arrive in a more fluid state that allows better interaction with it, causing an increase in the bond strength.

The contribution of a complementary powder (HA) with a CTE closer to the substrate favors the coating adherence with the substrate. Incorporating HA in the coatings as an anchor layer between the glass and the substrate and mixing it with the glass before spraying improved notably adhesion. The minor mismatch of the CTE between the coating layers and the substrate reduces the residual stress formed by the rapid cooling to room temperature after deposition. HA has the role of mitigating residual stresses in the coatings.

Heating the substrate prior to deposition of the glass material causes an improvement in the adhesion of the coatings. This improvement is due to a reduction in the temperature difference between the substrate and the deposited material, leading to a less drastic cooling to room temperature and, therefore, less residual thermal stress is generated.

The oxides that form the bioactive glasses also affect the adherence of the coatings since the microstructure obtained is marked by each component. In particular, with the free sodium composition (62W), no porosity was observed in the cross-sections of these coatings since the volatilization of sodium and phosphorus mainly causes it during spraying. Furthermore, the absence of porosity resulted in a high adhesion value in the as-sprayed coating and after one day of immersion in the physiological solution.

Several factors can affect, to different degrees, the bond strength of bioactive glass coatings, such as the morphology of the powders, the oxides that form the glass, the combination with other materials, and the application of heat treatments. In addition, in some cases, the combination of various strategies results in a more significant increase, as has been seen, for example, with the application of heat treatment to a coating produced with agglomerated glass.

Effect of glass composition on the microstructure and biological properties of the coating

The role of the elements forming the glass structure influences the properties of the coatings. For example, when comparing two glasses with the same oxides in different proportions (45S5 and S53P4), it could be appreciated that for a network structure less disrupted (with more networking formers), the release of ions occurs at a slower rate. Consequently, it has slower kinetics in forming the hydroxyl carbonate apatite layer since this is initiated in bioactive glasses by the ion exchange that occurs when it is in contact with the physiological fluid. Amorphous coatings have a more reactive response in physiological solutions than coatings containing crystalline phases since these phases include stronger bonds that results in more connected networks. Also, the presence of crystalline phases affects the ions released.

When less sodium and phosphorus oxides are present in a glass composition, less porosity is appreciated in the cross-sections of the coatings. These fewer defective microstructures give rise to enhanced mechanical properties, as occurs for 62W and S53P4 compositions compared to 45S5.

The elements present in the composition of bioactive glasses affect the biological response of the coatings. In particular, the free-sodium composition containing magnesium oxide showed a notable improvement in the proliferation of human bone cells, respect the other compositions tested. Magnesium is an essential cation that plays a crucial role in many physiological functions. The presence of magnesium in a system has been shown to accelerate the generation of new bone, but the mechanisms by which the magnesium ion stimulates cellular activity remain uncertain.

In addition, the phosphate-based glasses studied have very high solubility since high-phosphorus glasses have a highly distorted structure with weak bonds. Therefore, its bioactive capacity is compromised since its permanence in contact with the substrate is short in time.

Some properties of the coatings that are closely linked to the osseointegration process are affected by the glass composition, such as the capacity and kinetic of the apatite layer formation, the dissolution behaviour, or the stimulation and growth of bone tissue.

Another part of the study has focused on obtaining glass coatings using CGS, as it is an economical and fast method that at the same time maintains the chemical characteristics of the feedstock material. However, the brittleness of the glasses and the low temperatures involved during the process make it a challenge. When dense and brittle particles are deposited by cold spray, they rebound on the substrate, and a coating is not achieved.

Strategies based on polymeric composite coatings

By spraying a mixture of polymer with glass powder, the polymer facilitated the deposition of the glass, and the deposition of 45S5 glass particles was possible using CGS by a composite of PEEK and 45S5.

The polymer particles are above their glass transition temperature during spraying, which means they can be plastically deformed without breaking. So in this state, the polymer forms a dense and continuous matrix, where the glass particles are embedded. The glass particles maintain their initial characteristics since, at the process temperature, they do not experience any change. In the coatings, the distribution of particles is homogeneous, and even glass particles are found on the surface where the polymer does not completely surround them. This is because the polymer undergoes the necessary deformation to adapt to the

morphology of the glass particles, thus retaining the particles that are sufficiently embedded so as not to detach.

The ability of the composite to retain glass particles is limited to about one-third of the glass volume in the sprayed mixture. The presence of glass in the mixture negatively affects the deposition efficiency. When glass particles impact other glass particles, they cause erosion. So, the sprayed glass must find polymeric zones when it reaches the surface, which, if it is polymeric, deform locally and manage to retain the glass particles.

Some aspects such as the particle size of the feedstock powder influence the deposition efficiency, being more efficient when spraying smaller particles since they experience the heating and deformation necessary to adapt to the glass particles quickly.

As the glass particles are dense and hard, their presence in the coatings improves their mechanical properties, both in hardness and wear resistance. The incorporation of glass improves the biological response of the coatings, but since the glass is found in small quantities on the surface, it does not represent a notable improvement.

Effect of the glass composition on the viscosity behaviour of the material

The softening temperature of the glass is reduced by the incorporation of CaF_2 instead of CaO in silicate-based glasses, which are very stable and require high temperatures for processability. Adding some elements to the composition can disrupt the network and thus diminish the required temperatures being processed. Phosphate-based glasses become more processable at lower temperatures due to the less interconnected network. However, this remarkably open network also makes them suffer intense degradation, compromising their durability as coating material.

The properties of the glass result from the present elements and the way they are linked to form the structure. The elements with a smaller atomic radius generate denser structures with stronger bonds due to their proximity to the nucleus. Alkaline earth elements are denser than alkaline ones since they have a smaller atomic radius. Thus, replacing alkaline earth oxides with alkaline oxides allows for a less interconnected and less durable network, as observed in the binary systems studied ($CaO\text{-}P_2O_5$ and $Na_2O\text{-}P_2O_5$).

Figure 5.2 shows the deposition mechanism suffered by silicate-based glasses (45S5) compared to the newly developed composition (NaP_50 in the $Na_2O\text{-}P_2O_5$ system). The viscosity behaviour of the new composition is most proper for CGS and the particles are heated above their glass transition temperature, allowing their deformation and, consequently, their deposition.

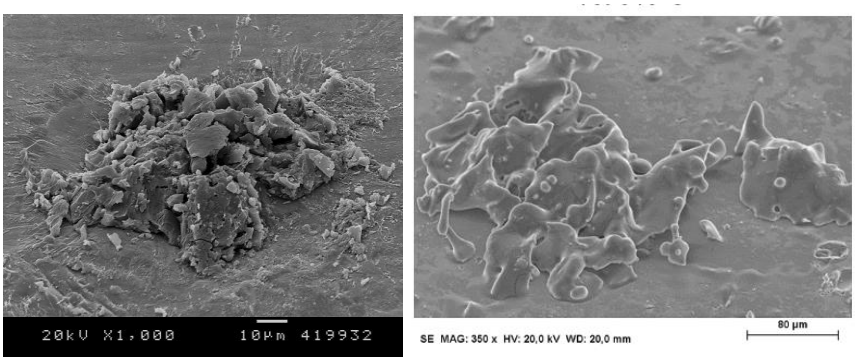

Figure 5.2 Splats particles of 45S5 (left) and NaP_50 (right) deposited by LPCGS

Among the different strategies explored to enable the deposition of brittle particles, a coating wholly made of glass was achieved using CGS by modifying the viscosity behaviour of the feedstock glasses. However, the durability of the coating is not adequate for being used in implants.

Alternatives for the deposition of bioactive glass particles by cold gas spray

This thesis has evaluated different methods for the deposition of bioactive glasses by cold spray technology. First, it has been observed that these glasses can be deposited in mixtures, remaining embedded in a polymeric matrix and keeping their properties intact. However, with this strategy, the amount of glass deposited in the composite is limited. Second, the modification of the composition has been evaluated to alter the properties of the glass so that by making it more susceptible to the working temperatures of cold spray, it is possible to deposit coatings entirely of glass. However, for the glasses to have the properties that make them suitable for the technique, the bioactive capacity of the glasses is compromised, in this case being compositions with high solubility. Despite it, this strategy has allowed us to see that cold spraying can deposit dense and brittle powder materials.

Recent Aerosol Deposition (AD) studies describe the possibility of creating ceramic films at room temperature by optimizing the particle diameter and deposition conditions. In this technique, the kinetics of the particles is related to their size (Ref 107).The different interactions that ceramic particles of different sizes can experiment by AD are represented in Figure 5.3. Particles between 200 nm and 2 µm are fractured by impact and experiment plastic deformation that lets them adhere to the substrate and form a film.

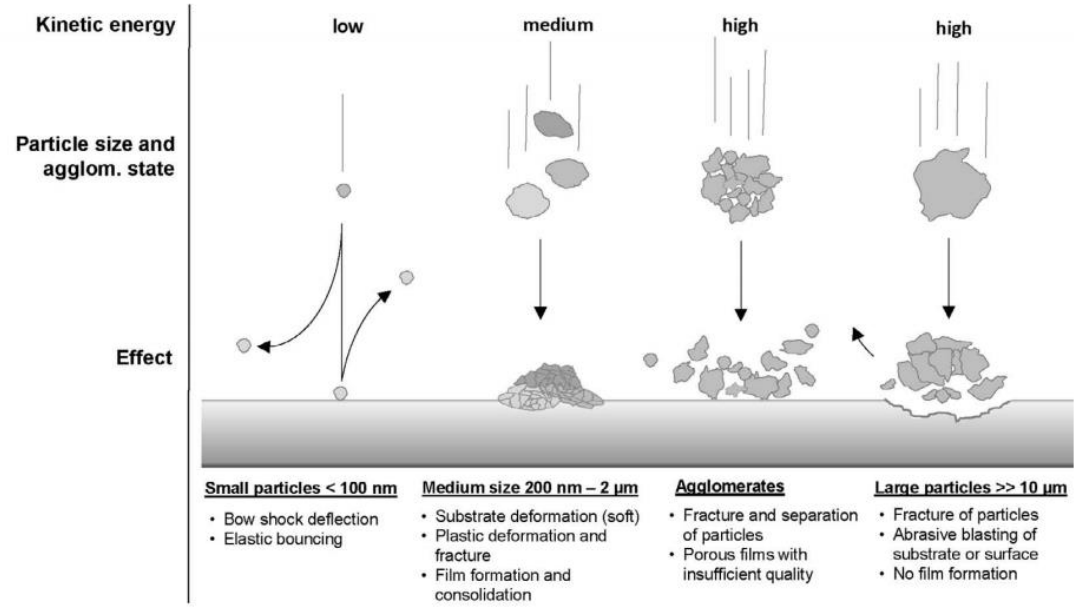

Figure 5.3 Illustration of possible particle-substrate interactions based on the speed and kinetic energy of the ceramic particles. Figure from (Ref 108)

The similarity between AD and CGS makes it possible for ceramic particles to experience a similar mechanism when sprayed by CGS.

In addition, the role of the powder and its architecture is a critical factor for the deposition and impact behaviour of brittle particles. Recent studies on cold gas spray for brittle materials include powders in the form of agglomerates (Ref 109, 110). The porous nature and the nano-metric grains of the particles could be involved with a micro-plasticity effect under the strong impact, allowing certain deformation capacity that causes the adherence of these materials.

The deposition of brittle materials by CGS is still a challenge. Using micrometric particles of bioactive glass formed by nano-agglomerates would be one of the possible lines of continuation of the study developed in this thesis.

6. Chapter: Concluding remarks

6. Chapter: Concluding remarks

In the different sections of this thesis, specific conclusions have been presented that finally lead to general conclusions summarized below:

- It has been possible to obtain bioactive glass coatings with enhanced bond strength by means of atmospheric plasma spraying, reaching the values required by the international regulations.
    - It has been proven that, by modifying the morphology of the powder feedstock the cohesion between coating and substrate is increased.
    - The use of hydroxyapatite in combination with bioactive glass, as a mixture of both powders and also as an anchor layer between substrate and glass, provides an improvement in the affinity of the coating with the substrate, increasing its adherence.
    - Applying a pre-heating to the substrate immediately prior to deposition can enhance the coating adhesion. This improvement in adhesion is even higher when a thermal post-treatment above glass transition temperature of the glass is applied.
    - Some oxides in the glass composition can generate pore-free microstructures, such as MgO, which contributes to form coatings with greater adherence.
- For the different bioactive glass compositions studied, the elements forming the structure of the glass and also their proportion alter the microstructure and properties of the coatings produced by atmospheric plasma spraying. Also, post-treatments have an effect on the characteristics of the final coatings.
    - The content of network-forming oxides and network modifiers in the composition affects the reaction of the coatings in physiological solution. In the case of glasses with less interconnected structures, the reaction rate is greater, generating coatings with more bioactivity.
    - The resulting microstructure from the application a post-thermal treatment, where crystalline phases are generated, significantly affects the reaction of the coating in physiological solution causing a delay in the rate of reaction.
    - The different elements forming the glass cause a different mechanical and biological response. In vitro tests with osteoblasts have shown that the non-commercial 62W composition gets a better cellular response compared to the commercial formulations. Furthermore, the 62W coatings achieve the best bond strength values, which are suitable for the desired application. Coatings produced with bioactive glass 62W are optimal candidates to promote a more efficient osseointegration than the current implants.

- For the first time, it has been possible to obtain glass coatings deposited by cold gas spraying.
    - The use of a mixture of PEEK and bioactive glass has allowed to obtain glass-containing coatings by cold spraying. The brittle particles have been embedded in a polymeric matrix and provide enhanced mechanical and biological properties to that polymeric biomaterial. The deposition efficiency obtained for these composites is high in relation to other polymeric coatings obtained by cold spraying, and it is negatively affected by the glass content in the mixture.
    - The design of new glass formulations with a viscosity behaviour adjusted to the temperatures reached during cold spraying allowed the deposition of glass powder by low pressure cold gas spraying. However, the high dissolution rate of the designed glass compromises the bioactive behaviour of the 100% glass coatings obtained.
    - The use of dense and brittle powders results in a particular bonding mechanism where the particles are fractured and adhered to the substrate but do not allow the formation of a cold spray glass coating. On the contrary, specially designed agglomerated powders composed of nano-sized glasses could enable the coating formation by the material microplasticity under the conditions of cold spraying.

References

References

1. H. Kaul and Y. Ventikos, “On the Genealogy of Tissue Engineering and Regenerative Medicine,” *Tissue Engineering - Part B: Reviews*, 2015.
2. S.D. Gross, A System of Surgery, Pathological, Diagnostic, Therapeutic, and Operative, *Am. J. Med. Sci.*, 1865, **49**(97), p 1102, doi:10.1097/00000441-186501000-00026.
3. H. An, Yuehuei, C.R. Burgoyne, M.S. Crum, and J.A. Glaser, Current Methods and Trends in Fixation of Osteoporotic Bone, *Internal Fixation in Osteoporotic Bone*, Y.H. An, Ed., (Stuttgart), Georg Thieme Verlag, 2002, p 73–107, doi:10.1055/b-0034-52188.
4. B. Jessney, Joseph Lister (1827-1912): A Pioneer of Antiseptic Surgery Remembered a Century after His Death, *J. Med. Biogr.*, 2012, **20**(3), p 107–110.
5. S. Sauerbier, R. Schön, J.E. Otten, R. Schmelzeisen, and R. Gutwald, The Development of Plate Osteosynthesis for the Treatment of Fractures of the Mandibular Body - A Literature Review, *J. Cranio-Maxillofacial Surg.*, 2008, **36**(5), p 251–259.
6. C.M. Court-Brown, Skeletal Trauma: Basic Science, Management and Reconstruction., *J. Bone Joint Surg. Br.*, 2003, **85**-**B**(7), p 1089–1089.
7. H.K. Uhthoff, P. Poitras, and D.S. Backman, “Internal Plate Fixation of Fractures: Short History and Recent Developments,” *Journal of Orthopaedic Science*, 2006, p 118–126.
8. C.S. Venable, W.G. Stuck, and A. Beach, THE EFFECTS ON BONE OF THE PRESENCE OF METALS; BASED UPON ELECTROLYSIS, *Ann. Surg.*, 1937, **105**(6), p 917–938.
9. A. Ruys, Alumina Bearings in Orthopedics: Origin and Evolution, *Alumina Ceramics*, 2019.
10. B.D. Ratner, A.S. Hoffman, F.J. Schoen, and J.E. Lemons, “An Introduction to Materials in Medicine,” *Biomaterials Science*, second ed., Academic Press, 2004.
11. Z. Li and K. Aik Khor, Preparation and Properties of Coatings and Thin Films on Metal Implants, *Encyclopedia of Biomedical Engineering*, 2019, p 203–212.
12. Introduction, *Definitions of Biomaterials for the Twenty-First Century*, Elsevier, 2019, p 1–14, doi:10.1016/B978-0-12-818291-8.00001-8.
13. D.F. Williams, On the Nature of Biomaterials, *Biomaterials*, Elsevier, 2009, **30**(30), p 5897–5909.
14. Biomaterials and Biomedical Materials, *Definitions of Biomaterials for the Twenty-First Century*, Elsevier, 2019, p 15–23.
15. L.H.M. Antunes and C.R.P. de Lima, Cobalt-Chromium Alloys – Properties and Applications ☆, *Reference Module in Materials Science and Materials Engineering*, Elsevier, 2018.
16. S. Pfanner, G. Munz, G. Guidi, and M. Ceruso, Universal 2 Wrist Arthroplasty in Rheumatoid Arthritis, *J. Wrist Surg.*, 2017, **06**(03), p 206–215.
17. N.J. Hallab and J.J. Jacobs, Orthopedic Applications, *Biomaterials Science: An Introduction to Materials: Third Edition*, Academic Press, 2013, p 841–882.
18. H.A. Zaman, S. Sharif, M.H. Idris, and A. Kamarudin, Metallic Biomaterials for Medical Implant Applications: A Review, *Appl. Mech. Mater.*, Trans Tech Publications, Ltd., 2015, **735**, p 19–25.
19. J.S. Hayes and R.G. Richards, “The Use of Titanium and Stainless Steel in Fracture Fixation,” *Expert Review of Medical Devices*, 2010.
20. M. Kaur and K. Singh, “Review on Titanium and Titanium Based Alloys as Biomaterials for Orthopaedic Applications,” *Materials Science and Engineering C*, 2019, p 844–862.
21. C.N. Elias, J.H.C. Lima, R. Valiev, and M.A. Meyers, “Biomedical Applications of Titanium and Its Alloys,”

JOM, 2008.

22. A. Ruys, Introduction to Alumina Ceramics, *Alumina Ceramics*, 2019, p 1–37.

23. A. Mehjabeen, T. Song, W. Xu, H.P. Tang, and M. Qian, “Zirconium Alloys for Orthopaedic and Dental Applications,” *Advanced Engineering Materials*, 2018.

24. G.R. Chilukoti and A.P. Periyasam, Ultra High Molecular Weight Polyethylene for Medical Applications, *Tech. Textilien*, 2012, **55**(3).

25. S. Verma, N. Sharma, S. Kango, and S. Sharma, “Developments of PEEK (Polyetheretherketone) as a Biomedical Material: A Focused Review,” *European Polymer Journal*, 2021, p 110295, doi:10.1016/j.eurpolymj.2021.110295.

26. S. Parithimarkalaignan and T. V. Padmanabhan, “Osseointegration: An Update,” *Journal of Indian Prosthodontist Society*, 2013, p 2–6.

27. P. Moreo, J.M. García-Aznar, and M. Doblaré, Bone Ingrowth on the Surface of Endosseous Implants. Part 1: Mathematical Model, *J. Theor. Biol.*, 2009, **260**(1), p 1–12.

28. A.S. da S. Mello, P.L. dos Santos, A. Marquesi, T.P. Queiroz, R. Margonar, and A.P. de Souza Faloni, Some Aspects of Bone Remodeling around Dental Implants, *Rev. Clínica Periodoncia, Implantol. y Rehabil. Oral*, 2016.

29. L.L. Hench, Opening Paper 2015- Some Comments on Bioglass: Four Eras of Discovery and Development, *Biomed. Glas.*, 2015, **1**(1), p 1–11.

30. S. Raghavendra, M.C. Wood, and T.D. Taylor, Early Wound Healing around Endosseous Implants: A Review of the Literature., *Int. J. Oral Maxillofac. Implants*, 2005, **20 3**, p 425–431.

31. M. Sundfeldt, L. V. Carlsson, C.B. Johansson, P. Thomsen, and C. Gretzer, “Aseptic Loosening, Not Only a Question of Wear: A Review of Different Theories,” *Acta Orthopaedica*, 2006, p 177–197.

32. U. Dapunt, B. Prior, J.P. Kretzer, T. Giese, and Y. Zhao, Bacterial Biofilm Components Induce an Enhanced Inflammatory Response against Metal Wear Particles, *Ther. Clin. Risk Manag.*, 2020, **16**, p 1203–1212.

33. J. Raphel, M. Holodniy, S.B. Goodman, and S.C. Heilshorn, “Multifunctional Coatings to Simultaneously Promote Osseointegration and Prevent Infection of Orthopaedic Implants,” *Biomaterials*, 2016.

34. P.A. Revell, Biological Causes of Prosthetic Joint Failure, *Joint Replacement Technology*, Woodhead Publishing, 2021, p 299–371.

35. A.G. Gristina, Biomaterial-Centered Infection: Microbial Adhesion Versus Tissue Integration, *Science (80-.).*, 1987, **237**(4822), p 1588–1595, doi:10.1126/science.3629258.

36. A.G. Gristina, P.T. Naylor, and Q. Myrvik, The Race for the Surface: Microbes, Tissue Cells, and Biomaterials, *Molecular Mechanisms of Microbial Adhesion*, 1989, p 177–211.

37. N.L. Davison, F. Barrère-de Groot, and D.W. Grijpma, Degradation of Biomaterials, *Tissue Engineering: Second Edition*, Academic Press, 2014, p 177–215.

38. J.R. Jones, Bioactive Glasses, *Bioceramics and their Clinical Applications*, Woodhead Publishing, 2008, p 266–283.

39. A. Pedone, T. Charpentier, G. Malavasi, and M.C. Menziani, New Insights into the Atomic Structure of 45S5 Bioglass by Means of Solid-State NMR Spectroscopy and Accurate First-Principles Simulations, *Chem. Mater.*, 2010, **22**(19).

40. A. Tilocca, Structural Models of Bioactive Glasses from Molecular Dynamics Simulations, n.d.

41. R.G. Hill and D.S. Brauer, Predicting the Bioactivity of Glasses Using the Network Connectivity or Split Network Models, *J. Non. Cryst. Solids*, 2011, **357**(24), p 3884–3887.

42. R. Hill, An Alternative View of the Degradation of Bioglass, *J. Mater. Sci. Lett.*, 1996, **15**(13), p 1122–1125.

43. M. Edén, The Split Network Analysis for Exploring Composition-Structure Correlations in Multi-Component Glasses: I. Rationalizing Bioactivity-Composition Trends of Bioglasses, *J. Non. Cryst. Solids*, 2011, **357**(6).

44. K.E. Wallace, R.G. Hill, J.T. Pembroke, C.J. Brown, and P. V. Hatton, "Influence of Sodium Oxide Content on Bioactive Glass Properties," *Journal of Materials Science: Materials in Medicine*, 1999.

45. M. Ojansivu, S. Vanhatupa, L. Björkvik, H. Häkkänen, M. Kellomäki, R. Autio, J.A. Ihalainen, L. Hupa, and S. Miettinen, Bioactive Glass Ions as Strong Enhancers of Osteogenic Differentiation in Human Adipose Stem Cells, *Acta Biomater.*, 2015, **21**.

46. M. Bosetti and M. Cannas, The Effect of Bioactive Glasses on Bone Marrow Stromal Cells Differentiation, *Biomaterials*, 2005, **26**(18).

47. F. Barrère, M. Ni, P. Habibovic, P. Ducheyne, and K. de Groot, Degradation of Bioceramics, *Tissue Engineering*, 2008.

48. R.Z. LeGeros, Properties of Osteoconductive Biomaterials: Calcium Phosphates, *Clin. Orthop. Relat. Res.*, 2002.

49. S. V Dorozhkin, "Calcium Orthophosphates in Nature, Biology and Medicine," *Materials*, 2009, p 399–498, doi:10.3390/ma2020399.

50. L. Wang and G.H. Nancollas, Calcium Orthophosphates: Crystallization and Dissolution, *Chem. Rev.*, 2008, **108**(11), p 4628–4669.

51. S. V. Dorozhkin, "A Detailed History of Calcium Orthophosphates from 1770s till 1950," *Materials Science and Engineering C*, Elsevier, 2013, p 3085–3110.

52. J. Jeong, J.H. Kim, J.H. Shim, N.S. Hwang, and C.Y. Heo, "Bioactive Calcium Phosphate Materials and Applications in Bone Regeneration," *Biomaterials Research*, 2019.

53. C. Guzmán Vázquez, C. Piña Barba, and N. Munguía, Stoichiometric Hydroxyapatite Obtained by Precipitation and Sol Gel Processes, *Rev. Mex. Fis.*, 2005, **51**(3), p 284–293.

54. T. Kokubo, H.M. Kim, and M. Kawashita, Novel Bioactive Materials with Different Mechanical Properties, *Biomaterials*, 2003, **24**(13), p 2161–2175.

55. A. Slepko and A.A. Demkov, First Principles Study of Hydroxyapatite Surface, *J. Chem. Phys.*, 2013, **139**(4).

56. H.R. Fernandes, A. Gaddam, A. Rebelo, D. Brazete, G.E. Stan, and J.M.F. Ferreira, "Bioactive Glasses and Glass-Ceramics for Healthcare Applications in Bone Regeneration and Tissue Engineering," *Materials*, 2018.

57. M. Montazerian and E. Dutra Zanotto, "History and Trends of Bioactive Glass-Ceramics," *Journal of Biomedical Materials Research - Part A*, 2016, p 1231–1249.

58. S. Oliver, B.A. Proctor, C.. May, and V.E. Annamalai, Degradation of Glass and Glass Ceramics, *Reference Module in Materials Science and Materials Engineering*, 2016.

59. Tadashi Kokubo, Bioactive Glass Ceramics: Properties and Applications, *Biomaterials*, 1991.

60. E. Fiume, J. Barberi, E. Verné, and F. Baino, "Bioactive Glasses: From Parent 45S5 Composition to Scaffold-Assisted Tissue-Healing Therapies," *Journal of Functional Biomaterials*, 2018.

61. P.N. De Aza, A.H. De Aza, P. Pena, and S. De Aza, Bioactive Glasses and Glass-Ceramics, *Bol. la Soc. Esp. Ceram. y Vidr.*, Sociedad Española de Cerámica y Vidrio, 2007, **46**(2), p 45–55, doi:10.13039/501100003359.

62. Q. Chen, C. Zhu, and G.A. Thouas, Progress and Challenges in Biomaterials Used for Bone Tissue

Engineering: Bioactive Glasses and Elastomeric Composites, *Prog. Biomater.*, 2012, **1**(1), p 2.

63. P. Fauchais and A. Vardelle, Thermal Sprayed Coatings Used Against Corrosion and Corrosive Wear, *Advanced Plasma Spray Applications*, 2012.

64. R.S.C. Paredes, S.C. Amico, and A.S.C.M. D'Oliveira, The Effect of Roughness and Pre-Heating of the Substrate on the Morphology of Aluminium Coatings Deposited by Thermal Spraying, *Surf. Coatings Technol.*, 2006, **200**(9), p 3049–3055.

65. P.L. Fauchais, J.V.R. Heberlein, and M.I. Boulos, Overview of Thermal Spray, *Thermal Spray Fundamentals: From Powder to Part*, (Boston, MA), Springer US, 2014, p 17–72, doi:10.1007/978-0-387-68991-3_2.

66. M.M. Verdian, Finishing and Post-Treatment of Thermal Spray Coatings, *Comprehensive Materials Finishing*, 2017, p 191–206.

67. K. Bobzin, M. Öte, and M.A. Knoch, Surface Pre-Treatment for Thermally Sprayed ZnAl15 Coatings, *J. Therm. Spray Technol.*, 2017, **26**(3).

68. R. Huiskes, H. Weinans, and B. Van Rietbergen, "The Relationship between Stress Shielding and Bone Resorption around Total Hip Stems and the Effects of Flexible Materials," *Clinical Orthopaedics and Related Research*, 1992.

69. E. Wintermantel, J. Mayer, T.N. Goehring, and S.N. Aqida, Composites for Biomedical Applications, *Reference Module in Materials Science and Materials Engineering*, 2016.

70. P. Fauchais, M. Vardelle, and S. Goutier, "Atmospheric Plasma Spraying Evolution Since the Sixties Through Modeling, Measurements and Sensors," *Plasma Chemistry and Plasma Processing*, 2017.

71. P. Fauchais, "Understanding Plasma Spraying," *Journal of Physics D: Applied Physics*, 2004.

72. L. Pawlowski, Thermal Spraying Techniques, *The Science and Engineering of Thermal Spray Coatings*, 2008, p 67–113.

73. M. Lorenzo-bañuelos, A. Díaz, D. Rodríguez, I.I. Cuesta, A. Fernández, and J.M. Alegre, Influence of Atmospheric Plasma Spray Parameters (APS) on the Mechanical Properties of Ni-Al Coatings on Aluminum Alloy Substrate, *Metals (Basel).*, 2021, **11**(4).

74. S. Janisson, A. Vardelle, J.F. Coudert, E. Meillot, B. Pateyron, and P. Fauchais, Plasma Spraying Using Ar-He-H2 Gas Mixtures, *J. Therm. Spray Technol.*, 1999, **8**(4), p 545–552.

75. M. Vardelle, P. Fauchais, A. Vardelle, K.I. Li, B. Dussoubs, and N.J. Themelis, Controlling Particle Injection in Plasma Spraying, *J. Therm. Spray Technol.*, 2001, **10**(2), p 267–284.

76. A. Nouri and A. Sola, Powder Morphology in Thermal Spraying, *J. Adv. Manuf. Process.*, 2019, **1**(3).

77. X.J. Ning, J.H. Jang, and H.J. Kim, The Effects of Powder Properties on In-Flight Particle Velocity and Deposition Process during Low Pressure Cold Spray Process, *Appl. Surf. Sci.*, 2007, **253**(18).

78. T. Schmidt, H. Assadi, F. Gärtner, H. Richter, T. Stoltenhoff, H. Kreye, and T. Klassen, From Particle Acceleration to Impact and Bonding in Cold Spraying, *J. Therm. Spray Technol.*, 2009, **18**(5–6), p 794–808.

79. F.S. Da Silva, N. Cinca, S. Dosta, I.G. Cano, J.M. Guilemany, and A.V. Benedetti, "Cold Gas Spray Coatings: Basic Principles, Corrosion Protection and Applications," *Ecletica Quimica*, 2017, p 9–32.

80. S. Singh, R.K.S. Raman, C.C. Berndt, and H. Singh, Influence of Cold Spray Parameters on Bonding Mechanisms: A Review, *Metals (Basel).*, 2021, **11**(12), p 2016, doi:10.3390/met11122016.

81. K. Sakaki, The Influence of Nozzle Design in the Cold Spray Process, *The Cold Spray Materials Deposition Process: Fundamentals and Applications*, Woodhead Publishing, 2007, p 117–126.

82. V.K. Champagne, "The Cold Spray Materials Deposition Process," *The Cold Spray Materials Deposition Process: Fundamentals and Applications*, Woodhead Publishing Limited, 2007,

doi:10.1533/9781845693787.

83. H. Tabbara, S. Gu, D.G. McCartney, T.S. Price, and P.H. Shipway, “Study on Process Optimization of Cold Gas Spraying,” *Journal of Thermal Spray Technology*, 2011, p 608–620.

84. M. Ghosh, A. Roy, A. Ghosh, H. Kumar, and G. Saha, Antibacterial and Antimicrobial Coatings on Metal Substrates by Cold Spray Technique: Present and Future Perspectives, *Green Approaches in Medicinal Chemistry for Sustainable Drug Design*, Elsevier Inc., 2020, p 15–45.

85. P. Vuoristo, Thermal Spray Coating Processes, *Comprehensive Materials Processing*, S. Hashmi, Ed., Elsevier, 2014, p 229–276, doi:10.1016/B978-0-08-096532-1.00407-6.

86. H. Assadi, F. Gärtner, T. Stoltenhoff, H. Kreye, F. Ga, T. Stoltenhoff, and H. Kreye, Bonding Mechanism in Cold Gas Spraying, *Acta Mater.*, 2003, **51**, p 4379–4394.

87. T. Schmidt, F. Gärtner, H. Assadi, and H. Kreye, Development of a Generalized Parameter Window for Cold Spray Deposition, *Acta Mater.*, 2006, **54**(3), p 729–742.

88. J. Henao, A. Concustell, S. Dosta, G. Bolelli, I.G. Cano, L. Lusvarghi, and J.M. Guilemany, Deposition Mechanisms of Metallic Glass Particles by Cold Gas Spraying, *Acta Mater.*, 2017, **125**, p 327–339.

89. M. Gardon, H. Melero, N. Garcia-Giralt, S. Dosta, I.G. Cano, and J.M. Guilemany, Enhancing the Bioactivity of Polymeric Implants by Means of Cold Gas Spray Coatings, *J. Biomed. Mater. Res. - Part B Appl. Biomater.*, 2014, **102**(7), p 1537–1543.

90. N. Cinca, A.M. Vilardell, S. Dosta, A. Concustell, I. Garcia Cano, J.M. Guilemany, S. Estradé, A. Ruiz, and F. Peiró, A New Alternative for Obtaining Nanocrystalline Bioactive Coatings: Study of Hydroxyapatite Deposition Mechanisms by Cold Gas Spraying, *J. Am. Ceram. Soc.*, 2016, **99**(4), p 1420–1428.

91. H. Melero Correas, Recubrimientos Biocompatibles de Hidroxiapatita-Titania Obtenidos Mediante Proyección Térmica de Alta Velocidad (HVOF), *TDX (Tesis Dr. en Xarxa)*, Universitat de Barcelona, 2014, http://www.tdx.cat/handle/10803/132160. Accessed 12 June 2018.

92. H. Melero, G. Fargas, N. Garcia-Giralt, J. Fernández, and J.M. Guilemany, Mechanical Performance of Bioceramic Coatings Obtained by High-Velocity Oxy-Fuel Spray for Biomedical Purposes, *Surf. Coatings Technol.*, 2014, **242**, p 92–99.

93. H. Melero, C. Madrid, J. Fernández, and J.M. Guilemany, “Comparing Two Antibacterial Treatments for Bioceramic Coatings at Short Culture Times,” *Journal of Thermal Spray Technology*, 2014, p 684–691.

94. H. Melero, N. Garcia-Giralt, J. Fernández, A. Díez-Pérez, and J.M. Guilemany, Comparison of in Vitro Behavior of As-Sprayed, Alkaline-Treated and Collagen-Treated Bioceramic Coatings Obtained by High Velocity Oxy-Fuel Spray, *Appl. Surf. Sci.*, 2014, **307**, p 246–254.

95. H. Melero, M. Torrell, J. Fernández, J.R. Gomes, and J.M. Guilemany, Tribological Characterization of Biocompatible HAp-TiO2 Coatings Obtained by High Velocity Oxy-Fuel Spray, *Wear*, 2013, **305**(1–2), p 8–13.

96. H. Melero, J. Fernández, S. Dosta, and J. Guilemany, Caracterización de Nuevos Recubrimientos Biocompatibles de Hidroxiapatita-TiO2 Obtenidos Mediante Proyección Térmica de Alta Velocidad, *Bol. la Soc. Esp. Ceram. y Vidr.*, 2011, **50**(2), p 59–64.

97. A.M. Vilardell, N. Cinca, N. Garcia-Giralt, S. Dosta, I.G. Cano, X. Nogués, and J.M. Guilemany, In-Vitro Comparison of Hydroxyapatite Coatings Obtained by Cold Spray and Conventional Thermal Spray Technologies, *Mater. Sci. Eng. C*, 2020, **107**, p 110306, doi:10.1016/j.msec.2019.110306.

98. A.M. Vilardell, N. Cinca, S. Dosta, I.G. Cano, and J.M. Guilemany, Feasibility of Using Low Pressure Cold Gas Spray for the Spraying of Thick Ceramic Hydroxyapatite Coatings, *Int. J. Appl. Ceram. Technol.*, 2019, **16**(1), p 221–229.

99. A.M. Vilardell, N. Cinca, N. Garcia-Giralt, C. Müller, S. Dosta, M. Sarret, I.G. Cano, X. Nogués, and J.M. Guilemany, In-Vitro Study of Hierarchical Structures: Anodic Oxidation and Alkaline Treatments onto

Highly Rough Titanium Cold Gas Spray Coatings for Biomedical Applications, *Mater. Sci. Eng. C*, 2018, **91**, p 589–596.

100. A.M. Vilardell, N. Cinca, N. Garcia-Giralt, S. Dosta, I.G. Cano, X. Nogués, and J.M. Guilemany, Functionalized Coatings by Cold Spray: An in Vitro Study of Micro- and Nanocrystalline Hydroxyapatite Compared to Porous Titanium, *Mater. Sci. Eng. C*, 2018, **87**, p 41–49.

101. A.M. Vilardell, N. Cinca, N. Garcia-Giralt, S. Dosta, I.G. Cano, X. Nogués, and J.M. Guilemany, Osteoblastic Cell Response on High-Rough Titanium Coatings by Cold Spray, *J. Mater. Sci. Mater. Med.*, 2018, **29**(3).

102. A.M. Vilardell, N. Cinca, I. Pacheco, C. Santiveri, S. Dosta, I.G. Cano, J.M. Guilemany, M. Sarret, and C. Muller, Hierarchical Structures of Anodised Cold Gas Sprayed Titanium Coatings, *Trans. Inst. Met. Finish.*, 2018, **96**(2), p 71–78.

103. A.M. Vilardell, N. Cinca, I.G. Cano, A. Concustell, S. Dosta, J.M. Guilemany, S. Estradé, A. Ruiz-Caridad, and F. Peiró, Dense Nanostructured Calcium Phosphate Coating on Titanium by Cold Spray, *J. Eur. Ceram. Soc.*, 2017, **37**(4), p 1747–1755.

104. A. Vilardell, N. Cinca, A. Jokinen, N. Garcia-Giralt, S. Dosta, I. Cano, and J. Guilemany, Real-Time Protein and Cell Binding Measurements on Hydroxyapatite Coatings, *J. Funct. Biomater.*, 2016, **7**(3), p 23.

105. C. Sara Rodrigo-Vázquez, M.A. Rodríguez, and A.H. De Aza, Devitrification Study of a Novel Bioactive Glass Designed on the CaSiO3 – Ca3(PO4)2 – MgCa(SiO3)2 System, *J. Non. Cryst. Solids*, 2020, **528**.

106. D. Geldart, E.C. Abdullah, A. Hassanpour, L.C. Nwoke, and I. Wouters, Characterization of Powder Flowability Using Measurement of Angle of Repose, *China Particuology*, 2006, **4**(3–4), p 104–107.

107. J. Akedo, “Room Temperature Impact Consolidation (RTIC) of Fine Ceramic Powder by Aerosol Deposition Method and Applications to Microdevices,” *Journal of Thermal Spray Technology*, 2008, p 181–198.

108. D. Hanft, J. Exner, M. Schubert, T. Stöcker, P. Fuierer, and R. Moos, “An Overview of the Aerosol Deposition Method: Process Fundamentals and New Trends in Materials Applications,” *Journal of Ceramic Science and Technology*, 2015, p 147–181.

109. A.M. Vilardell, N. Cinca, I.G. Cano, A. Concustell, S. Dosta, J.M. Guilemany, S. Estradé, A. Ruiz-Caridad, and F. Peiró, Dense Nanostructured Calcium Phosphate Coating on Titanium by Cold Spray, *J. Eur. Ceram. Soc.*, 2017, **37**(4), p 1747–1755.

110. M. Yamada, H. Isago, H. Nakano, and M. Fukumoto, Cold Spraying of TiO 2 Photocatalyst Coating With Nitrogen Process Gas, 2010, **19**(December), p 1218–1223.